From THE DEPARTMENT OF ONCOLOGY AND METABOLISM, University of Sheffield, UK

THE CONTRIBUTION OF INTERLEUKIN-34 IN INFLAMMATION AND OSTEOSARCOMA

Kristina Schiavone

Thesis for Doctoral Degree (Ph.D.)

University of Sheffield, 2019

The Contribution of Interleukin-34 in Inflammation and Osteosarcoma

A thesis submitted to the University of Sheffield for the degree of Doctor of Oncology in the Faculty of Medicine, Dentistry and Health

By

Kristina Schiavone

Principal Supervisor:

Professor Dominique Heymann
INSERM
European Associated Laboratory
"Sarcoma Research Unit"
University of Sheffield

Co-supervisor:

Dr. Robin Young
Department of Oncology and Metabolism
University of Sheffield

I would like to dedicate this thesis to those who are fighting osteosarcoma, to those who are related to, or have befriended an osteosarcoma patient, and to those who have lost someone to osteosarcoma. I hope that one day, science can fight and win this battle.

STANDARD DECLERATION

I declare that this thesis was composed by myself, and that the work contained herein is my own except where explicitly stated otherwise in the text, and that this work has not been submitted for any other degree or processional qualification except as specified.

ACKNOWLEDGEMENTS

First and foremost I would like to thanks my supervisor, Professor Dominique Heymann for his invaluable supervision throughout my PhD. Thank you for your guidance and for sharing your vast knowledge with me. Thank you for always pushing me further, and for mentoring me into the researcher that I am today. For that I will always be grateful.

My sincere thank you also goes to my co-supervisor Dr. Robin Young for all the advice and guidance he's given me.

A special thank you goes to Dr. Hannah Brown, Dr. Marcus Keating, Dr. Katy Henry, Dr. Stuart Hunt, Dr. Frederic Deschaseaux and Professor Steven Renshaw. The support and guidance of these people has been fundamental for the work carried out in this thesis. Thank you for welcoming me into your groups and letting me be part of the research environment.

Thank you to my friends and relatives, too numerous to name, who have encouraged me and supported me during this long process of my academic journey. Thank you everyone for always being there, especially when times got though!

And last but not least, my deepest gratitude and appreciation goes towards my parents, whose support and belief in me were always my main incentive. Their encouragement and support throughout this journey has been invaluable, and without it I wouldn't be where I am today.

ABSTRACT

Interleukin-34 is a cytokine sharing functional similarities with the macrophage-colony stimulating factor (M-CSF). It is responsible for the proliferation/differentiation/survival of myeloid cells. Upregulation of IL-34 contributes to disease progression and growth of osteosarcoma. IL-34 is therefore a novel prognostic biomarker, and a target for therapeutic intervention of osteosarcoma. This study aimed to investigate the role of IL-34 and its signalling/communication with the tumour stroma via extracellular vesicles, and in development and function using a zebrafish model. To determine the therapeutic effect of IL-34 targeting in osteosarcoma murine pre-clinical models where used. **METHODS:** Extracellular vesicles were isolated from osteosarcoma cells and mesenchymal stem cells. Proliferation, differentiation of lineage abilities and protein contents were assessed. In the second part of the study, anti-IL-34 monoclonal blocking antibodies were used in xenograft and allograft murine models, at 4mg/kg and administered (i.p) three times weekly. The effects on tumour growth and histological markers were investigated. We also evaluated the potential therapeutic benefit of combining the IL-34 blocking agent, in combination with doxorubicin as a combination treatment. Finally, using CRISPR/Cas9 system a loss of function model of IL34 was developed. Expression of the cytokine was determined by RT-qPCR and *in-situ* hybridization, while tail-fin injury assays were used characterize the expression of IL-34 in response to inflammation. **RESULTS:** Exosomes from osteosarcoma cells induced the commitment of mesenchymal stem cells towards adipogenesis whilst exosomes isolated from mesenchymal stem cells induced the proliferation of osteosarcoma cells indicating a tumour supportive role. In murine models, administration of blocking IL-34 antibody, inhibited tumour progression in both syngeneic and xenogeneic models. The treatment had no effect on bone associated remodelling after analysis by microCT. IHC analysis showed an increase in F4/80 infiltrates, and a tendency towards lower vascularisation as marked by CD31. CRISPR/Cas9 created a stable loss of function zebrafish mutant line deficient of IL-34. Investigation of IL-34 expression revealed low expression of the cytokine in larval development, that becomes upregulated in response to inflammation. A decrease in the number of macrophages in IL-34 morphants was also seen. **CONCLUSION:** This study represents the first characterization of IL-34 function and expression in zebrafish by a loss of function model. In osteosarcoma, the inhibition of IL-34 specific blocking antibodies demonstrates that the therapeutic benefit to abrogate IL-34.

LIST OF SCIENTIFIC PAPERS

I. Brown, H., **Schiavone**, K., Tazzyman, S., Heymann, D. & Chico, T. J. Zebrafish xenograft models of cancer and metastasis for drug discovery. *Expert Opin. Drug Discov*. 12, 379–389 (2017).

II. Brown, H., **Schiavone K.**, Gouin, F., Heymann, M. & Heymann, D. Biology of Bone Sarcomas and New Therapeutic Developments. *Calcif. Tissue Int*. 102, 174–195 (2017).

III. Heymann, M.F., **Schiavone K**., Garnier, D., Heymann, D.. The heterogeneity of osteosarcoma: the role played by osteosarcoma stem cells. *Advances in Experimental Medicine and Biology*, *In press*.

IV. Heymann, M.F., **Schiavone K.,** Heymann, D.. Bone sarcomas in the immunotherapy era. *British Journal of Pharmacology*, *Submitted*

V. **Schiavone, K.,** Keating, M., Henry, K., Renshaw, S., Heymann, D. Zebrafish model to assess the role of IL-34 in inflammation, *Unpublished Manuscript*

VI. **Schiavone, K.,** Brown, H., Young, R., Heymann, D**.** Blocking IL-34 as a potential therapeutic target for the treatment of osteosarcoma, *Unpublished manuscript*

VII. **Schiavone et al.** Generation of IL-34 knockout mice, *Unpublished manuscript*

TABLE OF CONTENTS

LIST OF FIGURES

LIST OF TABLES

LIST OF ABBREVIATIONS

ANOVA – Analysis of variance

ASC – Adipose derived mesenchymal stem cells

BCIP- 5-bromo-4-chloro-3-indolyl-phosphate

BME – Bone Microenvironment

BMSC – Bone marrow derived mesenchymal stem cells

BP – Base pair

BSA – bovine serum albumin

BV – Bone volume

CCL - Chemokine ligand

CD – Cluster of differentiation

CDK - Cyclin-Dependent Kinase

cDNA – complementary DNA

CDP – Cisplatin

CM – Conditioned Media

CRISPR – Clustered regularly interspaced short palindromic repeats.

CS- Chondroitin Sulfate

CSF-1 - Colony Stimulating Factor-1

CXCL – Chemokine C-X-C motif ligand

DAPI - 4′,6-diamidino-2-phenylindole

DC – Dendritic cells

DEPC – Diethyl polycarbonate

DMARDs – disease modifying antirheumatic drugs

DMEM – Dulbecco's Modified Eagle's Medium

DMSO – Dimethyl Sulfoxide

DNA – Deoxyribonucleic acid

DNase – deoxyribonuclease

DOX – Doxorubicin

DPF – Days post fertilization

DSB – Double Strand Break

ECFC – Endothelial Colony Forming Cells

EDTA – Ethylenediaminetetraacetic acid

EF1α – Elongation factor 1-alpha

EGFR – Endothelial growth factor

ELISA – Enzyme-linked immunoadsorbent assay

ENU – N-ethyl-N-nitrosurea

ERK – Extracellular signal-related kinases

ESCRT – Endosomal sorting complexes

EVs – Extracellular Vesicles

FBS – Foetal Bovine Serum

GAPDH – Glyceraldehyde 3-phosphate dehydrogenase

GFP – Green fluorescent protein

GM-CSF - Grannulocyte-macrophage- colony-stimulating-factor

gRNA – Guide Ribonucleic acid

HCL – Hydrochloric acid

HDTMX – High dose methotrexate

HEK – human embryonic kidney

HIF – Hypoxia inducible factor

HPF – Hours post fertilization

HRP – Horse radish peroxidase

HSP70 – Heat shock protein 70

HSP90 - Heat shock protein 90

HUVEC – Human Umbilical Vein Endothelial Cells

IBD – Inflammatory bowel disease

IFNy – Interferon gamma

IFO – Ifosfamide

IL – Interleukin

IL-1β – Interleukin – 1 Beta

JNK – C-Jun N-terminal kinases

KIT – Tyrosine kinase

KO – Knockout

M-CSF – Macrophage- Colony Stimulating Factor

MAP – Methotrexate, cisplatin and doxorubicin

MAPIE - Methotrexate, cisplatin, doxorubicin and ifosfamide

MAPK – Mitogen activated protein kinase

MCS-F – Membrane Macrophage-Colony Stimulating Factor

MCSF-R – Macrophage-Colony Stimulating Factor Receptor

MDM2 – Murine Double-Minute Type 2

MHC – Major histocompatibility complex

miRNA – micro RNA

mRNA – messenger RNA

MSC – Mesenchymal Stem Cells

MV – Microvesicle

MVB – Multivesicular bodies

MWCO – Molecular weight cut-off

NBT – Nitro blue tetrazolium

NCBI – National centre for biotechnology information

NF-κB – Nuclear factor kappa-light-chain-enhancer of activated B cells

NK – Natural killer

NMD – Non-sense mediated decay

OS – Osteosarcoma

PAM – Protospacer Adjacent Motif

PAMPS – Pathogen Associated Molecular Patterns

PBI – posterior blood island

PBS – Phosphate Buffered Saline

PBS-T - Phosphate Buffered Saline + Tween 20

PCR – Polymerase chain reaction

PD-L1 – Programmed death-ligand 1

PFA – Paraformaldehyde

RANKL - Receptor Activator of Nuclear Kappa-B Ligand

RB1 – Retinoblastoma

RECQL4 – REC Q Helicase 4

RIPA - Radioimmunoprecipitation assay

RNA – Ribonucleic acid

RNase – ribonuclease

RPTPβ/ζ – Receptor Protein Tyrosine Phosphatase Beta/Zeta

RT-qPCR – Real-time quantitative polymerase chain reaction

SD – Standard Deviation

SDF-1 – Stromal derived factor -1

SEM – Standard error of mean

SSC – saline sodium citrate

TALEN – Transcription activator-like effector nuclease

TAM – Tumour Associated Macrophages

Tb. N – Trabecular number

Tb. S – Trabecular spacing

Tb. Th – Trabecular thickness

Tg – Transgenic line

TGF- β – Transforming growth factor-beta

TNFα - Tumour necrosis factor alpha

TP53 – Tumour Protein P53

TRAF6 – TNF receptor associated factor 6

TRPS – Tunable resistive pulse sensing technology

TV – Tumour volume

U-2OS – human bone osteosarcoma epithelial cells

UTR – Untranslated region

UV – Ultraviolet

VEGF – Vascular endothelial growth factor

WHO – World health organisation

WISH – Wholemount in-situ hybridization

WT – Wild type

ZFIN – Zinc finger nuclease

CHAPTER 1

GENERAL INTRODUCTION AND THESIS OUTLINE

The biological importance of the skeleton has in the last few decades been revealed as more than just a protective framework for organs. Bone has been shown to contain some remarkable properties (e.g. mechanical, endocrine) with a myriad of genetic factors, stem cells, cytokines, transcription factors, growth factors and hormones all amenable to study bone development. The skeleton is also the most important site of metastatic disease and bone metastasis has a devastating impact on the quality of life. Knowledge on the pathogenesis of bone tumours has seen considerable progress over the last two decades with the identification of key regulators of bone remodelling (such as the RANK/RANKL system), and a better understanding of dialogs between tumour cells and their microenvironment. By extension, research on bone sarcomas has highly benefitted from this progress with the interactions between tumour cells and the bone microenvironment at the heart of research on bone sarcomas.

1.1 Classification of Bone Sarcomas

Bone tumours can be classified into two major categories; benign and malignant tumours. Amongst the malignant tumours, are bone sarcomas and bone metastases. Malignant bone tumours can originate from either sarcomas or carcinomas. These differ in the origination of their tissues. Sarcomas develop from mesodermal tissues such as bone or muscle, while carcinomas originate from epithelial tissues (endodermal or ectodermal origin) such as the lining of the breast, colon or prostate. Malignant primary bone tumours, named bone sarcomas, originate from mesenchymal tissues (bone marrow, cartilage, bone) whilst bone metastases (or secondary tumours) mainly originate from carcinomas even if sarcoma cells can induce bone metastatic foci. Carcinoma cells can metastasize to bone through the lymphatic or blood circulation (Ferrari *et al.,* 2016).

The two main types of sarcomas are soft tissue sarcomas and bone sarcomas. Soft tissue sarcomas develop from cells that support, surround, and protect extremities and organs of the body including fat, muscle, connective tissue, nerves and blood vessels. Primary bone tumours are composed of heterogeneous histological entities (Brown *et al.,* 2018). The three main types of bone sarcomas are: osteosarcoma (OS), Ewing sarcoma and chondrosarcoma. OS and Ewing sarcomas are associated with the development of metastases to the bone, or more frequently to the lungs, whereas chondrosarcomas are characterized by a high risk of local recurrence and metastases depending on their grading (Brown *et al.*, 2017). Primary bone tumours are exceptionally rare and account for only 0.2% of all malignant tumours. In 2010, 443 patients were diagnosed with bone sarcomas in England (Francis *et al.*, 2013). OS and Ewing sarcomas pre-dominate in children and teenagers, (mostly OS and Ewing sarcoma, whilst chondrosarcoma is more common at the 4th decade). Soft tissue sarcomas increase in the middle age group.

1.2 Osteosarcoma Epidiemology

OS has an annual worldwide incidence of 3-5 per million in males, and 2-4 per million in females (Grimer *et al.,* 2013). It exhibits a bimodal age distribution primarily affecting children and young adults at a peak incidence of around 18 years. The second peak incidence is observed in older adults following radiotherapy or in association with Paget disease. Despite their rarity, osteosarcomas are the most common form of primary malignant bone tumours, representing around 56% of bone cancers in children. Incidence is higher in males than in females (male to female ratio of 1.5:1). This difference may be related to the skeletal growth period, which is longer in males than females. However it peaks earlier in females (12 years for females versus 16 years for males), due to the relatively earlier growth spurt experienced by girls (Longhi *et al.*, 2006).

1.3 Characteristics of Osteosarcoma

OS generally develops within the metaphysis of long bones, in particular the distal femur, proximal tibia and proximal humerus, as these regions undergo rapid growth phases (Figure 1). Sixty percent of cases originate in the knee, however they can also occur in the axial skeleton (<10% of cases in pediatric age group), most commonly in the pelvis. Conventional OS is characterized as a high-grade malignant tumour of spindle-shaped mesenchymal cells that produce an osteoid matrix (Heymann & Rédini, 2011) (Figure 2). OS cells express osteoblastic markers such as osteocalcin (OC), Alkaline phosphatase (AL-P) and bone sialoprotein (BS) (Brown *et al.,* 2017). OS tumours are generally locally aggressive, and tend to produce early systematic metastasis. Around 25% of patients present with detectable metastatic disease usually after 36 months from diagnosis. The most frequent site for metastases is the lung, with some also developing into other bones and soft tissues sites (Luetke *et al.*, 2014).

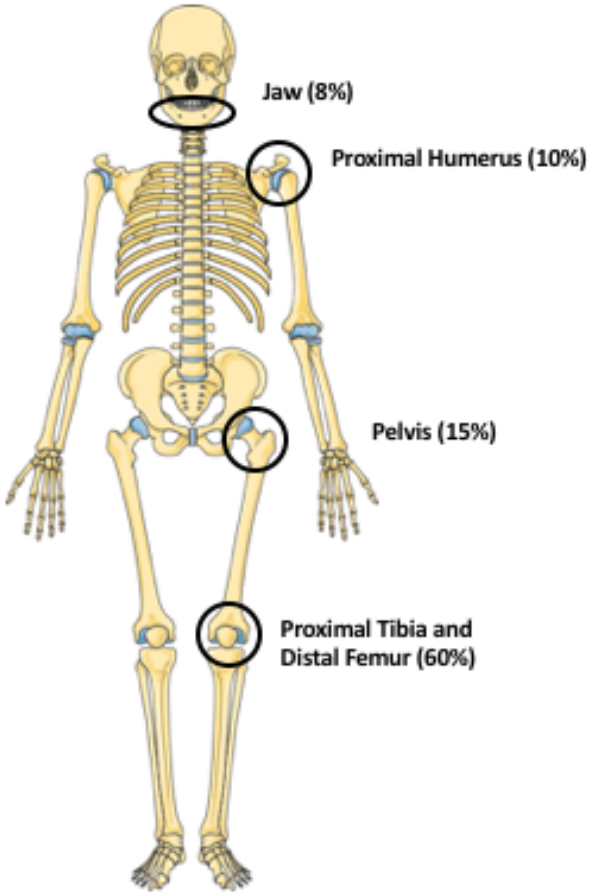

Figure 1: Schematic diagram of a human skeleton showing common sites for distribution of osteosarcoma. The primary sites for development of osteosarcoma include the jaw, proximal humerus (shoulder) pelvis, distal femur and proximal tibia.

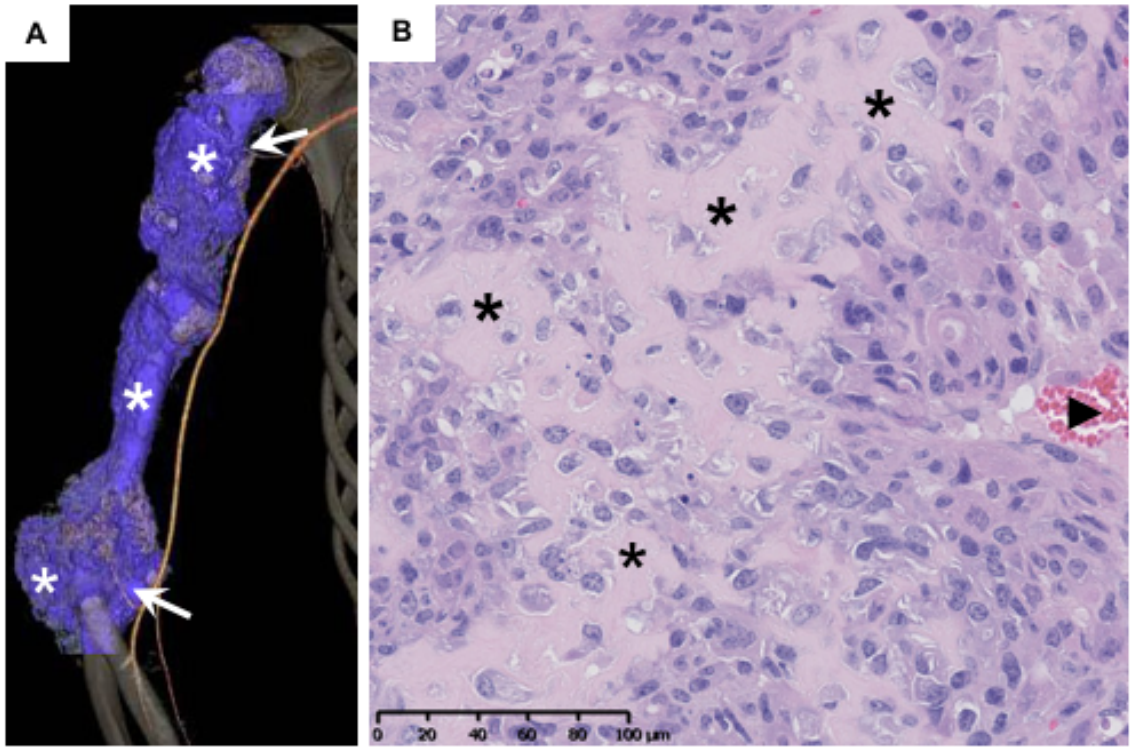

Figure 2: Representative X-ray and histological view of osteoblastic osteosarcoma. A) A computed tomography of an OS in a 15-year old patient. The tumour tissue is composed of mineralized component (indicated by *) and is associated with the vasculature (indicated by arrows). B) Typical histological view of OS showing osteoid extracellular matrix produced by OS cells (*), tumour tissue is vascularized (black arrow head). Adapted from "Bone Cancer" 1st Edition, Ed. Heymann D., Academic Press, 2009).

The type of OS is subdivided on tumour cell morphology and organisation, including the components of the extracellular matrix. There are three major subtypes: osteoblastic, chondroblastic and fibroblastic (Luetke *et al*., 2014). The main difference between these subtypes is attributed to the origin of the disease according to the oncogenic events occurring during cell differentiation. Apart from these subtypes, other subtypes include; telangiectatic, small cell, parosteal, periosteal, and low-grade central OS. Telangiectatic OS constitutes blood filled cystic spaces separated by thin septa, while small cell OS is characterized by sheets of round cells that produce an osteoid matrix which is often confused with Ewing sarcoma (Marina *et al*., 2004).

The 5-year survival rate for patients with localized forms of sarcomas are 70-75%. Survival rates become significantly lower around 30% for pulmonary disease. (Stiller *et al.,* 2001). Tumour resection together with chemotherapy allows for successful management of localized OS, however metastatic disease still poses as one of the main challenges for clinicians and researchers, thus highlighting the need to develop new therapeutic strategies.

1.4 Origin of Osteosarcoma Cells

Mesenchymal stem cells (MSCs) are stromal cells progenitors of osteoblasts (bone cells), chondrocytes (cartilage cells), adipocytes (fat cells), smooth muscle cells and striated muscle cells. To date, the majority of studies report that OS originates from MSCs located in the bone marrow, trabecular bone or periosteum. This has been demonstrated in transgenic mouse models and in comparisons of gene expression between malignant cells and MSCs (Lin *et al*., 2009; Chan *et al*., 2013). However these authors also report that MSCs show lack of specificity and may give rise to other types of sarcomas such as poorly differentiated soft-tissue sarcomas. Additionally, they also report that on deletions of *p53* and *RB1*, the incidence of OS drops to 29% whilst poorly differentiated soft-tissue sarcomas dominate.

Evidence is emerging that OS may arise from mutations occurring in MSCs committed to the osteoblastic lineage (Mutsaers & Walkley, 2014) Osteoblasts are specialized cells that regulate the formation of bone by depositing new bone tissue through the production of matrix proteins. Osteoblasts develop from MSCs through a series of intermediate pre-cursor cell populations called pre-osteoblasts. These acquire osteoblast-specific properties as they differentiate, and express several transcription factors known to regulate the differentiation such as Runx2 and Osterix-1 (Rodda & McMahon, 2006). Malignant transformation of these precursor cells by at least two or more oncogenic events, leads to the initiation of OS (Figure 3). Evidence comes from mouse studies whereby deleting *p53* at different points along the osteoblast lineage, increased the occurrence of OS (Walkley *et al.*, 2008). Further *in vivo* work by deleting promoter genes highly expressed in the osteoblastic lineage, such as *Osterix*, *Col1α1* and *Osteocalcin*, resulted in mouse models with a relatively high incidence of OS (Nakashima *et al.*, 2002).

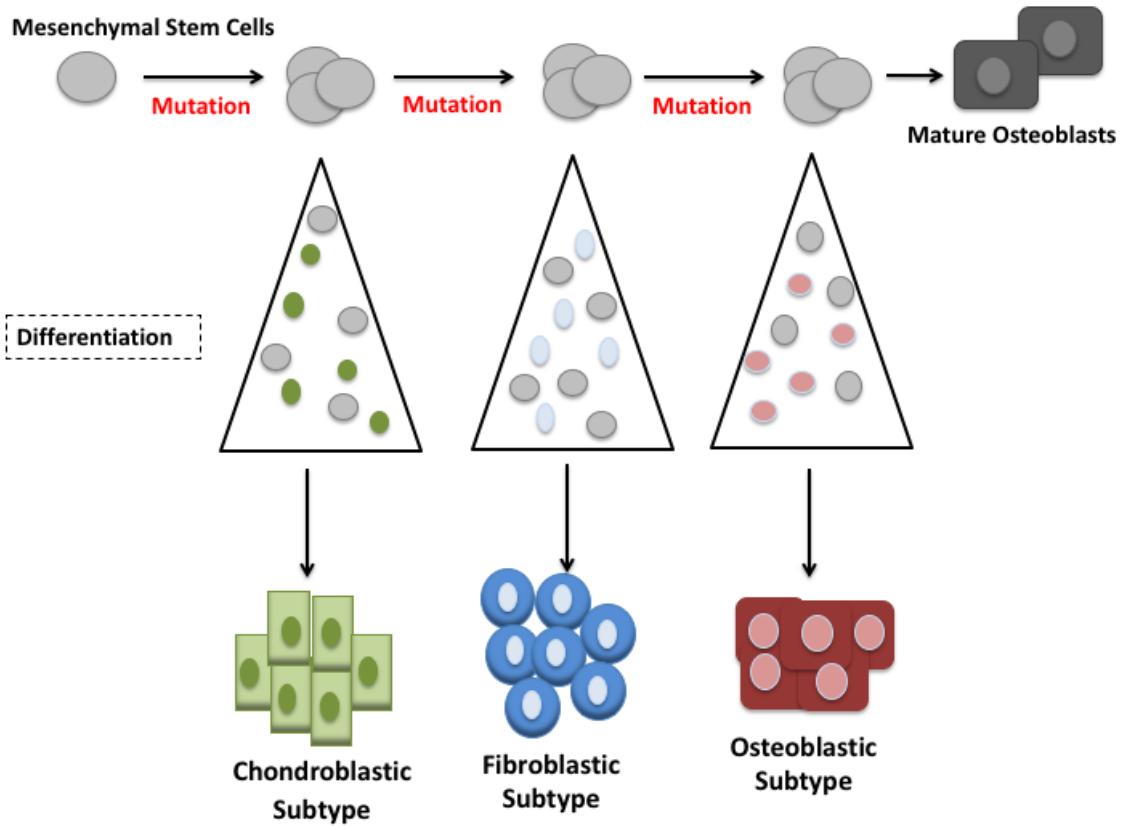

Figure 3: Schematic representation of the cell of origin in osteosarcoma. Specific sub-types of OS arise from cells undergoing differentiation in the lineage hierarchy from mesenchymal stem cells to osteoblasts. Oncogenic events in pre-osteoblast cell populations, give rise to subtypes of OS, thus the stage of differentiation within the osteoblastic linage at which the transformation occurs determines the subtype. Adapted from Mutsauers and Walkley 2014, and Brown *et al.,* 2017.

Altogether, this data supports the hypothesis that the cellular origin of OS comes from cells committed to the osteoblastic lineage and not from MSCs. Furthermore, the data also suggests that the stage of cellular differentiation where the mutations occur might determine the resulting OS sub-type (Mutsaers & Walkley, 2014). Further studies are required to confirm this hypothesis using more purified populations of pre-osteoblasts than those used in the studies carried out to date.

1.5 Genetics of Osteosarcoma

Despite this increasing evidence, the origin of OS remains enigmatic in part due to its rarity. OS is a genetically unstable tumour characterized by multiple chromosomal translocations, amplifications and deletions. Recently, human sarcomas have been found to contain fusion genes associated with cellular motility, thus highlighting the high genetic instability that is characteristic of OS. Transcriptome sequencing identified two recurrent fusion genes, *LRP1-SNRNP25* and *KCNMB4-CCND3*, known to be associated with cancer progression and where seen to promote OS cell migration and invasion (Yang *et al*., 2014).

Genome wide association studies have also led to progress in understanding the genetic origins of OS. A number of alterations and inactivating mutations have been found to play a role in initiating OS tumour development. These include mutations in the tumour suppressor genes *Tp53* and retinoblastoma (*RB1*), as well as mutations in *c-MYC* and *RECQL4* oncogenes, and down-regulation of the Wnt signaling pathway (Broadhead *et al*., 2011). These mutations lead to specific and rare syndromes associated with a predisposition to developing OS: inherited syndromes including hereditary bilateral retinoblastoma (mutation of *RB1* gene), Li–Fraumeni syndrome (germline mutations of the *p53* tumor suppressor gene), Bloom syndrome (mutation of *BLM* gene coding for a DNA helicase), and Rothmund–Thomson syndrome (mutation of the *RECQL4* gene encoding a DNA helicase). These syndromes then identify several master genes regulating the pathogenesis of OS. OS may also develop in association with multiple exostoses and Paget's disease.

Despite the recent advances in understanding the genetic origins associated with OS, the majority occur without any familial predisposition, and the number of cases associated with germline mutations is approximately 3% (Martin *et al.,* 2012) It should be noted that these data were drawn from analysis of small cohorts of tumour samples, and that none of the mutations are recurrent or specific therefore their use in diagnostics is limited.

OS tumours have also been linked to BRCAness signature in a study by Kovac *et al*. In this exome sequencing study, 123 OS were analysed for driver gene mutations, and 14 genes were identified as the main drivers. However none of the drivers were found to be responsible for the majority of tumours. The authors however report that over 80% of OS show large-scale instability signatures characteristic of BRCA1/2 deficient tumours. The findings therefore imply that during the evolution of OS, several oncogenic pathways drive chromosomal instabilities leading to the acquisition of BRCA-like traits (Kovac *et al*., 2015).

A number of studies have reported difficulties in differentiating low-grade OS from benign lesions, as both present with similar radiographic appearances. Low-grade OS constitutes between 5–7% of all osteosarcomas, and is subdivided into two subgroups subject to its location to the bone cortex, parosteal OS and low-grade central OS. Inability to correctly diagnose these lesions may lead to inappropriate treatment (Mackall *et al.,* 2002). Low-grade OS is characterised by supernumerary ring chromosomes encompassing the amplification of chromosome 12q13–15, in conjunction with cyclin dependent kinase 4 (CDK4) and murine double-minute type 2 (MDM2) gene region. The incidence of these amplifications is more prevalent in low grade OS rather than high-grade classical OS and thus MDM2 and CDK4 immunohistochemistry is the current technique used to differentiate between low grade OS and benign fibrous and fibro-osseous lesions, especially in patients with atypical radio-clinical presentation and/or limited biopsy samples (Dujardin *et al*., 2011).

Although several studies have been performed to determine the events leading to the development of OS, its pathogenesis still remains unclear. However, rather than looking at the genetic origin of OS, its pathogenesis can be viewed in terms of its cellular origin, and how oncogenic events in its precursor cells lead to malignant transformation and initiation of the tumour. To date, the most accepted theory is that initially, a mutational event (most

probably in *p53* or *RB*) results in clonal population with chromosomal instability, that leads to further chromosomal alterations and additional mutational events, ultimately resulting in a polyclonal populations of cells. Within tumour sites, the local environment then helps it to survive and proliferate thus contributing further to the survival and propagation of the tumour.

1.6 Conventional Therapy

Complete surgical resection termed as resection en-bloc-large (resection until healthy margins) remains the cornerstone for treatment of OS, however, surgery alone is not enough to cure patients, and most die as a result of metastasis. As a result, adjuvant chemotherapy was established by Rosen *et al* in the late 70's, and this approach is still applicable nowadays (Longhi *et al.*, 2006).

Following staging investigations and a diagnostic biopsy, initial treatment usually consists of intensive polychemotherapy with combinations of doxorubicin (adriamycin), cisplatin (CDP), ifosfamide (IFO) and high-dose methotrexate (HDMTX). Together these drugs are known as neoadjuvant chemotherapy (Rosen *et al.,* 1975) and are administered prior to surgical resection. Following surgery, post- operative chemotherapy is given, and is known as adjuvant chemotherapy. The goal of the adjuvant chemotherapy is the eradication of micro-metastases that have already spread at the time of diagnosis.

On the other hand, the goal of neoadjuvant chemotherapy besides the eradication of micro-metastases, is the destruction of primary tumour cells with reduction of tumour burden and the possibility to evaluate the histological response to preoperative chemotherapy. The level of bone tumour necrosis after preoperative chemotherapy is a prognostic factor that correlated with disease free and overall survival of OS (*ESMO*, 2014). The resected tumour is thus scored on the percentage number of residual viable tumour cells according to the Huvos scale (grade I > 50%, grade II from 11-50%, grade III from 1-0%, grade IV: no detectable viable cancer cells) (Huvos, 1991). In practice, patients are divided into good responders if <10% of viable tumour cells are found, and poor responders if >10% of viable tumour cells are present. A recent international EURAMOS-1 study was carried out to determine the effect on survival of changing post-operative chemotherapy based on this

histological response. Poor responders were randomized between continuing MAP (methotrexate, doxorubicin and cisplatin), and MAPIE (addition of ifosfamide and etoposide). Results showed that there was no significant difference in the outcome between the regimens of drugs administered and therefore post-operative chemotherapy is not adapted according to response (Whelan *et al.*, 2015). Radiotherapy is also administered when surgery is not possible (such as neck, head, spine), or when resection margins are considered as inadequate, however osteosarcomas are usually considered as radioresistant (Brown *et al.,* 2017).

1.7 The Local Microenvironment in Osteosarcoma

Several other theories have been proposed to explain the development of cancer cells in bone. One such is based on the 'seed and soil' theory initially proposed by Stephen Paget in the late 19th century and focuses on the local environment of OS (Paget, 1989). When tumour cells invade bone, a cycle is established between the tumour cells and their microenvironment, where the functional equilibrium between osteoblasts (bone forming cells) and osteoclasts (bone resorption cells) is deregulated. OS cells dysregulate the microenvironment by activating osteoclast differentiation and resorption, which in turn stimulate tumour growth by releasing proliferative factors stored in the extracellular matrix. An inflammatory environment that promotes the growth of tumour cells is therefore established (Heymann *et al*., 2011). This leads to the development of the 'bone niche', in which the bone microenvironment promotes the progression of cancer initiating cells and provides the right conditions for their survival and development. Cancer initiating cells are defined as cells with self-renewal ability, tumour-initiating capacity, and ability to give rise to more differentiated progeny (Zhang *et al*., 2003). This not only occurs in primary sarcomas, but also during the development of secondary bone metastases (Figure 4).

The niche is a highly complex environment and is not only restricted to bone related cells. Other types of cells including endothelial cells, and macrophages are also present. These set up niches of their own, a 'vascular niche' and an 'immune niche', which contribute to the tumour microenvironment by modifying the vascularization and altering the local immunity respectively (Andersen *et al*., 2009; Heymann *et al*., 2017). Other more specific niches are also present, such as muscles and lung parenchyma for invading and metastatic

cells. This bilateral dialogue established between cancer cells and their neighbours is a central aspect of the development of bone sarcomas. There are several ways by which cells communicate such as by direct soluble factors (chemokines and cytokines), direct cell to cell communication for example through gap junctions, as well as by extracellular vesicles (Melzer *et al*., 2016). Extracellular vesicles are small membrane bound vesicles loaded with proteins, miRNA, and mRNA. Studies have demonstrated that OS cells can become chemoresistant through the transfer of resistance factors via exosomes (Torreggiani *et al*., 2016). Recently, Baglio *et al* described how EVs secreted by highly malignant OS cells selectively incorporate TGFβ, which induces proinflammatory IL-6 production by MSCs. IL-6 is associated with tumour growth, establishing a cycle between MSCs and OS cells (Baglio *et al*., 2017).

The niches play a role in keeping cancer cells dormant and triggering the development of tumours both locally or to distant organs. This has been demonstrated in studies of OS that developed from benign lesions after patients underwent bone curettage and grafting, following long periods (7-28 years) of being disease free (Picci *et al*., 2011). To explain the development of these secondary-induced primary bone tumours, the authors suggest that tumour growth was promoted by MSCs in the inserted scaffold. Perrot *et al*., also reported a delayed local reappearance of OS. This came after 13 years from initial diagnosis, and 18 months following a lipofilling procedure. Perrot *et al*. investigated the relationship between tumour growth, fat injections, and mesenchymal stem/stromal cell like cells present in fatty tissue. Results showed that fat grafts and progenitor cells promote tumour growth, indicating that dysregulation of tumour niches may reactivate tumour proliferation (Perrot *et al*., 2010; Avril *et al*., 2016).

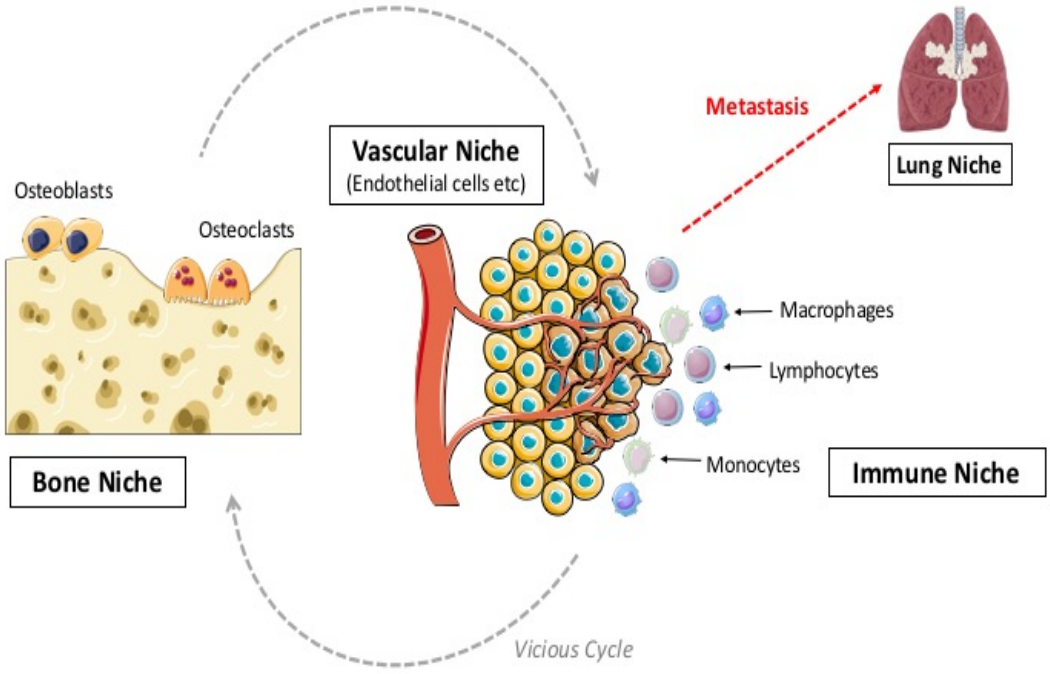

Figure 4: Diagram showing the tumour niches in osteosarcoma. The bone microenvironment is composed of a diversified cell population forming specific niches (vascular, immune, bone, muscular and pulmonary niches (metastatic niche). A dynamic relationship between sarcoma cells, and the bone microenvironment is established, where the cancer cells create favourable conditions for the growth and dissemination of the tumour including modifications in local immunity, vascularisation and bone cell function. Adapted from Brown *et al.,* 2017

The immune infiltrate of OS comprises one of the most important niches. This immune environment is composed of several types of immune cells including T-lymphocytes, macrophages, as well as sub-populations of B-lymphocytes and mast cells. OS cells are able to control the differentiation and recruitment of immune infiltrating cells to establish a local immunosuppressive environment that is able to promote tumour growth and metastasis, and increase drug resistance (Heymann *et al*., 2017). Macrophages are one of the most important immune infiltrates in the microenvironment, followed by T-lymphocytes. These cellular sub-types and their role in OS will be described in the following sections.

1.8 Tumour Associated Macrophages

Macrophages were originally thought to generate anti-tumour activities by recruiting helper T-cells. However, clinical and experimental data have shown that certain macrophage phenotypes are correlated with enhanced tumour progression, induction of angiogenesis and promotion of immunosuppression (Sica *et al*., 2008; Coffelt *et al*., 2010).

Macrophages demonstrate functional plasticity as a result of signals generated from stromal cells and tumour cells. They can differentiate into M1 or M2 type macrophages. M1 macrophages induce inflammatory responses and anti-tumour immunity, whilst M2 type induces anti-inflammatory responses and pro-tumorigenic properties through the induction of neo-angiogenesis (Knowles & Harris, 2007). Macrophages that infiltrate tumours are known as tumour associated macrophages (TAMs). They resemble closely M2 type macrophages and are recruited to tumours as a result of overexpression of growth factors such as macrophage colony stimulating factor (M-CSF), CC Chemokine ligand 2 (CCL-2) and vascular endothelial growth factor (VEGF) (Chockalingam & Ghosh, 2014). The M2 subtype has been seen to promote the tumour growth and minimize the efficacy of therapy using a combination of mechanisms. Primarily, they reinforce the presence of cancer cells by inhibiting anti-tumour responses and stimulate cell proliferation. Secondly, TAMs regulate angiogenesis by enhancing the angiogenic switch (the phenotypic switch to angiogenesis), and promoting the proliferation of endothelial cells. TAMs contribute to tumour progression by assisting in cancer cell invasion, seeding, extravasation, survival and proliferation of cancer cells at metastatic sites (Sica *et al*., 2008). Additionally, TAMs accumulate in conditions of hypoxia within the tumour and up-regulate the expression of hypoxia-inducible factors, which in turn triggers transcription of various growth factors including VEGF (Lewis & Murdoch, 2005). Classical cell surface markers for M1 type macrophages include IBA1, iNOS and MHCII, whereas ARG1, CD163, IL-10 and CD23 are some of the markers used for identification of M2 subtypes.

In many cancers, the presence of TAMs leads to poor prognosis (Knowles & Harris, 2007). However, Buddingh *et al*., recorded that the expression of TAM-associated genes in pre-treatment biopsies of OS, correlated with a lower risk of metastases. The authors observed an expression of macrophage-associated genes in hematopoietic cells and not in OS tumour cells. They also found that TAMs in post-chemotherapy resections and metastatic lesions,

led to improved survival. The authors reported a heterogenous population of M1 and M2 phenotypes in OS tumours, and that there was an association between macrophage infiltration and higher micro-vessel density. This suggests that the influx of macrophages may support certain aspects of tumour growth. However overall, in OS, direct or indirect anti-tumour activity of macrophages outweighs their possible tumour supporting effects (Buddingh *et al.*, 2011).

Dumars *et al.,* demonstrated (Dumars *et al*., 2016) the association of TAM to a better overall survival of OS patients. These authors observed a dysregulation of the macrophage balance in favour of M1 cells in non-metastatic patients. The above findings are backed by a clinical trial of 662 OS patients using muramyl tripeptide (MTP), a macrophage-activating agent. (Mori *et al*., 2008). Addition of this peptide to chemotherapy regimens of doxorubicin, cisplatin, and methotrexate resulted in a statistically significant improvement in 6-year overall survival, from 70% to 78% ($p = 0.3$, hazard ratio = 0.71, 95% CI, 0.52 to 0.96) (Meyers *et al*., 2008). It is therefore possible that the M1 and M2 macrophage ratio may regulate metastasis in OS, and that once a threshold of either phenotype is reached, the tumour microenvironment may be changed to one that favours metastasis. However, results from this study are considered controversial due to beneficial effect of LMTP-PE in a non-adapted control group. Thus MTP for OS has not been universally adopted and further investigation into this mechanism is needed.

In 2006, a phase 3 trial (OS2006) of zoledronic acid, did not improve outcome for patients with OS. To investigate this, infiltrating tumour cells were investigated in the pre-therapeutic biopsies. The authors report that CD163 positive macrophages although usually associated with an M2 macrophages sub-type, were associated with Th1 responses – (proinflammatory and tumoricidal activity), whilst CD8-positive tumour infiltrating lymphocytes played a major role in delaying OS metastases. Thus reporting a correlation between the presence of CD8 positive lymphocytes at the time of diagnosis, and a better overall survival for patients treated with zoledronic acid. Thus in the microenvironment the balance between M1/M2 can be variable and associated with increased survival (Gomez-Brouchet *et al*., 2017).

Based on these observations, a number of therapies targeting macrophages have been developed. Most notable is the liposome-encapsulated muramyl tripeptide (L-MTP-PE) which acts as an immunoregulator by triggering macrophages and T-cell reactions (to be discussed in more detail in Chapter 3).

1.9 Tumour Infiltrating Lymphocytes

Lymphocytes are the second most abundant cell types in OS infiltrates. Tumour infiltrating lymphocytes (TILs) are detectable at around 75% in OS patients, which increases to 86% in metastatic conditions (Muthana *et al*., 2013). The key role played by TILs in the tumour microenvironment was demonstrated by Fritzsching *et al*. (2015). The authors demonstrated that a $CD8^+/FOXP3^+$ ratio in biopsies prior to chemotherapy, is correlated with prolonged survival. From 150 included cases, patients with complete treatment were identified and assigned to the discovery (diagnosis before 2004) or the validation cohort (diagnosis 2004–2012). Highly standardized immunohistochemistry of $CD8^+$ and $FOXP3^+$, which was validated by methylation-specific gene analysis, was performed followed by whole-slide analysis and clinical outcome correlations. Osteosarcoma patients with higher (above the median- 3.08) intratumoral $CD8^+/FOXP3^+$ ratios at time of diagnosis where shown to have a much better outcome than patients with lower (below median) $CD8^+/FOXP3^+$-ratios. No patients with a $CD8^+/FOXP3^+$-ratio above the third quartile died within the observation period (median follow-up 69 mo). Patients with a ratio higher than 3.08 showed improved survival strengthening the key role of TILs in OS (Fritzsching *et al*., 2015). T-lymphocytes express PD-1 and/or B7-1 which bind to PDL-1 expressed on the surface of OS cells. The binding of PDL-1 to PD-1 is associated with inhibition of their cytotoxic properties and associated downstream signalling. This negatively regulates the activating signal initiated by T-cell receptor after the presentation of tumour peptides associated with the MHC system. This leads to enhanced local immunosuppression and then tumour progression (Maekawa *et al*., 2016). The expression of PD-1 by TILs led to the development of therapeutic benefits in the PD-1 and PD-L1 interaction in OS. Three clinical trials using anti PD-1 antibody are currently undergoing for patients with metastatic OS (to be discussed in more detail in chapter 3).

1.10 Macrophage Colony-Stimulating Factor

The macrophage colony-stimulating factor (M-CSF or CSF-1) is a cytokine required for proliferation, differentiation and survival of cells from the hematopoietic lineage including monocytes, macrophages, and osteoclasts (Yoshida *et al.*, 1990). The effects of M-CSF are regulated through a type III tyrosine kinase receptor called MCSF-R (also known as c-fms, CD115 and CSF-1R) which is encoded by the proto-oncogene *c-fms*. The importance of M-CSF in bone has been demonstrated *in vivo* using mutant osteopetrotic *(op/op)* mice (Wiktor-Jedrzejczak *et al.*, 1991). The mice exhibited a number of skeletal abnormalities (e.g. stunted growth, domed skull, stubby appearance of the tarsals, metatarsals, femur and humerus), a toothless phenotype, and deficiencies in macrophages and osteoclasts. This phenotype resulted from a null mutation in the *CSF-1* gene by insertion of a single base pair, and led to a deficiency in the production of osteoclasts (Yoshida *et al.*, 1990). A similar but more severe phenotype was also obtained when the CSFR-1 gene was inactivated leading to $Csf1^{-}/Csf1^{-}$ (Dai *et al.*, 2002). Preliminary experiments indicated that the above effects might be restored by injecting the recombinant form of human M-CSF to the *op/op* mice. This resulted in correction of the observed osteopetrotic phenotype, as well as restoration of the number of macrophages and osteoclasts (Wiktor-Jedrzejczak *et al.,* 1991). However it did not overcome all the defects observed, indicating that other variants of M-CSF or other cytokines, might be acting in combination to regulate the activity of osteoclasts.

1.11 M-CSF in Cancer

Lymphocytes, osteoblasts, stromal cells and tumour cells secrete M-CSF in order to sustain the continuous proliferation of the tumour by a direct or indirect effect depending on the expression of M-CSFR in cancer cells. M-CSF can act as an autocrine, paracrine and endocrine factor. Increased expression of M-CSF has been found in a number of cancers including breast, pancreatic and colorectal cancer. High expression levels of M-CSF in ovarian cancer correlate with increased tumour aggressiveness and poorer prognosis (Chockalingam & Ghosh, 2014).

M-CSF has also been suspected in the process of tumour metastasis in breast cancer. A recessive null mutation of *CSF-1* gene resulted in delayed lung metastasis and tumour progression in a murine breast cancer model. This reduction was explained by the authors as arising due to lack of TAMs (M1 type). Restoring local concentrations of M-CSF, resulted in the promotion of tumour development. These pro-tumoral actions are exerted through macrophages, suggesting that lack of macrophages in tumours of *Csf1op*/*Csf1op* mice is primarily due to the systematic loss of CSF-1, and that other chemo attractants are present in mice to recruit macrophages into the tumour site (Lin *et al*., 2001). Other studies have reported that M-CSF has the potential to bring about anti-tumour responses as well. Rat T9 glioma cells transfected with membrane bound isoforms of macrophage M-CSF (mM-CSF; a non-secreted isoform of M-CSF) were killed by macrophages in a dose dependent manner. Killing of mM-CSF expressing tumour cells by macrophage *in vitro* occurred through phagocytosis (Jadus *et al*., 1996). Although these reports are contradictory, the tumour promoting actions of M-CSF are well documented, and overall it is regarded as a "pro-tumour" cytokine. Another cytokine with a high functional selectivity represented by stimulating monocyte survival in a CSF-1R-dependent manner, is interleukin-34 (IL-34). The discovery of IL-34 emerged much later than that of M-CSF rendering the actions of M-CSF as currently known partially redundant.

1.12 Interleukin-34

In 2008, Lin et al discovered a novel cytokine IL-34 by producing recombinant forms of proteins from cDNA's encoding both secreted proteins and extracellular domains of trans-membrane proteins. They transfected these cDNAs into HEK 293T cells and screened the biological activities of cell supernatants through a number of cell-based assays (e.g. monocyte proliferation, signalling assays). They identified a new soluble factor called IL-34 that transduced signaling pathways through the M-CSF receptor, and also showed that IL-34 induced the formation of colony forming unit macrophages in human bone marrow cultures with the same effectiveness as M-CSF (Lin *et al.,* 2008). In light of this study, it was hypothesized that IL-34 shared common features with M-CSF and thus a functional overlap between both cytokines was revealed.

1.13 Structure of IL-34, M-CSF and Their Receptor

IL-34 is a 27.5 KDa secreted dimeric glycoprotein consisting of 242 amino acids. The gene encoding IL-34 is located on human chromosome 16q22.1 and is organized into 11 exons. Human IL-34 shows sequence identity of 71%, 72% and 99.6% with mouse, rat and chimpanzee respectively, thus showing that it is highly conserved across species (Zhou *et al.*, 2016). IL-34 is evolutionary distant but structurally related to M-CSF in that they are both N-glycosylated proteins. (Nakamichi *et al.*, 2013).

Functional studies demonstrated that both M-CSF and IL-34 stimulate macrophage differentiation and up-regulate monocyte activity (Wei *et al.*, 2010) (Lin *et al.,* 2008). However several phenotypic differences were observed in the resulting macrophages. These differences predicted that IL-34 uses an alternative binding mode from M-CSF on binding to the MCSF-R receptor. Further structural analysis showed that IL-34 and M-CSF bind to the extracellular domain of MCSF-R in a similar way, but through two distinct contact points (Figure 5). Binding of IL-34 or M-CSF to MCSF-R leads to receptor dimerization and differential auto-phosphorylation on its eight tyrosine residues (Garceau *et al.*, 2010). M-CSF/MCSF-R and IL-34/MCSF-R crystals have a similar shape, but the IL-34/M-CSFR complex is more stable. Chihara *et al*. showed some differences in the kinetics of MCSF-R phosphorylations and in the nature and intensity of phosphorylated tyrosine residues after IL-34 binding, partly explaining the differences in the signalling pathways they elicit, and also revealing in part their functional overlap (Chihara *et al.*, 2010)

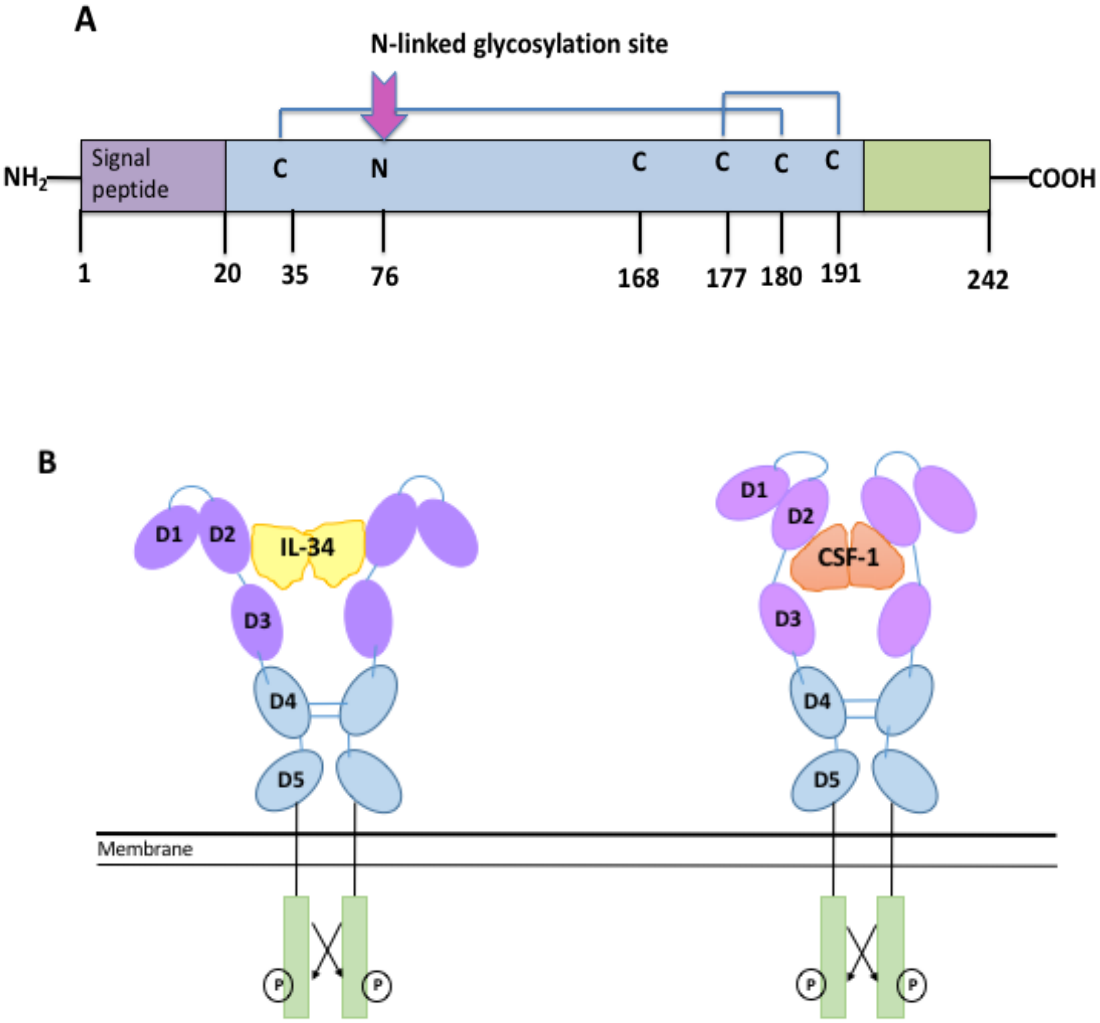

Figure 5: Schematic representation of IL-34 and MCSF-R cytokines A) The structure of IL-34 showing an N-linked glycosylation region. Disulphide bridges are indicated by solid blue lines. B) The CSF-1 receptor is composed of five immunoglobulin-like domains (D1-D5). The interdomain flexibility between D2 and D3 is the main feature allowing the receptor to bind to both IL-34 and M-CSF. IL-34 binds to the cleft between D2 and D3 leading to autophosphorylation of specific tyrosine kinases within the intracellular domain. Adapted from Nakamichi *et al.,* 2013

1.14 Expression of IL-34

In human and murine tissues, IL-34 is widely expressed in the brain, heart, liver, kidney, mammary glands and prostate, but most notably in the spleen; consistent with a role in myeloid cell regulation. An interesting observation comes from the study of Wei *et al.* (2010) which provides new insights on the expression patterns of M-CSF and IL-34. When studying the expression levels of these two cytokines during mouse development, they showed that their expression levels differ substantially in a spatiotemporal manner. Thus IL-34 although it has overlapping functions with M-CSF, it could be considered as a local molecular effector according to the spatial and temporal situation rather than at the systemic level. For example to coordinate the cellular communication network between osteoblasts, macrophages and osteoclasts at the microenvironment level (Wei *et al.*, 2010). The authors found that while M-CSF mRNA levels were increased in embryos and placenta, IL-34 mRNA levels were low and did not increase. Additionally, IL-34 mRNA was differentially more expressed then M-CSF mRNA in adult brains. However, this aspect needs to be elucidated further since it might have further implications on the bone niche and how IL-34 plays a role in maintaining the survival and proliferation of sarcoma cells.

1.15 Receptors of IL-34

IL-34 is highly expressed in post-natal and adult brains. MCSF-R is also highly present in early development, but dramatically decreases, almost undetected, in adult brains. This high expression of IL-34 in adult brains without expression of its receptor, suggested that other receptors for this cytokine exists (Nandi *et al.*, 2012). Indeed, the receptor protein tyrosine phosphatase (RPTPβ/ζ) has been identified on the glioblastoma cell line U251, as another receptor for IL-34 through its cell surface chondroitin sulphate (CS) chains. By using IL-34 affinity chromatography of solubilized mouse brain membrane followed by mass spectrometric analysis, Nandi *et al* reported that IL-34 selectively binds to cell surface RPTP-ζ and initiates downstream signalling leading to inhibition of cell proliferation and motility. They also showed that IL-34 binding to RPTP-ζ is dependent on the presence of CS chains (Nandi *et al.*, 2013).

Similarly, syndecan-1, also a proteoglycan with CS chains, was able to modulate IL-34-induced M-CSFR signalling pathways. Syndecan-1 also increases the migration M2 macrophages induced by IL-34. In addition, it was proved that IL-34 induced myeloid cell migration, is dependent on syndecan-1 (Segaliny *et al.*, 2015). Therefore in addition to MCSF-R, RPTPβ/ζ and syndecan-1 are key regulators of IL-34 activity, and may play a role in bone inflammatory diseases and bone sarcoma development (Figure 6).

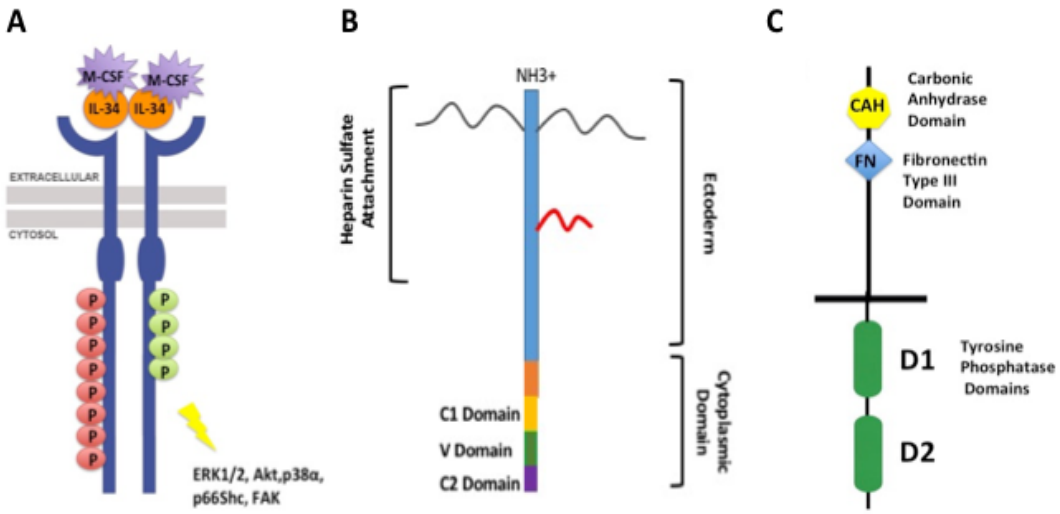

Figure 6: Schematic representation of the receptors of IL-34. Diagram showing the three proposed receptors for IL-34. (A) MCSF-R Receptor; IL-34 and M-CSF bind to the MCSF-R receptor by two distinct contact points. Binding induces the auto-phosphorylation of different tyrosine residues (red for M-CSF and green for IL-34) and subsequently different biological responses (B) Syndecan-1; a proteoglycan with CS chains, able to regulate IL-34-induced M-CSFR signalling pathways. Syndecan-1 also increases the migration of M2 macrophages induced by IL-34. (C) RPTPβ/ζ; Binding of IL-34 to PTP-ζ is dependent on the presence of CS chains. IL-34 selectively binds to cell surface PTP-ζ and initiates downstream signalling leading to inhibition of cell proliferation and motility. MCSF-R, RPTPβ/ζ and syndecan-1 are key regulators of IL-34 activity, and may play a role in bone inflammatory diseases and bone sarcoma development.

When IL-34 binds to the extracellular domain of MCSF-1R, autophosphorylation of specific tyrosine residues within the intracellular domain occurs. These phosphorylated residues recruit other kinases and adaptor proteins, to activate several signaling pathways including ERK1/2, PKB/AKT, focal adhesion kinase (FAK), STAT3, and NF-κB (Figure 7). Together these signaling pathways play major roles in proliferation, differentiation, survival, cell migration, adhesion as well as cytokine and chemokine expression. Activation of such signaling pathways can be observed in cells expressing the MCSF-1R such as myeloid cells, epithelial cells, fibroblasts, and cancer cells (Baghdadi *et al.,* 2018). A recent study has also reported that activation of CSF-1R by IL-34 activates signaling pathways related to autophagy and caspase by the increased expression of AMP-activated protein kinase (AMPK)-1 and UNC-51 like autophagy activating kinase 1 in monocytes (Boulakirba *et al.*, 2018).

As for activation of RPTP-ζ, this induces the tyrosine phosphorylation of FAK and paxillin, resulting in inhibition of proliferation, clonogenicity, and motility in specific cellular targets such as glioblastoma cells (Figure 7). On the other hand, IL-34 induced activation of signalling pathways is importantly modulated by the interaction between IL-34 and chondroitin sulphate chains of syndecan-1. Low to moderate expression of syndecan-1 may result in limited activation of IL-34 and MCSF-1R signals, whereas on increased expression of syndecan-1 activation of IL-34 through MCSF-1R could be enhanced (Segaliny *et al*., 2015)

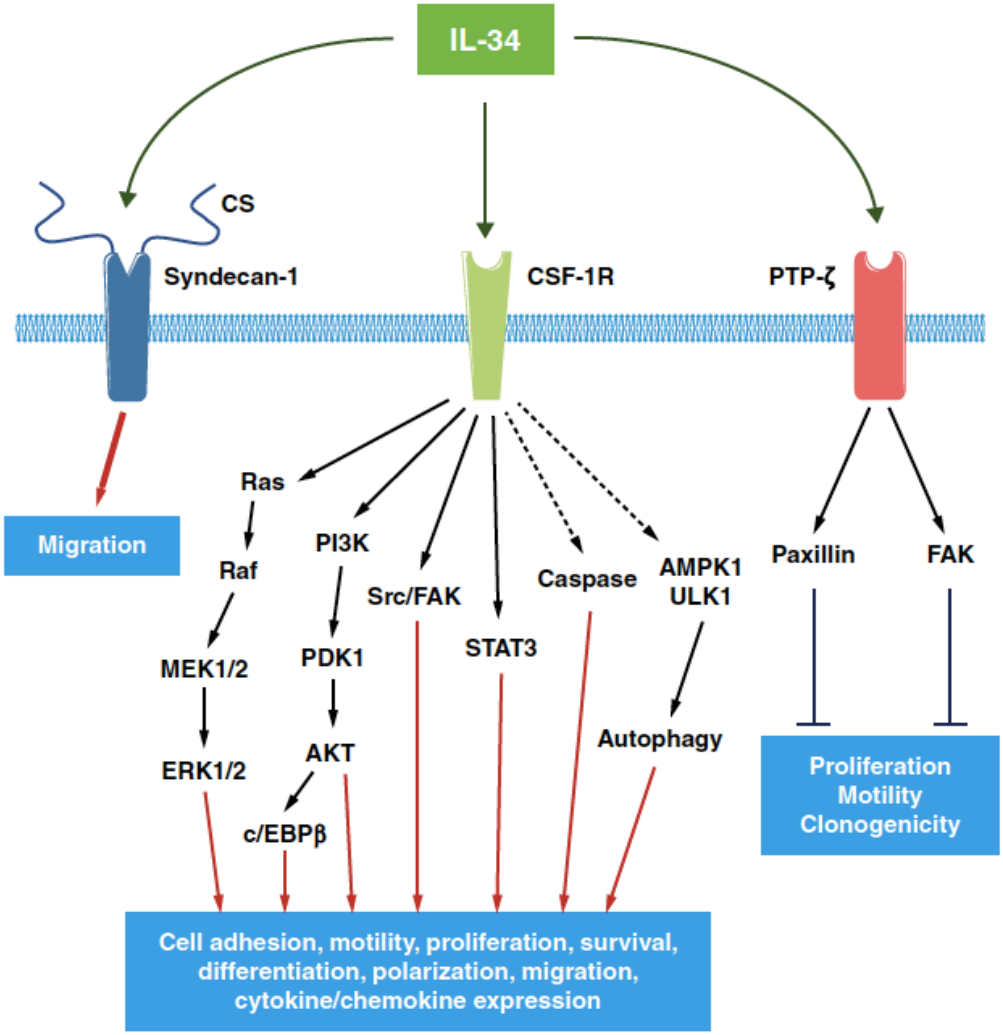

Figure 7: Diagram of the signalling networks of IL-34. IL-34 binds to the extracellular domains of its receptors (MCSF-1R, RPTP-ζ and chondroitin sulfate chains of syndecan-1) to elicit the activation of a number of signalling pathways. These are involved in the regulation of several major functions including proliferation, differentiation, survival, adhesion and migration (Baghdadi *et al.,* 2018).

1.16 Role of IL-34 in Bone Biology and Monocyte Differentiation

M-CSF and IL-34 play a central part in bone remodelling through osteoclastogenesis, the process by which osteoclasts break down bone. Osteoclastogenesis and the differentiation of osteoclasts are mainly dependent on M-CSF and RANKL. In association with RANKL, IL-34 can replace M-CSF to induce osteoclast formation by stimulating the proliferation and adhesion of osteoclast precursors. IL-34 can completely substitute for M-CSF during this process, thus defining a novel pathway for osteoclastogenesis. IL-34 was highly expressed in osteoclast-like cells found in giant cell tumours of bone. In contrast to osteoblasts, osteoclasts showed very strong staining for IL-34, suggesting a potential role in the pathogenesis of bone sarcomas by promoting osteoclast formation (Baud'Huin *et al.*, 2010). The role of M-CSF in osteoclastogenesis, as demonstrated in the osteopetrotic *op/op* mice, was previously described (Wiktor-Jedrzejczak *et al.*, 1991). Similarly IL-34 can contribute to osteoclastogenesis. The effects of IL-34 in *op/op* mice, was studied by Wei *et al.* in 2010 and they demonstrated that IL-34 expression was able to recover the main defects observed in op/op mice. Using *in vitro* murine and human models of osteotogenesis, Baud'Huin *et al.* 2010) showed that IL-34 was able to support RANKL-induced osteoclastogenesis in the absence of M-CSF. IL-34 stimulated RANKL-induced osteoclastogenesis by promoting the adhesion and proliferation of osteoclasts progenitors, solidifying further the hypothesis that M-CSF and IL-34 exhibit a functional overlap.

Similar to M-CSF, IL-34 was shown to promote the differentiation of monocytes into immunosuppressive M2 macrophages. It was shown that IL-34 gives rise to macrophages with an IL-10^{high} and IL-12^{low} phenotype, suggestive of a typical M2 phenotype. Moreover these macrophages are immunosuppressive similar to that induced by M-CSF (Foucher *et al.*, 2013). Moreover, IL-34 induces M2 macrophages via the M-CSF receptor and independently of M-CSF. Furthermore, GM-MCSF and IFNy prevented their generation, and that IFNγ skews established IL-34 driven macrophages into an immunostimulatory IL-12^{high} and IL-10^{low} phenotype.

In the placenta, IL-34 contributes to the local immune tolerance of the microenvironment due to M2 macrophage polarisation. IL-34 was found at the foetal-maternal interface in 49 women, in both the foetal placenta and maternal decidua and it was able to polarize monocytes in macrophages of the decidual phenotype (Lindau *et al.*, 2018).

Further studies demonstrate that both IL-34 and M-CSF have the ability to promote the survival and differentiation of monocytes into macrophage phenotypes with some differences. For example the study by Barve *et al.,* which compared downstream transcriptional profiles and pathways of IL-34 and M-CSF and found differences in the expression of the differentiation marker C-C chemokine receptor type 2 (CCR2) (Barve *et al.,* 2013). Furthermore, IL-34 but not M-CSF was demonstrated to be involved in the follicular dendritic cell-induced monocytic cells *in vitro* (Yamane *et al.,* 2014). All this data collectively demonstrates that a vital role for IL-34 and MSCF-R in cell regulation and differentiation.

1.17 Regulation of IL-34 Expression

Since the functions of IL-34 and M-CSF are similar, this would indicate that similarly to M-CSF, the production of IL-34 from osteoblasts could potentially be induced by inflammatory cytokines. Eda *et al*. (2011) showed that pro-inflammatory cytokines such as IL-1β and TNF-α stimulate IL-34 mRNA expression in osteoblasts. Among four inflammatory cytokines (IL-1β, IL-6, IL-17, and tumour necrosis factor-a (TNF-α), IL-34 mRNA expression level was dramatically induced by IL-1β (17- fold) and TNF-α (74-fold). On investigating the involvement of the intracellular mitogen-activated protein kinases (MAPKs) in IL-1β and TNF-α mediated induction of IL-34 mRNA expression, the authors found that IL-1β and TNF-α activated p44/42 MAPK, c-Jun N-terminal kinase (JNK) as well as nuclear factor- B (NF-kB) but not p38 (Eda *et al*., 2011).

IL-1β and TNF-α mediated induction of IL-34 mRNA expression was decreased by JNK inhibitor. Interestingly, although treatment of MEK-1/2 inhibitor showed no reduction in the increase of IL-34 mRNA expression by cytokines, combination of MEK-1/2 inhibitor and JNK inhibitor significantly inhibited IL-1β and TNF-α mediated IL-34 mRNA expression level compared to those by each inhibitor alone. In comparison, IL-1β and TNF-

α mediated induction of M-CSF mRNA was not affected by p38, JNK, and MEK-1/2 inhibitors. However, NF-κB inhibitor completely inhibited the elevation of M-CSF mRNA expression by these cytokines. These results therefore show that pro-inflammatory cytokines, IL-1β and TNF-α, induced the expression of IL-34 mRNA via JNK and p44/42 MAPK but not p38 in human osteoblasts while p38, JNK, and p44/42 MAPK were not involved in the induction of M-CSF mRNA expression by these cytokines (Eda *et al*., 2011). How this differential regulation between M-CSF and IL-34 underlies the differences in IL-1β and TNF-α induced signalling pathways in osteoblasts still remains to be clarified. Other studies also showed the activation of IL-34 by inflammatory cytokines such as that reported by Yu et al. In this study, MC3T3-E1 mouse osteoblastic cells, produced IL-34 in response to TNF-α through the NF-κB signalling pathway in a dose and time dependent manner (Yu *et al*., 2014). Some recent data suggests that other than inflammatory cytokines, an active metabolite of vitamin D known as 2MD, enhances expression of IL-34 in mouse spleen and bone via vitamin D receptor mediated signalling. Splenectomy and knockdown of IL-34 inhibited the 2MD-induced osteoclastogenesis (Covaleda *et al.,* 2010). Further studies, also revealed an association between IL-34 and microRNAs. Overexpression of miR-28-5p leads to suppression of IL-34 in hepatocellular carcinoma (Zhou *et al.*, 2016).

1.18 Inflammation and IL-34

Most of the cytokines previously described (TNF-α, IL-1β, IL-6 and IL-17) are reported to stimulate the generation of osteoclasts through the induction of M-CSF production by osteoblasts. Therefore, this indicates that IL-34 may also be induced in the site of bone destruction in degenerative bone diseases such as rheumatoid arthritis and periodontal inflammation.

Rheumatoid arthritis is an autoimmune disorder characterized by inflammation of the synovial joints, and cytokines play a role in driving the synovial cell activation that leads to joint destruction. The role of IL-34 in rheumatoid arthritis has been confirmed by several studies. IL-34 is produced by synovial fibroblasts in response to stimulation by the inflammatory cytokines TNF-α and IL-1β as already described and is released into the synovial fluids of patients. IL-34 was in fact found in significantly higher levels in the synovial fluids of rheumatoid arthritis patients in comparison to osteoarthritis patients, and correlated with leucocyte number and inflammation intensity (Chemel *et al.*, 2012). IL-34 levels also correlated with disease activity index (DAS28), inflammation parameters, auto-antibody production as well as concentration of other inflammatory mediators (IL-6, IL-17 and MMP-3) (Tian *et al.*, 2013; Chemel *et al.*, 2017). Upon treatment with DMARDs or TNF-α antagonist therapy (infliximab or eternacept) a significant decrease of IL-34 serum levels was observed (Hwang *et al.*, 2012).

Given that IL-34 and M-CSF are both simultaneously expressed in synovial fluids of patients with RA, blocking the activity of both, or blocking the MCSF-R would be needed to produce a therapeutic benefit. To determine the effect of blocking either IL-34 or M-CSF or else their receptor (MCSF-R) in RA synovial explants, *Garcia et al.* tested this in intact synovial biopsy samples. Single blockade of either cytokines, did not effect the secretion of IL-6 by synovial tissue. However, treatment with anti MCSF-R antibody (huAB1) reduced levels of IL-6 compared with samples treated with isotype control (Garcia *et al.*, 2016). Moreover, treatment with huAB1 suppressed the production of chemokines CCL-2, CCL-7, CXCL-8 as well as secretion of IL-1β, TNF-α and MMP-2. These results therefore suggest that inhibition of the M-CSF receptor may be an effective therapeutic target for the treatment of RA.

In periodontal inflammation, IL-34 was found to be expressed in gingival fibroblasts, and its expression also enhanced by TNF-α and IL-1β. They also confirmed once more that IL-34 was able to support RANKL-induced osteoclastogenesis of bone marrow macrophages independently of M-CSF (Bostrum & Lundberg, 2013). IL-34 has also been associated with other autoimmune disorders linked to its role in monocyte proliferation. IL-34 is overexpressed in inflamed salivary glands in patients with Sjorgen's syndrome, an immune disorder affecting exocrine glands (Ciccia *et al.*, 2013). An important component of Sjorgen's syndrome lesions are macrophages, and their levels are increased in areas with severe lesions. Expression of IL-34 was associated with an increase of inflammatory cytokines, and pro-inflammatory monocytes ($CD14^{bright}$ and $CD16^{+}$) suggesting a potential regulation of monocyte and macrophages by IL-34 in SS. Il-34 has also been associated with inflammatory bowel disease (IBD) where a positive correlation was seen between levels of inflammation and overexpression of IL-34 in inflamed mucosa of Crohn's disease and ulcerative colitis, as well as level of monocytes. This suggests a role for IL-34 in amplifying the immune inflammatory response in patients with IBD (Zwicker *et al.*, 2015).

A positive correlation has been documented between insulin-resistant type II diabetes and overexpression of IL-34. Serum IL-34 levels are significantly elevated in such patents in comparison to controls. Finally in obesity, IL-34 is expressed by adipocytes and increased in serum of obese patients as IL-34 increases insulin resistance (Baghdadi *et al.*, 2018)

1.19 IL-34 and Cancers

IL-34 is expressed in a number of cancers such as breast, ovarian, colorectal, lung, skin, and brain and plays an important role in the tumour microenvironment through alternations of the niches (Zins *et al.*, 2018) IL-34 expression correlates with tumour progression as observed in OS and lung cancer as well as metastasis and angiogenesis. In lung cancer, IL-34 was seen to correlate with tumour progression and poor survival. High co-expression of both IL-34 and M-CSF, was associated with the poorest survival compared to patients in which these cytokines where absent or present at low levels (Baghdadi *et al.,* 2018). Recently, Franze *et al.* (2018) showed that IL-34 was able to support pro-tumourigenic signal in colon cancer.

This study unveils how two ligands of the same receptor can co-exist and exert their function in the same microenvironment. Even though it would be expected for these ligands to act as competitors, Il-34 and M-CSF have the ability to exhibit additive effects on proliferation and viability at certain conditions. Il-34 has the potential to interact with M-CSF and form a heteromeric cytokine to induce specific activation on MCSF-R (Segaliny *et al*., 2015). Therefore, in tumours that naturally express both ligands, or have the ability to produce both cytokines, Il-34 can potentially interact with M-CSF and consequently the M-CSF receptor and bring about unique functions in cancer cells and myeloid cells. Based on these observations, co-expression of both IL-34 and M-CSF, naturally or induced under therapeutic conditions, can characterize malignancies with an enhanced aggression pattern and has an impact on the clinical outcome of cancer therapy.

IL-34 expression in tumours may therefore be a critical prognostic biomarker correlating with tumour malignancy. In light of the pro-tumourigenic functions described above, Il-34 makes an attractive therapeutic target. Inhibition of CSF-1 targeting alone, will be insufficient to block the signaling of IL-34 since IL-34 binds to several other receptors including syndecan-1 and *RPTPβ/ζ* which are frequently expressed in various cancers. Thus targeting the signaling pathway that controls the production of IL-34 in the tumour microenvironment may be effective in multi-agent chemotherapy.

1.20 The Role of IL-34 in Osteosarcoma

Il-34 is expressed by OS cells as determined by qPCR and immunohistochemistry of 12 human biopsies osteosarcoma, as well as through a series of transcriptomic data. The expression of IL-34 was also assessed in four conventionally used OS cell lines (HOS, U2OS, MG63 and SaoS2) and proven positive in all of these cell lines. Additionally, IL-34 was upregulated in a dose response manner on induction by TNF-α and IL-1β as previously determined (Segaliny *et al.,* 2015). Since an inflammatory environment is established during tumour development, Il-34 produced by tumour cells would facilitate the recruitment of macrophages and formation of blood vessels within the tumour microenvironment.

The potential involvement of IL-34 in the pathogenesis and progression of OS was therefore then demonstrated both *in vitro* and *in vivo*. *In vitro,* analysis on human umbilical vascular endothelial cells (HUVEC) and endothelial cell precursors (ECFC) were performed to assess the role of Il-34 in angiogenesis and adhesion of myeloid cells. IL-34 stimulated the proliferation of endothelial cells and vascular cord formation in cultures of ECFCs, and increased the number of adherent monocytes in co-cultures with HUVECs. The authors also showed that IL-34 modulated FAK, Src, Akt and ERK1/2 signalling pathways in endothelial cells proving that these signalling molecules are involved in IL-34 mediated angiogenesis (Segaliny *et al.,* 2015).

More importantly were the results from *in vivo* studies using mouse models inoculated with OS cells overexpressing IL-34. In comparison to control OS cells, OS cells overexpressing IL-34 resulted in larger primary tumours and increased number of lung metastases. *In vivo,* IL-34 increased the recruitment of M2 TAMs into the tumour tissue as demonstrated by immunohistochemical staining of Arginase-1 in OS tumours. This data is in agreement with previous *in vitro* studies showing that like M-CSF, IL-34 is involved in macrophages survival, migration and polarization. *In vitro* IL-34 drives the differentiation of macrophages towards an immunosupressive M2 sub-type and thus strengthen the role of IL-34 in inflammation and associated cancer development. IL-34 can maintain the inflammatory process associated with cancer by facilitating the extravasation of mononuclear phagocytes and drive their differentiation towards an M2 phenotype. Consequently, the pro-angiogenic effect of IL-34 related to M2 macrophage polarization and/or recruitment will come into play to increase tumour vasculature as demonstrated *in vivo*. IL-34 acting in this paracrine manner at the tumour microenvironment is one of the main pathways to promote tumour progression.

A paracrine effect for IL-34 is also associated with chemoresistance. It is well documented that chemoresistance is enhanced when chemotherapeutic agents increase the frequency of M2 macrophages, which in turn limit the efficacy of chemotherapy. In lung cancer, IL-34 secreted by chemoresistant cells enhanced monocyte differentiation into the M2 type and additionally, humanized mouse models of OS chemoresistant tumours producing IL-34, were highly infiltrated with M2 macrophages and suppressing anti-tumour responses under conditions of chemotherapy (Baghdadi *et al.,* 2016) The authors also reported that under conditions of chemoresistance, IL-34 can function in an autocrine manner by acting on

CSFR-1 expressing tumour cells and TAMs. IL-34 induces the phosphorylation of CSFR-1 which in turn leads to activation of C/EBPβ via the AKT mediated pathway. This enhances the pro-tumourigenic and immunosuppressive functions of TAMs which consequently contribute to therapeutic resistance in cancers. This helped overcome strict conditions of chemotherapy, and identifies IL-34 as a promising target to help overcome chemoresistance in future therapeutic treatments.

1.21 Thesis Outline

The work presented in this thesis investigates the role of IL-34 in the pathogenesis of osteosarcoma, as well as its role in the inflammatory response. The studies summarized in this introduction indicate a central role for IL-34 in myeloid cell survival, differentiation as well as in the progression of OS by modifying the "bone niche", promoting the formation of new tumour blood vessels, and attracting immune cells to tumour sites. IL-34 thus acts as a key regulator in OS tumour cells, and in the tumour microenvironment.

In **Chapter 2**, the aim was to investigate the dialog established between OS cells and their microenvironment. The functional role of extracellular membrane vesicles as mediators of intracellular communication for modulating OS tumour development are explored. The work aims to better characterise extracellular vesicles in cell-to-cell interactions, as well as the communication between OS cells and other cells in the tumour microenvironment, with a focus on the contribution of IL-34 in this dialog. Specific aims:

1. To isolate and characterise exosomes derived from OS cell lines as well as exosomes from mesenchymal stem cells (bone marrow derived, and adipose derived)
2. To assess the biological functions of OS derived exosomes on mesenchymal stem cells including specifically proliferation, and differentiation of lineage abilities.
3. To determine whether IL-34 is present in vesicles isolated from OS cell lines, and whether it is involved in cell-to cell dialog between OS cells.
4. To gather more information and study the roles of mesenchymal stem cell derived exosomes, and their biological contributions on OS cells with particular focus on their protein cargo, proliferation and uptake by OS cells.

To study the potential of IL-34 as a therapeutic target for the treatment of OS, *in-vivo* murine models were used. The setting up of these models and the work done to determine the therapeutic effect of blocking IL-34 are described in **Chapter 3.** By using a rat anti-mouse blocking antibody, the effect of IL-34 blockade on OS development and the potential mechanisms by which this is achieved was investigated. Specific aims

1. To set up allograft and xenograft models of OS using mouse (MOS-J) and human (MNNG-HOS) OS cells respectively.
2. To perform a dose-response analysis of IL-34 blocking antibody and evaluate the response on tumour growth.
3. To investigate the treatment effectiveness of anti-murine and anti-human IL-34 blocking antibody on tumour progression.
4. To evaluate the impact of combining anti-murine IL-34 with the chemotherapeutic agent doxorubicin.
5. Using a combination of immunohistochemistry and analysis of bone architecture, the effects of the treatments and any potential mechanisms on tumour physiology are to be investigated.

To study the role of IL-34 in inflammation and its role in the innate immune phenotype, a zebrafish knockout model deficient for IL-34 was developed. **Chapter 4** includes the development and use of CRISPR/Cas9 to generate a zebrafish IL-34 knockout line, and the subsequent analysis on the immune phenotype so to establish to role of IL-34 as an inflammatory cytokine. Specific aims:

1. To generate an *il34* loss of function model and stable mutants using the CRISPR/Cas9 mechanism.
2. To assess the resulting loss of function phenotype in terms of the development and function of *il34* in larval zebrafish, including the effect on the bone phenotype.
3. To extend further the knowledge about the expression patterns of *il34* in wild type zebrafish.
4. To investigate the effects of il34 deficiency on inflammatory responses and innate immune cell populations in larval zebrafish.

In a conclusive **Chapter 5**, the findings from this work are summarized and discussed. This chapter also includes the future perspectives for the continuation of the work presented here, and possible avenues that can be considered to continue to increase our knowledge on the role of IL-34.

CHAPTER 2

EXOSOMES AS COMMUNICATORS IN OSTEOSARCOMA AND IN THE TUMOUR MICROENVIRONMENT

2.1 INTRODUCTION

Tumour progression is correlated with a number of molecules released by tumour cells into the extracellular space. These target other cells in an autocrine or paracrine manner, to induce changes in cells from the same tumour, or to other neighbouring cells such as stromal or endothelial cells within the metastatic niche (Jerez *et al.,* 2017). On characterisation of the secreted proteome, studies have confirmed that this secretome contains molecules supporting cell proliferation, cell migration, survival, angiogenesis, immune system evasion and metastasis. These events occur through a set of complex mechanisms and a number of pathways, including a "non-classical" mechanism of exporting molecules via exosomes and extracellular vesicles (EV's) (Miller & Grunewald, 2015). Exosomes are a sub-type of extracellular membrane bound vesicles. The term extracellular vesicles (EVs), is a term used to cover different heterogeneous classes of membrane-bound vesicles with sizes ranging from 30-2000nm, whereas the term exosomes is used to those vesicles restricted to 40-100nm in diameter

The three main types of EVs are; exosomes, microvesicles and apoptotic bodies (Min *et al.*, 2016). Exosomes are defined and separated from other vesicles based on their source, method of isolation, size and surface markers. Exosomes are thus specifically restricted to those vesicles being 40-100 nm diameter. They can be secreted by a wide-range of cell types including lymphocytes, platelets, red blood cells and tumour cells, as well as in several body fluids such as urine, saliva and blood. They consist of a lipid bilayer surrounding a cytosol devoid of organelles, that contains proteins, lipids and nucleic acids originating from the cell source and type (J. Liu *et al.,* 2017). Exosomes are formed by the

endocytic pathway, where inward budding of multivesicular bodies occurs, which then fuse with plasma membrane to release exosomes into the extracellular space (Figure 8).

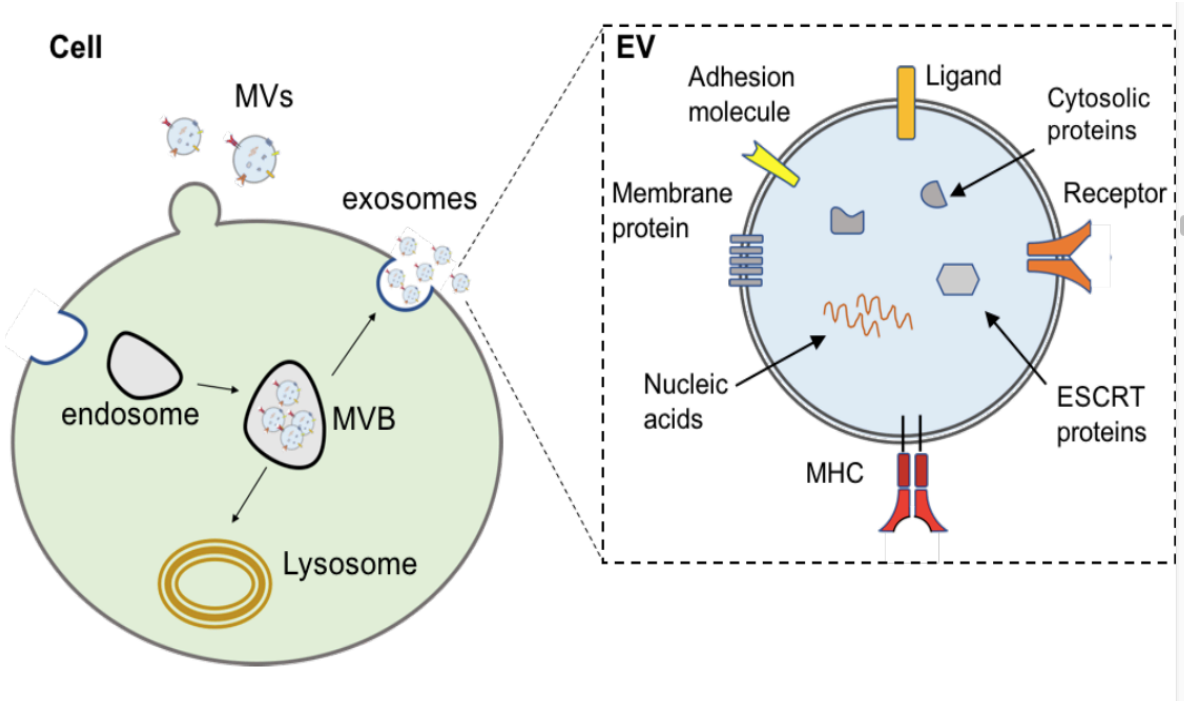

Figure 8: Illustration of the biogenesis of exosomes and their composition. The left panel shows a representation of EV biogenesis in which exosomes arise from the inward budding of endosomal multivesicular bodies (MVB). MVBs can be degraded upon fusion with the lysosome or can release intraluminal vesicles (ILVs) into the extracellular space upon fusion with the plasma membrane, being designated as exosomes. On the right, an enlarged exosome showing the components in particular, nucleic acids (DNA and RNA species) and they can also harbour a plethora of proteins (e.g. adhesion molecules, tetraspanins, cytosolic proteins and endosomal sorting complexes required for transport (ESCRT) components). Adapted from Colombo *et al.,* 2014)

2.1.1 Isolation, Detection and Analysis of Exosomes

Exosomes have been successfully isolated from cell culture media, and several body fluids. There are several methods by which they can be isolated, however this field is particularly challenging due to their small size, high heterogeneity and different sources from which they originate. Some of the main considerations that need to be taken into account when choosing a method for isolating exosomes are a) high recovery b) purity – should not be contaminated and c) integrity – should be kept intact (Rupert *et al*., 2017). Sample collection and processing for exosome isolation is therefore a complex process that ultimately depends on the starting material. Due to the nature of the data presented in this thesis, only the processing of cell culture medium by differential centrifugation, and quantification by TRPS analysis will be covered. Differential centrifugation is regarded as the "gold standard" technique for isolating vesicles, at it involves a series of sequential centrifugation steps, with increasing force. The popularity of differential centrifugation as an isolation technique may be due to its simplicity and short preparation time. Typical differential centrifugation of EVs from culture media is shown in Figure 9.

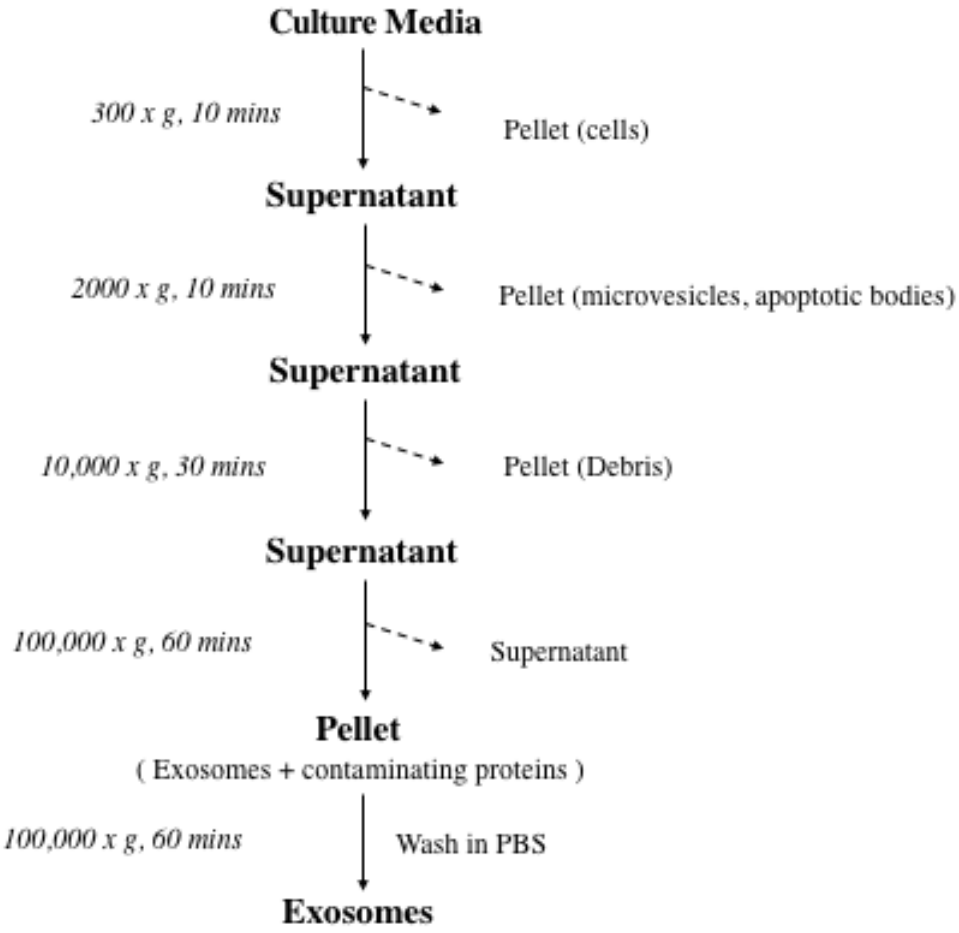

Figure 9: Workflow of ultracentrifugation. The scheme represents the workflow for exosomal purification by differential centrifugation. Three low to medium-speed centrifugation steps deplete the supernatant of cells, debris and contaminating vesicles. Exosomes are then purified and washed by ultracentrifugation at 100,000 x g.

This method however has several drawbacks, mainly that it produces low yields, and that it increases the risk of contamination with proteins and nucleic acids (Théry *et al*., 2006) . As a result, several other techniques have been developed, aimed to improve the isolation process and include size exclusion techniques, precipitation methods, affinity binding techniques, and microfluidics.

At present, exosomes can be detected by a number of methods most common being; a) electron microscopy; used to determine their ultrastructure, b) flow cytometry; to analyse surface phenotypic markers, and c) western blotting. The major proteins used as markers for the detection of exosomes include tetraspanins (CD9, CD63, CD81 and CD82), heat shock proteins (HSP70 and HSP90), ESCRT- associated proteins (TSG101), adhesion molecules (integrins) and fusion proteins (Annexins) (Min *et al.,* 2016).

The characterisation of exosomes is an area of great contention in the field of EV research, that is currently undergoing development. Due to their small size and often complex environment, several technical challenges arise when it comes to characterising and quantifying exosome samples. Due to this, and added with the limitations of isolating pure exosomes, there is no exclusive approach to detected EVs and their characterisation requires a combination of techniques. Usually, quantification methods are an added measure, especially important when it comes to comparing samples.

Methods for the quantification of EVs rely on both optical or non-optical techniques, and are used to quantitate both the size and concentration. This thesis describes the use of tunable resistive pulse sensing (TRPS) technology for the quantification and size profiling of exosomes. Currently the only platform available for TRPS is the qNano instrument (Izon Science, Christchurch, New Zealand). TRPS consists of a non-conductive membrane, separating two fluid cells and punctuated with a nano-sized pore. One of the fluid cells is filled with particle free electrolyte, and the other with the sample of interest (Figure 10A). By applying a combination of voltage and pressure, an electric current is established. When the particles transfer through the pore (Figure 10B), the current becomes altered. The particles create a ‘resistive pulse’ or ‘blockade signal’ that is detected and measured by the application software. The resistive pulse is proportional to the particle volume (Figure 10C). The rate at which these blockade signals occur, results in particle concentration. Since concentration and rate of blockade are linearly proportional, by using a simple calibration sample of a known concentration and size, the concentration and size distribution of an unknown sample can be measured (Maas *et al.*, 2014).

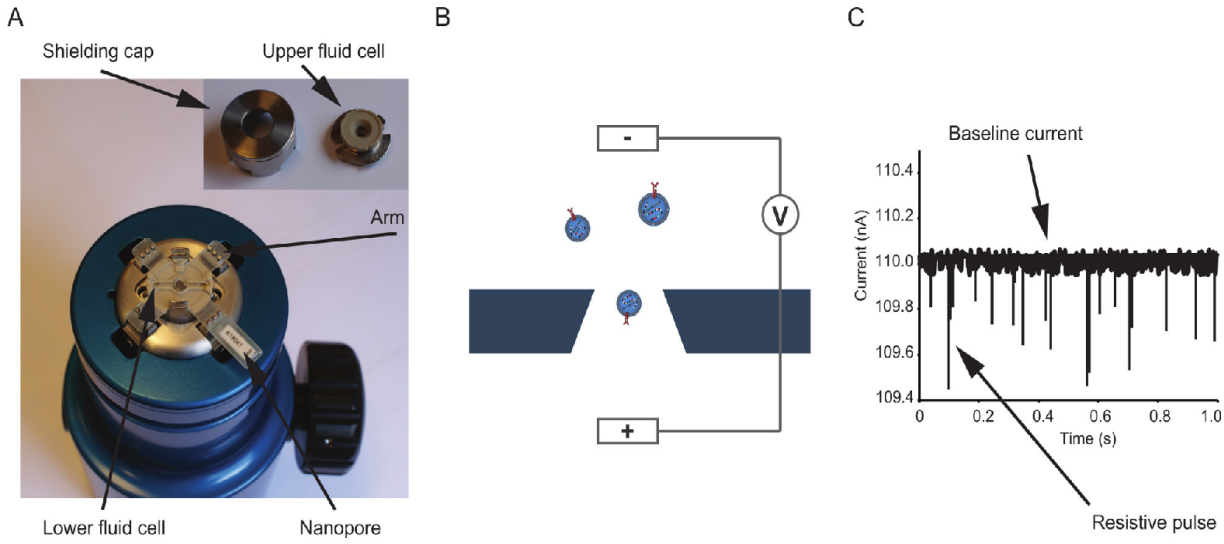

Figure 10: The qNano instrument and mode of operation (A) Photograph of the instrument showing a nanopore. A shielding cap protects the fluid cells from environmental electrical interference. (B) Illustration of tunable resistive pulse sensing (tRPS). A non-conductive elastic nanopore separates two fluid cells. Once a voltage is applied, an electric current is established through the pore and as EVs pass through the nanopore, the ionic flow is altered and detected as a resistive pulse. (C) Example of resistive pulses. The magnitude of a resistive pulse is proportional to the volume of the particle (Maas *et al.,* 2014).

2.1.2 Role of Extracellular Vesicles in Cancers

The main function of exosomes is to transport their bioactive molecules from donor cell to recipient cell for the exchange of genetic material and re-programming of recipient cells. This intracellular communication between tumour cells through EVs is a mechanism that tumour cells utilise to promote tumour survival and progression. Compiling evidence suggests that exosomes play these vital roles through evasion of the immune system, modulation of the microenvironment and promotion of angiogenesis and metastasis (Min *et al*., 2016). Each of these mechanisms will be discussed in short below.

Tumourigenesis: Tumour cell EVs assist in tumour progression by enhancing stromal re-modelling. EVs from cancer cells drive the transition of stromal fibroblasts towards a myofibroblast phenotype, via the transfer of TGF-β and induction of α-smooth muscle actin expression (Liu *et al*., 2018) (Figure 11). In OS, EVs have been reported to be associated with the Wnt/β-catenin signaling pathway. A pathway known to be associated with the progression of OS when aberrantly activated driving cell proliferation and tumourigenesis. Chen *et al*. demonstrated that activation of autocrine Wnt/β-catenin signaling in the tumor cell-derived EVs would enhance the development and survival of OS cells *in vitro* (Chen *et al*., 2015).

Immunosupression and/or immunomodulation: Exosomes can lead to immune escape by supressing antigen specific responses, or by upregulating immunosuppressive cell differentiation. Tumours use EVs to evade immune recognition by shedding the ligand for natural killer receptor (NKG2D) thus avoiding the destruction of immune cells by cytotoxic NK cells and $CD8^+$ T cells (Clayton *et al*., 2008) (Figure 11).Transfer of TGF-β by tumour derived EVs, additionally, prevents antigen presentation by dendritic cells and promotes the transition of $CD8^+$ cytotoxic T cells towards a regulatory T cell phenotype (Clayton *et al*., 2007).

Angiogenesis: Exosomes are also implicated in the induction of neo-angiogenesis and help tumours to grow by increasing their metastatic potential. EVs facilitate tumour-mediated angiogenesis by targeting expression of VEGF. Breast tumour EVs harbour VEGF as well as notch ligand D114 to stimulate local angiogenesis (Figure 11). Alternatively, EVs can carry a mutated version of EGFR that is transferred to other tumour cells increasing expression of VEGF and oncogenic activity in these cells (Cho *et al*., 2012). EVs are also highly secreted in hypoxic cancer cells and enriched with angiogenic proteins in a hypoxia-inducible factor (HIF)- dependent manner. As a result, further stimulating tumour-mediated angiogenesis *in vivo*. In OS, Bhattacharya *et al.* found that TGF-β1-containing EVs promoted tumour development and metastasis via angiogenesis (Bhattacharya *et al.,* 2008).

Metastasis: As one of the major hallmarks of malignant tumours, metastasis is a complex process that involves optimisation of the microenvironment to one that favours both local and distant metastasis. Evidence suggests that cancer derived exosomes, selectively transfer signals to neighbouring cells to modify the local environment in favour of local metastatic conditions, as well as to distant sites via the circulation, assisting in the formation of the pre-metastatic niche (Liu *et al.,* 2018). In melanoma, exosomes have been confirmed to accumulate in lymph nodes, to induce recruitment of tumour cells, and remodelling of the extracellular space in favour of metastasis. Interchangeably, stromal cells can produce exosomes that stimulate cancer cell motility and metastasis by the activation of several pathways. Exosomes from bone-marrow derived mesenchymal stem cells induced the dormancy of breast carcinoma cells with the effect of reducing proliferation and their chemosensitivity to facilitate their survival in the metastatic niche (Ono *et al.*, 2014).

Modulation of microenvironment: Exosomes can modulate and manipulate the microenvironment via intracellular communications, and additionally by modulating adjacent stromal cells. The consequences of such modifications lead to enhanced tumour growth, invasion, and a more malignant phenotype. Stimulating surrounding fibroblast with cancer derived EVs towards a myofibroblast-like phenotype, has been shown to be one of the major mechanisms by which cancer cells achieve this (Webber *et al.,* 2015). TGF-β from EVs, have been reported to trigger the SMAD-dependent pathway to promote myofibroblast differentiation with angiogenic responses. For example as seen in breast cancer derived exosomes, where adipose derived mesenchymal stem cells stimulated the differentiation into myofibroblast like cells that secrete VEGF and stromal derived factor-1 (SDF-1) to promote tumour progression (Cho *et al.,* 2012). Similarly the transmission of the oncogenic protein tyrosine kinase (KIT) in gastrointestinal stromal tumours via vesicles to adjacent stroma, has been shown to enhance tumour promoting properties of smooth muscle rich stromal cells downstream of KIT. The end result is supported tumour invasiveness, and thus further contribution towards the metastatic spread (Atay *et al.*, 2014).

The interplay between tumour and its microenvironment is also described by the actions of EVs produced by stromal cells, which can themselves secrete vesicles to contribute to changes in the microenvironment. For example fibroblast exosomes promotes the migration of breast cancer cells via the uptake of $CD81^{+}$ exosomes by cancer cells and interaction of Wnt11 (Valcz *et al*., 2018).

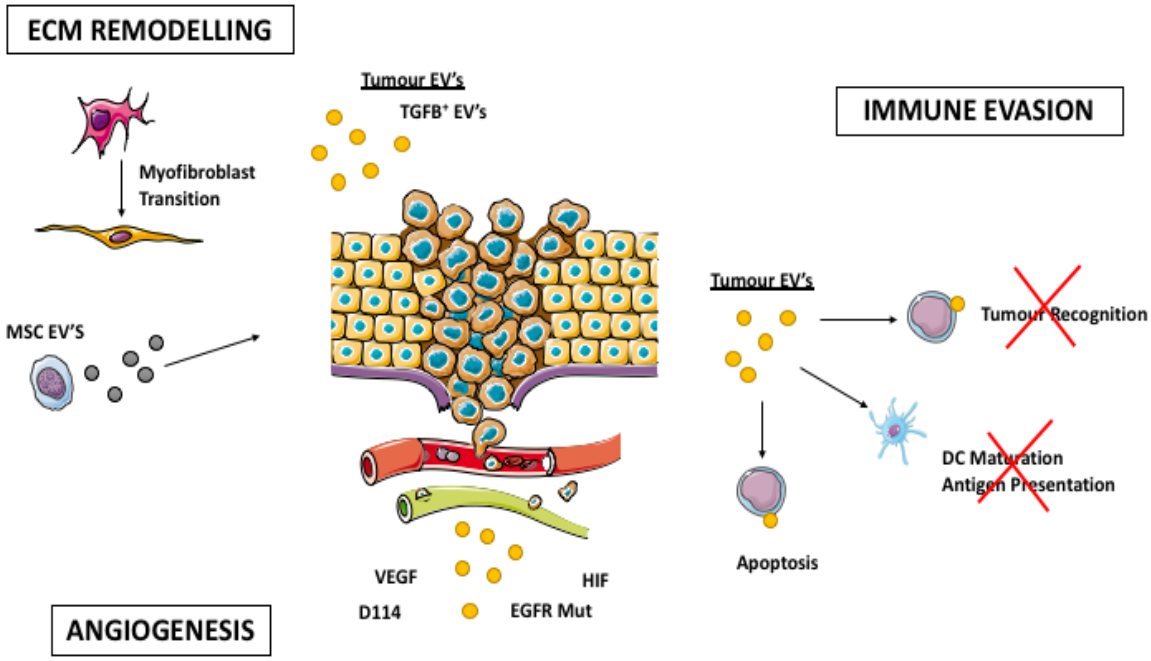

Figure 11: Diagram illustrating the role of EVs in cancer. The diagram depicts the role of EVs in the tumour microenvironment depicting roles in ECM-remodelling, angiogenesis and immune evasion. TGF-β = Transforming growth factor-β, VEGF = vascular endothelial growth factor, HIF = hypoxia inducible factor, EGFR = endothelial growth factor receptor, D114 = delta-like 4, MSC = mesenchymal stem cell, DC = dendritic cell

2.1.3 Role of Mesenchymal Derived Extracellular Vesicles

Since exosomes are involved in cell to cell communications, there has been much focus on research about exosomes derived from mesenchymal stem cells and their effects on diseases, as well as on tumour cells and their microenvironment. This, however comes with contrasting views in the literature as both tumour promoting properties, and tumour inhibiting effects by MSC derived vesicles have been reported (Yu *et al*., 2014).

One mechanism associated with tumour promoting effects *in vivo*, is the ERK1/2 mediated promotion of tumour derived VEGF. MSC exosomes in conjunction with tumour cells, resulted in increased breast tumour incidence and growth *in vivo,* via stromal myofibroblasts and promotion of angiogenesis (Zhu *et al*., 2012). In myeloma, a similar effect was observed whereby myeloma educated MSC's release exosomes with a different profile of adhesion molecules, oncogenic proteins, and contents capable of promoting tumour growth (Roccaro *et al*., 2013). Contrastingly, bone marrow derived MSC vesicles were reported to impair myeloma growth by down-regulating VEGF expression in tumours both *in vitro* and *in vivo*. Mir-16, a miRNA enriched in MSC derived exosomes and known to target VEGF, is responsible for this angiogenic effect (Lee *et al*., 2013). Also, depending on the type of stem cell, the effect on tumour proliferation can be different. Del Fattore *et al* demonstrated that exosomes from bone marrow MSC's, supressed cell proliferation, whilst adipose stem cell derived vesicles exerted the opposite effect. These properties, taken together demonstrate the importance of exploring stem cell derived exosomes, and thus aim to bridge the gap in the knowledge of how MSC derived vesicles exert their biological functions in OS and it's microenvironment (Del Fattore *et al*., 2015).

2.1.4 Rationale

The roles of exosomes in the biological and pathophysiological processes of OS, are still not yet fully understood. Some studies have reported that exosomes derived from OS supernatants, are enriched with proteins associated with angiogenesis, cell adhesion, immune evasion and cell migration, in comparison to proteins in exosomes from non-malignant cells (Bracha *et al.*, 2018; Garimella *et al.*, 2014; Ruby *et al.*, 2017)However, despite this, there is still a large gap in the knowledge about OS derived vesicles, with the molecular mechanisms of how they assist in tumour progression and metastasis needing further investigation.

Similarly, although literature on mesenchymal derived exosomes and their biological functions in tumours are increasing, there is still nothing known about the interactions of MSC derived exosomes with the microenvironment in OS. Much still needs to be elucidated about this dialogue, especially in the transfer of contents between host cell and recipient cell. Intercepting the environmental factors sustaining OS pathogenesis and progression, may therefore increase our knowledge of the field and will be beneficial for providing novel therapeutic options.

2.1.5 Aims and Objectives

The general focus of this chapter was to explore extracellular vesicles from OS as a novel mechanism of signalling *in vitro* whilst learning about the current limitations of the field. The aims of this chapter where to characterize OS derived vesicles, and determine their biological effect on recipient cells. The goal was to better characterize the functional communications between OS cells and mesenchymal stem cells, through the contribution of exosomes in this dialog.

Specific aims:

1. To isolate and characterise exosomes derived from OS cell lines as well as exosomes from mesenchymal stem cells (bone marrow derived, and adipose derived)

2. To assess the biological functions of OS derived exosomes on mesenchymal stem cells including specifically proliferation, and differentiation of lineage abilities.
3. To determine whether IL-34 is present in vesicles isolated from OS cell lines, and whether it is involved in cell-to cell dialog between OS cells.
4. To gather more information and study the roles of mesenchymal stem cell derived exosomes, and their biological contributions on OS cells with particular focus on their protein cargo, proliferation and uptake by OS cells.

2.2 METHODS

This chapter was carried out in collaboration with the School of Clinical Dentistry under the supervision of Dr. Stuart Hunt (School of Clinical Dentistry, Sheffield UK). Thanks to this collaboration regular access to qNano system for measurement was possible.

2.2.1 Materials, Reagents and Equipment used

A. MATERIALS & REAGENTS	
0.22 μm Vivaspin 500 Filters; VS0161	Sartorius
96-well plate; 3595	Costar
Pierce BCA Protein Assay Reagent A; 23221	Thermo-Fischer
Pierce BCA Protein Assay BCA Reagent B; SZBF3500V	Fluka Analytical
BSA Protein Standard; P08343	Sigma-Aldrich
Cell Tracker CM-Dil C7000 Kit	Thermo- Fischer
DMSO; D2650	Sigma-Aldrich
Dulbecco's Modified Eagle's Medium (DMEM), High Glucose GlutaMax, pyruvate; 31966	Gibco
Foetal Bovine Serum; 10270-106	Gibco
Hoeschst Solution; 33342	Thermo- Fischer
Penicillin-Streptomycin (PenStrep), P0781	Thermo-Fischer
Performaldehyde (PFA); 158127	Sigma- Aldrich
Phosphate Buffered Saline (PBS);	Gibco
Pore membrane; NP100A	Izon Science
RIPA Buffer; R0278	Sigma-Aldrich
Round bottomed 35mm dishes with No 1.5 coverslip; P35G-1.5-20C	Mattek
SuperSignal West Pico Chemiluminescent Substrate; 34580	Thermo- Fischer
Cell culture multi-flasks T175; 353143	Falcon
Trypsin; T4174	Sigma-Aldrich
Ultra-Clear polycarbonate tubes; 362305	Beckmann Coulter
VivaSpin 100 kDA MWCO Polyethersulfone tubes; GE28-9322-37	GE Healthcare
XTT Cell Titer 96® Proliferation Assay	Promega

B. ANTIBODIES	
Mouse secondary; P0260	DAKO
Rabbit monoclonal Anti-CD9 Antibody; AB92726	Abcam
Rabbit monoclonal Anti-Vinculin Antibody; AB129002	Abcam
Rabbit polyclonal Anti-CD63 Antibody; SC15363	Santa Cruz Biotechnology
C. KITS	
Human IL-34 ELISA Kit; P1659	Diaclone
Proteome Profiler XL Human Cytokine Array; ARY022B	R&D Systems
D. EQUIPMENT	
ChemiDoc XRS Imager; 1708265	Bio-Rad
Confocal Laser Scanning Microscope; LSM510	Zeiss
High speed centrifuge ; Avanti J-26 XPi	Beckmann Coulter
Micro-plate reader ; SpectraMax M5	Molecular Devices
MSE Sanyo Harrier top-bench centrifuge 18/80R	Sanyo
qNano System	Izon Science
Sanyo CO_2 Incubator; MCO-20AIC	Richmond Science
Ultracentrifuge; Optima TL-100	Beckmann Coulter
E. SOFTWARE	
GraphPad Prism Version 7	Graph Pad Software
Image Lab Software V5.2.1	Bio-Rad
Izon TRPS Software (Check version)	Izon Science
Zen Lite Imaging Software V	Zeiss

For the duration of this chapter and for any part of the thesis relating to exosomes, the term **extracellular vesicles** (EVs), is used to refer to membrane-bound vesicles with sizes ranging from 30-2000nm, whereas the term **exosomes** is used for those vesicles restricted to 40-100nm in diameter

2.2.2 Cell Lines

For the following part of the work, exosomes where isolated from four cell lines. Two human OS cell lines; MG63 and KHOS, and two primary cell cultures bone marrow derived mesenchymal stem cells (BMSCs) and adipose derived mesenchymal stem cells (ASCs). Their characteristics and can be summarised in the table below (Table 1)

Table 1: Table outlining the cell-lines used for isolation of exosomes.

	MG63 overexpression of Il-34 or GFP (control)	**KHOS* overexpression of Il-34 or GFP (control)**	**Adipose mesenchymal stem cells (ASCs)**	**Bone marrow mesenchymal stem cells (BMSCs)**
Source	14 year-old male, OS	13 year old, female, OS	Human fat samples	Human bone marrow aspirates
Morphology	Osteoblast-like	Epithelial	Spindle shaped, fibroblast like	Spindle shaped, fibroblast like
Acquired From	Originally ATCC, Modified cells established by Segaliny et al., 2015; Heymann Lab: (INSERM, FR)	Originally ATCC, Modified cells established by Segaliny et al., 2015; Heymann Lab: (INSERM, FR)	STROMALab INSERM, University of Toulouse, France	STROMALab INSERM, University of Toulouse, France
Media for culturing	DMEM + High GlutaMax (Gibco) and 10% FBS (Gibco)	DMEM + High GlutaMax and 10% FBS	α-MEM + High GlutaMax (Gibco), 10% FBS & 1% PenStrep (Sigma)	α-MEM + High GlutaMax, 10% FBS & 1% PenStrep

KHOS cells: Cell line derived from HOS by transformation using Kirsten murine sarcoma virus (Ki-MSV). Properties are similar to parent HOS and are tumourigenic in mice. This cell line is different from MNNG-HOS which is transformed by MNNG (a carcinogenic nitrosamine) and is tumourigeneic in nude mice.

2.2.3 Cell Culturing

Cells were maintained in adherent monolayers in tissue culture flasks T175 flasks, (Corning, UK) for production of exosomes in their respective medium. For exosome isolation, the medium was supplemented with foetal calf serum (FBS) depleted of exosomes by overnight ultracentrifugation. FBS was depleted of exosomes by overnight centrifugation at 100,000g at 4 ^{o}C, followed by filter sterilisation. For primary cell lines, culture media were supplemented with 1% Penicillin-Streptomycin solution (Thermo-Fischer) to prevent bacterial growth. All cells were grown in humidified 37^{o}C, 5% CO_2.

2.2.4 Isolation of Exosomes by Ultracentrifugation

Exosomes were purified from cell culture media following a protocol consisting of successive rounds of centrifugation (Figure 9, Figure 12). Cells were first grown to a sub-confluent state (80%) in exosome-depleted FBS for 72 hours. Conditioned media was then collected, and centrifuged at 300 g for 10 minutes in 50 mL centrifuge tubes, followed by a centrifuge at 2,000 g for 20 minutes to remove any residual cells (Top-bench centrifuge, Sanyo). The supernatant was collected, and centrifuged at 10,000 g for 30 minutes in a high-speed centrifuge (J-26 XPi, Beckmann Coulter). This step was to eliminate and residual debris in the media.

The remaining supernatant was then concentrated using 100 kDA MWCO viva protein concentrator columns (GE Healthcare) and subjected to centrifugation at 3,500rpm for 15mins. To pellet exosomes, the concentrated media was transferred into polycarbonate tubes (Beckmann Coulter), and centrifuged at 100,000 g for 60 minutes using a TL-100 ultracentrifuge (Beckmann Coulter). The pellet was washed once with cold sterile PBS, re-centrifuged at 100,000 g for 60 minutes and re-suspended in 50 μL of PBS. For long-term storage exosome pellets were stored in -80°C. All centrifugations were performed at 4°C.

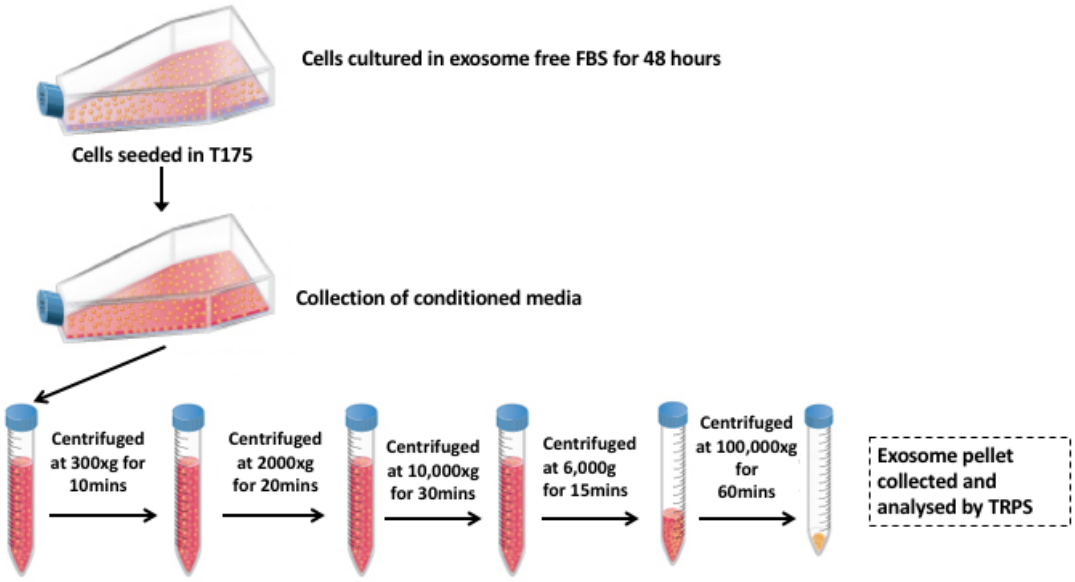

Figure 12: Workflow for isolating exosomes from cell culture media by ultracentrifugation.

2.2.5 Sizing and Quantification of Exosomes

Size distribution analysis was performed using the qNano system (Izon Science, New Zealand). Samples were diluted (1:5 in PBS) and passed through a 0.22 μm filter (Sartorius). TRPS was operated using an NP100A pore membrane (Izon Science), applied pressure of 10cm, and voltage of 0.5V. The sample was recorded for a minimum of 600 blockade events. Sample size distributions were calibrated by Izon Control Suite 2.2 using beads of known size, diluted in PBS and measured at identical settings. Data was analysed with TRPS software (Izon Science) to calculate the size and concentration of the particles.

2.2.6 Estimation of Protein Concentration by BCA Assay

The BCA protein assay was used to measure the amount of proteins present in the purified exosomes, thus giving an idea of the total amount of exosomes secreted by the cells. Isolated exosomes were re-suspended in lysis buffer in the presence of protease inhibitors (5x RIPA Buffer, Sigma Aldrich), sonicated for a few seconds to permeabilise the vesicles, and left on ice for about 15 minutes.

For the standard curve, serum albumin was diluted to concentrations ranging between 0-1000 μg/mL. Exosome samples were diluted with lysis buffer and made into working solutions of not larger than 20 μL. BCA reagent was prepared by mixing 50 parts of BCA reagent A, with 1 part of BCA reagent B. Following that, 20 μL of standards and diluted samples were pipetted out on a 96-well plate, and 200 μL of reagent was added to each. The plate was incubated at 37^{o}C for 30 minutes after which the absorbance was measured at 540 nm by a plate reader (SpectraMax M5, Molecular Devices).

2.2.7 Immunodetection by Western Blotting

Exosomal surface markers CD63 and CD9 were examined by western blot analysis. Based on the BCA estimate of protein concentrations, around 5 μg of exosome sample, was resolved by 12% SDS-PAGE and transferred to a polyvinylidene difluoride (PVDF) membrane. To prevent unspecific antibody binding, the membrane was blocked for 1h with 5% dry milk. After blocking, the membrane was incubated with the primary antibodies diluted in 2.5% milk over night at 4^{o} C. CD9 antibody (Abcam, Ab 92726) was incubated at a dilution of 1:2000, whereas CD63 antibody (Santa Cruz Biotechnology SC: 15363) was used at a dilution of 1:200. Vinculin antibody (Abcam, Ab129002) was used as a loading control (1:2000) The following day, membranes were incubated for 1 hour with horseradish peroxidase (HRP)- conjugated secondary mouse antibody at 1:2000 (Dako). Immunoreactive protein bands were visualized using the Super signal west-pico chemiluminescence detection kit (Thermo Scientific), and imaged using a ChemiDoc XRS+ Imager (Bio-Rad).

2.2.8 Proliferation Assays

Proliferation assays were used to study the biological effects of cellular communication and interaction between stem cells and tumour cells via exosomes. To set up the assays, cells were seeded in 96-well plates and cultured to 50-60% confluency. For cell densities, ASC cells were seeded at 2,000 cells/well, MG63 cells (parental cell line) seeded at 2,000 cells/well and KHOS (parental) cells seeded at 1,000cells/well. The next day, media was removed and exchanged with fresh media containing the purified vesicles. Each of the following experiments were performed in triplicate.

- **Experiment 1** – Adipose derived stem cells (ASCs) treated with OS exosomes from MG63-IL-34 and MG63-GFP (ctrl) (3 serial dilutions 1:1, 1:2 and 1:4 for each) – also treated with respective conditioned media (prepared over 24hrs)
- **Experiment 2** - Adipose derived stem cells (ASCs) treated with OS exosomes coming from KHOS-IL-34 and KHOS- GFP (ctrl) (3 serial dilutions 1:1, 1:2 and 1:4 for each) - also treated with respective conditioned media (prepared over 24hrs)
- **Experiment 3** – KHOS cell line treated with ASCs derived exosomes (5 serial dilutions 1:1, 1:2, 1:4, 1:8 and 1:10)
- **Experiment 4** – OS cell line MG63 treated with ASCs derived exosomes (5 serial dilutions 1:1, 1:2, 1:4, 1:8 and 1:10)

For all experiments cells where serum starved 24hrs prior to treatment. Cells cultured with no vesicles, (only 2% FBS) served as a control, whereas cells in 10% FBS were used as positive control. 5% DMSO was used as an additional control. XTT assay (Promega) was done and read at 24hrs, 48 hrs and 72hrs. The XTT assay is based on the cleavage of a tetrazolium salt XTT, in the presence of an electron coupling reagent, to produce a soluble formazan salt. A conversion that occurs only in viable cells. Absorbance was measured at 570 nm using SpectraMax M5 (Molecular Devices) plate reader.

2.2.9 ELISA

Enzyme-linked immunosorbent assays (ELISA) was used to quantify the levels of IL-34 in MG63 and KHOS derived exosomes, in comparison with their respective cell lysates, and conditioned medium. Exosomes were derived from KHOS and MG63 cell lines overexpressing IL-34 and GFP as previously described. Isolation of exosome contents was performed by addition of lysis buffer and sonication as previously outlined.

The human IL-34 cytokine sandwich ELISA was purchased from Diaclone (France). All experiments were performed in triplicate, and according to the manufacturer's protocol. Briefly, samples and standards were added into the plate and incubated at room temperature for 2 hours. Wells were then washed with wash buffer, and left with biotinylated anti-IL-34 antibody for 1 hour at room temperature. Streptavidin - horse radish peroxidase (HRP) was then used for detection by adding 100 µL to each well, and left to incubate for 30 minutes. For detection, the substrate solution was added and samples were left to incubate with it for 25 minutes (away from any direct light). At the end, the colour-change reaction was halted by adding 100 µL of stop solution.

Plates were subject to measurement of absorbance at 450 nm and 650 nm (for wavelength correction) using the SpectraMax M5 (Molecular Devices) plate reader. Wavelength correction adjusted results to account for any optical imperfections in the plate. All measurements occurred within 10 minutes from completion of the assay. Cytokine standards provided with each kit were used to produce standard curves and determine unknown concentrations. The standard curve was generated by plotting the log of mean absorbance for each standard against the log of its known concentration (to produce linearized data).

2.2.10 Internalization of Exosomes

2.2.10.1 Fluorescent staining of exosomes

Imaging of *in vitro* transfer of adipose stem cell derived exomes to either KHOS or MG63 OS cells was performed so as to visualize the internalization of exosomes. To achieve this, the exosomes were fluorescently labelled using a lipophilic membrane dye that incorporates within the lipid membrane of the vesicles.

ASCs derived exosomes were labelled using the Cell Tracker™ CM-DiI C7000 Kit (Thermo-Fischer), according to the manufacturer's recommendations. In brief, 1mg/ml of dye solution was resuspended in PBS to make the stock solution. 2 µl of the stock labelling solution was then mixed with 1mL of exosome suspension (exosomes re-suspended in sterile PBS) and transferred to an eppendorf tubes, covered with foil to keep light away, and incubated for 10 minutes at 37°C. After labelling, samples were washed with PBS and centrifuged at 100,000 g for 1hour at 4°C. A control was prepared by adding CM-Dil solution to PBS. Controls were prepared in parallel with exosomes. The exosomes were then resuspended in 200 µL of exosome depleted media. To remove any un-bound dye, labelled solutions where filtered through 100K MWCO centrifugal exosome filters (GE Healthcare).

2.2.10.2 Co-culturing stained exosomes

The MG63 and KHOS cells were plated in round-bottomed 35 mm dishes with No 1.5 coverslip (Matek) (seeded at 5,000 cells per dish) 24 hours prior to exosome addition. The cells were incubated in DMEM media supplied with exosome depleted FBS. After cells were allowed to settle, the media was replaced with 200 µL of labelled exosome suspension, and left to settle for 1 hour. The dishes where then topped up with more media and left to incubate for the time required (6 hours or 24 hours) after which they were labelled with a nuclear stain and fixed.

For fixing, the media was first removed and the cells were washed with PBS after which they were fixed with 4% paraformaldehyde for 15 min at room temperature. The cover slips were then mounted on a cover glass using Hoechst Solution (1:10 dilution) (Thermo

Scientific). Pictures were taken using a confocal laser microscope Zeiss LSM510 (Zeiss MicroImaging GmbH) with 40x/1.3 oil immersion objective.

2.2.11 Cytokine Profile of Exosomes

The Proteome Profiler Human XL Cytokine Array Kit (R&D systems), was used to simultaneously analyse the cytokine content in the exosomes. These nitrocellulose membranes are pre-embedded with capture antibody spots that bind to specific target proteins present in the sample. Captured proteins can then be detected with biotinylated detection antibodies, and visualised using chemiluminescent detection reagents. The signal produced is proportional to the amount of protein bound.

Exosomes derived from BMSCs and ASCs were purified and permeabilised, and protein content measured by BCA assay. The cytokine array procedure was performed according to manufacturer's protocol. As per its consideration, 50 μg of total exosomal protein, was loaded onto each membrane. Samples were prepared by diluting the desired quantity (according to results of BCA assay) to a final volume of 1.5 mL with array buffer 6. Membranes were then incubated (on a rocking platform) in sample solutions overnight at 2-8°C. Following this incubation, membranes were washed with wash buffer and incubated with detection antibody cocktail buffer for 1 hour. After another set of washes, membranes were covered with streptavidin-HRP followed by coverage in chemiluminescent reagent, spread evenly only to membrane, and incubated for 1 minute.

Membranes were imaged using a ChemiDoc XRS+ Imager (Bio-Rad). Intensities of samples on the membrane (pixel density) were quantified using Image Lab Software (Bio-Rad) Raw output was given as mean pixel density. Assays were normalised to the pixel density of the reference spots for consistency between membranes.

2.2.12 Differentiation of Mesenchymal Stem Cells

This part of the project was done in collaboration with Dr. Frederic Deschaseaux and Jean-Gerard Descamps from STROMALab (https://www.stromalab.fr/) at the French National Institute for Health and Medical Research (Inserm), University of Toulouse, France.

To identify the potential effects of OS derived exosomes on stem cells, the phenotype of undifferentiated mesenchymal stem cells following the addition of OS exosomes was studied. Exosomes derived from MG63 and KHOS were added to the cultures and lineage markers were evaluated by RT-PCR at day 3 or day 7 (RT-qPCR method outlined in Zebrafish section 4.2.4.5). The transcript analysed (see Table 2), were associated with osteoblastic, chondroblastic, and adipocytic phenotypes, that is characteristic of their differentiation abilities.

2.2.13 Statistical Analysis

Data were analysed using GraphPad Prism (version 7.0) software (Graphpad). N numbers for all experiments donated by the prefix n and all errors bars shown denote the mean ± Standard error of the mean. All data analysed with either T test, or a two-way ANOVA with Dunnett's multiple comparison test, for parametric data.. Significance values denoted as follows: Non-significant (ns): $p > 0.05$, *: $p<0.05$, **: $p<0.01$, ***: $p<0.001$ and ****:$p<0.0001$.

Table 2: List of primers to analyse the differentiation of mesenchymal stem cells by RT-qPCR.

	Forward Primer	**Reverse Primer**
Osteoblastic		
RUNX2	5'-GGC CCA CAA ATC TCA GAT CGTT-3'	5' -CAC TGG CGC TGC AAC AAG AC-3'
DLX5	5'-GCC ACC AAC CAG CCA GAG AA-3'	5'-GAC GAG AAG AAT TAC CAG GGA AAC A-3'
PTHR1	5'-ACA TCT GCG TCC ACA TCA GGG-3'	5'-CCG TTC ACG AGT CTC ATT GGT G-3'
SP7 (osterix)	5'-CTC CTG CGA CTG CCC TAA T-3'	5'-GCC TTG CCA TAC ACC TTG C-3'
BGLAP	5'-GAG GGC AGC GAG GTA GTG AAG A-3'	5' -CGA TGT GGT CAG CCA ACT CG-3'
Chondroblastic		
COL2a1	5' – CTG CAA AAT AAA ATC TCG GTG TTC T – 3'	5' – GGG CAT TTG ACT CAC ACC AGT- 3'
COL10	5'- GGT ATA GCA GTA AGA GGA GAG CA-3′	5'- AGG ACT TCC GTA GCC TGG TTT-3′
Sox9	5' -CAA GAC GCT GGG CAA GCT CT-3'	5' -TCT TCA CCG ACT TCC TCC GC-3'
Aggrecan	5'- CCT CTG GAC AAC CAG GTG TT-3'	5'- AAA CCA GCT CAG GGA CTC CT-5'
Adipocytic		
AP2	5′-GGC ATG GCC AAA CCT AAC AT-3′	5′-TTC CAT CCC ATT TCT GCA CAT-3′
PPARG2	5' -AAG GCG AGG GCG ATC TTG AC-3'	5' -GCA GGG GGG TGA TGT GTT TG-3'

2.3 RESULTS

The aim of this chapter was to characterize OS derived exosomes and better study the functional communications between OS cells and their environment with a specific focus on the contribution of mesenchymal stem cell derived vesicles in this dialog. The work detailed in this chapter was conducted at the beginning of my PhD as I was learning about the practicalities of working with extracellular vesicles and the field-wide lack of standardization. The lab was fortunate to have regular access to the qNano system at the School of Clinical Dentistry (University of Sheffield). This presented a good opportunity to not only to make use of a novel technique in the field of EVs, but also to learn about the relative benefits and weaknesses related to this emerging field. These results are therefore preliminary and focused towards methodological aspects and considerations of processing EVs.

2.3.1 Cell Origin

The EVs investigated in the initial part of the study were isolated from human MG63 and KHOS cell lines. The cells were cultured in exosome-depleted serum, since FBS contains high levels of naturally occurring exosomes. This would otherwise be problematic on analysing the vesicles as background signal from exosomes in FBS would make it difficult to distinguish which vesicles are being secreted by the cells of interest, and which are secreted by FBS, and could thus lead to skewed results. Cells were cultured in exosome depleted FBS 28-48 hours prior to EV harvest (depending on initial seeding density). EVs were also isolated from human BMSCs and ADSCs (See section 2.3.9). Similar culture conditions were applied, with the difference that incubation in exosome depleted FBS was longer (24-72 hours) owing to the slower growth rates of these primary cells.

2.3.2 Isolation of Extracellular Vesicles and Associated Limitations

Cell culture media was collected and processed as explained in the materials and methods section. The approach used for isolation of exosomes was based on ultracentrifugation, and the procedure was optimised throughout the study. The main steps however were a series of low-speed serial centrifugation steps to remove dead cells and debris, followed by high-speed ultracentrifugation to pellet the vesicles. Based on several reports, this method can increase the risk of contamination and can have a negative impact on the integrity of the vesicles collected (Rupert *et al*., 2017; Théry *et al*., 2006). This is because the sample may also contain soluble proteins and protein aggregates that deposit with the vesicle pellet. Therefore some regard this method as less reliable for obtaining vesicles. There is still a lack of standardisation in this field due to the variety of biological resources from which EVs can be derived. Despite this, it was decided to use this conventional method for ease of comparison to the literature.

Another major limitation when it comes to characterising the exosomes, is the storage and processing of the samples. Again, a lack of standardisation makes comparisons between studies difficult. Therefore, for these steps of the experiments, we aimed to tackle some of the issues encountered with sample preparation and storage in relation to exosome size and concentration.

Since exosomes are classified as being submicron, a 0.22 μm filter was used to remove any potential contaminants from the suspension prior to TRPS analysis. On analysis, an NP100A pore membrane was used. The choice of nanopore for the TRPS analysis was based on previous experiments by the team of Dr. Stuart Hunt (Peacock *et al*., 2018). Other than pore size, other factors affecting the yield and concentration of samples are freezing and filtering prior to analysis. Freezing was found to greatly reduce the concentration, and so did filtering. However unfiltered and fresh exosomes could not be detected due to frequent pore blocking, so filtering had to be performed.

2.3.3 Size and Concentration Analysis of Exosomes by TRPS

Since different types of EVs can have a wide range of sizes, their size was utilized as a means for their identification and classification. Typical analysis generated by TRPS for EVs derived from IL-34- or GFP- overexpressing MG63 and KHOS cells, are illustrated in Figure 13. TRPS analysis gave measurement of the size distribution (nm) and concentration of EVs (particles/mL). This data shows that the vesicles isolated from both cell lines have a similar particle diameter ranging from 50-300nm, with the majority falling within the range of 50-100 nm, which is equivalent to the classification size for exosomes.

The average size distribution profiles of isolated exosomes as determined by TRPS, is shown in Figure 14. There was no significant difference between the size of exosomes isolated from GFP-overexpressing KHOS (KHOS-GFP) and IL-34-overexpressing KHOS (KHOS-IL-34) cells (78 nm vs 80 nm, p=0.4380, SD = 3.6 Fig.14a). In contrast, the mean particle diameter for control MG63 was slightly higher than the exosomes from IL-34 overexpressing cells (64 nm vs. 75 nm, *p value* = 0.0181, SD = 2.5 Fig.14b).

Next, the concentration of the isolated exosomes per cell after 24 hours was determined for each cell line. An estimation of the maximum amount of exosomes that can be produced from these cells was required, so that these values can then be used for future work, for example when using these exosomes to treat other types of cells. Conditioned media following 24 hours of incubation in exosome-depleted serum was collected, and the yield was calculated by TRPS as illustrated in the figure below. The data sets reveal that the highest yield of exosomes was generated from KHOS-IL34 cells with 1742 extracellular vesicles/cell compared to 628 vesicles/cell for KHOS-GFP (p = 0.0265, SD = 320.4, Fig 14c). In comparison, the MG63-IL34 cells yielded 447 particles per cell while MG63-GFP cells had 1010 particles (p = 0.0025, SD= 48.64 Fig14d). As shown in this data the presence of IL-34 did to some degree interfere with the concentration of the exosomes.

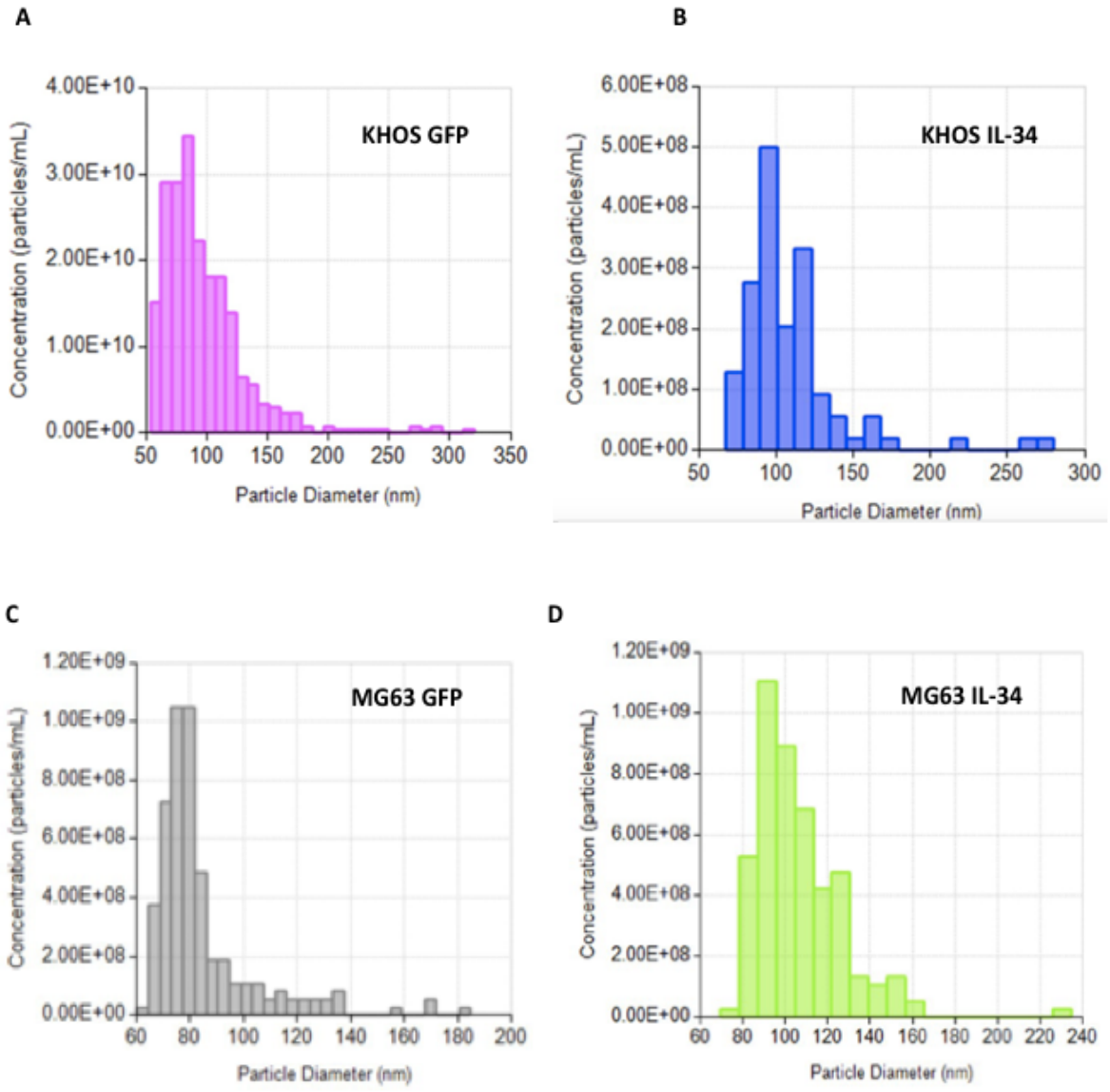

Figure 13: TRPS analysis of exosomes isolated from OS cell lines. EVs were isolated from cell culture media of (A) KHOS-GFP, (B) KHOS-IL-34 (C) MG63-GFP and (D) MG63-IL-34. Histograms are the result of the analysis of a minimum of 500 individual EV events. The size distribution is correlated to the concentration (particles / mL) of that sized particle in the sample.

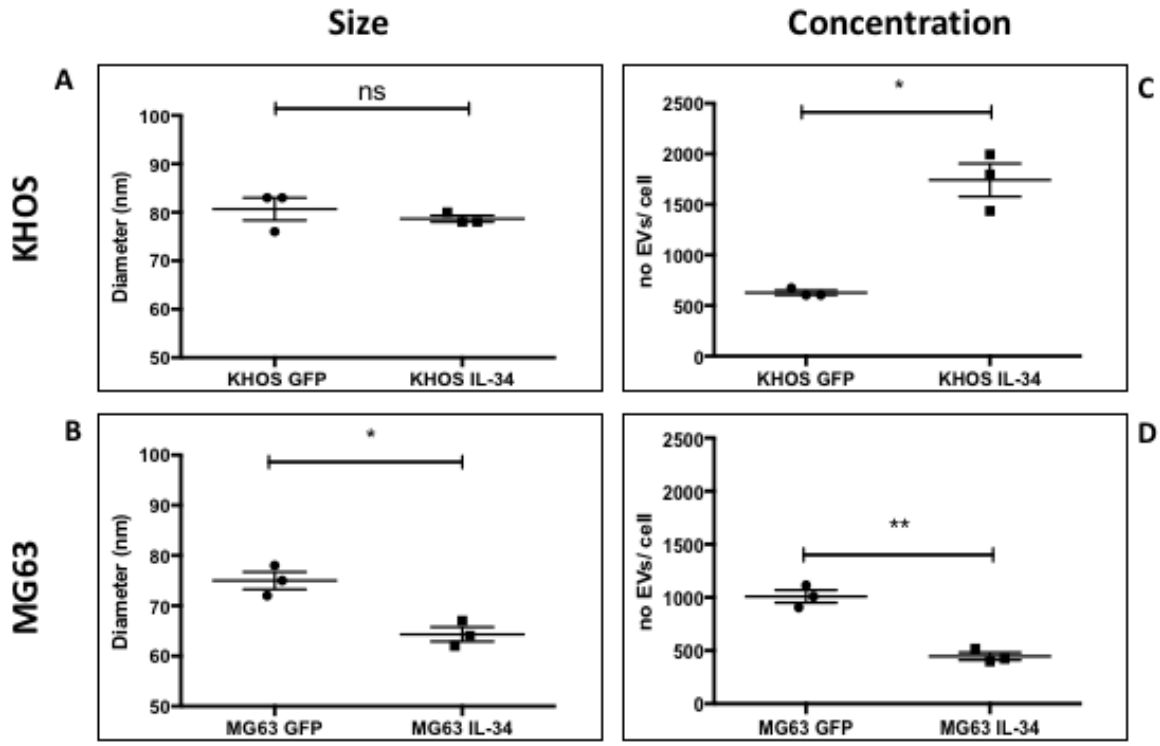

Figure 14: Size distribution and concentration profiles of exosomes. Panel A-B : Scatter plots for mean diameter in nanometers (nm) of exosomes isolated from KHOS and MG63. Panel C-D: Scatter plots for yield of exosomes showing the number of EVs/cell for HOS and MG63 after 24 hours in culture. Data is presented as ± SEM and n=3. Analysis by paired t-test, * $p < 0.05$, ** $p<0.01$ and ns = not significant.

2.3.4 Analysis by Western Blot

Following identification of size by TRPS, samples were next analysed by western blotting for well characterised exosomal markers CD63 and CD9. These tetraspanins are known to be specific, and present on the surface of most exosomes. Results are shown in Figure 15 confirming that CD63 and CD9 positive exosome populations were recovered with ultracentrifugation. Taken together, these results demonstrate that the protocols used, successfully isolated $CD9^+$, $CD63^+$ exosomes of 50-100 μm diameter from human OS cell lines.

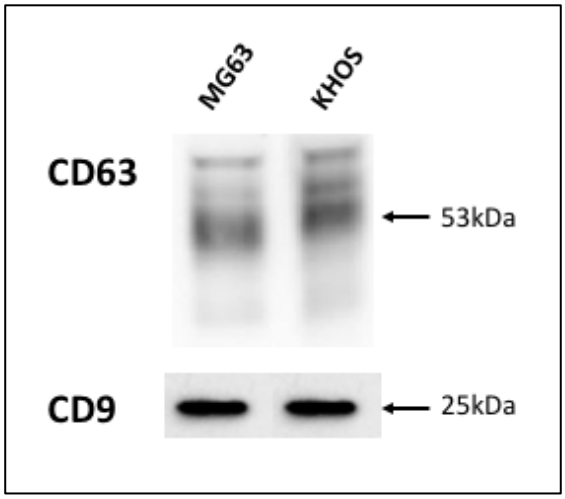

Figure 15: Western blot of CD63 and CD9. MG63 and KHOS derived exosomes expressed exosomal markers CD63 and CD9 as shown by Western blot.

2.3.5 Quantification of Exosomes

To measure the total amount of exosomes (proteins) present in the prepared exosome suspensions, the Bradford protein colorimetric assay was used. This gave an estimate of the amount of exosomes secreted by the cells, and needed as a quantitative measure for when preparing exosome samples for immunoblots. This method is currently the most common way of quantifying EVs in the literature (Théry *et al*., 2006), and is used to also quantify vesicles before they are added to other cells, in several activity assays (proliferation, migration, survival etc).

This method however, may have bias as EV samples may also contain soluble proteins and other protein aggregates, leading to errors in the quantification. This is an area of great contention in the EV field, where lack of standardisation makes comparisons difficult to interpret. Therefore, for the following experiments exosomes were quantified in terms of their concentration (vesicles/ml) as determined from the TRPS analysis, rather than as total protein content.

2.3.6 Osteosarcoma Derived Exosomes and Their Effect on the Proliferation of ADSCs

Given the relationship between tumour and stromal cells in tumour microenvironment, we aimed to determine whether exosomes from the OS cell lines, are able to influence the proliferation of adipose stem cells. We examined the effects of treating ADSCs with OS-derived exosomes; GFP- and IL-34-MG63 and KHOS overexpressing cells. Proliferation of adipose stem cells was measured in the presence of three different dilutions of exosomes (1:1, 1:2, 1:4), and conditioned media (C.M.) from the respective cell line prepared over 24 hours. Additionally, we examined the effect of proliferation of the ADCS treated with 5% DMSO for negative control, 10% FBS for positive control and no EVs (CTRL, 2% FBS) to assess proliferative effects in serum deprived conditions.

From the graphs presented in Figure 16, exosomes from OS did not modulate the proliferation of ADSCs at any of the concentrations applies. A two-way ANOVA with Dunnett's multiple comparison test, showed no significance between the optical density reading for either KHOS GFP/IL-34 or MG36 GFP/IL-34 derived exosomes (Figure 16). A significance was observed for the positive control (10% FBS) for each time point – 24, 48 and 72 hours indicating that as expected ADSCs with supplemental media proliferate at a higher rates than those supplied with normal media (No EVs).

However, OS cell conditioned media, effectively proliferates the adipose stem cells. Conditioned media from respective cell lines, had a positive effect on the proliferation rates, with the highest increase in optical density 24 hours after the media was added. This result suggests that conditioned media contains stimulatory factors to proliferate ADSCs, and in fact this effect has also been observed and reported in a similar study (Palumbo & Li, 2012

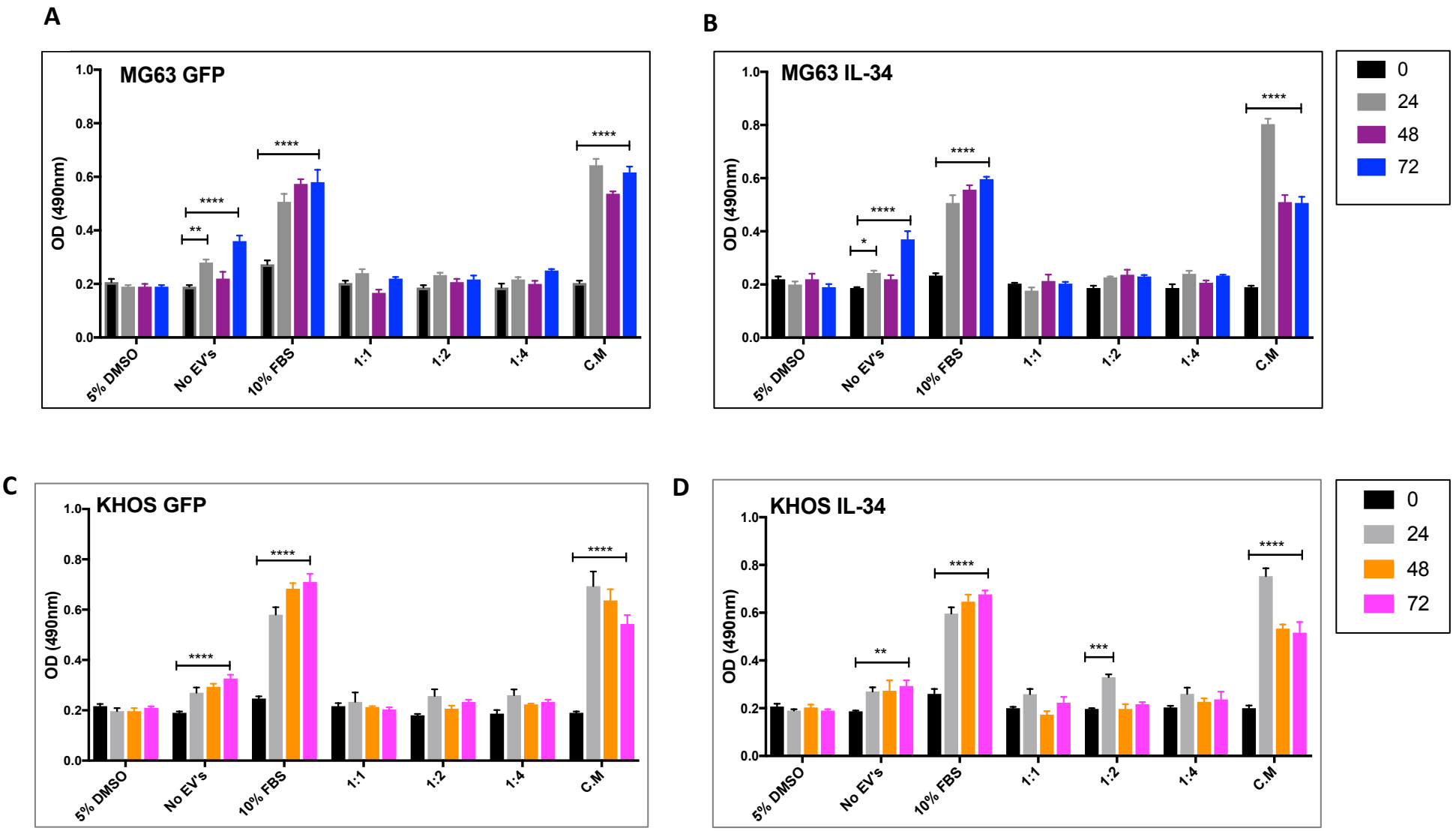
A
MG63 GFP
OD (490nm)
1.0
0.8
0.6
0.4
0.2
0.0
**
****
****
****
5% DMSO
No EV's
10% FBS
1:1
1:2
1:4
C.M
B
MG63 IL-34
*
****
****
****
0
24
48
72
C
KHOS GFP
****
****
****
D
KHOS IL-34
**
****
***
****

Figure 16: Effect of OS derived exosomes on proliferation of ADSCs. ADSCs were exposed to exosomes from osteosarcoma cell lines (A) MG63 GFP (B) MG63 Il-34 (C) HOS GFP and (D) HOS IL-34 in three decreasing dilutions (1:1, 1:2, 1:4) and conditioned media from respective cells. ADSCs were also supplemented with media containing no exosomes, 10% FBS (positive control), and 5% DMSO (negative control). Cell proliferation was assessed at different time points (0, 24, 48 & 72 hrs) by XTT assay and quantified by a microplate reader. Data is presented as mean ± SEM, and n=3. P values calculated by two-way ANOVA with Dunnett's multiple comparison tests. *p < 0.05, **p < 0.01, ***p < 0.001, ****p < 0.0001

2.3.7 Detection of IL-34 in Exosomes by ELISA

Despite the fact that knowledge on the involvement of IL-34 in the pathogenesis of OS is expanding, little is known about the functional communications of this cytokine in the microenvironment of OS or of any other cancer types. In parallel, since vesicles are emerging as some of the main protagonists in this dialog, the next step was to investigate whether the exosomes obtained from OS cells contained IL-34. For this a human enzyme-linked immunosorbent assay (ELISA) was used.

Exosomes purified from MG63 and KHOS cell lines overexpressing IL-34 or GFP, were assessed. For comparison, we used lysates from each of the respective cell lines, as well as lysates from parental MG63 and KHOS (not overexpressing) and HOS-GFP cell lines. Based on the ELISA results, there was no detectable IL-34 in the exosomes derived from OS cells overexpressing IL-34. In comparison, as expected, the lysates from their cell lines, marked positive for IL-34 with MG63-IL-34 having 160 pg/mL of IL-34 and IL34-KHOS having a mean of 580 pg/mL (Figure 17). This data indicates that internalisation of cytokines and associated proteins, is far from random, but is a complex event dependent on cell source, biogenesis and culturing conditions.

Following the results from this analysis, any plans to study the role of EVs and the contribution of IL-34 in this dialog were put on hold, and instead the focus was shifted on the role of primary cells in the cross communication between their exosomes and the microenvironment in OS.

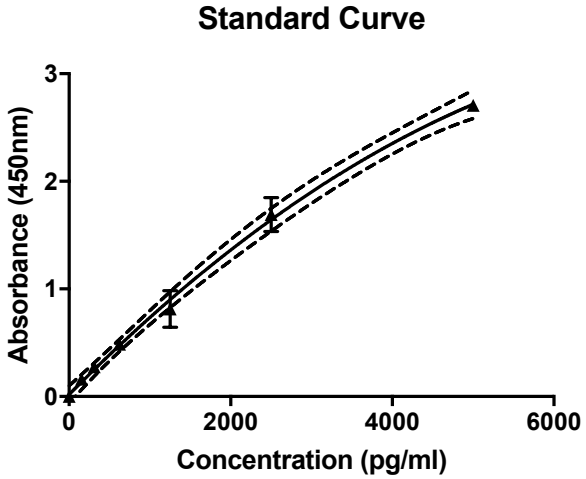

Concentration (pg/ml)	OD at 450nm
5000	2.70315
2500	1.80525
1250	0.69285
625	0.47535
312.5	0.27055
156.25	0.18715
0	0.07245

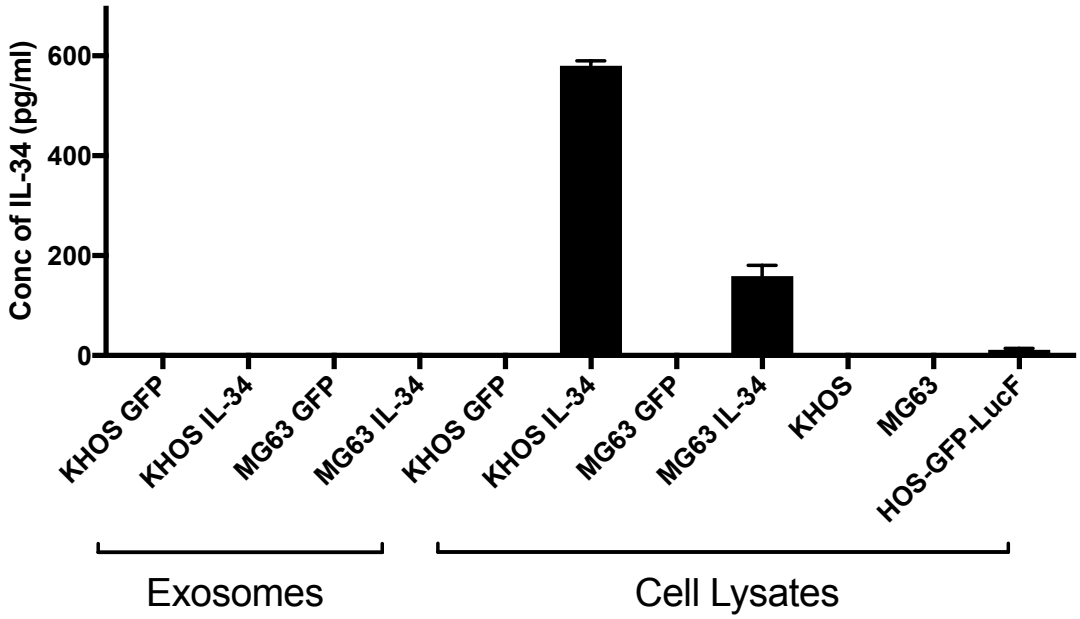

Figure 17: ELISA of IL-34 from osteosarcoma derived exosomes. To determine concentration of IL-34, 100ul of GFP/IL-34-KHOS and GFP/IL34-MG63 exosomes were subject to ELISA. In comparison, cell lysates from the respective cell lines were also tested. (A) Standard curve of known concentrations of human IL-34 (B) ELISA results showing concentration of IL-34 in exosomes and lysate samples. Data were normalised for total protein content. Results represent the mean ± SEM obtained from n=3 exosomes or lysate samples.

2.3.8 Exosomes Isolated from OS cells, Induced the Commitment of BMSCs and ADSCs Towards Adipogenesis

Based on the previous ELISA results, IL-34 did not seem to be present in the exosomes isolated from KHOS or MG63 Il-34 overexpressing cells. Therefore the experiments that followed from this point forward, were more focused on the relationship between osteosarcoma cells and their microenvironment rather than on the role of IL-34 and extracellular vesicles in osteosarcoma.

In the next analysis, the influence of OS derived exosomes on the differentiation of BMSCs was examined. Exosomes were purified from KHOS cells and cultured with naive BMSCs, with or without KHOS exosomes for 7 days. Gene expression of factors associated with MSC differentiation- osteogenic, chondrogenic and adipogenic factors were assessed at days 3 and 7 by RT-qPCR (Figure 18). This experiment was performed by Dr. Frederic Deschaseaux and Jean-Gerard Descamps from STROMALab (https://www.stromalab.fr/) at the French National Institute for Health and Medical Research (Inserm), University of Toulouse, France.

Data shows that the exosomes increased differentiation into adipocytes by upregulating gene expression of adipogenic factors. AP2 and PPARG2 were evaluated after 7 days of stimulation by the exosomes (Figure 18C). This indicated that EVs derived from OS promote adipogenic differentiation on MSCs. On the other hand, no effects were noted for chondroblastic differentiation whereas for osteoblastic differentiation, it can be noted that the osteogenic markers decreased on day 7 when treating with OS derived vesicles.

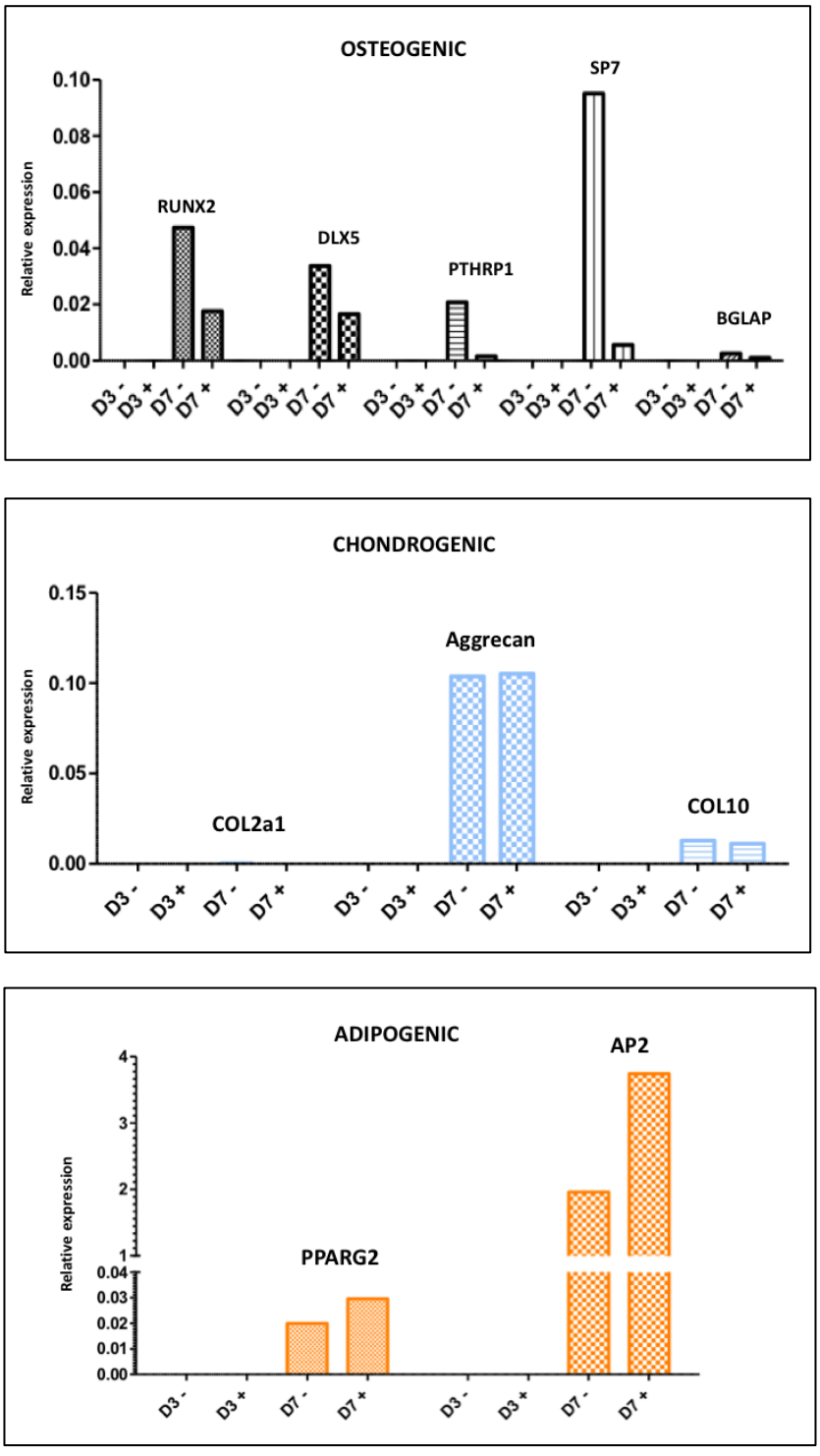

Figure 18: RT-qPCR of MSC lineage markers after co-culture with OS derived exosomes. Exosomes from KHOS cells were added into cultured MSCs, after differentiation into (A) osteoblastic, (B) Chondroblastic and (C) Adipogenic lineages. Exosomes were added (+) or not (-) into the cultures and lineage markers were evaluated by RT-qPCR at day 3 or day 7.

The next part of the results, are preliminary investigations on the two-way communication between OS and its microenvironment through exosomes derived from BMSCs and ADSCs. Human mesenchymal stem cells were isolated from human bone marrow aspirates, while adipose derived stem cells were obtained from human fat samples removed from patients who underwent abdominal liposuction in the plastic surgery department (Dr Frédéric Dechaseaux, Toulouse, FR). These cells were cultured and harvested for exosomes, with the methods described in previous section. The influence of BMSCs and ADSCs derived exosomes on the proliferation of OS cells, as well as their trafficking and protein composition are presented below.

2.3.9 Isolation of Exosomes From BMSCs and ADCSs

Similarly to previous experiments, exosomes were isolated from cell culture supernatants of BMSCs and ADSCs after incubation in exosome free serum for 72 hours. Following purification of the media by ultracentrifugation, the exosome pellet was analysed by TRPS for confirmation of size and concentration of exosomes (Figure 19). It could be noted that in comparison to OS cells, these primary cells secrete less exosomes, probably due to the lower proliferation rates that is characteristic of these cells.

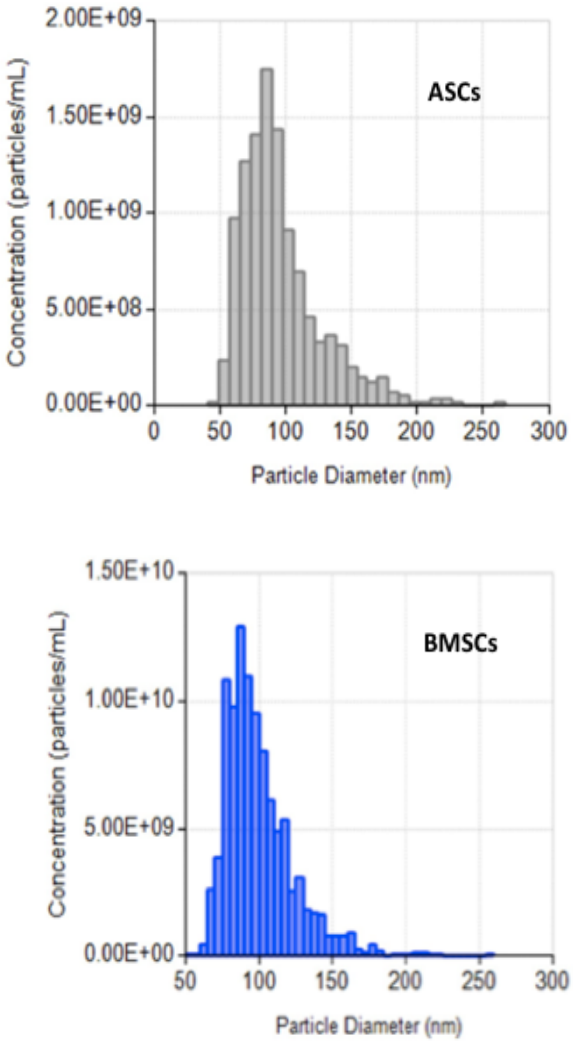

Figure 19: TRPS analysis of exosomes isolated from ADSCs and MSCs. TRPS results for (A) Adipose derived mesenchymal cells and (B) bone marrow derived mesenchymal stem cells. Histograms are the result of the analysis of a minimum of 500 individual EV events. The size distribution is correlated to the concentration (particles /mL) of that sized particle in the sample.

2.3.10 Exosomes from ADSCs Are Incorporated Into Osteosarcoma Cells.

To investigate whether exosomes from ADSCs can interact with OS cells, purified ADSC derived exosomes were labelled with a fluorescent dye (CM-Dil) prior to incubation with MG63 and KHOS cells. The cells were labelled with DAPI to visualize the nuclei, and cellular uptake of the exosomes was performed by confocal laser microscopy. CM-Dil labelled exosomes, were internalised by both OS cell lines, whereby exosome internalisation was observed from 6 hours, up until 24 hours from incubation, implying that exosomes derived from primary cells can be internalised by OS tumours (Figure 20 and Figure 21).

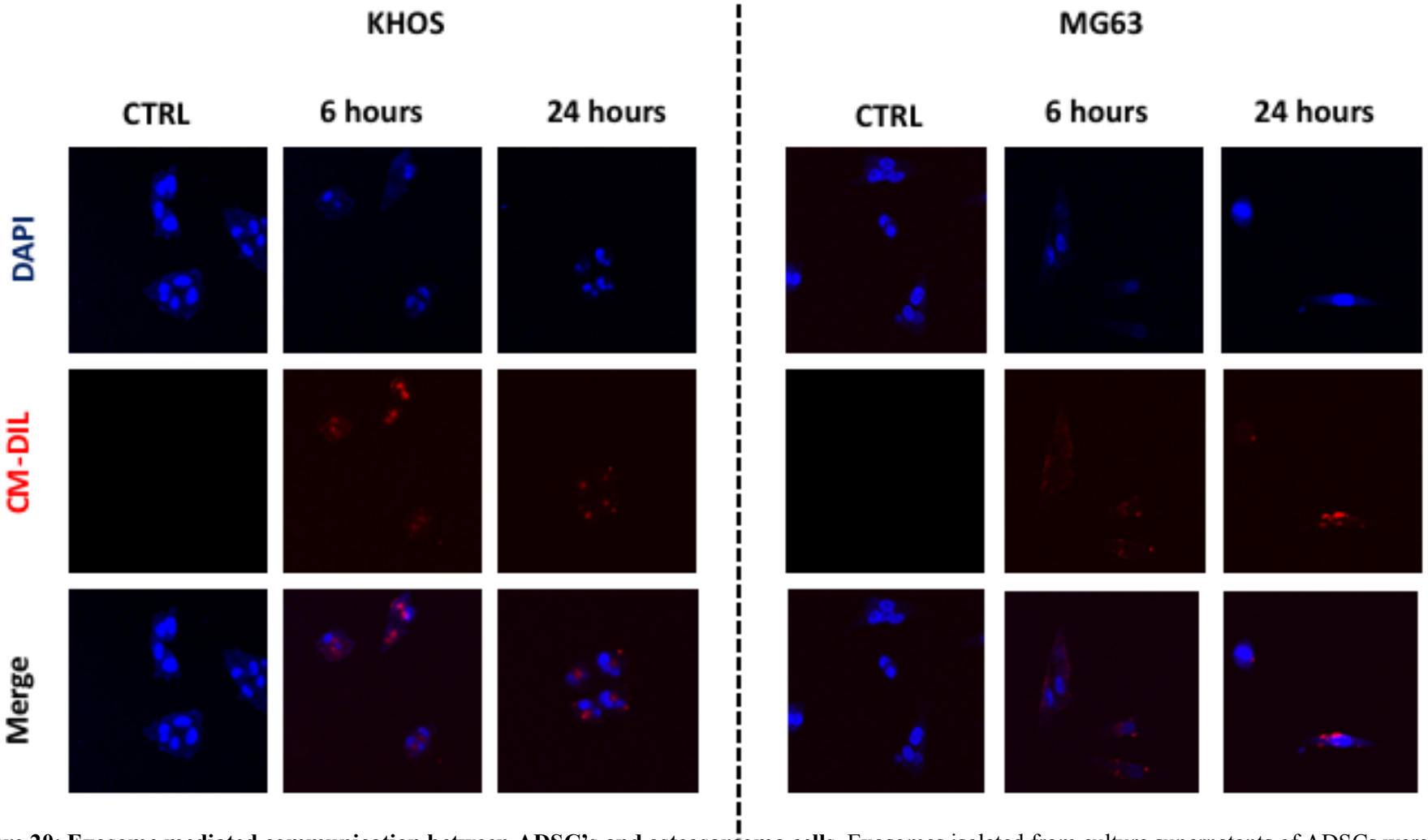

Figure 20: Exosome mediated communication between ADSC's and osteosarcoma cells. Exosomes isolated from culture supernatants of ADSCs were labelled with CM-Dil dye (red) and incubated with OS cells MG63 and KHOS for 24 hours. Nuclei were counterstained with DAPI (blue). Original magnification: x40

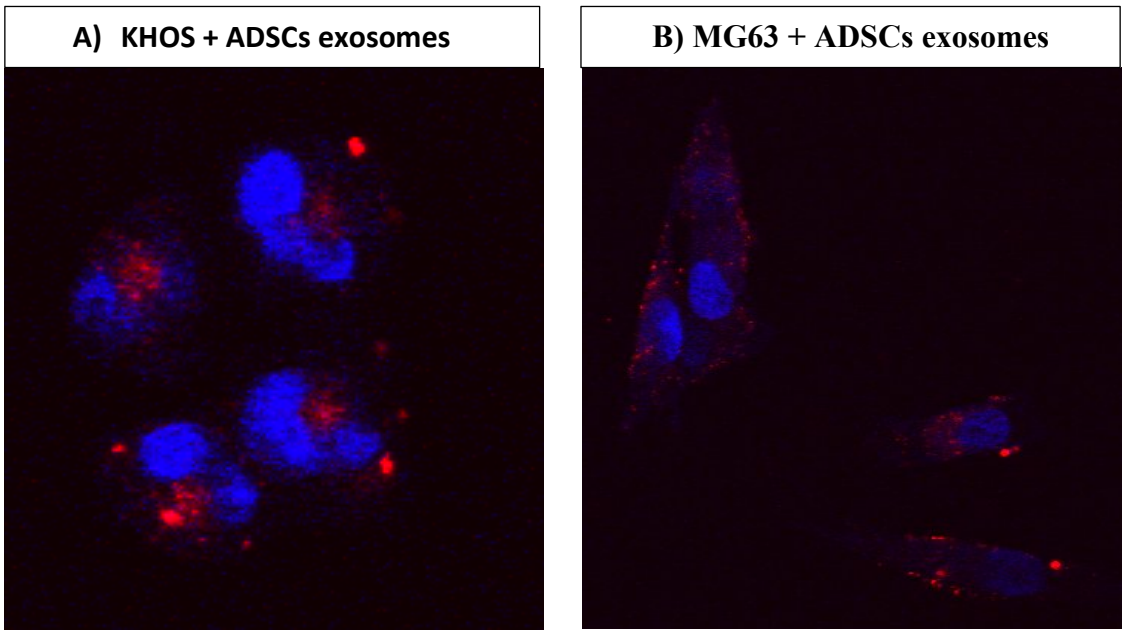

Figure 21: Confocal images of ADSC exosomes after incubation with OS cells. ADSC exosomes were co-cultured for 24hours with A) KHOS and B) MG63 cells. Blue: nuclei observed by DAPI staining, Red : exosomes. Magnification x40

2.3.11 Mesenchymal Derived Exosomes and Their Effect on the Proliferation of Osteosarcoma Cells

Next, to study the role of exosomes derived from primary stem cells on OS proliferation, we added preparations of these vesicles to MG63 and KHOS parental cell lines, and monitored proliferation rates by XTT assay. Proliferation was measured without exosomes present (No EVs) and in the presence of different dilutions of exosomes (1:1, 1:2, 1:4, 1:8 and 1:10). Additionally, we examined the effect of proliferation of the OS cells treated with 5% DMSO for negative control, 10% FBS for positive control.

Exosomes from ADSC cells, significantly increased the proliferation of MG63s in a timely (increase from 0 till 72 hours) (Figure 22A). This result can be examined in comparison to when no vesicles were supplied (control), confirming that the increase detected was an effect of exosomes. On the other hand, no difference in KHOS proliferation rates were observed between treatment with ADSCs derived exosomes in comparison to control (treatment with no exosome) (Figure 22B). These data demonstrate the involvement of exosomes in stem cell induced promotion of OS proliferation, and the cross-communication involved between these cell types

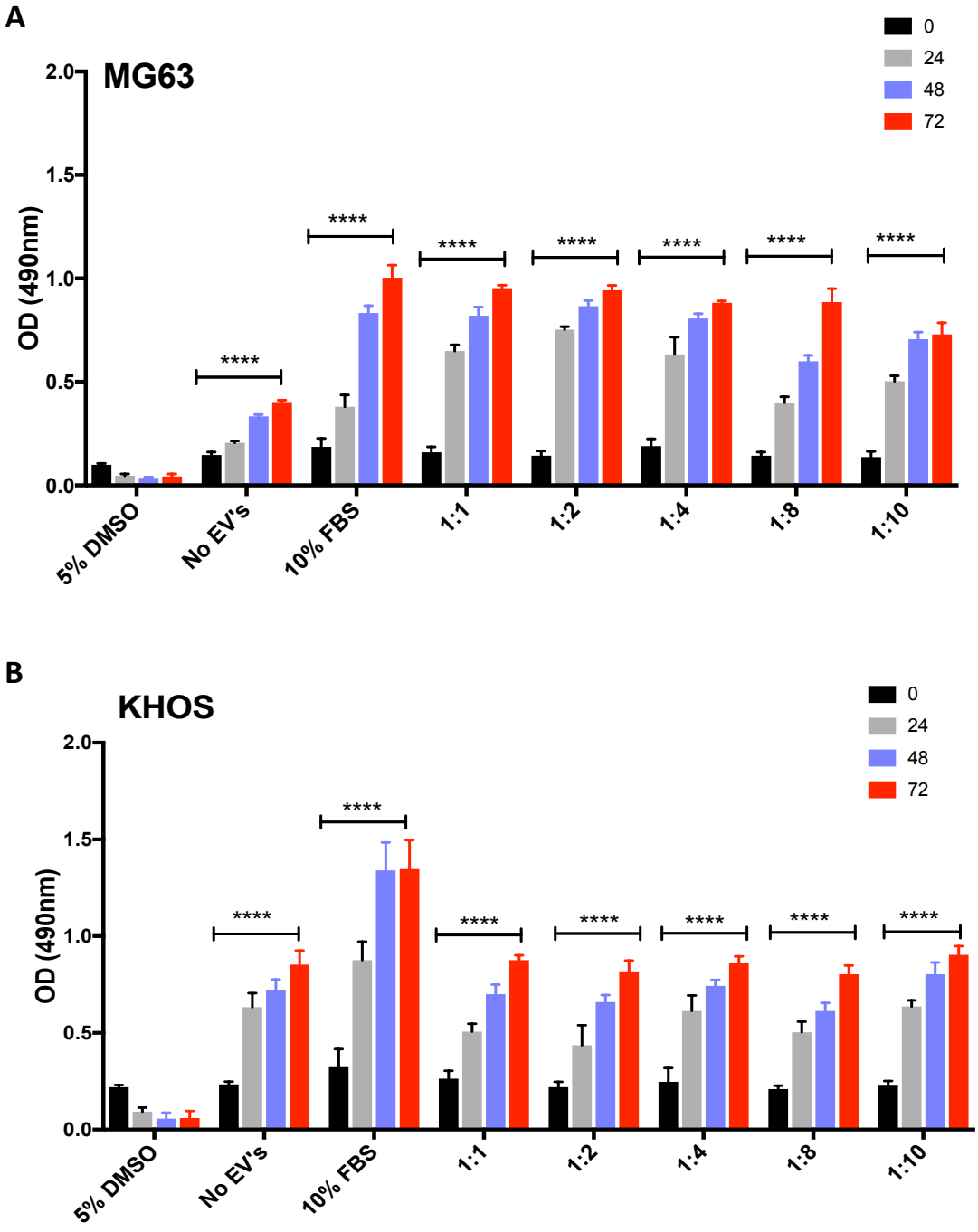

Figure 22: Effect of ADSCs derived exosomes on the proliferation of osteosarcoma cells. OS cells (A) MG63 and (B) KHOS were exposed to exosomes from ADSC cells in five decreasing dilutions (1:1, 1:2, 1:4, 1:8 and 1:10) OS cells were supplemented with media containing no exosomes (No EVs, CTRL) 10% FBS (positive control), and 5% DMSO (negative control). Cell proliferation was assessed at different time points (0, 24, 48 & 72hrs) by XTT assay and quantified by a microplate reader. Data is presented as mean SEM, and n=3. P values were obtained by two-way ANOVA with Dunnett's multiple comparison test, ****$p < 0.0001$

2.3.12 Analysis of Exosomes Content from BMSCs and ADSCs

Previous studies have shown that EV cargo is loaded with specific protein, mRNA, miRNAs, and lipids that may be transferred to target cells. The composition of these exosomes is still understudied, especially with regards to mesenchymal stem cells derived vesicles. To identify and characterise cytokines and chemokines that may play roles in the cross-communication in the tumour microenvironment, or by autocrine ways a human cytokine array was utilised.

Exosomes were purified from cell culture supernatants of BMSCs and ADSCs, and treated with RIPA buffer, to permeabilise their membranes and release the contents. The BCA assay was then used to quantify the protein content. The resulting supernatants were assayed for cytokine/chemokine levels, using a human cytokine array kit. Pixel densities for the different array proteins were defined and plotted (Figure 23). Both bone marrow and adipose derived mesenchymal stem cells released measurable levels of Serpin E1, Thrombospndin-1, Endoglin, Pentraxin-3, IGFBP-3, Osteopontin, IL-8, IL-6, IL-17A and FGF19 (Table 3). These results indicate that mesenchymal stem cells contain a specialised cargo and are able to exchange cytokines through exosome secretion and uptake. Refer to appendix for full list of cytokines.

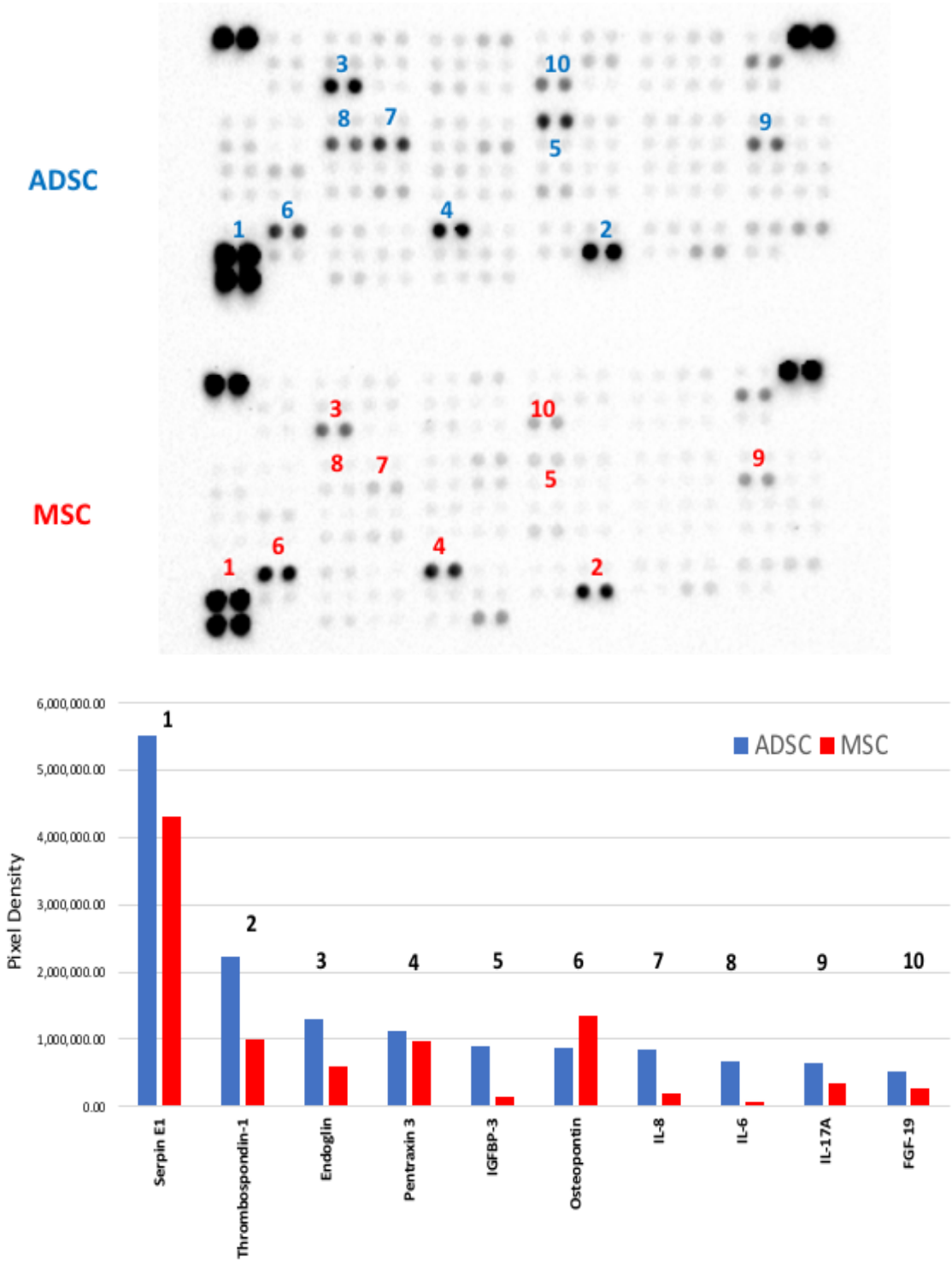

Figure 23: Cytokine and chemokine profile of exosomes released from BMSCs and ADSCc
Exosomes from primary cell lines were purified by ultracentrifugation and 50ug of total exosomal protein was harvested for immune cytokines using the Proteome Profiler Human XL Cytokine Array. (A) Cytokine array comparing content between ADSCS and BMSCS (B). The pixel densities for each spot were calculated using Image J software and plotted. (see supplemental Table 1 for arrangement of ABS on the array, and appendix for full list of cytokines).

Table 3: Table highlighting the characteristics of the cytokines found in BMSCs and ADSCs exosomes by cytokine profile array

Serpin E1	Serine protease inhibitor, often found upregulated in migratory cancer cells (Humphries *et al*., 2019)
Thrombospondin-1	A glycoprotein with anti-angiogenic functions. In OS, TSP-1 overexpression inhibited angiogenesis and tumour growth (Jian *et al*., 2019)
Endoglin	Membrane glycoprotein with a central role in angiogenesis, therefore important for tumour growth, survival and metastasis (Tian *et al*., 2017)
Pentraxin-3	Glycoprotein induced by pro-inflammatory cytokines thus a modulator of inflammation in tumours, correlated with grade and severity of tumours (Giacomini *et al*., 2018)
Insulin-like growth factor-binding protein 3 (IGFBP-3)	Stimulates cell proliferation but also inhibits apoptosis. A combination of these mitogenic and antiapoptotic effects has a profound impact on tumour growth (Yu & Rohan, 2018)
Osteopontin	Extracellular matrix glycoprotein implicated in the pathogenesis of a variety of disease states, including cancer, and several chronic inflammatory diseases (Lund *et al*., 2009)
Interleukin-8 (IL-8)	Cytokine that is a mediator of inflammation and acts as a chemoattractant for neutrophils and T-cells, also associated with cancer stem-cell like properties (Corrò *et al*., 2019)
Interleukin-6 (IL-6)	A pro-inflammatory cytokine associated with tumorigenesis and metastasis (Taniguchi & Karin, 2014)
Interleukin 17-A (IL-17A)	A pro-inflammatory cytokine. Upregulated during inflammation and contributes to disease severity including cancers by enhancing neutrophil infiltration and the production of pro-inflammatory chemokines (Fabre *et al*., 2018)
Fibroblast growth factor-19 (FGF-19)	Fibroblast growth factor implicated in the pathogenesis of several cancers (Somm & Jornayvaz, 2018)

2.4 SUMMARY

In this first chapter, we investigate the role of extracellular vesicles, specifically exosomes, derived from OS cells – MG63 and KHOS. Exosomes were successfully isolated using a series of centrifugation techniques, followed by size analysis and quantification by TRPS analysis using the Q-Nano platform. On estimation of the amount of exosomes that these cells produce, it was found that compared to MG63, KHOS cells produce higher yields of exosomes. Characterisation by Western blotting, revealed classical surface membrane markers CD9 and CD63 present on these isolated vesicles. Exosomes from these two OS cell lines, did not seem to have any proliferative effect on mesenchymal stem cells, however they induced the commitment of these cells towards adipogenesis. From these results it can therefore be proposed that OS exosomes can have an effect on differentiation and lineage abilities of stromal cells in tumour microenvironment.

Similarly, exosomes were also purified from bone marrow and adipose derived mesenchymal stem cells. Assays to study the functional role of these exosomes revealed that they are incorporated into OS cells - determined by confocal microscopy, and that they are able to induce proliferation of OS cells when compared to cells grown under serum-deprived conditions alone. Characterisation of the components of these vesicles by cytokine arrays showed that these exosomes contain a number of proteins associated with several biological processes including those related to tumour progression. Taken together, these data indicate a tumour supportive role for MSC derived exosome

CHAPTER 3

IL-34 AS A POTENTIAL THERAPEUTIC TARGET FOR OSTEOSARCOMA

3.1 INTRODUCTION

3.1.1 Mouse Models of Osteosarcoma

Mouse models of sarcoma have been highly important for investigating the mechanisms of tumorigenesis and metastasis, as well as for testing various possible therapeutic regimens. Models to represent primary bone tumours are numerous and can be generated via several ways (Uluçkan *et al.*, 2015). Injecting cell suspensions of either human (xenograft) or murine cells (allograft), is the most common method used to establish pre-clinical models of OS in mice. The cells are injected into either immunocompetent or immunodeficient animals, with the main advantage being that these models allow the growth of tumours whilst still keeping the original tumour architecture (Jacques *et al.,* 2018).

Orthotopic models: Establishing syngeneic or xenogeneic models is achieved by two methods of cell-injections. The first, is injecting cells close to the bone, usually in close proximity to the tibia or femur, and is termed as "para-osseous inoculation". The second method is by injecting directly into the bone termed as "intra-osseous inoculations" with the latter being more technically difficult to perform. The advantages of these orthotopic models is that the original site for tumour development is reproduced (Jacques *et al.,* 2018).

Induction of primary bone tumours by para-osseous cell injections are commonly used with MOS-J cells for the set up syngeneic models, or with human MNNG-HOS cells to generate xenogeneic models (Gobin *et al.,* 2013; Lamoureux *et al.,* 2014). Similarly, induction of bone sarcomas by intra-osseous injection of cancer cells can be achieved by human 143B

or K7M2L2 OS cells in SCID or nude mice. This model is able to reproduce highly metastatic conditions with the formation of lung nodules (Meier *et al.,* 2017).

Heterotopic models: Other models for directly inoculating cancer cells include those where cells are injected into heterotopic sites. These include subcutaneous cell injections, or intraperitoneal into the muscle, renal capsule or kidney (Jacques *et al*., 2018). Human 143B, as well as c-Fos transgenic mouse OS cells have been successfully injected subcutaneously to form tumour masses containing bone (Grigoriadis *et al*., 1993; Zhou *et al*., 2017). An added approach to subcutaneous injections has been developed in which cells are incorporated into a Matrigel based matrix providing a scaffold of active bio-molecules that is able promote cell engraftment. This was successfully performed by Duan *et al*., using KHOS OS cells in a 1:1 Matrigel matrix ratio (Duan *et al*., 2017) and similarly also Saos-2. Cell inoculation into heterotopic sites was also achieved intraperitoneally by injection of Saos-2 in nude mice, and resulted in the induction of xenograft models of OS (Chen *et al*., 2017).

The main advantage of heterotopic inoculations is the ease of execution coupled with the large variety of cancer cells and diverse injection sites. This method can also be used to explain whether cells have the potential to form tumours *in vivo* in a cell-autonomous way, in the absence of a bone environment. Despite these advantages, these models lack a fundamental property, in that they fail to reproduce the bone microenvironment and the vicious cycle established in this dialog, and therefore do not emulate fully the steps of tumour development (Cherrier *et al*., 2005; Grimaud *et al*., 2002).

The model of choice ultimately depends on the aim of the study, with each model having both advantages and limitations. Models should aim to address the issue of genetic heterogeneity, in that they should be close to human tumours as much as possible, and to imitate the natural characteristics of the disease with an adapted tumour microenvironment (Guijarro *et al*., 2014).

Tumour transplantations: Transplantation of tumour fragments from a donor to a recipient addresses these issues by maintaining cellular heterogeneity and genetic background (Guijarro *et al*., 2014). Primary bone tumours induced by this method can be achieved by injecting cells subcutaneously or in close contact to the bone. Tumour fragments from HOS-osteosarcoma cells were successfully transplanted into the rear flank of nude mice (Westrøm *et al*., 2016) and similarly, murine POS-1 cells were inoculated in the hind footpath of C57BL6 mice (Lamoureux *et al*., 2007).

Genetically engineered models: Genetically engineered mouse models of OS address some of the limitations present with orthotopically induced models; mainly the possible instability of cell lines with repeated passages, and difficulty in assessing whether metastasis originates from the primary tumour mass, or is a result of escape from injections at the time of inoculations. In these models, spontaneous formation of OS is genetically provoked (Grigoriadis *et al*., 1993). The mice have genetic mutations in tumour suppressor genes leading to OS forming as a secondary malignancy and thus forming tumours very close to the human context. The main disadvantage of such models is that they cannot reflect the high molecular heterogeneity of the disease (Botter *et al*., 2015).

3.1.2 Immunotherapy as a Therapeutic Approach for Osteosarcoma.

As stated in the introductory chapter, there is an urgent need for new therapeutic options for the treatment of OS and mostly for patients that are in high risk groups i.e.- patients who are poor responders, patients with high metastatic disease, or patients in relapse. Various new therapeutic approaches are emerging that target not only tumour cells directly, but also the tumour niche by acting on signalling molecules involved in apoptosis, drug resistance and cell proliferation (Luetke *et al*., 2014). For the purpose of this thesis, a brief overview of current immunotherapies and immunomodulators will be given.

The local immune tolerance and immune cells recruited by cancer cells in the tumour, is a major key component of cancers. A promising avenue of treatment is the use of checkpoint inhibitors/immune modulators. These target molecules serving as the “checks and balances” of the immune responses. By activating stimulatory molecules and/or blocking

inhibitory molecules, these treatments show promising anti-cancer immune response (Brown *et al*., 2017; Heymann *et al*., 2016).

One such molecule that has become strategic in targeting the immune response, is programmed cell death ligand 1 (PDL-1). PDL-1 is a cell surface protein that represses cytotoxic $CD8^+$ T-cell mediated immunity, and is frequently expressed in numerous cancers including OS (Miwa *et al*., 2019). Increased expression of PDL-1 and infiltration of T lymphocytes has been shown to be correlated with metastatic high grade OS (Sundara *et al*., 2017). Two major anti-PD-1 antibodies are currently in progress in OS. A phase II study of Prembozilumab (NCT02301039) in patients with advanced sarcoma, and a phase I/II of Nivolumab (NCT02304458) in younger patients with recurrent or refractory sarcoma (Tawbi *et al*., 2017).

Infiltration of macrophages contributes towards the progression of OS, and therefore several strategies have been developed to target this aspect. One such agent is mifamurtide (L-MTP-PE) which activates the production of macrophages. Administration of mifamurtide in combination with chemotherapy resulted in improved overall survival by 10% (Meyers *et al*., 2008). There is however controversy on the execution and design of the above study, and therefore this agent is not universally admitted. A phase II/III clinical study of mifamurtide (NCT01459484) administered post-surgery in combination with chemotherapy to overall 200 patients, is currently underway (NIH Clinical Trials, 2019).

Another major avenue of immunotherapy for OS is adoptive T-cell therapy. In this treatment, T-cells are removed from the patient and genetically modified to enhance their activity, after which they are re-introduced into the patient with the aim to bring about improved anti-tumour response (Brown *et al*., 2017). A phase I trial of the chimeric antigen receptor (CAR) T cells genetically modified to express a protein receptor that recognises GD2, a protein found on most OS cells, is currently underway for both children and adults with OS (NCT019553900, NCT02107963). Similarly, a phase 1 trial of T-cells engineered to recognise and target several tumour antigens (NY-ESO-1, MAGEA4, PRAME, SSX and survivin) is currently underway for patients with solid tumours of OS, synovial sarcoma and rhabdomyosarcoma (NCT02239861) (NIH Clinical Trials, 2019).

Preparation of other immune cells such as natural killer (NK) cells and dendritic cells are in evaluation for phase I/II clinical trials, with the main aim of re-activating the immune response against cancer cells thus improving the local immune tolerance. Example is clinical trial NCT02409576 in which activated, haploididentical NK cells are administered and the effect on clinical response is analysed (Heymann & Heymann 2017).

The use of monoclonal antibodies to target specific antigens in tumours is another major therapeutic approach based mostly on targeting the immune niche. A phase II trial to target RANKL and associated bone remodelling, called denosumab (NCT02470091) is underway in children with OS (Miwa *et al.,* 2019). A second major therapy using monoclonal antibodies are two phase II clinical trials of dinutuximab which targets GD2, a marker of cancer stem cells found on OS cells, in patients with recurrent OS (NIH Clinical Trials, 2019) (Brown *et al*, 2017).

3.1.3 Rationale

Based on recent studies on the role of the immune system in OS development, it is evident that the immune niche comprises several new potential therapeutic biomarkers and targets for the treatment of OS. The survival rates of sarcoma patients have not been improved over the last four decades, and there is therefore an urgent clinical need to identify new therapeutic targets, and develop new therapeutic approaches in order to improve patient survival rate.

The cytokine IL-34 has been proposed to be a major protagonist in the immune niche and based on previous work (Chemel *et al.,* 2012; Segaliny *et al.,* 2015) it could be a potential new candidate for immunotherapies in patients. The goal is to target this cytokine by anti-cytokine treatment, and translate our pre-clinical investigations into clinical applications, with the final goal being to improve survival rates and quality of life (development of drugs with less toxicity and side effects) to patients with this malignancy.

3.1.4 Aims and objectives

The main objective of this chapter is to investigate IL-34 as a potential new therapeutic target by the use of pre-clinical *in vivo* mouse models of OS. By using an anti-cytokine antibody, the effects of IL-34 blockade on OS tumor development and progression will be investigated.

Specific aims

6. To set up allograft and xenograft models of OS using mouse (MOS-J) and human (MNNG-HOS) OS cells respectively.
7. To perform a dose-response analysis of IL-34 blocking antibody and evaluate the response on tumour growth.
8. To investigate the treatment effectiveness of anti-murine and anti-human IL-34 blocking antibody on tumour progression.
9. To evaluate the impact of combining anti-murine IL-34 with the chemotherapeutic agent doxorubicin.
10. Using a combination of immunohistochemistry and analysis of bone architecture, the effects of the treatments and any potential mechanisms on tumour physiology are to be investigated.

3.2 METHODS

3.2.1 Materials, Reagents and Equipment Used

A. CELL CULTURE REAGENTS	
DMEM Medium + GlutaMAX, 2026753	Gibco
Fetal Bovine Serum, 10270-106	Gibco
Phosphate Buffered Saline, 10010023	Gibco
RPMI 1640 Medium + GlutaMAX, 11879020	Gibco
Trypsin Solution (10x), 59427C	Gibco
B. IN-VIVO REAGENTS	
Doxorubicin; 141210070	ITH Pharma
Ethylenediaminetetraacetic acid (EDTA); 6381-92-6	Fisher Scientific
Mouse anti-human (Clone: B-T34) IL34; RSP-R160513	Diaclone (france)
Rat anti-murine (Clone: Sheff5) Il-34; 160719-Sheff5	Diaclone (France)
Isofluorane ; 6064291	Zoetis
Performaldehyde; 30535-89-4	Fisher Scientific
C. IMMUNOHISTOCHEMISTRY REAGENTS	
Bovine Serum Albumin (BSA); SLBR0417V	Sigma-Aldrich
DAB Peroxidase Substrate Kit; SK4100	Vector Labs
DPX Mountant for Histology; BCBH4393V	Sigma-Aldrich
Eosin; E6003	Sigma-Aldrich
Ethanol, Absolute 99.8%; 64-17-5	Fischer Scientific
Goat serum blocking solution; S1000	Vector Labs
Gills Haematoxylin No 2; GHS216	Sigma-Aldrich
Hydrogen Peroxide; 7722-84-1	Fisher Scientific
Methanol, 99.9% Analytical reagent Grade; 67-56-1	Fisher Scientific
Paraffin; SL9176	Leica
PBS Tablets; BR0014G	Oxoid
Paraformaldehyde; 30525-89-4	Fisher Scientific
Rabbit serum blocking solution; S5000	Vector Labs

Target Retrieval Solution, Citrate pH6 ; S1699	DAKO
Tris Base; BCBL6643V	Sigma-Aldrich
Triton-X; T9284	Sigma-Aldrich
Tween-20; 9005-64-5	Fisher Scientific
Vectastain Elite ABC HRP Kit; PK-6100	Vector Labs
Xylene (Analytical Reagent Grade); 1330-20-7	Fisher Scientific
D. ANTIBODIES	
Biotinylated goat anti-rabbit IgG antibody; BA-1000	Vector Labs
Biotinylated rabbit anti-rat (mouse adsorbed) IgG antibody; BA-4001	Vector Labs
Rabbit monoclonal (EPR19518) anti-CD163 antibody; Ab182422	Abcam
Rabbit monoclonal (SP6) anti-Ki67 antibody; Ab16667	Abcam
Rabbit polyclonal (ASP175) anti-caspase-3 antibody; 9661	Cell Signalling
Rat monoclonal (CI: A3-1) anti- F4/80 antibody; MCA497R	Bio-Rad
Rat monoclonal (SZ31) anti-CD31 antibody ; DIA-310	Dianova
E. SOFTWARE	
Graph Pad Prism Version 7	Graph pad software
QuPath	OmicX

3.2.2 Animal Investigations

Animals were housed at the University of Sheffield Biological Services Unit. All experiments were conducted according to the institutional ethical guidelines under the Home Office project licence P4C7433CD, and personal licence number IO6008638.

3.2.3 Set-up of Osteosarcoma Models

To study the effects of inhibiting IL-34 on OS growth, metastasis, and bone associated re-modelling, xenograft and allograft models were set up. Tumour cells were inoculated into immunocompromised mice for xenogeneic models, and immunocompetent mice for syngeneic models. The different cell lines used for the paratibial *in vivo* models are described in the table below (Table 4).

Table 4: Table outlining the cell lines used for setting up *in vivo* osteosarcoma models

Model	Cell Line (Species)	Origin	Mouse strain
Xenogeneic Model	HOS-MNNG (human)	HOS from ATTC and transformed with MNNG (a carcinogenic nitrosamine) (Lamoureux *et al*., 2014)	BALB C/Nude
Syngeneic Model	MOS-J (mouse)	Murine osteogenic cell line from spontaneous chondroblastic OS (Lamoureux *et al*., 2014) Provided by Prof Len Schultz, Jackson Lab, USA (Joliat *et al*., *2002)*	C57BL/6J

3.2.4 Paratibial Injections of Osteosarcoma Cells

3.2.4.1 Preparation of cells

Five-week old mice were purchased from Charles River (UK) and allowed to acclimatize for a week after arrival. Mice were maintained under pathogen free conditions throughout the duration of the experiment. Animals were no older than 6 weeks on the day of tumour cell inoculation. On the day of injection, MNNG-HOS or MOS-J cells were trypsinized, washed two-times with PBS to remove serum residues, spun down and resuspended in PBS before inoculation. Mice were anesthetized by inhalation of isofluorane/air mixture (2%, 1 L/min). Complete anaesthesia was assessed by pinch reflex, and the procedure was only carried out if animals did not withdraw the paw.

3.2.4.2 Paratibial inoculations

The anaesthetised mice were slowly injected with the cell suspension by maintaining the legs outstretched between the thumb and the index finger, and then applying the needle perpendicular to the tibia. Before injecting the cells, the bone was scratched with the tip of the needle in order to activate the periosteum. Twenty microliters of cell suspension containing up to 250,000 MNNG-HOS cells or 125,000 MOS-J were injected per mouse in close contact to the activated periosteum. The animals were then monitored closely post injection and placed into an incubator at 33°C to recover. The weight of the mice was measured before they were injected, and monitored twice a week throughout the duration of the experiments.

3.2.4.3 Tumour volumes

The above way of inoculating tumour cells, known as paratibial inoculations, leads to rapid tumour growth in the soft tissue with secondary contiguous bone invasion. Tumours appeared at the injection site 10 days later, and the tumour volumes were measured 3 times weekly using calipers for the duration of the experiments. Tumour volumes were calculated by measuring two perpendicular diameters (mm) on each tumour, using the following formula: $V=0.5 \times L \times (S)^2$ in which L and S are the largest and smallest perpendicular

diameters respectively (Lamoureux *et al*., 2014). The mean diameter of the tumours was not allowed to exceed 1.5 cm.

3.2.5 Preparation of Injectables

3.2.5.1 PBS injections

PBS served to function as a vehicle control. 0.1 mL of sterile PBS was injected using a 1 mL sterile syringe and a 25-gauge needle. All vehicle control injections where given intraperitoneal.

3.2.5.2 IL-34 antibodies injections

Anti Il-34 blocking antibodies where provided by Diaclone (France). Such antibodies are currently not commercially available, with Patent number WO 2016/097420 AI. Anti-murine IL-34 (SHEFF-5) was supplied at 2.48 mg/mL, whilst anti-human IL-34 (B-T34) was supplied at 1.5 mg/mL. Each antibody was made up to a stock solution of 1 mg/kg diluted in PBS and stored at 4°C until use. The antibody was administered accordingly, depending on the dose required, using a 1 mL sterile syringe and a 25-gauge needle, via the intraperitoneal route.

3.2.5.3 Doxorubicin injections

Doxorubicin was purchased from ITH Pharma (London) at a stock concentration of 2 mg/kg. The required concentrations (1 mg/kg, 2 mg/kg and 3 mg/kg) where prepared by diluting DOX in sterile PBS and administering the drug at 0.1 mL increments using a 1 mL sterile syringe and 23-gauge needle. The drug was given by intravenous injections weekly or bi-weekly (depending on dose needed to be administered).

3.2.6 Evaluating the Impact of Injecting Different Cell Concentrations of MOS-J Cells, on Tumour Growth and Lung Metastasis

The aim of the initial *in vivo* experiment was to assess kinetics of tumour growth upon injecting different cell concentrations of MOS-J cells for setting up a syngeneic model. The objective was to determine the ideal cell concentration for use in future experiments, and assess the impact of such concentrations on lung metastasis.

Six-week old immunocompetent C57BL/6 mice were used. Three groups of 3 mice were formed, one for each different cell concentration; (Group 1: 125,000 cells/mouse, Group 2: 250,000 cells/mouse and Group 3: 500,000 cells/mouse). The mice were monitored for 21 days and tumour growth was measured three times weekly.

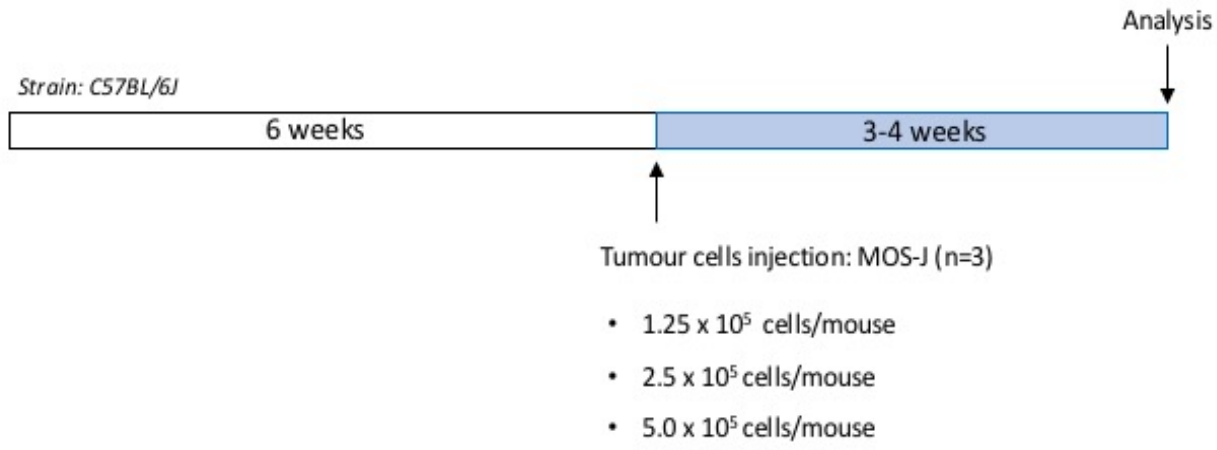

Figure 24: Experimental design of tumour kinetics in an allograft model of osteosarcoma.

3.2.7 Evaluating the Dose-response of Anti-murine IL-34 Antibody on Tumour Growth in a Syngeneic Osteosarcoma Model

Following the determination of the optimal cell concentration for MOS-J cells, we proceeded to perform a dose response analysis of the antibody in order to determine the optimal dose and best efficacy. Anti- IL34 antibody was given at three different doses with an intermediate dose set as 4 mg/kg. Two additional doses were given: a lower dose (1 mg/kg) and a higher dose (8 mg/kg). Intra-peritoneal injections were given three times weekly, as previous experiments.

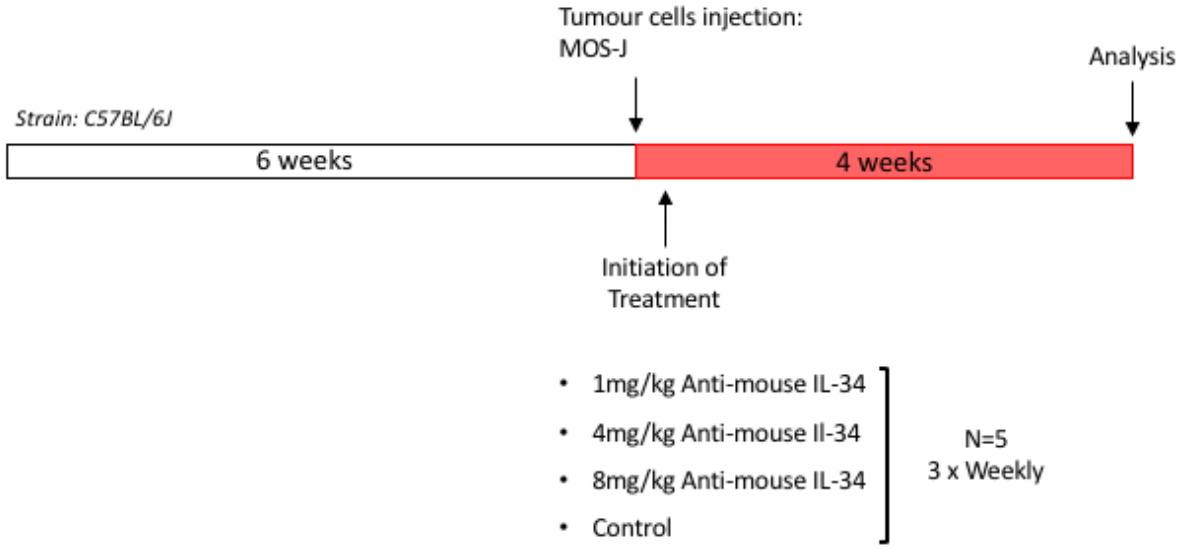

Figure 25: Experimental design of a dose response analysis of anti-Il34 antibody (doses: 1 mg/kg, 4 mg/kg and 8 mg/kg, intraperitoneal, three times/week) in an allograft model of OS.

3.2.8 Evaluating the Treatment Effectiveness of Anti-murine IL-34 Antibody in a Syngeneic Osteosarcoma Model

The previous *in vivo* study showed that the dose of antibody used had a positive impact on tumour reduction, and therefore this was established as a potential working dose. For the next experiment, we proceeded to determine the effectiveness of the anti-murine IL-34 antibody for an allograft model. Mice (n=12) where treated with 4mg/kg of anti-murine IL-34, three times weekly, and PBS as control. Tumour growth kinetics was assessed as previously described.

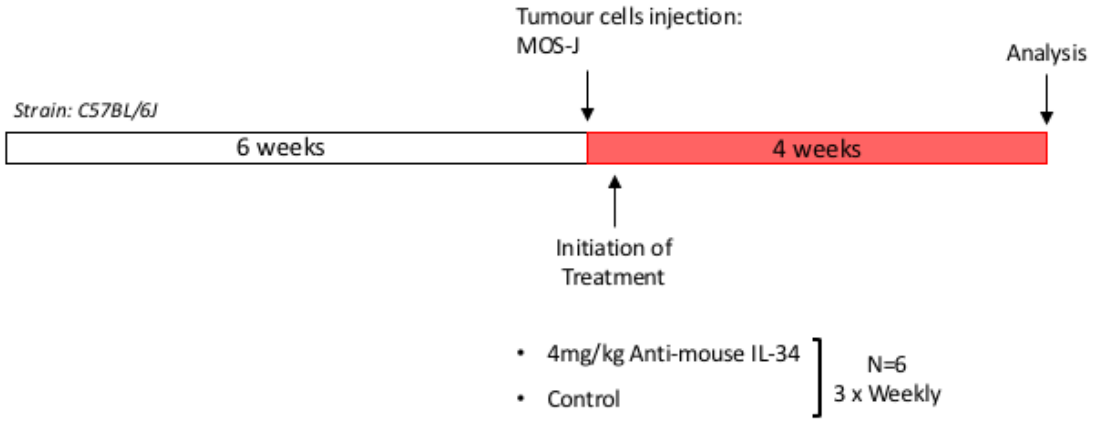

Figure 26: Experimental design of a syngeneic model of osteosarcoma.

3.2.9 Evaluating the Efficacy of Anti-murine and Anti-human IL-34 Antibody on Tumour Growth in a Xenogeneic Osteosarcoma Model

The aim of the next *in vivo* experiment was to establish a xenogeneic model and (i) assess the therapeutic efficacy of anti-IL-34 antibodies on OS tumour growth, and (ii) to determine which is the most effective way to potentially block IL-34 i.e. blocking tumour derived IL-34 (treating with anti-human IL-34) or blocking IL-34 in the tumour microenvironment (treating with anti-murine IL-34).

Six week old, female Balb/C nude mice were each injected with 250,000 MNNG-HOS cells. The mice where then randomly divided into three groups (n=6) and treated intraperitoneally with either anti-mouse IL-34 antibody or anti-human Il-34 antibody, at 100 μg/mouse, three times weekly for 3 weeks. PBS and control isotypes were used as a vehicle controls. Tumour growth was monitored by measuring tumour volumes twice weekly, whilst tolerance to the treatment was assessed once a week by measuring weight.

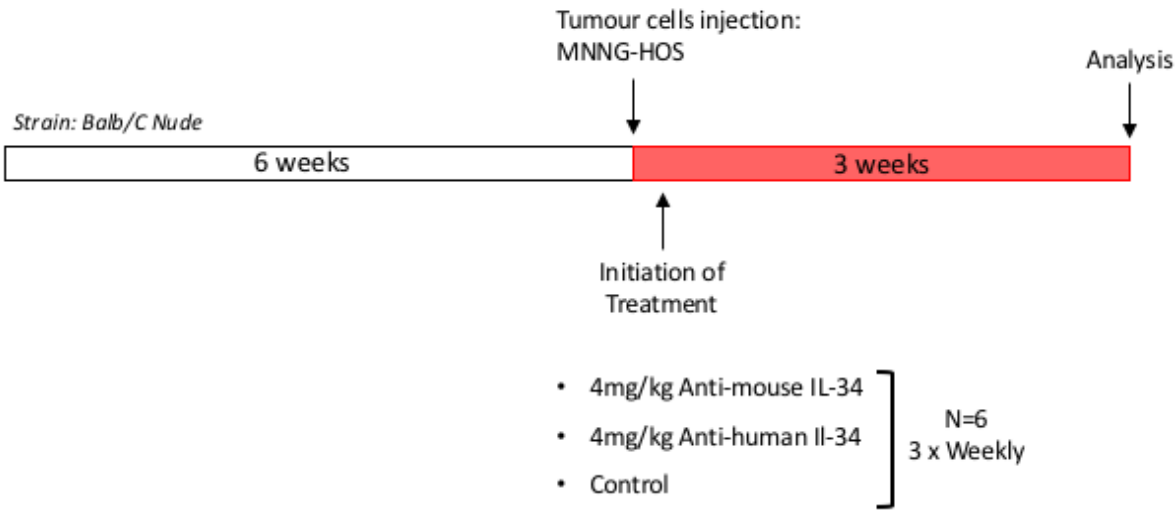

Figure 27: Experimental design of a xenogeneic model of osteosarcoma. Anti-IL34 antibodies (anti-mouse and anti-human IL-34, intraperitoneal, 4 mg/kg, three times/week) where given to asses their therapeutic efficacy on tumour growth and metastasis.

3.2.10 Tolerance and Effectiveness of Doxorubicin in the Mouse MOS-J Osteosarcoma Model

Following the results from the previous experiments and having established that blocking IL-34 in the microenvironment of OS delays tumour growth, the potential of treating with anti-IL34 antibody in combination with a chemotherapeutic drug was investigated.

In order to choose the optimal chemotherapy dose for the MOS-J model, we aimed to compare the effect on tumour growth when treating with different doses of the chemotherapeutic agent doxorubicin. Three groups of 3 mice each (n=3) where set up and 125,000 MOS-J cells where injected per mouse. Each group received different doses of doxorubicin: 2 mg/kg, 3 mg/kg and 4 mg/kg weekly, plus a control group.

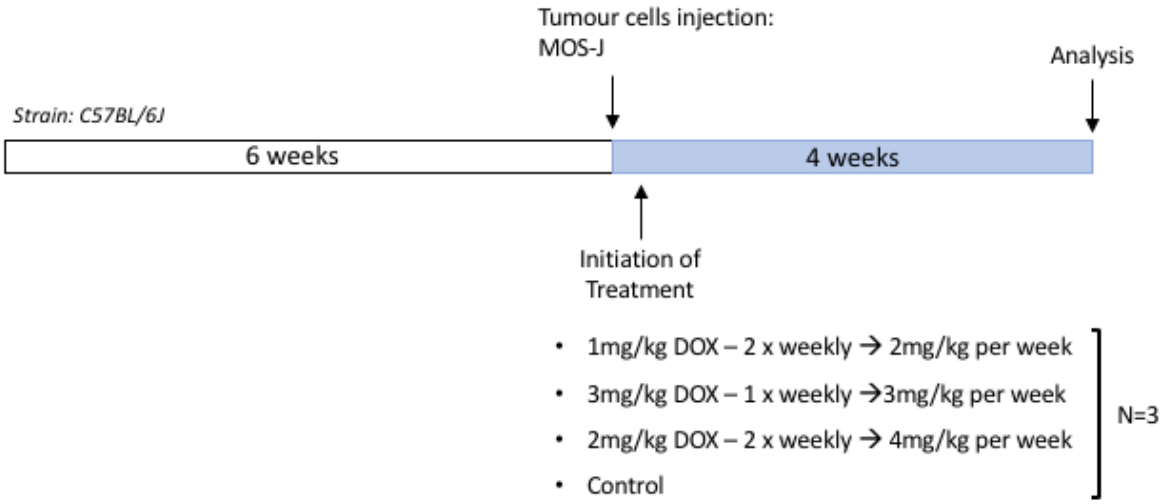

Figure 28: Experimental design of a dose response analysis of doxorubicin in allograft model of osteosarcoma.

3.2.11 Evaluating the Impact of Combining Anti-murine IL-34 and Doxorubicin on Tumour Growth in the Syngeneic MOS-J Osteosarcoma Model

After establishing the optimal doses for both doxorubicin and anti-IL34, we aimed to investigate the potential of treating with anti-IL34 antibody in combination with doxorubicin, and whether this could enhance the efficacy of both treatments.

A syngeneic model with six-week old female mice was set up as previously outlined. Mice were randomly assigned into 4 groups (n=8): control (PBS, intraperitoneal, 3x weekly), anti-murine IL-34 (4 mg/kg, intraperitoneal, 3x weekly), doxorubicin (3 mg/kg, intravenous, 1x weekly) and anti-murine IL-34 + doxorubicin (combined therapy). Tumour volumes were measured three times weekly for 28 days.

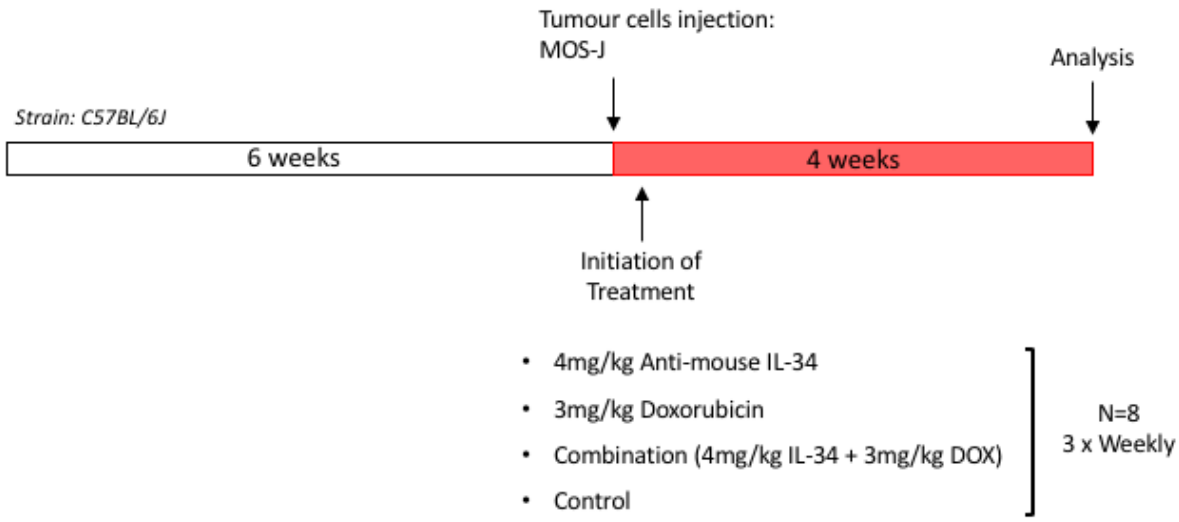

Figure 29: Experimental design for combination therapy in an allograft model of OS. Anti-IL-34 antibody was administered intraperitoneal (4 mg/kg, three times/week) and doxorubicin administered intravenously, (3 mg/kg, one time), plus their combination and PBS as control.

3.2.12 Processing of Samples

3.2.12.1 Blood samples

Blood was collected at the end of each study in order to establish a biological cohort. For sacrificing, the mice were injected with by 0.5 mL of pentabarbiturate. Animals were monitored after injection and deep anaesthesia was confirmed by pinch reflex. A fresh 1ml syringe and 25-gauge needle was used to retrieve blood from the heart before cervical dislocation. The blood was then placed into a 1.5 mL Eppendorf tube after removing the needle to reduce sheer stress. Blood was left on ice until further processing. The blood samples were centrifuged at 10,000 g for 20 minutes at 4°C in order to separate serum and cellular components. The clear serum was carefully collected into fresh Eppendorf and stored at -80°C.

3.2.12.2 Tissue samples

On the day of sacrifice, lungs, spleen and liver tissues were removed and immediately placed into 4% PFA in PBS into labelled bijou tubes. These where left to fix in 4% PFA for 48-72 hours, on rotation at 4°C. After fixation, the tissues were placed into labelled histology cassettes, and into a solution of 70% EtOH and sent for processing into wax. All tissue samples were processed by the bone analysis laboratory at the University of Sheffield (See section 3.2.14)

3.2.12.3 Bone samples

A. Histology assessment

Tumour legs, as well as contralateral legs (excised and stripped) were placed in 4% PFA in PBS at 4°C for 48-72 hours as described above. In some cases micro-computed tomography (MicroCT) was performed at this stage (See section below). After fixation, the solution was changed to a decalcifying solution (0.5M EDTA, 0.5% PFA in PBS, pH8). The solution was changed three times weekly for two weeks whilst all samples were kept on rotation at 4°C. Bone samples were then placed into labelled histological cassettes, and washed in PBS three times for 1 hour before being processed and embedded in paraffin (See section 3.2.14)

B. Micro-computed tomography analysis

Legs were scanned using a high-resolution microcomputed tomography (SkyScan 1272, bruker) at 50 kV and 200 mA, 0.5 mm aluminium filter and a resolution of 4.3um for both trabecular and cortical analysis. After obtaining the X-Ray Scans, the SkyScan Necron Program was used to reconstruct the images with a thresholding of 0.009 to 0.09 and a beam hardening correction of 20%. Trabecular, cortical and ectopic bone formation were analysed using the SkyScan Ctan program and calculated according to the recommendations published in Journal of bone and mineral research (Bouxsein et al., 2010)

C. Trabecular analysis

For the proximal tibia and the distal femur, the mineralised cartilage bridge was used as a reference point. Trabecular structures positioned 0.2 mm below the growth plate were quantified over a length of 1mm. Bone Volume (BV) and Tumour Volume (TV) of tumour legs and contralateral legs were measured.

D. Cortical analysis

Similar to the trabecular analysis, cortical analysis was performed at on offset of 1.00 mm from the mineralised cartilage bridge and quantified over a length of 1 mm. Cortical bone Volume (BV), Trabecular Number (Tb.N), Trabecular Spacing (Tb.Sp) and Trabecular Thickness (Tb.Th).

E. Ectopic bone analysis

Ectopic bone (also referred to as ectopic ossification), refers to the spontaneous formation of bone in soft tissue (Segaliny *et al.,* 2015; Lamoureux *et al.,* 2014, Gobin *et al.,* 2015) Ectopic bone analysis was performed in the tibia and fibula at a resolution of 8 μm. Two points of reference were used, firstly the mineralised cartilage bridge in the tibia, and the secondly the merging of the fibula with the tibia. Tumour bearing tibia and fibulae were analysed separately and compared to their contralateral non-tumour bearing tibia and fibulas.

3.2.13 Embedding and sectioning of tissues

Tissue embedding was performed by the bone analysis laboratory at the University of Sheffield. Legs and tissues were paraffin embedded with a tissue processor. Samples underwent various stages of dehydration in ethanol solutions, clearing in butanol and embedding in paraffin. Tissues were cut on a Leica microtome, and sections of 3 μm were mounted on microscope slides.

3.2.14 Immunohistochemistry

3.2.14.1 Dewaxing and dehydrating of paraffin embedded sections

Paraffin embedded tissue sections were first de-waxed prior to applying any staining procedures. This was carried out as follows:

1. Sections dewaxed in fresh xylene twice for 5 minutes each
2. Sections were incubated in 100% ethanol for 5 minutes and 3 minutes respectively to remove the xylene
3. Sections incubated in 95% ethanol for 3 minutes.
4. Sections rinsed in tap water for 1 minute

Sections of tumour bearing legs were then stained with a number of different stains (See sections below). Following staining sections were dehydrated prior to mounting in the following steps:

5. Sections incubated in 70% Ethanol for 3 minutes
6. Sections incubated in 90% Ethanol for 3 minutes
7. Sections incubated in 95% Ethanol for 3 minutes
8. Sections incubated in 100% Ethanol twice for 3 minutes each.
9. Sections incubated in Xylene twice for 5 minutes each
10. Mount coverslips with DPX mounting fluid

3.2.14.2 Haematoxylin and eosin staining

Haematoxylin and eosin staining is a dye used generally in histology based on its ability to clearly demonstrate a difference between different tissue structures. Haematoxylin stains cell nuclei blue, whilst eosin stains cell cytoplasm and most connective tissues pink. To stain for H&E, slides were dewaxed, stained with Gill's haematoxylin solution for 90 seconds followed by a wash in tap water for 5 minutes. Next, slides were incubated in 1% eosin in 1% (w/v) calcium carbonate solution for 5 minutes, washed in tap water for 2 minutes and dehydrated before mounting.

3.2.14.3 Immunohistochemistry

Immunohistochemistry for five different stains marking cell proliferation (Ki67), cell-death (Caspase-3), total macrophages (F4/80), M2 macrophages (CD163) and vascularisation (CD31) was carried out on a minimum of three non-serial sections at 3 μm each. An outline of the methodology used for each marker studied is described below. Each stain was modified for antigen retrieval and dilution of primary antibodies as described in Table 5.

Slides were first dewaxed and then blocked in endogenous peroxidase with 3% H2O2 in methanol for 30 minutes at ambient temperature, followed by washes in PBS-T (0.1%), twice for 5 minutes each. Antigen retrieval was then achieved with the respective method for each stain (Table 5), followed by two-5 minute washes in PBS-T (0.1%). Unspecific binding sites were blocked by incubating slides in serum prepared in 1% BSA/PBS-T for 1 hour at room temperature. This was then followed by an overnight incubation in the primary antibody at a made up in 2% serum. For a negative control, slides were incubated with serum only.

The next day, sections were washed in PBS-T (twice for 5 minutes each) followed by incubation in secondary antibody at a dilution of 1:200 made up in 2% serum, for 1 hour at room temperature. Slides were washed in PBS-T (twice for 5 minutes each) prior to incubation in ABC solution (made up at least 1 hour prior to use: 1 drop of A, 1 drop of B in 2.5 mL PBS) for 30 minutes at ambient temperature and further washes and incubation in DAB. Finally slides were washed in water to stop the DAB reaction, counterstained in haematoxylin for 30 seconds, and dehydrated and mounted in DPX.

Table 5: Table summarising the immunohistostaining stains and techniques used for the preparation of immunohistochemical slides.

	Stain	Antigen Retrieval	Primary Antibody	Secondary Antibody	Serum
Ki67	Nuclear antigen present in mid G1, S, G2 and all the M-phase of the cell cycle and thus a marker for cell proliferation (Scholzen & Gerdes, 2000).	PT Module, 80°C for 45 minutes with 10 mM Citrate Buffer, pH6	Rabbit monoclonal antibody (SP6) (Abcam - AB16667). Reacts with both human and mouse Ki67. Dilution **1:100**	Biotinylated goat anti-rabbit IgG Antibody (Dako)	Goat
Caspase3	Cleaved Caspase-3 is associated with the initiation of the 'death cascade' and therefore marks the cell's entry point into the apoptotic signalling pathway. (Inwald *et al*., 2013)	PT Module, 80°C for 1 hour with 10mM Citrate Buffer, pH6	Rabbit monoclonal antibody (ASP175) (Cell Signalling – AB9661). Reacts with human and mouse Caspase -3. Dilution **1:200**	Biotinylated goat anti-rabbit IgG Antibody (Dako)	Goat
F4/80	F4/80 protein is restricted to mouse macrophages involved in the regulation of antigen specific efferent regulatory T (Treg) cells to suppress antigen-specific immunity (Lin, H *et al*., 2005)	Pressure cooker for 2 hours (30 sec at 121°C cycles plus cooling time).Target retrieval solution (DAKO), pH6 at 1/10 dilution.	Rat monoclonal antibody that recognises the murine F4/80 antigen (CI: A3-1) (Bio-Rad, MCA497R).	Biotinylated rabbit anti-rat IgG Antibody (Dako)	Rabbit

			Dilution: **1:50**		
CD31	Known as platelet endothelial cell adhesion molecule (PECAM-1), is expressed on the surface of endothelial cells. Interactions of endothelial cells with each other, as well as receptors that mediate such interactions, are fundamental in the process of angiogenesis (Naeem & Hassan, 2018).	PT Module, 80°C for 45 minutes with 10 mM Citrate Buffer pH6	Monoclonal rat antibody (SZ31) (Dianova, DIA-310) that detects mouse CD31. Dilution **1:50**	Biotinylated rabbit anti-rat IgG Antibody (Dako)	Rabbit
CD163	Cell surface glycoprotein receptor highly expressed on subsets of tissue resident macrophages (Yang *et al*., 2015). Used to identify macrophages of the M2 subtype.	TRIS-EDTA solution pH 9 (10 mM Tris base, 1 mM EDTA solution). Slides immersed in boiling buffer solution for 5 mins, followed by immediate washings in cold PBS-T.	Monoclonal rabbit antibody (EPR19518) (Abcam 182422) detecting mouse CD163. Dilution **1:200**	Biotinylated goat anti-rabbit IgG Antibody (Dako)	Goat

3.2.14.4 Scoring of histological slides

Three non-serial sections per tumour sample were stained for Ki67, Caspase-3, CD31, CD163 and F4/80. Slides were first scanned using a digital slide scanner (Panoramic 250 Flash III, 3DHistech UK). Analysis of the IHC stained slides was performed using QuPath (Version 0.1.2, OmicsX), an open-source image analysis software.

All x40 scanned slides were imported into the programme. The region of interest equating to the tumour area was chosen by drawing a region of interest around the area, excluding any tissue folds. Positive staining was defined as the presence of any discernible DAB positivity localised in the membrane and/or cytoplasm. Quantitation was conducted as recommended in (Bankhead *et al.,* 2017). Briefly, intensity thresholds were set for cellular DAB detection. Percentage positive data was extracted from each slide and averaged across replicates.

3.2.15 Statistics

Data were analysed using GraphPad Prism (version 7.0) software (Graphpad). N numbers for all experiments donated by the prefix n and all errors bars shown denote the mean ± Standard error of the mean. All data analysed with either T test, one-way ANOVA with Dunnett's multiple comparison test or a two-way ANOVA. Significance values denoted as follows: Non-significant (ns): $p > 0.05$,*: $p<0.05$, **: $p<0.01$, ***: $p<0.001$, ****:$p<0.0001$

3.3 RESULTS

3.3.1 Development of Osteosarcoma Models *in-vivo*

3.3.1.1 Paratibial inoculation of tumour cells

Injection of a murine or human cancer cell line in close contact to the bone, i.e. at an orthotopic site, is one of the most frequently used methods to induce bone sarcomas in mice for the development of allograft and/or xenograft models (Guijarro *et al.,* 2014; Jacques *et al.,* 2018; Uluçkan *et al.,* 2015) In such models, cells are inoculated close to the bone generally into the femur or tibia diaphysis. These models have been previously shown to be highly effective with 80% tumour take rate and high reproducibility, with the para-tibial procedure being less invasive than intraosseous cell inoculations. These models, result in rapid tumour growth in the soft tissue with secondary contiguous bone invasion, and spontaneous pulmonary metastasis.

Two OS pre-clinical mouse models were set up for this part of the PhD. First, an allograft model using the mouse chondroblastic MOS-J cell line. These cells formed solid tumours when injected into immunocompetent syngeneic hosts (C57BL/6J mice), mimicking endochondral bone development. Histological assessment of decalcified tumour legs by H&E, revealed high grade tumours with multiple cells of varying size, with a highly osteoblastic phenotype. The transplantable tumours destroyed and invaded existing bone, as well as vessels in close proximity to the tumour (Figure 30A). These *in vivo* tumours are characterised by regions of necrotic areas towards the centre of the tumours and an area of highly proliferative cells located on the outside circumference.

Secondly, a human OS model by inoculation of MNNG-HOS cells was developed. This xenograft model induced the development of primary bone tumours in nude mice as confirmed by histological analysis of decalcified tumour legs stained by H&E (Figure 30B). The tumours formed are close to undifferentiated OS and induce bone associated remodelling and osteolytic lesions.

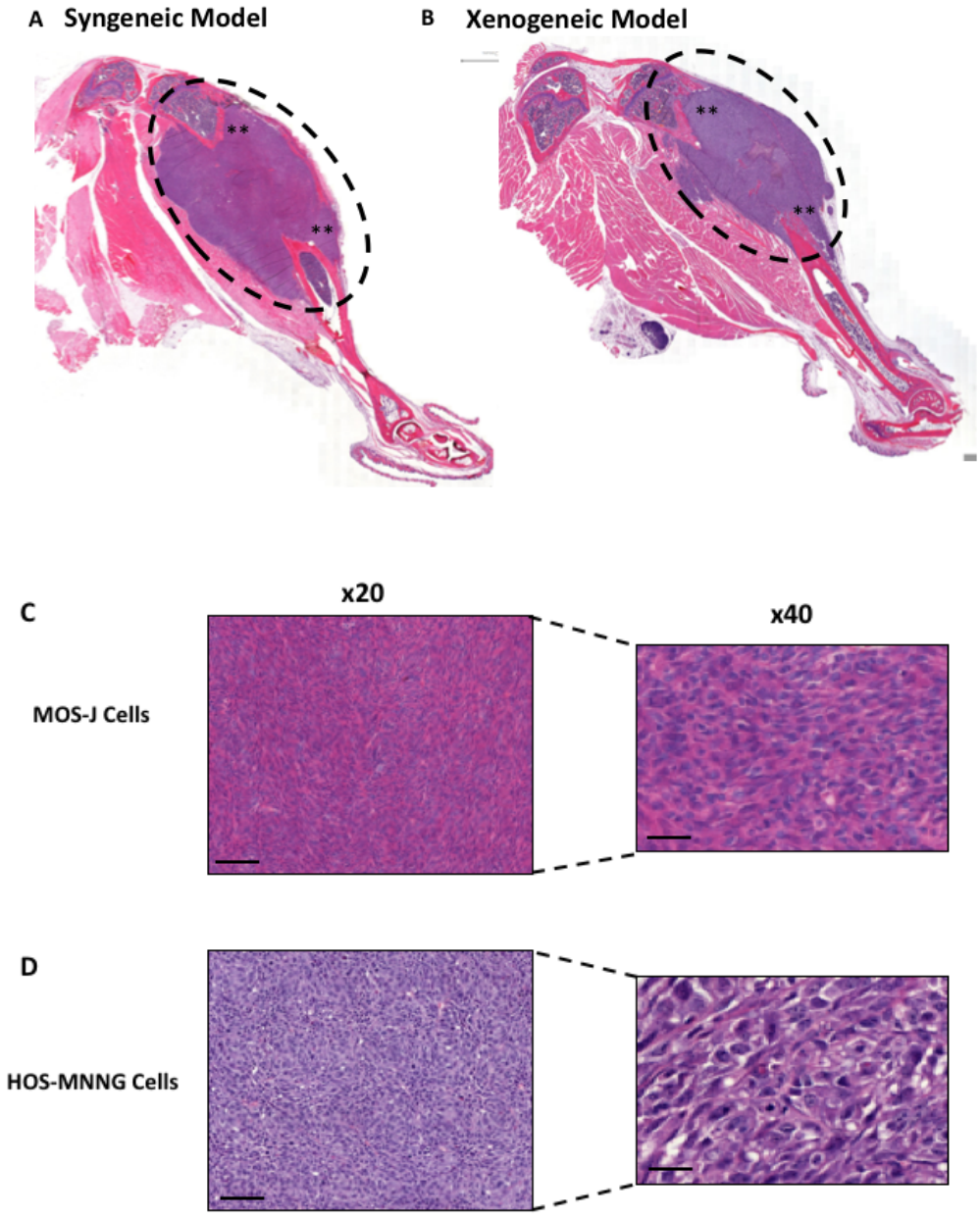

Figure 30: Haematoxylin and eosin staining of allograft and xenograft models of osteosarcoma. Two osteosarcoma *in-vivo* models were set up **A)** a mouse osteosarcoma model using 125,000 MOS-J cells. Image shows tumour mass (indicated by dashed lines) after 28 days from cell inoculation, and ** indicate position of growth plates. **B)** a human osteosarcoma models using 250,000 HOS-MNNG cells. Image shows tumour mass after 21 days from cell inoculations. In both cases, the tumour cells were injected in close contact to the tibia after activation of the periosteum. **C and D)** Immunohistochemical H&E stains of allograft and xenograft tumours with 20x and 40x fields showing representative sections. Scale bar = 100μm

3.3.1.2 Establishment of syngeneic osteosarcoma model and analysis of tumour growth

The first objective was to set up a working syngeneic model, and to determine the optimal cell concentration of cells to inject. To achieve this, a titration experiment using increasing number of MOS-J cells was performed and a kinetic of tumour growth were assessed.

Immunocompetent C57BL/6J mice (n=3 per group) where injected with the following MOS-J cell concentrations: 1.25 x 10^5, 2.5 x 10^5 and 5.0 x 10^5 per mouse. All the mice injected formed palpable tumours within 5-10 days of cell inoculation. The higher cell concentration (5.0 x 10^5 cells/mouse) displayed the larger tumour volumes with a mean of 280 mm^3. These mice had to be sacrificed at day 15 as the maximum limit of tumour size according to the project licence in place, was reached (1.5 cm). The data indicates that a lower cell number, that of 1.25 x 10^5 cells/mouse would be an ideal cell concentration to use in future experiments, in order for the mice to last for a duration of four weeks of more, thus giving ample time to asses treatment responses. All other mice where sacrificed when limits of tumour size was reached (Figure 31)

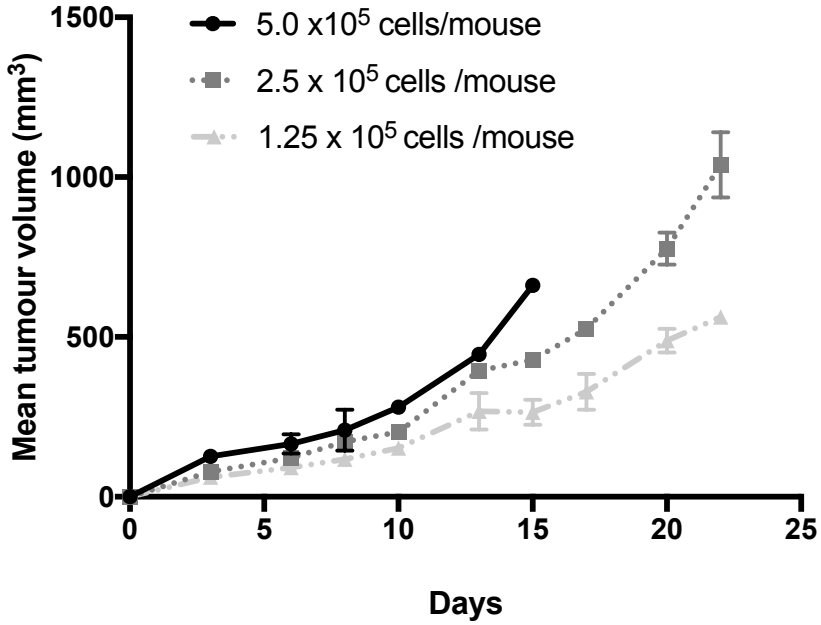

Figure 31: Mean tumour volumes of tumour kinetics in allograft model of OS. Following injection of three different concentrations of MOS-J cells into immunocompetent mice, mean tumour volumes were obtained for 23 days as measured by calipers.

With regards to setting up a similar preliminary titration study for the development of a xenograft model a previous experiment undertaken by Dr. Hannah Brown (University of Sheffield, UK) was successful in determining the optimal number of MNNG-HOS cells to set up a xenogeneic model in nude mice. Female Balb/C nude mice were injected with three different cell concentrations (100,000, 250,000 and 500,000 cells per mouse). Tumours were then left to grow for 28 days. The end result showed that inoculating 250,000 cells per mouse would be the ideal cell concentration, and therefore data from this study was used to set up the xenogeneic model.

The next objective of the in vivo investigations, was to determine the relevance of IL-34 as therapeutic target. The effects of anti-IL34 blocking antibodies on the progression of OS (e.g. tumour growth and pulmonary metastasis) were investigated in two pre-clinical models of OS described above. We investigated two newly available IL-34 blocking monoclonal antibodies; an anti-murine (SHEFF5) and an anti-human (B-T34).

3.3.2 Blocking Murine IL-34 in an Allograft Model of Osteosarcoma

3.3.2.1 Evaluation of a dose-response analysis of anti-murine IL-34

An *in vivo* dose-response experiment was carried out so as to decide the effective dose of anti-murine IL-34 antibody, and assess its ability to inhibit tumour growth. Treatment was administered three times weekly at three increasing doses 1 mg/kg, 4 mg/kg and 8 mg/ kg. A control group was injected with a PBS solution of the same volume. All mice showed palpable tumours after around 7-10 days of cell inoculation. Following the initial 15 days of tumour transplantation, differences in tumour sizes could already be observed. The 1mg/kg dose did not modulate the tumour growth, with an ANOVA between this group and the control showing no significant differences in tumour volumes. Tumour growth was seen to slow down with higher doses. Tumour growth slowed down by around 40% compared to control group after around 15 days. The blocking antibody inhibited tumour growth at a dose of 4 mg/kg 25 days post cell injection with a highly significant difference of ($p = 0.005$, One-way ANOVA). For the 8 mg/kg dose group, this also slowed down tumour growth in comparison to control ($p = 0.03$, One-way ANOVA) however, not as effectively as the 4 mg/kg dose (Figure 32). Taken together, this data shows that from the

doses administered, the 4 mg/kg dose was considered to be the most effective dose for inhibiting tumour growth, thus providing the first evidence that blocking anti IL-34 is a potential target for the treatment of OS.

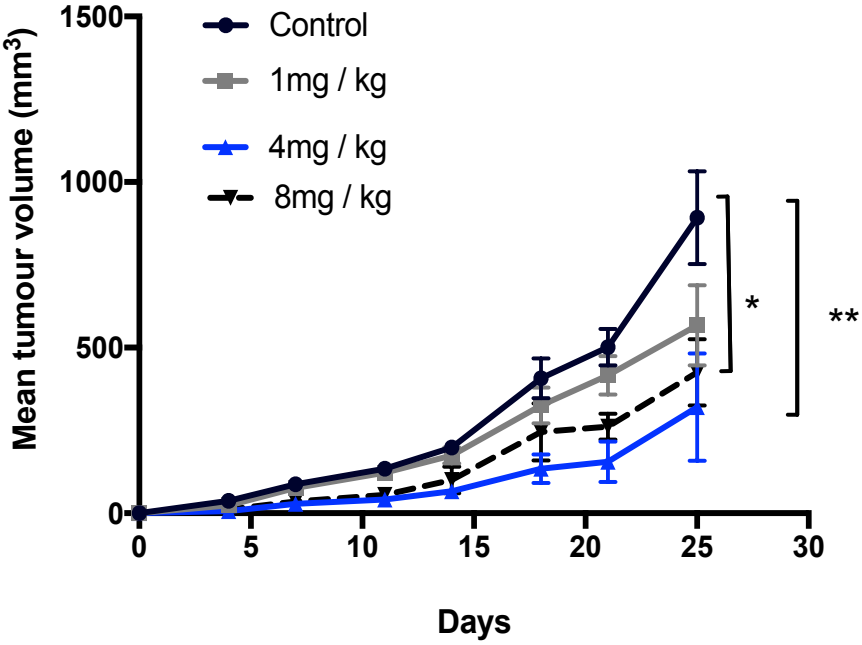

Figure 32: Mean tumour volumes for dose response analysis of anti- IL-34 antibody in an allograft model of osteosarcoma. Immunocompetent 6 week old, female mice were injected with 1.25 x10^5 cells by paratibial injections. Graph shows the mean tumour volume for each dose administered from day 2 after cell inoculation till day 25, as measured by calipers. Error bars are shown as mean ± SEM, n=5, p values calculated by One-way ANOVA *p < 0.05, **p < 0.01.

Next, the therapeutic potential of anti-murine IL-34 administration on lung metastasis, bone associated re-modelling and the resulting impact on tumour physiology by immunohistochemical analysis.

3.3.2.2 Effect of blocking anti-murine IL-34 on tumour growth and lung metastasis

Anti-murine IL-34 (4mg/kg, three times weekly) was administered in 6 weeks old female mice (n= 6 per group), 2 days after the local para-tibial injection of MOS-J cells (1.25 x 10^5) and continued until day 23. All animals treated with the antibody exhibited a significant decrease of tumour volume compared with control mice starting at day 10 (116 mm^3 for CT compared to 270 mm^3 for treated group) and after 23 days (tumour volume of 440 mm^3 for control and 190 mm^3 for treated) (p value = 0.0003). (Figure 33B). Animals were sacrificed at day 23 as the limit of the tumour size (1.5 cm) was reached and thus had to be ended in accordance with Home Office Regulations. When each animal is considered individually, the incidence of mice progressing with a tumour volume of less than 500 mm^3 was diminished by day 23 in treated animals (0/6), in comparison with controls (6/6) (Figure 33C). This data again reinforces the hypothesis that targeting IL-34 significantly delays OS tumour growth.

The presence of microscopic metastasis in the lungs was then examined by histology. At the time of necropsy, lungs were preserved in 4% paraformaldehyde and processed, cut into serial sections of 3μm and stained with H&E for the detection of pulmonary metastatic nodules. All of the mice, both in control and treated groups, showed no presence of metastatic nodules evidencing that the duration and timing of the experiment, in addition to the cell concentration used, were insufficient for metastasis to develop.

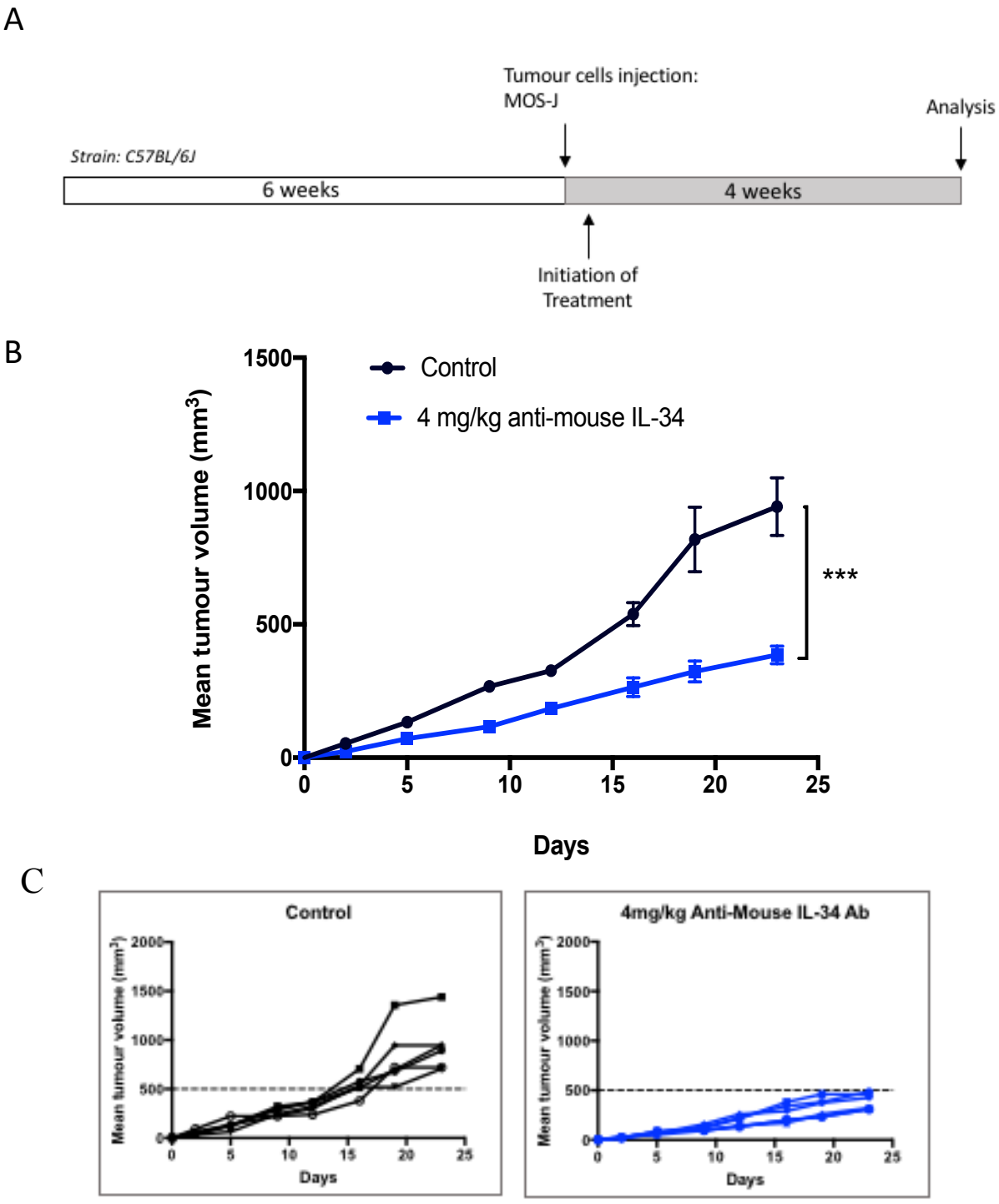

Figure 33: Anti-murine IL-34 antibody delays osteosarcoma growth in MOS-J allograft model. (A) Mice were treated with 4 mg/kg anti-murine IL-34 antibody via the intraperitoneal route, three times a week starting 2 days after paratibial cell inoculations, up until day 23 and tumour volumes measured by calipers. The mean (B) or the individual (C) tumour volumes of mice treated was compared with control group ± SEM, n=6, p values were calculated by One-way ANOVA, ***p > 0.001.

3.3.2.4 Effect of anti-murine IL-34 antibody on tumour associated bone lesions

Since OS-associated alteration of bone remodelling plays a central role in the development and progression of bone tumours, the ability of the antibody to alter tumour-associated bone remodelling was analysed. The bone microarchitecture in legs bearing tumours was examined at the end of the study (Day 23) using a high-resolution X-ray micro-CT system.

While tumour volumes were reduced following treatment with the antibody, analysis of bone architecture showed that the treatment failed to prevent tumour associated osteolysis. This is demonstrated in a number of analysis of bone morphometric parameters of both cortical and trabecular bone. (Figure 34B, 34D and 34E). Total bone volume also failed to show any differences between control and treated groups. Additionally, it was also examined whether the treatment would have any effect on the formation of ectopic bone. As shown in Figure 34C, no significant differences in bone volume (BV%) of either tumour bearing tibia or fibula was observed.

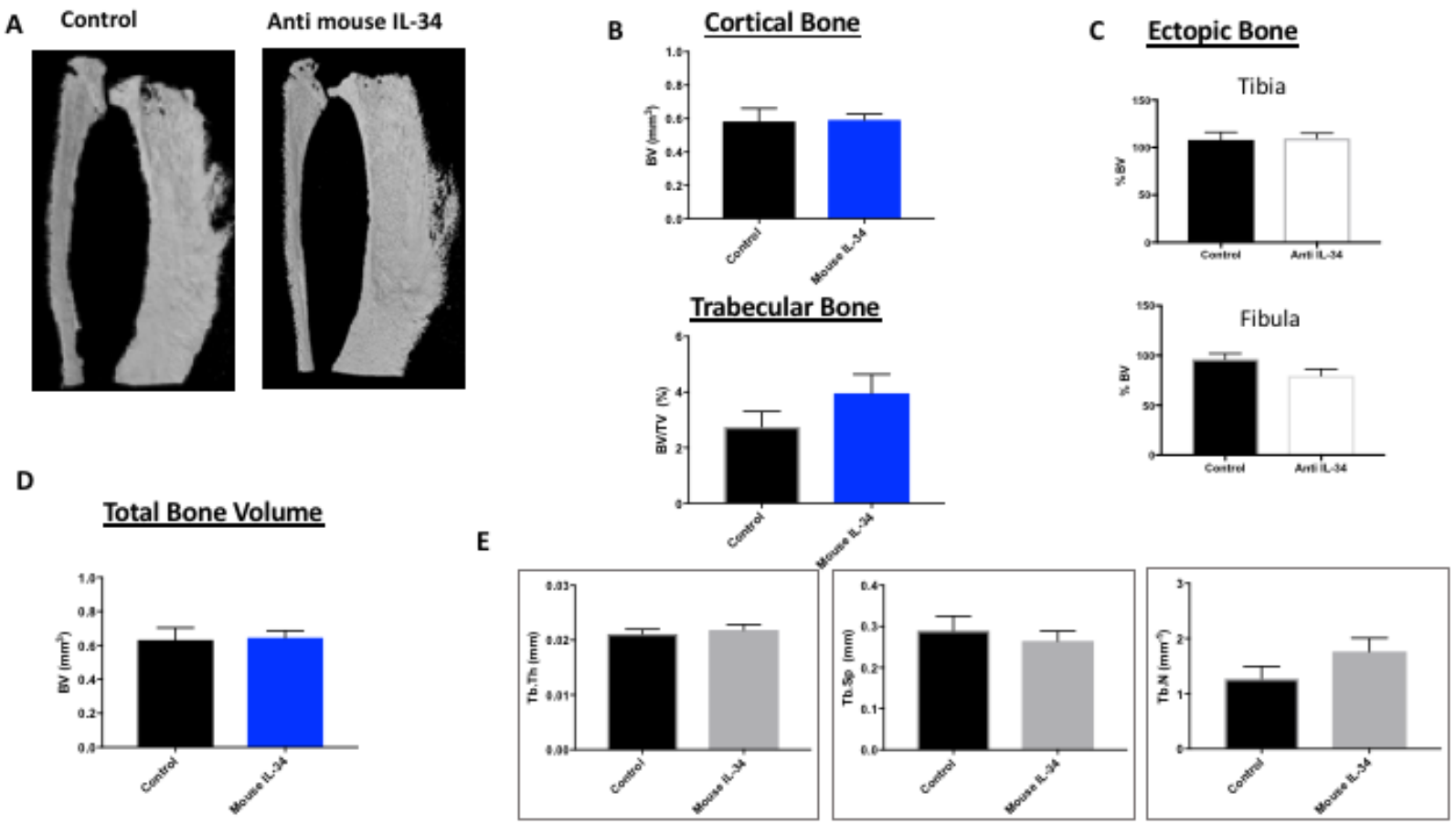

Figure 34: Effect of anti-murine IL-34 on tumour associated bone lesions in syngeneic osteosarcoma model. (A) 3D reconstruction of tibia and fibula of each group (control and treated) at the end of the experiment – day 23 (B) graphs showing bone volume (BV) of cortical bone in each of the groups as well as bone volume of trabecular bone (BV/TV). (C) graphs showing ectopic bone volume (BV%) in the tumour bearing tibia and fibula (D) total bone volume (BV), (E) trabecular thickness (Tb.Th), Separation (Tb. S) and Number (Tb.N) for tumour bearing tibia per group. Data area mean ± SEM, N=6 per group. T-test for all data sets showed no level of significance.

3.3.2.5 Immunohistochemical analysis

In order to analyse the mechanisms involved in the inhibition of tumour growth observed, the effects were studied by staining tumour biopsies with a number of markers mainly Ki67 for proliferation, caspase-3 for marked cell death, F4/80 for macrophages, CD31 as a marker of endothelial cells reflecting the amount of vascularisation, and CD163 for M2 type macrophages.

IHC analysis showed no difference in the proliferation rate between treated and non-treated groups, as determined by the proliferation marker Ki67 (Figure 35D). This is probably due to the high aggressiveness of the MOS-J tumours, as well as the method of action of blocking antibodies. Blocking antibodies, do not act directly on the proliferation of tumour cells (in contrast with cytotoxic drugs where the mechanism of action is to stall cellular growth). Similarly, the rate of apoptosis was not affected by the treatment (Figure 35H). Caspase-3 analysis is collected from tumours at the end-point of the experiment (around 4 weeks) and would have probably already undergone significant apoptosis.

A slight tendency towards a decrease in CD31 for treated groups was seen (Figure 35L). This could be explained given the role of IL-34 in mediating angiogenesis in OS by regulating the proliferation of endothelial cells (Segaliny *et al.,* 2015). Despite this however, the difference was not significant as can be observed in Figure 33L. This demonstrates once more that the aggressiveness of this model is responsible for the high SD observed, and the absence of significant differences.

An increase towards $F4/80^{+}$ macrophage infiltrates was detected in treated groups in comparison to control (Figure 35P). This higher incidence of macrophages can be attributed to high inflammation in the local environment of the tumour, and other cytokines which were non efficient before. This would lead to a dysregulated balance between M1/M2 macrophages, in favour of M1 phenotype and thus an increase in F4/80 marker.

CD163 was detected around the tumours, and in connective tissue at the periphery. The low number of CD163 positive cells in general, could be attributed to a dysregulation in the balance of M1/M2 macrophages favouring the M1 sub-population. Also, taking into consideration the low numbers detected in non-treated group (control) a further reduction in the treated group is possibly occurring but difficult to detect by IHC (Figure 35T)

Overall, the above immunohistochemical analyses indicate that the syngeneic model was highly aggressive, as can be seen by its high tumour volumes. This high variability and small animal numbers in each group could explain the high standard deviation obtained, and the absence of significant differences.

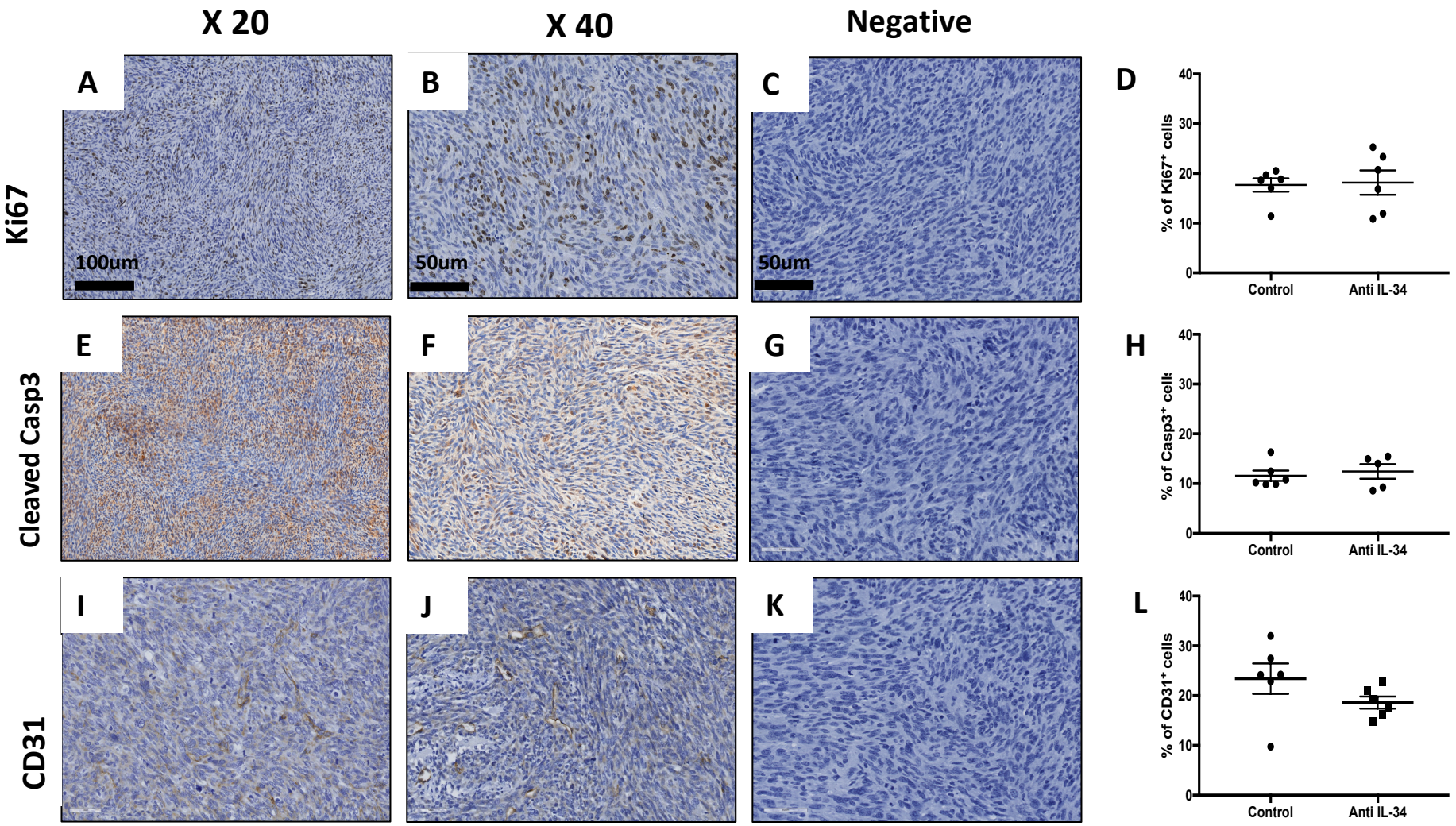
X 20
X 40
Negative
Ki67
Cleaved Casp3
CD31
A
B
C
D
E
F
G
H
I
J
K
L
100um
50um
50um
% of Ki67+ cells
% of Casp3+ cells
% of CD31+ cells
Control
Anti IL-34
0
10
20
30
40

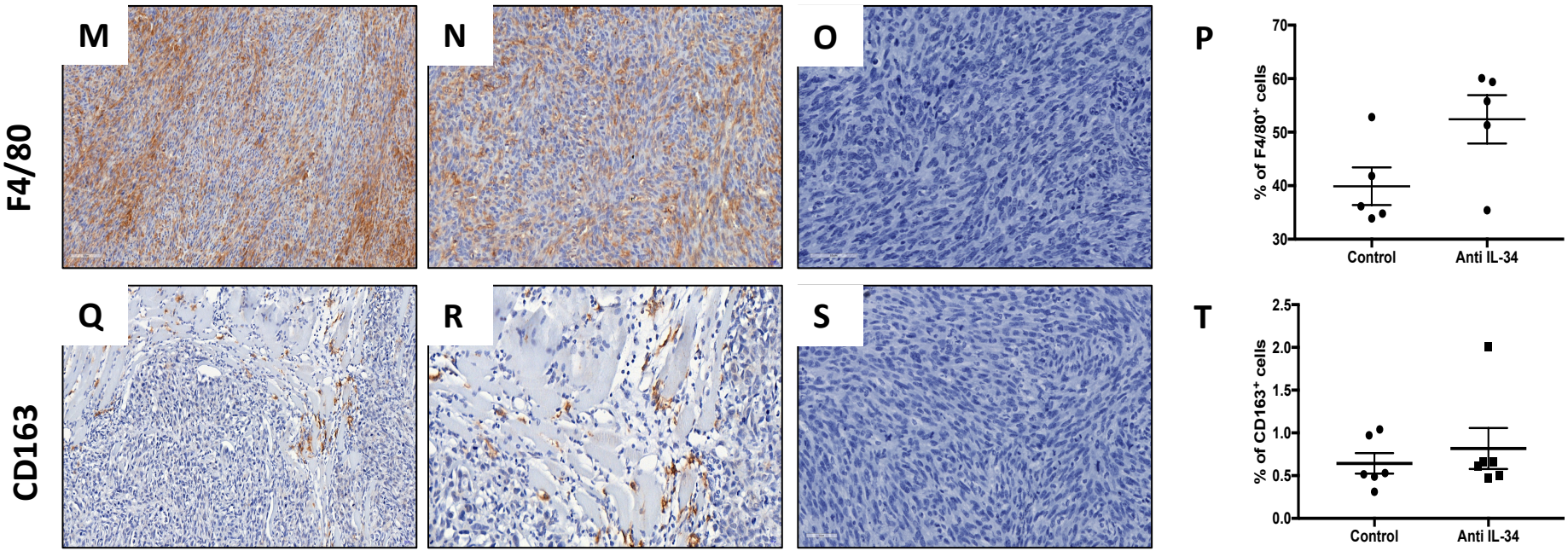

Figure 35: Immunohistochemical analysis of tumour biopsies in an allograft model of osteosarcoma. Images showing staining of tissues from MOS-J syngeneic mouse model for: **Ki67** (Panel A-D), **Caspase-3** (Panel E-H), **CD31** (Panel I-L), **F4/80** (Panel M-P), and **CD163** (Panel Q-T). 1st column: 40x objective and scale bar = 100 µm, 2nd column: 20x objective and scale bar = 50 µm, 3rd column: negative control, 4th column graphs showing data from all specimens scored and estimated as percentage of positive cells. Data are expressed as mean ± SEM and n=6 per group. T-test for all data sets showed no level of significance.

3.3.3 Blocking Human and Murine IL-34 in a Xenograft Model of Osteosarcoma

After determining the outcome of blocking IL-34 in a syngeneic model, the effect of blocking IL-34 in a MNNG-HOS model was next analysed. In addition to investigating whether blocking IL-34 in the surrounding tumour microenvironment would show similar effects in nude mice, it was investigated whether blocking IL-34 produced by tumour cells would have any effect on slowing down tumour growth.

The anti-human Il-34 antibody used in this experiment, is able to block the biological activity of IL-34 by inhibiting the interaction of IL-34 with M-CSFR. Indeed IL-34-dependent cell proliferation is blocked by this antibody. In addition intra-cellular signal transduction triggered by IL-34 binding to its receptor is inhibited. In such a manner, therefore this antibody is useful to target Il-34 produced by tumour cells. According to the antibodies patent (WO 2016/097420) the present antibody has a high affinity for IL-34 () and therefore the dose used for this experiment was similar to the one used for the syngeneic model.

3.3.3.1 Effect of blocking IL-34 on tumour growth and lung metastasis

An experimental model of OS induced by MNNG-HOS cells was set up as previously described. Anti-murine and anti-human IL-34 (4 mg/kg, three times weekly) were administered in 6 week old female mice (n= 6 per group), 2 days after the local para-tibial injection of MNNG-HOS cells (2.5 x 10^5) and continued until day 20. PBS was injected for the control group. Data for tumour volumes were collected by calipers as previously described. As plotted in the graph (Figure 36B), tumours treated with anti-human IL-34 showed no significant effect on the tumour volumes when compared to the control group. On the other hand, treatment with murine IL-34 antibody, showed a significant decrease of tumour volumes compared to control as previously seen in the allograft model ($p = 0.009$). When animals were taken individually, all the mice in the anti-murine treated group, progressed with a tumour volume of less than 50 mm^3, whereas those in the other two groups did not (6/6 control and anti-human treatment) (Figure 36C)

As in the previous model, the presence of lung metastasis was assessed by histological assessment of paraffin embedded sections of lungs collected at the end-point of the treatment (Day 21). None of the mice developed pulmonary nodules of metastasis, due to the short timing of the experiment and small tumour volumes.

3.3.3.2 Effect of blocking IL-34 antibody on tumour associated bone lesions

Similar to the previous model, the effect of the treatment on the bone microarchitecture of tumour bearing tibia was analysed using micro-CT. Visual inspection of the 3D reconstructions of the tibia suggests that the treatments did not alter the tumour-associated bone formation in the MNNG-HOS model (Figure 37A). Indeed, the total bone volume in mice injected with either anti-murine or anti-human antibodies, showed no significant change in either cortical bone or trabecular bone, neither in total bone volume when cortical and trabecular bone were analysed together (figure 37D). Bone osteolysis was further evaluated by evaluating the trabecular number (Tb.N), trabecular thickness (Tb.Th) and Trabecular Spacing (Tb. Sp) and neither of these parameters exhibited any differences. The treatment showed no effect on ectopic bone formation. Complementary with previous results ectopic bone formation was neither altered or improved in either tibia or fibula (Figure 37C).

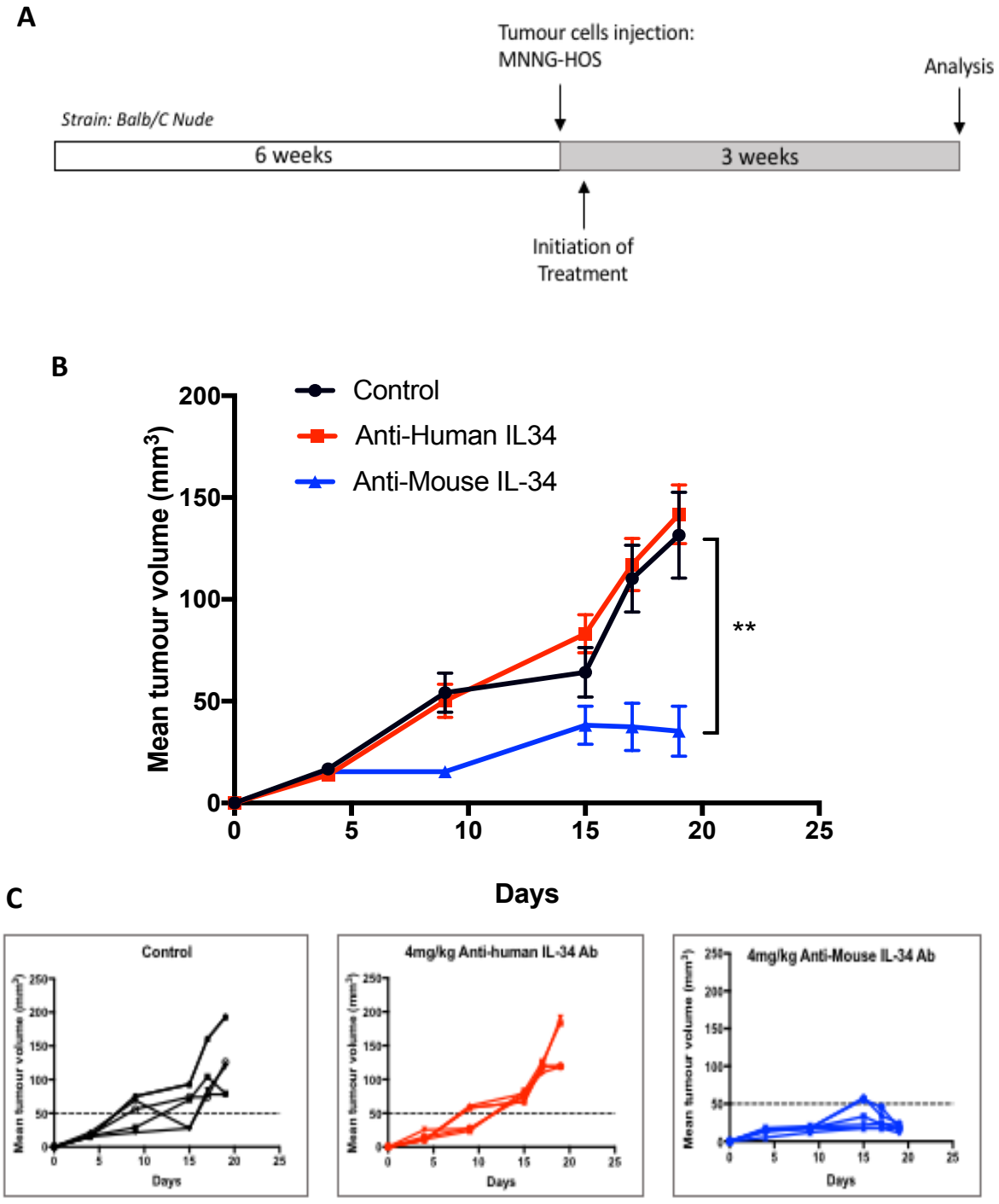

Figure 36: Mean tumour volumes following treatment with anti-human and anti-murine IL-34 in a xenogeneic osteosarcoma model. (A) Immunocompromised Balb C/ nude mice were injected with MNNG-HOS cells (2.5 x 10^5). Treatment with IL-34 blocking antibodies (4 mg/kg for each SHEFF5 and B-T34) was initiated 2 days after paratibial cell inoculations, and given 3 times weekly via intraperitoneal route for a duration of 21 days. (B) Mean tumour volumes were measured by calipers and calculated from day 1 to day 21 for each group (C) Individual tumour volumes of mice treated with each antibody compared with control group. Data area mean ± SEM, n=6 per group. P values calculated using Two-way ANOVA **p < 0.01.

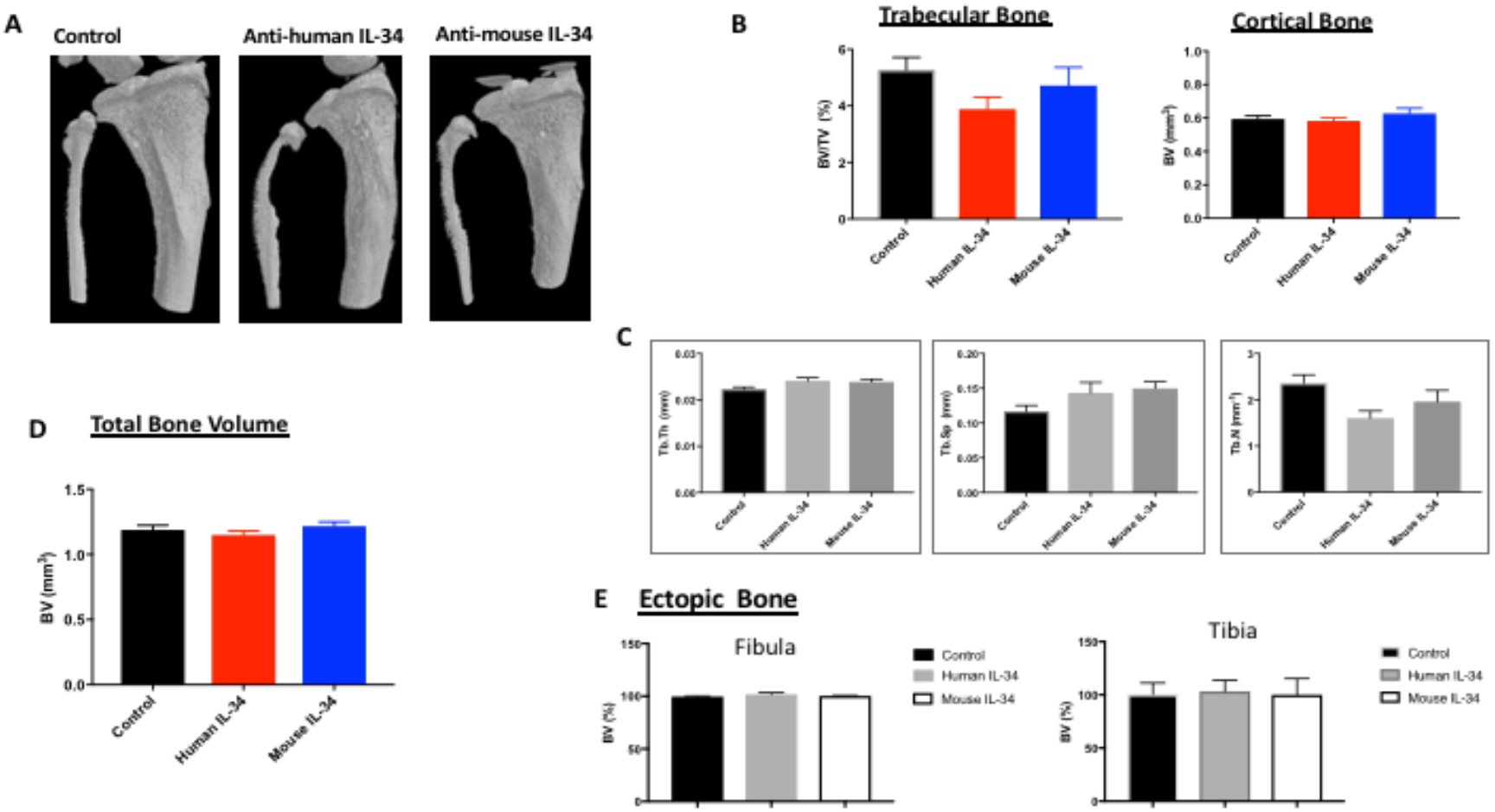

Figure 37: Effect of blocking IL-34 on tumour associated bone lesions in xenogeneic osteosarcoma model. (A) 3D reconstruction of tibia and fibula of each group (control, anti-murine and anti-human) at the end of the experiment – day 21 (B) graph showing bone volume (BV) of cortical bone in each of the groups and bone volume (BV/TV) for trabecular bone (C) trabecular thickness (Tb.Th), Separation (Tb. S) and Number (Tb.N) for tumour bearing tibia per group (D) graph showing total bone volume (i.e. cortical and trabecular) (E) graphs showing ectopic bone volume (BV%) in the tumour bearing tibia and fibula. Data area mean ± SEM, N=6. One-way ANOVA for all data sets showed no level of significance.

3.3.3.3 Immunohistochemical Analysis

Immunohistochemical analysis showed no difference in Ki67 or Caspase-3 expression after treatment with either anti-human IL34 or anti-mouse IL-34 blocking antibodies (Figure 38D and 38H). A significant decrease of CD31 expression in animals treated with anti-mouse blocking antibody in comparison to both the control or anti-human antibody was observed. This suggests that inhibition of tumour progression may result from a decreased rate of endothelial cell proliferation, resulting in a decrease of blood vessels and solidifying the role of IL-34 in angiogenesis (Figure 38L).

With regards to immunohistochemical analysis of macrophages in this model, there was an increase in F4/80 macrophages (Figure 38P) but no difference in the expression of CD163 (Figure 38T). Taken together this shows that there was no difference in the M2 population between treated and control, resulting in an increase of M1 macrophages. Although the xenograft model is less aggressive than the allograft, similar to previous results, the small animal numbers in each group could explain the high standard deviation obtained, and the absence of significant differences.

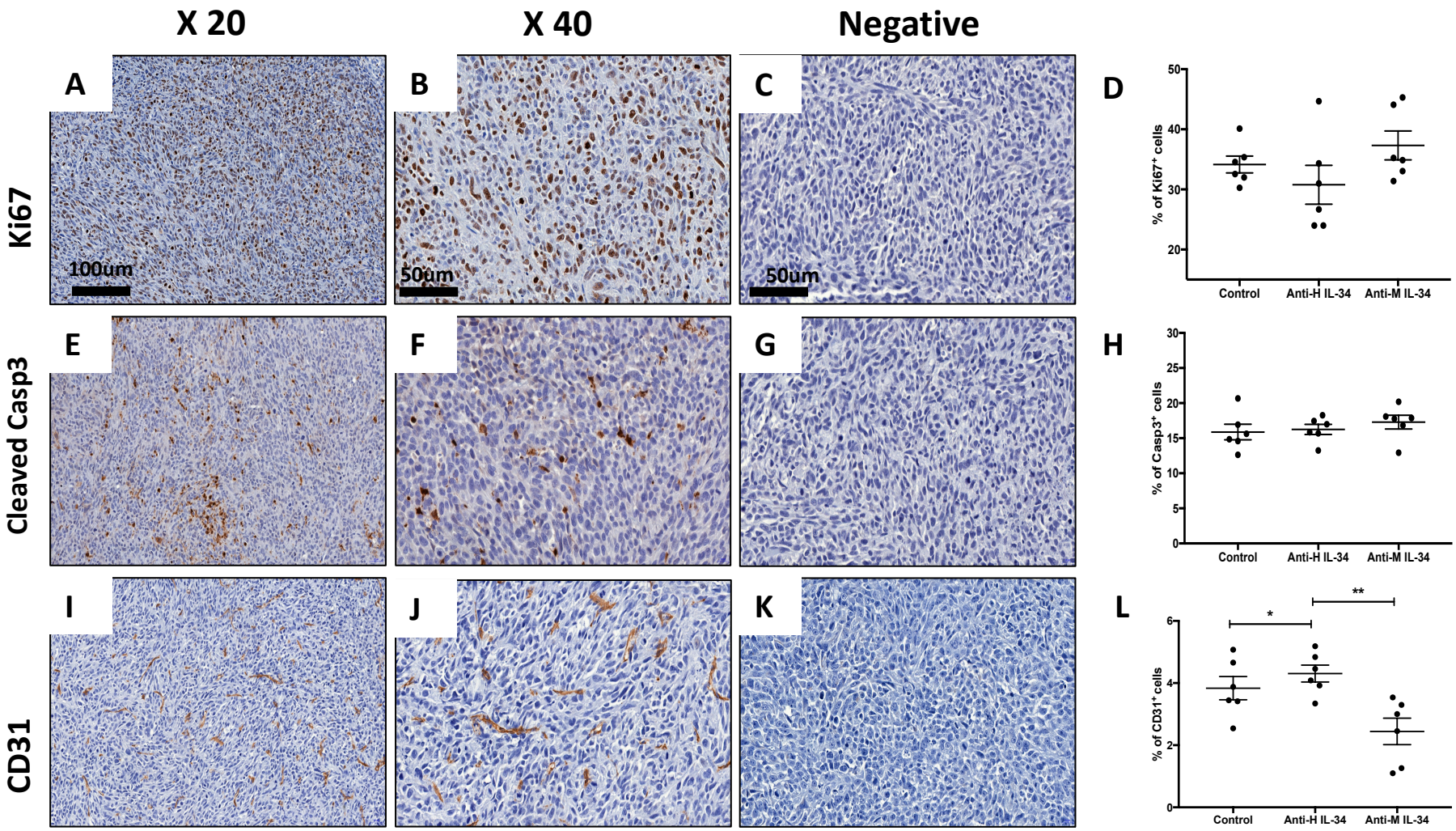
X 20
X 40
Negative
A
B
C
D
Ki67
100um
50um
50um
E
F
G
H
Cleaved Casp3
I
J
K
L
CD31
% of Ki67+ cells
% of Casp3+ cells
% of CD31+ cells
Control
Anti-H IL-34
Anti-M IL-34
*
**

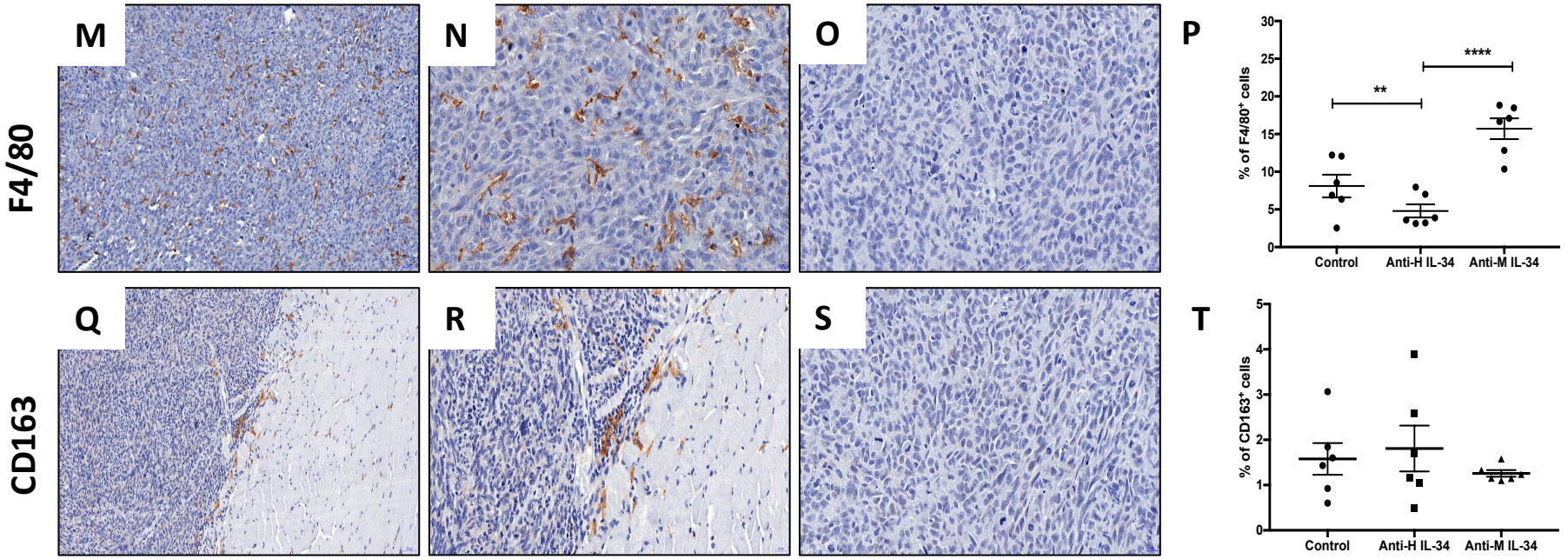

Figure 38: Immunohistochemical analysis of tumour biopsies in a xenograft model of osteosarcoma. Images showing staining of tissues from MNNG-HOS xenogeneic mouse model for: **Ki67** (Panel A-D), **Caspase-3** (Panel E-H), **CD31** (Panel I-L), **F4/80** (Panel M-P), and **CD163** (Panel Q-T). 1st column: 40x objective, 2nd column: 20x objective, 3rd column: negative control, 4th column graphs showing data from all specimens scored and estimated as percentage of positive cells. Data are expressed as mean ± SEM and n=5 per group. P values calculated using One-way ANOVA *p < 0.05 **p < 0.01, ****p < 0.0001.

3.3.4 Assessment of Tumour Necrosis

Histological analysis by H&E was used to measure levels of necrosis in both tumour models. MOS-J model was characterised by small necrotic foci distributed in the tumour mass while MNNG-HOS model was characterised by a significant and larger necrotic area at the centre of the tumour mass. No significant difference in necrosis rates was observed in either model, as well as no difference between treatments (Figure 39).

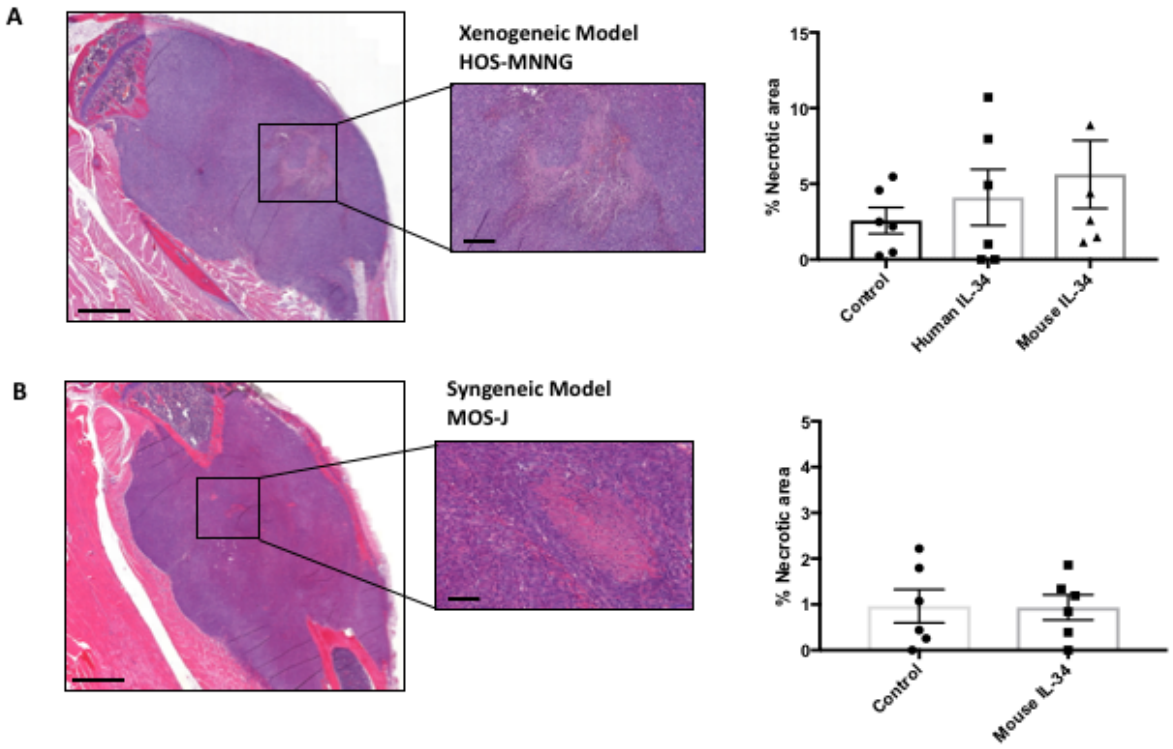

Figure 39: Quantification of necrotic areas from H&E sections. Representative tumour sections showing discolouration associated with necrosis in the central areas of the tumour and quantification of these areas for (A) HOS-MNNG model and (B) MOS-J model treated with Il-34 blocking antibodies Data are mean ± SEM (n=5 for xenogeneic model and n=6 for syngeneic model) Scale bar = 100um

3.3.5 Effect of Bi-therapy with IL-34 Blocking Antibody and Doxorubicin on Tumour Growth in Allograft Model of Osteosarcoma

On consideration of the data from both the allograft and xenograft models, the results demonstrate that targeting IL-34 in the microenvironment is effective at significantly inhibiting tumour growth and promoting tumour shrinkage. As a result, it was hypothesized that administering murine IL-34 in conjunction with other treatments already known to delay OS growth, would be a potential treatment regimen aimed at delaying OS tumour development.

In this respect, although several studies have already demonstrated the use of a single dose of doxorubicin to inhibit primary tumour growth in mouse models of OS, the aim was to evaluate the optimal dose of doxorubicin that was well tolerated without any possible toxicities in the MOS-J allograft models currently set up.

3.3.5.1 Evaluation of a dose-response analysis of doxorubicin

The tolerance and effectiveness of different doses of doxorubicin was evaluated in the MOS-J allografts model. Models were set up as previous, and mice were treated with three doses of doxorubicin all administered via the intravenous route: i) 2 mg/kg (2 x weekly of 1 mg/kg doses), ii) 3 mg/kg (1 x weekly of 3 mg/kg dose), and iii) 4 mg/kg (2 x weekly of 2 mg/kg doses). The efficacy of the drug was assessed by monitoring the primary tumour growth with digital calipers twice a week, until tumour diameter limits were reached (1.5 cm). No significant weight loss due to this chemotherapy was observed.

For this chemotherapy, two of the doses were effective at delaying tumour growth: 3 mg/kg and 4mg/kg ($p = 0.01$ for 3 mg/kg and $p= 0.002$ for 4 mg/kg) (Figure 40). This mean decrease in tumour volume although showing that both doses are effective, the 3mg/kg would be better suited so as to make sure that tumours are not completely diminished by the end of the biotherapy treatment.

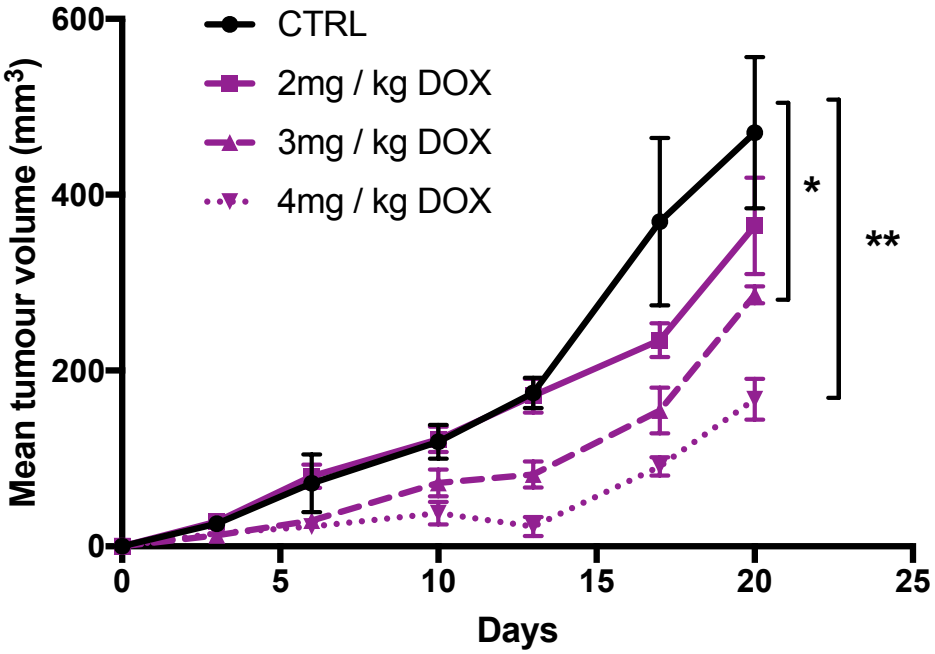

Figure 40: Dose response analysis of doxorubicin in a MOS-J model of osteosarcoma. Mice were injected with $1.25x10^5$ MOS-J cells and treated with 3 different doses of the chemotherapeutic agent doxorubicin via intraperitoneal route till day 21. Treatment was initiated 2 days after cell injections. Graph indicates mean tumour volumes for each dose and control treated mice as measured by calipers. Data are shown as mean ± SEM, n=3 per group. P values calculated using One-way ANOVA *p < 0.05 **p < 0.01

3.3.5.2 Effect of bi-therapy with IL-34 blocking antibody and doxorubicin on tumour growth

Thus, the next step was to evaluate whether the combination of IL-34 blocking antibody with doxorubicin, would have a synergistic effect. In addition to exhibiting a good therapeutic effect on tumour growth, whether combining the two treatments would prevent any tumour associated osteolysis. This bi-therapy study was conducted in the MOS-J model.

A total number of 32 immunocompetent mice (n=8/treatment group) were injected with MOS-J cells and assigned randomly into four treatment groups: i) PBS as control, ii) anti-murine blocking IL-34 (4 mg/kg i.p, 3 times weekly), iii) doxorubicin (3 mg/kg i.v, one time weekly), iv) bi-therapy of anti-murine IL-34 and doxorubicin (4 mg/kg i.p and 3 mg/kg i.v). Treatment was initiated 2 days post tumour cell injection.

The mean tumour volumes for IL-34 and doxorubicin monotherapy, indicate that when each of these therapies are administered individually, a significant decrease in tumour progression is observed (p value = 0.01 for IL-34 and p value = 0.0002 for Doxorubicin, Two-way ANOVA with Dunnett's multiple comparison test) This is in consistency with previous results obtained in this thesis (Figure 41). On the other hand, the combination of blocking antibody with doxorubicin, failed to act synergistically to prevent tumour growth. Slight decrease in mean tumour volumes when compared to the control group can be observed, however this is not at an improved rate than administering either of the monotherapies. This unexpected result could have been due to poor administration of the doxorubicin. These could be eluded from the individual graphs as seen in Figure 41, whereby a high discrepancy of tumour volumes between individual mice can be seen.

Taken together the data suggest that although individually the treatments are effective at slowing down OS tumour growth, when given together they did not completely prevent tumour growth. Administration of a combination treatment induced a slow but sustained reduction in tumour growth, and improvements to the therapeutic regimen, in terms of both doses and timing, will be required.

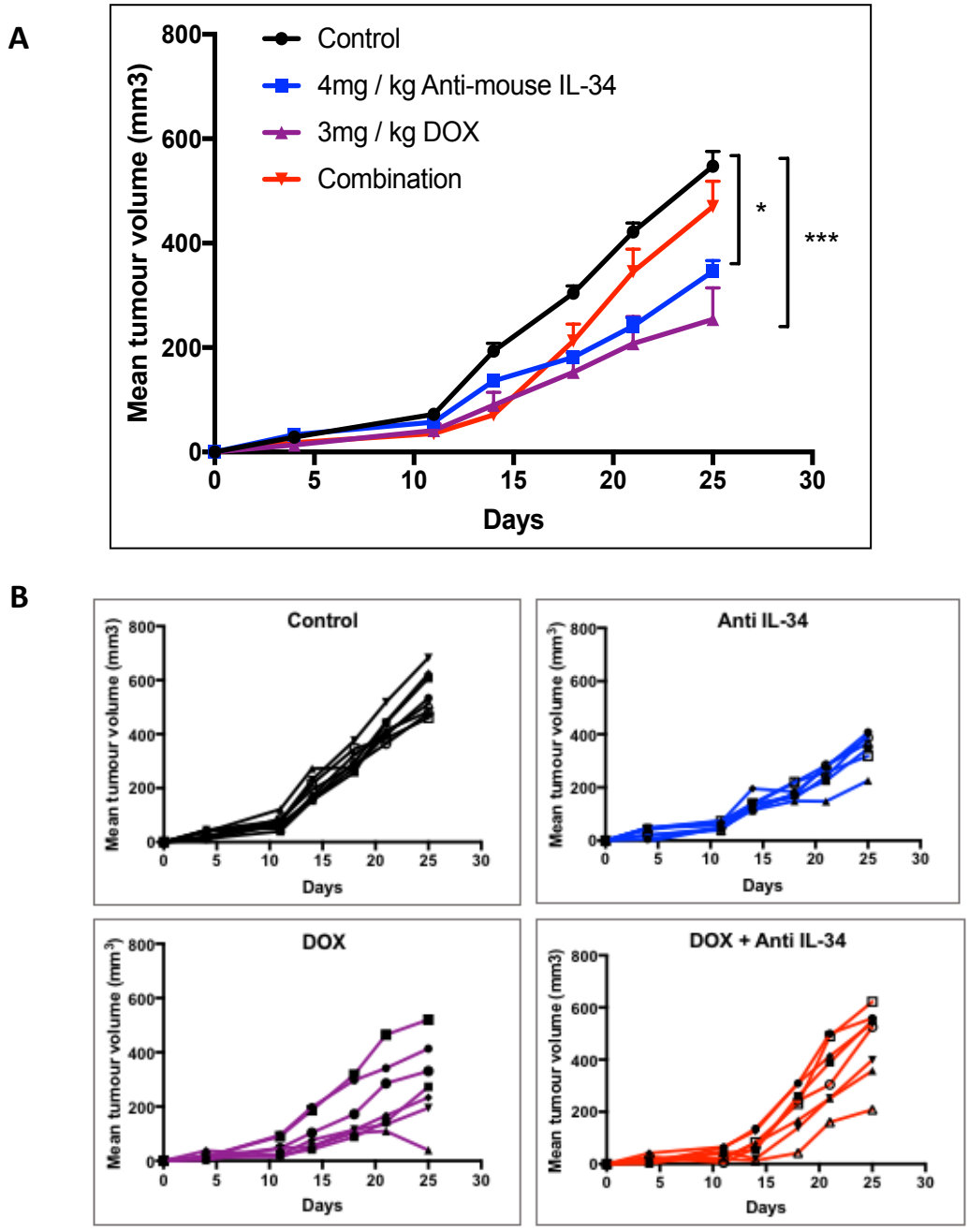

Figure 41: Mean tumour volumes for combination therapy (anti-IL-34 and doxorubicin) in an allograft model of osteosarcoma. Mice were treated three times a week with 4mg/kg anti-murine IL-34 antibody and one time weekly with 3mg/kg of doxorubicin starting 2-days after paratibial inoculation of tumour cells. (A) Mean tumour volumes and (B) individual tumour volumes compared between the four groups. Data is shown as mean ± SEM, n=8 per group. p values were calculated using Two-way ANOVA *$p < 0.05$, *** $p < 0.001$.

3.3.5.3 Immunohistochemical analysis

Consistent with the results obtained, immunohistochemical analysis showed that combination treatment failed to delay tumour progression as demonstrated by no effect on proliferation rates (Ki67), apoptosis (Caspase3), or vascularisation (CD31) (Figure 42A, 42B and 42C respectively). Macrophage populations (i.e. both M1 and M2 sub-types) were not affected by the treatment possibly due to dose timing. Similar to previous models, the expression of CD163 was detected more around tumours than in the tumour stroma.

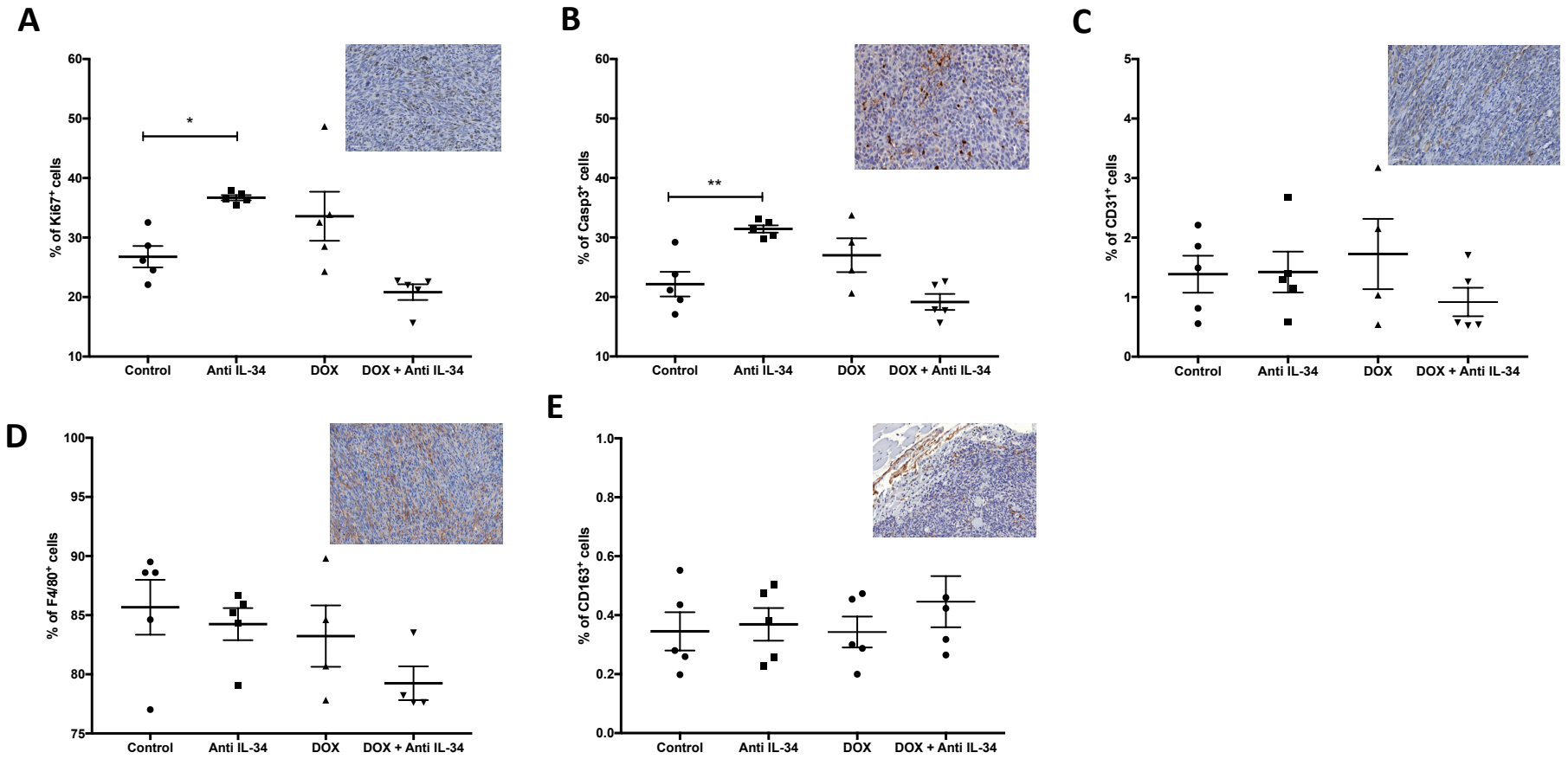

Figure 42: Immunohistochemical analysis of tumour biopsies for combination therapy. Data was obtained at the end-point of the study (Day 25) Graphs of A) cell proliferation with Ki67, B) cell death with caspase-3, C) vascularisation with CD31, D) number of pan macrophages with F4/80, E) number of M2 sub-type macrophages as CD163 all expressed as percentage of positive number of cells. Data expressed as mean SEM, n=8 per group (Control, 4mg/kg anti-murine IL-34, 3mg/kg doxorubicin, bi-therapy of IL-34 antibody and doxorubicin). P values obtained by One-Way ANOVA with the following threshold of significance: *p > 0.05, **p > 0.01.

3.4 SUMMARY

The present study aimed to determine the therapeutic effect of IL-34 targeting in OS by using murine pre-clinical models and anti-IL34 blocking antibodies. Two OS models were set up, a syngeneic mouse model in immunocompetent mice using the mouse MOS-J cell line, and a xenogeneic model in immunodeficient mice by the human MNNG-HOS cell line . In both cases, paratibial inoculations of tumour cells were used for the development of tumour growth in soft tissue. This involved injecting tumour cells in close contact to the tibia diaphysis following activation of the periosteum.

Firstly, a dose-response analysis was carried out to determine the optimal dose and best efficacy of the IL-34 blocking antibodies. After establishing that a 4mg/kg dose, three times weekly, is the optimal dose, the antibody was administered, in both models, for 3-4 weeks. The resulting effect was a reduction of tumour volume and growth compared to the control groups. In parallel, an antibody blocking human IL-34 was tested in the xenogeneic model, but no reduction of tumour growth was observed, concluding that the development of IL-34 appears to be mainly produced by the murine tumour microenvironment.

Next, microCT analysis was used to assess whether this treatment had any effects on bone associated remodelling, including formation of ectopic bone. Analysis of bone michroarchitecture of both cortical and trabecular parameters, revealed that the treatment had no significant effect on bone alterations. As a result, tumour histology by immunohistochemistry was studied. Analysis revealed a reduction in vascularisation by the marker CD31, and increase in pan macrophage marker F4/80. No differences in tumour proliferation or cell death by caspase-3 were detected possibly due to the high variability and/or the small animal number in each group.

We then evaluated the potential therapeutic benefit of IL-34 blocking agent, and doxorubicin as a combination treatment in these preclinical models. The effects of anti-murine IL-34 (4 mg/kg) and doxorubicin (3 mg/kg) were investigated in the syngeneic mice model. These two treatments administered together, failed to act synergistically as determined by clinical (tumour growth) and histological levels (immunohistochemical analysis). Most likely, problems in the administration of the DOX led to these unexpected

results. Macrophage populations, both for overall macrophages and macrophages of the M2 sub-type were not affected at the tumour site despite the treatment, possibly due to dose timing. A better strategy for testing this combination therapy would be needed.

In conclusion, IL-34 appears mainly produced by the murine tumour microenvironment. The inhibition of IL-34 specific blocking antibodies demonstrates that the therapeutic benefit to abrogate IL-34 in OS and thus IL-34 may be a novel therapeutic target in bone associated disease

CHAPTER 4

ZEBRAFISH AS A MODEL TO STUDY THE ROLE OF IL-34 IN THE IMMUNE RESPONSE

4.1 INTRODUCTION

To extend our findings on the role of IL-34 in steady state conditions, a murine knockout model for IL-34 is currently being developed. The work being carried out on this model and some of the initial data are being presented in sub-chapter 3.5 (Refer to appendix) in order to strengthen the relevance of this model in relation to the work carried out in this PhD.

4.1.1 The Zebrafish as a Model Organism

The zebrafish (*Danio rerio)* is a tropical freshwater fish established as a major model of human disease over the past 15 years. Even though the zebrafish is less closely related to humans than rodents, it offers several advantages as a model in biomedical research. These advantages allow the zebrafish model to be used as an addition to already existing models.

The popularity of the zebrafish as a model comes from the fact that zebrafish embryos develop rapidly and are transparent. Embryos develop from a single cell to a whole organism by 24 hours post fertilisation (hpf), with the entire body plan and major organs fully established. By 5-days post fertilisation (dpf), all major developments are complete (White *et al.,* 2013). Sexual maturity is reached by 2.5 months of age, making generation time small compared to other models, and therefore allowing for mutant colonies to be established quickly (Lieschke & Currie, 2007).

The fertilised egg develops external to the mother. This offers a significant advantage over mammalian models. The optical clarity of the embryo allows for direct imaging and visualisation of embryogenesis (Brown *et al*., 2017; Chico, 2008). When coupled with the use of fluorescent reporter lines, real-time imaging of pathologies and cellular interactions can be performed.

Due to their small size, zebrafish are cost effective. They are capable of producing large numbers of progeny, with a single female able to produce hundreds of eggs per week and can therefore be housed in large numbers (Lieschke & Currie, 2007). Breeding is easily controlled by a light cycle (14 hours light, 10 hours dark) and as a result, manipulation of embryos is easily achievable (Nasiadka & Clark, 2012).

Despite obvious differences between humans and zebrafish, over 70% of human genes have been recognised in zebrafish orthologues, and the sequencing of its genome is currently in its 11th version (Howe *et al*., 2013). Zebrafish are classified as a 'lower vertebrates', and play an important role when implementing the 3Rs. The 3Rs aim to limit the number of animals used in research purposes by replacement, reduction and refinement. There is also less rigorous oversight of studies when using early embryos in contrast with rodent embryos, making the zebrafish an attractive model for researchers (Seth *et al*., 2013).

Despite the above aforementioned qualities of the zebrafish as a suitable model for research, it also has some disadvantages. Fixing and sectioning of embryonic larvae is difficult owing to their small size. Histological analysis is also challenging, since only a few antibodies against zebrafish proteins are currently validated (although this is improving). Additionally, imaging can be applied only to embryos at early stages, and often requires the prevention of pigmentation by the use of Nacre or Casper mutant lines. As the animal becomes larger and more opaque, penetration of the tissue for imaging becomes more difficult, making the model disadvantageous at this point. An added complication, is that zebrafish possess more than a single orthologue of a human gene, (a genome duplication that occurred in teleosts after their divergence from mammals) and thus it is difficult to achieve consistency in parity of function (Brown *et al*., 2017)

Overall, the zebrafish model offers a good compromise between practical simplicity and intricacy making it an ideal intermediate between rodent models that is a better option than using invertebrate models.

4.1.2 Zebrafish Genetic Tools

A number of genetic tools are now available to generate genetic models of disease using the zebrafish. Targeted genome modifications and RNA interference strategies are used to study the consequences of loss of function mutations. RNA interference strategies include the use of Morpholinos to generate transient knockdown of protein coding and miRNA genes making them ideal in genetic inhibition studies. Stable mutants can be generated by large scale N-ethly-N-nitrosurea (ENU) mutagenesis screens that create random mutations. The generated mutants are then characterised and the responsible gene identified (Kettleborough *et al*., 2013)

More recent techniques have now been developed for precise genome editing including zinc-finger nucleases (ZFIN), transcription activator-like effector nuclease (TALEN) and the clustered-regularly-interspaced-short-palindromic-repeats (CRISPR) with associated protein 9 (Cas9) system. These are used to generate knockout mutant zebrafish lines relatively easily and quickly. They can also be used to generate knock-ins and specific point mutations through homology directed repair (Auer & Del Bene, 2014). In this thesis, the CRISPR/Cas9 system was utilized and therefore only this mechanism will be explained in more detail.

4.1.3 The CRISPR/Cas9 Mechanism

The mechanism of CRISPR/Cas9 is based on the adaptive immunity of bacteria, in which specific DNA sequences are recognized by an RNA-dependent recognition mechanism and a Cas9 nuclease (Bauer *et al*., 2015). This system has been modified to be used as a genomic engineering tool, and has made CRISPR one of the most popular approaches to generate knock-outs, activate or repress genes of interest.

The CRISPR/Cas9 system consists of two main constituents: a ‘guide’ RNA (gRNA) and Cas9 endonuclease. The gRNA is a synthetic RNA made of a ‘scaffold’ sequence that is

required for the binding of the Cas9, and a 'target' sequence that is specific and complementary to the genomic target of interest (Figure 52). The target region is around 20bp long, and should be present upstream of a Protospacer Adjacent Motif (PAM) sequence. This PAM sequence is needed for target binding of the endonuclease, and the exact nature of the sequence is dependent upon the species of the bacteria (5′ NGG 3′ for *Streptococcus pyogenes* Cas9) (Ablain *et al*, 2015). Once injected, the guide RNA and Cas9 protein form a riboprotein complex that goes through a conformational change from an inactive state, to a DNA-binding complex. When the Cas9-gRNA complex binds to the target DNA, the nuclease domains of the Cas9, cleave the strands of the DNA. This results in a double strand break (DSB) mediated by Cas9, within the target DNA (3-4 nucleotides upstream of the PAM sequence). These double strand breaks are repaired via homologous recombination or non-homologous end-joining, thus resulting in indels (insertions and/or deletions) or frameshift mutations. Ideally, the end result is a loss-of function mutation within the target gene (Bauer *et al*., 2015). Early exonic sequences are frequently targeted since this leads to gene disruption through frame-shifts or non-sense mutations.

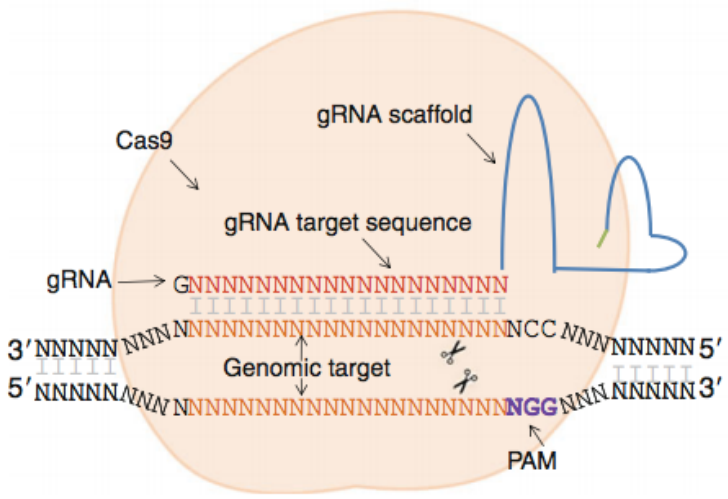

Figure 43: Schematic diagram of the CRISPR/Cas9 system. The CRISPR/Cas9 is composed of a Cas9 endonuclease and a single stranded guideRNA. The gRNA is designed to target a genome sequence of 19-23bp at the 5' side of a PAM motif. (Adapted from Ablain *et al*., 2015)

In zebrafish, injection of gRNAs and Cas9 mRNA into the one-cell stage embryo yields deletions/insertions at target sites with relatively high frequencies. Mutations are inheritable due to mosaic targeting of the germline, allowing rapid establishment of mutant strains. Gene inactivation by CRISPR/Cas9 is permanent, providing an effective and complementary approach to morpholinos (Chang *et al.,* 2013). In this study, CRISPR-Cas9 was used to generate a knockdown of IL-34 so as to investigate the effects of its loss on bone development and immune phenotype.

4.1.4 Zebrafish as a Model of Immunity

For decades, research has relied heavily on mouse models for experimental designs to study immunology. With the realisation that the innate immunity plays an important role in coordinating immune responses, further models (also including invertebrates) have been added. The zebrafish is both a powerful and versatile vertebrate model useful for immunological research.

The innate immune response forms the first line of defence against pathogens. In zebrafish, the innate immune system is functional by 2 dpf, and includes an extensive and heterogenous system similar to that of higher vertebrates including cytokines, neutrophils, macrophages, and interferons. The features of a multi-lineage myeloid system have been retained, with monocyte/macrophage cells capable of phagocytosis from 28 to 30 hpf, and granulocytic lineages that appear 32-48 hpf. One major difference is that zebrafish lack bone marrow and lymph nodes, and instead hematopoiesis occurs in the head kidney as in all other teleosts. Immune cells and blood cells arise from the hematopoietic, pluripotent stem cells in the whole kidney marrow. These cells then differentiate into either the myeloid or the lymphoid lineage (Trede *et al.,* 2004).

The zebrafish is an excellent model to study the development of immune cells due to their external development and optically transparent embryos. Following fertilisation, larvae survive with only the innate immune responses because the adaptive immune system is morphologically, and functionally mature at 4-6 weeks post fertilisation. This temporal separation therefore provides a suitable model to study the innate immune response *in vivo* (Novoa & Figueras, 2012). The use of zebrafish *in vivo* studies can also be used in parallel

with human *in vitro* experiments to help study immune cell function and immune cell interactions.

One of the most important advantages of using the zebrafish as a model of immunity, is the establishment of transgenic zebrafish. Specific cells, organelles and structures can be fluorescently labelled to track cells and study cell morphologies and cell-to-cell interactions. The use of fluorescent tags coupled with the transparency of the larvae, allow for ease of visualisation of the whole organism as inflammation is initiated and subsequently resolves (Feng *et al.,* 2010). *In vivo* imaging in zebrafish has allowed for a better understanding of the development of cellular components, insights into their distribution, and identification of tissue locations as well as migratory behaviours. The detailed visualisation in real-time allows for the detection of intracellular damage and cell death with minimal interference (Henry *et al.,* 2013).

Genetic manipulation offers a way to understand the molecular controls and functions of the cellular components of both the adaptive and innate immune counterparts. The zebrafish can be genetically manipulated, using a wide variety of techniques, as discussed in section 4.1.2, making it an ideal model for genetic studies. Several lines of evidence suggest that the zebrafish have a complete set of genes for the establishment of a fully functional immune system similar to the mammalian immune system. Many protein and gene families involved in the innate mechanisms have been described, showing that several signalling pathways in mammals are conserved in teleost fish. This includes several cytokines that arise from macrophages, lymphocytes, granulocytes, DC's and mast cells (Traver *et al.,* 2003, Abo-al-ela *et al.,* 2018). Cytokines are secreted proteins with growth, differentiation, and activation functions that regulate the nature of immune responses. They are the earliest mediators of infection and are involved in several steps of the immune response from induction of the innate response to generation of cytotoxic T-cells, and production of antibodies. Cytokines modulate the immune response through autocrine or paracrine manner upon binding to the corresponding receptors (Reyes-Cerpa *et al.,* 2012). In the zebrafish, several cytokines have been identified and studied such as IL-1β, TNF-α, IL-18, Interleukin-2, Interleukin-4, Interleukin-6, Interleukin-8, Interelukin-11, etc (Bird & Tafalla, 2015; Zou & Secombes, 2016).

4.1.5 Interleukin-34 in Zebrafish

In zebrafish IL-34 was first identified and sequenced by Wang *et al*. They identified IL-34 from five teleost fish, and showed that they had similar gene organisation with loci syntenically conserved (Wang *et al*., 2013). Using comparative expression studies, they demonstrated that IL-34 is differentially expressed in tissues, suggesting a homeostatic role of IL-34 for the macrophage lineage in fish. Later in 2018, a study by Wu *et al*., reported that IL-34 is a driver of the migration of microglial precursors to the brain, and that its overexpression enhanced microglial colonisation (Wu *et al*., 2018).

4.1.6 Rationale

Since its initial identification, there has been little development on the role of *il34* in zebrafish. Its expression pattern, biological processes and molecular functions have not yet been fully investigated. Moreover, the effect of IL-34 on macrophages *in vivo* is still in initial stages, and is not yet understood. For these reasons, and in view of the importance of this cytokine in the monocyte/macrophage lineage, we sought to identify, characterise and describe the expression of *il34* in zebrafish.

4.1.7 Aims and objectives

The general focus of this chapter was to develop a zebrafish knockout model to study the role of il34 in terms of its contribution towards the immune phenotype. The main objective was to develop and characterise a loss of function mutant. Following that, the focus was to study the
contribution and role of *il34* in the immune environment.

Specific aims:

1. To generate an *il34* loss of function model and stable mutants using the CRISPR/Cas9 mechanism.
2. To assess the resulting loss of function phenotype in terms of the development and function of *il34* in larval zebrafish, including the effect on the bone phenotype.

3. To extend further the knowledge about the expression patterns of *il34* in wild type zebrafish.
4. To investigate the effects of il34 deficiency on inflammatory responses and innate immune cell populations in larval zebrafish.

4.2 METHODS

This chapter was carried out in the zebrafish facility at The Bateson Centre, at the University of Sheffield. The work was conducted as a collaboration with Professor Stephen Renshaw. Thanks to this collaboration, access to the zebrafish facility and use of zebrafish project licence was possible.

4.2.1 Materials, Reagents and Equipment Used

A. MATERIALS & REAGENTS	
2 X BioMix Red	Bioline
Agarose	Sigma Aldrich
Ammonium acetate	Ambicon
Anti-dig Antibody	Sigma Aldrich
BCIP	Thermo Fischer
Bovine Serum Albumin (BSA)	Sigma Aldrich
Cas9 Protein	NEB
Chloroform	Fisher Scientific
Ethanol	Fisher Scientific
Ethidium Bromide	Thermo-Fisher
Formamide	Fisher Scientific
Glycerol	Sigma Aldrich
Heparin	Thermo-Fisher
Isopropanol	Acros Organics
Magnesium Chloride	Sigma Aldrich
Methanol	Fisher Scientific
Methylene Blue	Sigma Aldrich
NBT	Sigma Aldrich
NTP-DIG-RNA-Mix	Roche
Paraformaldehyde	Fisher Scientific
Phenol Red	Sigma Aldrich
Phosphate-Buffered Saline Tablets	Fisher Scientific
Proteinase K	Sigma Aldrich

RNAse inhibitor	Agilent Biotechnologies
Sheep Serum	Sigma Aldrich
Sodium Chloride	Fluka Analytical
Sodium Citrate	Sigma Aldrich
Sodium Hydroxide	Fisher Scientific
SP6 polymerase	Promega
SYBR Green	Sigma Aldrich
T7 Polymerase	Promega
TAE Buffer	Life Technologies
Taq Polymerase	Promega
Transcription Buffer	Promega
Tricaine	Life Technologies
Tris	Sigma Aldrich
Trizol	Life Technologies
tRNA	Sigma Aldrich
Tween-20	Sigma Aldrich
B. KITS	
DNA-Free Kit	Invitrogen, Life Technologies
Megashortscript T7 Transcription Kit	Invitrogen, Life Technologies
One Shot Competent Cells Kit	Invitrogen, Life Technologies
QIAquick PCR Purification Kit	Qiagen
SuperScript II First-Strand Synthesis Kit	Thermo Fisher Scientific
TOPO TA Cloning Kit	Invitrogen, Life Technologies
C. RESTRICTION ENZYMES	
Bsi1	NEB
BSR1	NEB
MWo1	NEB
D. PRIMERS & ULTRAMERS	
Primers for genotyping and for RT-qPCR	Integrated DNA Technologies
Ultramers for guideRNA's	Sigma-Aldrich

E. EQUIPMENT	
Spectrophotometer ND-1000	Nanodrop
Thermal Cycler Touch C1000	Bio-Rad
Prism Centrifuge	Lab-Net
Inverted Microscope – Eclipse TE2000	Nikon
SMZ1500 Stereomicroscope	Nikon
Bio-Doc Gel Imaging System	UVP
RT-PCR System HT7900	Agilent Biosystems
Gel Pack	Bio-Rad
Stereo Microscope MZ9.5	Leica
F. SOFTWARE	
Elements Software	Nikon
Graph Pad Prism V7	Graphpad
Snap Gene Viewer	GSL Biotech
Ap-E Plasmid Editor	University of Utah

4.2.2 Generation of *il-34* Mutant Zebrafish by CRISPR/Cas9

4.2.2.1 Identification of Interleukin-34 gene in zebrafish

A BLAST search for Interleukin-34 zebrafish (*Danio rerio*) protein on both ENSEMBL and NCBI databases led to the identification of a single zebrafish orthologue of human and mouse IL-34 (ENSDARG00000091003.2).

4.2.2.2 Identification of sequences to target with the CRISPR/Cas9

The exons chosen as CRISPR targets were Exon 2, Exon 3 and Exon 5. Early exons were chosen so as to increase the chance of full loss-of-function occurrence. Each exon sequence was inputted into the software SnapGene viewer to locate CRISPR sites. To identify sites, PAM sites (NGG or CCN) were located within each of the exon sequences. Sequences with a built-in restriction site were chosen, so that once a mutation is generated, the restriction site is disrupted and restriction digest can be used to screen for mutants. Since restriction enzymes are used to monitor the occurrence of a cleavage, it was crucial that the restriction enzyme chosen presented only once within the CRISPR target. The chosen sequence (20 bp upstream of the PAM site) was noted and placed into a guideRNA (gRNA) template (underlined sequences in Table 6. The remaining part of the template contained a sequence for the guide RNA to recruit the Cas9 and the T7 promoter (shown in bold). The sequences were ordered as single stranded ultramers from Sigma Aldrich.

Table 6: Target sequences designed for CRISPR mediated knockdown of *il34* in zebrafish. Highlighted regions are target sequences, bold sequences are T7 promoter regions.

gRNA	Enzyme	Sequence
Exon 2 – gRNA1	BSi1	5'-AAAGCACCGACTCGGTGCCACTTTTTCAAGTT GATAACGGACTAGCCTTATTTTAACTTGCTATTTC TAGCTCTAAAACCCAGCATTCGGACTGGACCATG G**CTATAGTGAGTCGTATTA** -3'
Exon 3 -gRNA 2	BsrI	5'-AAAGCACCGACTCGGTGCCACTTTTTCAAGTT GATAACGGACTAGCCTTATTTTAACTTGCTATTTC TAGCTCTAAAACCCAGTGTGCAGTAGTGCAGCTC C**CTATAGTGAGTCGTATTA** -3'
Exon 5 –gRNA 3	Mwo1	5'- AAAGCACCGACTCGGTGCCACTTTTTCAAG TTGATAACGGACTAGCCTTATTTTAACTTGCTATT TCTAGCTCTAAAACCCAGTGCTGCCGAGAGATCT CCC**CTATAGTGAGTCGTATTA**-3'

4.2.2.3 Transcription of gRNA

Transcription of the gRNAs from the oligonucleotide templates was performed using the MEGAshortscript T7 kit (Life Technologies). The transcription reaction mixture was assembled as follows: 1 µL oligonucleotide, 1 µL enzyme, 1 µL each dNTP, 1 µL buffer and 3µL nuclease free water. The mixture was incubated at 37°C for at least 4 hours. Following this incubation period, 1 µL of DNAse was added in order for any remaining nucleotides to degrade. Nuclease-free water was added to top up the reaction volume to 100 µL. 15 µL of cold 10 M ammonium acetate solution, and 300 µL ice cold ethanol were then added to the mixture and mixed so as to purify the RNA. The RNA was precipitated for at least 30 minutes at -20°C. To pellet the RNA, the mixture was centrifuged for 15 minutes at 13,000 g at 4°C. The supernatant was removed, and the pellet air-dried and resuspended in 10 µL of nuclease-free water. The RNA concentration was measured using a nanodrop spectrophotometer and stored at -80°C until further use.

4.2.2.4 Zebrafish husbandry

All zebrafish used for this project were located in the aquaria at The Bateson Centre, at the University of Sheffield. Zebrafish were present in tanks at a density of no more than four zebrafish per litre, with a 14 hour light and 10 hour dark cycle, at a temperature of 28°C. All experimental procedures were carried out in accordance with the Animals (Scientific Procedures) Act 1986 under the authority of UK Home Office Project Licence PPL70/8178 and Personal Licence IO6008638.

4.2.2.5 Maintenance and collection of zebrafish embryos

For collection of zebrafish embryos, a marble tray was placed in the fish tank the night before. This stimulates mating at the beginning of the light cycle in the morning. If careful staging was to be done, zebrafish were pair mated by pairing. To pair mate, a male and female zebrafish were placed on either side of a divided tank overnight. The divider was then removed in the morning at the desired time and the zebrafish were allowed to mate for collection of embryos. Embryos and larvae were kept at a temperature of 28ºC in 1X E3 media (containing 2 drops of methylene blue antifungal agent). Zebrafish were placed in 10 cm petri dishes, with no more than 60 fish in one plate. Larvae were not kept past the point of legal protection at 5.2 dpf unless they were being raised to adulthood. To cull, live embryos were terminally anaesthetised in tricaine (0.016%).

4.2.2.6 Microinjection of gRNAs into zebrafish embryos

Prior to injection, it was made sure that embryos did not develop past the four-cell stage, as this is not ideal for injection of genetic constructs; ideally they should be at the one cell stage. Eggs were lined up against a microscope slide for ease of injection, whilst the needle was lowered toward the eggs, piercing the surface of the chorion and entering the yolk sac in one stroke. Each gRNA was injected together with Cas9 protein. The injection mixture was made up of the following; 1 µL of Cas9 protein, 1 µL of gRNA and 0.5 µL phenol red. 1 nanoL of this mixture was injected into the yolk of each embryo. Several uninjected embryos were kept as a control (Figure 53).

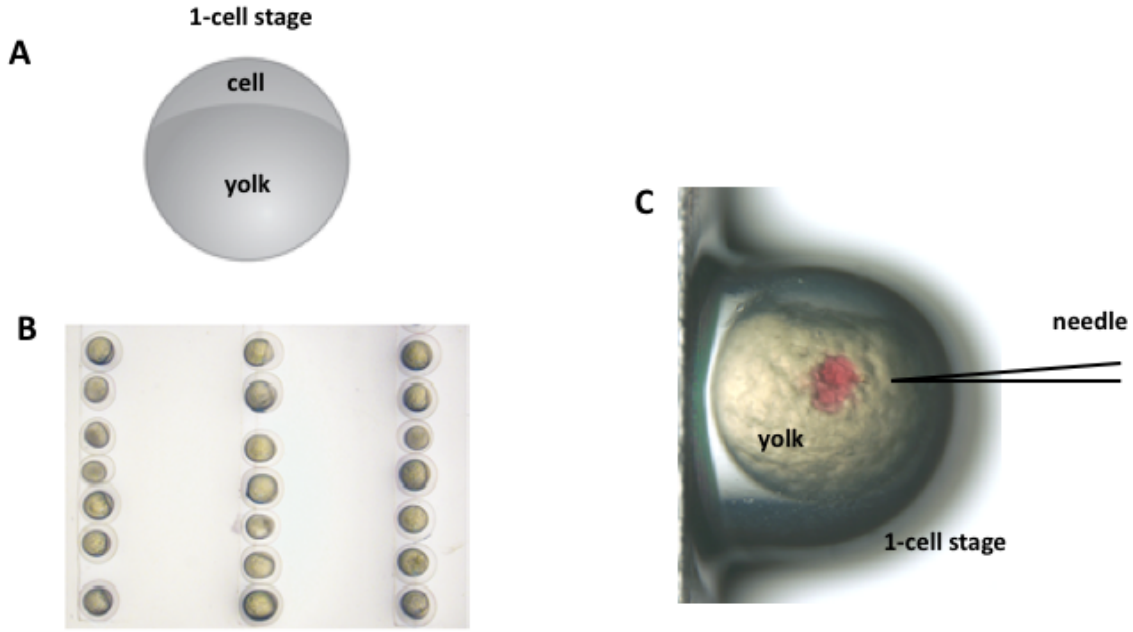

Figure 44: Figure showing microinjection of zebrafish embryos. (A) An illustration of a zebrafish embryo at the one-cell stage (B) Alignment of one-cell stage embryos prior to injection (C) image showing needle and injection of construct directly into the yolk as marked by the red phenol. Adapted from (Rosen *et al*., 2009)

4.2.2.7 Testing of CRISPR efficacy

Twenty-four hours post injection, the DNA of eight injected embryos and un-injected embryos were collected. Each sample was subjected to PCR with primers for each of the CRISPR targets and PCR products were then digested with the relevant restriction enzymes (Table 6). If the CRISPR was successful, the restriction site would be disrupted, and an undigested band was visible. Embryos that showed a mutant band on the gel were raised. This was required for germline integration of the transgene. Screening for founder fish (F0) that carry the *il34* mutation in their germ cells was performed when they reached sexual maturity (see section 4.2.3.2).

4.2.2.8 Primers for PCR

A forward and a reverse primer were designed for each of the target sequences using primer 3 (http://primer3.ut.ee/). Primers were supplied by Integrated DNA Technologies Ltd (Belgium). Upon arrival, the primers were re-suspended in dH2O, to a final concentration of 100 μM. The primer sets for each of the guide RNA's injected are listed in the table below (Table 7).

Table 7: List of PCR Primers for each target sequence

Guide RNA	Sequence
gRNA 1	Fw Primer 5'- GATATTTTTTGCAGGTGTTTAATA - 3' Rv Primer 5'- CATCTGACATTTTGTCATTTTTA - 3'
gRNA 2	Fw Primer 5'- TCAGCCAATAAATATCAGATCCA- 3' Rv Primer 5'- CGTCTCCTTAAGGTTGCATTT - 3'
gRNA 3	Fw Primer 5' - GCGAACCACAAAAAGTTGAA- 3' Rw Primer 5'- TGGTCTTCGTGATTCCCTTC- 3'

Fw: forward, Rv: reverse

4.2.2.9 Nucleic acid extractions

Genomic DNA was extracted from whole embryos by boiling them in sodium hydroxide. 100 µL of NaOH was added to one embryo, and heated at 95°C for 5 minutes. This was followed by vigorous vortexing. 10 µL of 1 M Tris HCl pH8, was added for neutralization of the solution, and the sample was then centrifuged at 1,000 g for 1 minute to pellet any large debris. The supernatant was collected for further analysis.

4.2.2.10 Polymerase Chain Reaction

Amplicons were amplified with the primer sets in a 10µL PCR reaction (5 µl Biomix Red (Bioline), 1 µl each forward and reverse primer, 2 µL dH_2O, and 1 µL ultramer). The PCR cycle was as follows: 95°C for 3 minutes, 35 cycles of 95°C for 30 seconds, respective annealing temperatures for 30 seconds, and 72°C for 20 seconds. The reaction was then incubated for 5 minutes at 72°C. 2 µL of the PCR reaction was electrophoresed on an agarose gel to confirm that the PCR was successful. The amplified ultramer was then stored at -20°C until needed.

4.2.2.11 DNA gel electrophoresis

To visualise the PCR and restriction digest products, DNA gel electrophoresis was used. A 1.5% agarose gel was made by dissolving agarose in TAE buffer (20 mM acetic acid, 40 mM Tris, 1 mM EDTA). 4µL ethidium bromide was added per 50mL of agarose and mixed by swirling the molten agarose gel. Samples were run at 150 V for 15-30 minutes. DNA bands were visualised with UV light using the BIODOC ITTM imaging system (UVP).

4.2.2.12 Screening for stable founders and identification of mutation by sequencing

To identify founders with germline transmission of *il34* mutation, F0 adult fish (at 3 months of age) were outcrossed with wild-type AB fish. Embryos at 1-2 dpf from such matings, were screened for *il34* heterozygous allele (*il34* +/-). Following the identification of such mosaic founders (F0), these where outcrossed to wild-type adults. The resultant offspring of founder fish, termed the F1 generation, are either WT or else carry the heterozygous alleles of the transgene in their genome (Figure 54). Following an additional 3 months, F1 fish were outcrossed to wild-type and their embryos used to sequence the mutation. Cloning was performed for direct insertion of Taq polymerase- amplified PCR products into a plasmid vector for sequencing.

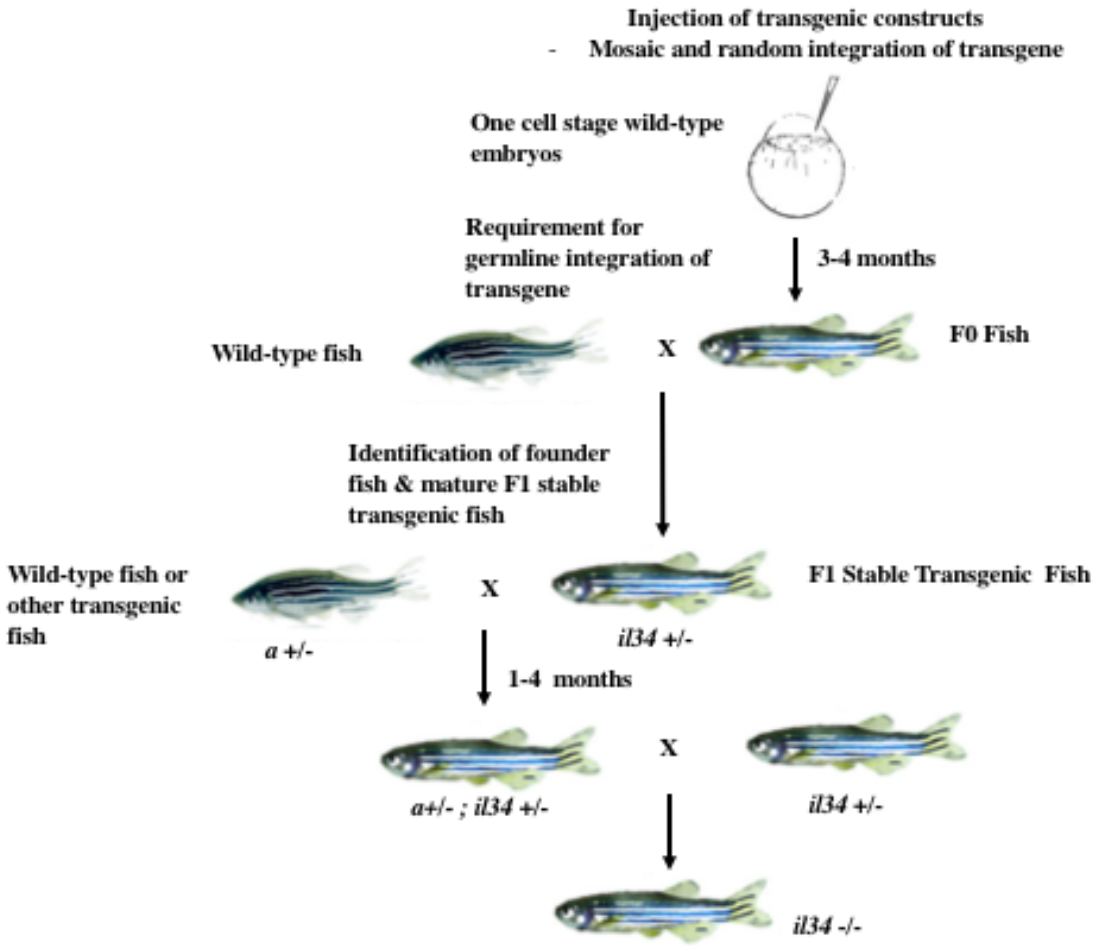

Figure 45: Strategy and timeline for generating a stable il34 mutant line. The DNA construct (gRNA with Cas9) is first injected into one-cell stage wild-type zebrafish embryos, where the transgene is allowed to integrate into the fish genome. This integration is required in order to generate a stable mutant line where both individuals and their offspring carry the il34 mutation. After reaching sexual maturity, F0 generation fish are outcrossed to wild-type to screen for founders with the germline transmission. The offspring of such founder fish, will be the F1 generation, and these carry the heterozygous allele in their genome. The F1 generation is then outcrossed to wild-type for the continuation of the mutant transgenic line (ideally outcrossed until F3 is reached), or crossed to other transgenics (termed a in diagram) to create transgenic lines mutated for il34.

4.2.2.13 Cloning and transformation

To perform molecular cloning, the TOPO TA cloning® kit (Invitrogen, Life technologies) was used. The PCR product was first purified using the QIAquick PCR purification KIT (Qiagen). Following this, 4 μl of purified freshly purified DNA, 1 μl of TOPO vector and 1 μl of salt solution were mixed together and left to incubate at room temperature for 30 minutes. In the meantime, chemically competent DH5β (NEB) cells were defrosted on ice for a few minutes. To initiate the transformation, the cloning products were added to the cells, and incubated on ice for 30 minutes. Cells were then heat shocked at 42ºC for 30 seconds followed by an additional 5 minutes on ice. 900 μl of SOC media (Sigma) was then added, and left to incubate on a shaker for 1 hour at 37°C. While incubation occurs, agar plates with ampicillin at a concentration of 0.1 mg/ml were left in the incubator to dry. 100 μl of the transformation reaction was plated onto the agar plates and distributed evenly using a cell spreader. The plate was then incubated overnight at 37 ºC. In order to determine whether the TOPO cloning was successful, colony PCR was performed.

4.2.2.14 Colony PCR

After the transformation plate was incubated overnight, the colonies were picked for analysis. A PCR master mix was made up using M13 primers from TOPO TA cloning® kit. For the DNA portion of the reaction, a single colony was picked using a sterile p10 pipette tip and dabbed into the PCR reaction. PCR was performed on all reactions and gel electrophoresis was then performed. Reactions positive for PCR cassette were sent for sequencing with M13 primers.

4.2.3 Genotyping and Maintenance of il-34 Mutant Line

4.2.3.1 Fin Clipping

In order to genotype, adult fish were anesthetised in a solution of tricaine (80 μg/mL). Using sterile surgical scissors, a small portion of the caudal fin was removed. The clipped fish were moved to individual tanks, until the genotype was established.

4.2.3.2 Genotyping

Genotyping was performed by extracting DNA from the caudal fins by the sodium hydroxide method. This was followed by a PCR and subsequent DNA electrophoresis. The *il34* 50 bp deletion was genotyped using the following primer pair for the whole duration of the project:

Forward Primer 5'-TCAGCCAATAAATATCAGATCCA- 3'
Reverse Primer 5'-CGTCTCCTTAAGGTTGCATTT- 3'

A product of size 300 bp was WT (*il34* +/+). A product of size 250 bp was homozygous (*il34* -/-) for 50 bp deletion. Two products of both these sizes were heterozygous (*il34* +/).

Following the identification of a (heterozygous) allele in the F1 generation containing a 50 pb deletion (*il34* +/-), the F1 generation was outcrossed to WT until the F3 generation was reached. Zebrafish homozygous for this 50 bp deletion (*il34* -/-) used for all experiments, were generated from an incross of F3 heterozygotes *il34*+/-

4.2.3.3 Combination of il34 mutant line with other transgenic lines

Since *il34* is hypothesised to be involved in the generation and proliferation of myeloid cells, combining the mutant line with other transgenic lines where myeloid cells (namely macrophages and neutrophils) are fluorescently labelled would be beneficial. This would allow imaging and examination of the individual contributions these cells play during inflammation without the presence of *il34*. We therefore crossed *il34* mutant zebrafish to two other transgenic lines:

1. *Tg*(mpx:GFP)^{i114} : a transgenic zebrafish line that expresses GFP under the neutrophil-specific myeloperoxidase (*mpx*) promoter (Renshaw & Loynes, 2006)
2. *Tg*(fms:GFP)^{SH377}: a transgenic zebrafish line that expresses GFP under the control of csf1r receptor (Dee *et al.,* 2016)

Zebrafish heterozygous for il34 allele (*il34*+/-) were crossed with zebrafish homozygous for the respective line to generate transgenics mutated for *il34*. Following the crossings, embryos positive for GFP fluorescence, where selected and raised. Adults were genotyped for *il34* mutations and heterozygous individuals were identified and kept for further experiments.

4.2.4 Characterising *il-34* Expression in Wild Type Zebrafish

4.2.4.1 Spatial expression of il34

To characterise *il34* in WT zebrafish, we assessed the level of expression through 1-5dpf larvae, and adult organs (head kidney, brain, gut, spleen, liver, and heart) by conventional Q-PCR as well as RT-PCR. Additionally we performed whole mount *in situ* hybridisation on 3dpf larvae to determine site expression of this orthologue.

4.2.4.2 RNA extractions

To extract RNA required for cDNA generation; 20 larvae and/or organs, were collected and placed in an eppendorf tube. All E3 media was removed and samples were washed in PBS. 300μl of TRIzol® (Life Technologies) was added and the larvae homogenised with a mechanical pestle (approx. 15 pulses per sample), followed by incubation on ice for 5 minutes. At this stage, homogenised samples were put put into liquid nitrogen for snap freezing and stored at -80 ºC until further use. Otherwise RNA extractions where performed immediately after this step.

60 μl of Chloroform were added; the tube was inverted a few times, then left to incubate for a further 5 minutes at room temperature and vortexed to ensure chloroform is mixed. Samples were then centrifuged for 15 minutes at 13,000 g at 4ºC. 100 μl of the supernatant were removed and placed into a new sterile microcentrifuge tube. 150 μl of isopropanol were added, the tube was inverted to precipitate the RNA. Samples were then incubated overnight at -20ºC. Following overnight incubation, samples were centrifuged again using the same settings. All supernatant was discarded, and the RNA pellet washed with 70% ethanol and centrifuged for 5 minutes at 7,000 g at 4°C. The supernatant was discarded again, and the RNA pellet air dried for 3 minutes, followed by re-suspension in 20 μl DEPC treated H_2O.

For embryos at 1-5dpf, 20-30 larvae were used per sample, and for organs, 2-3 of each organ was pooled. These experiments where repeated three times to achieve three biological repeats.

4.2.4.3 DNase treatment

The DNA-Free KIT ™ (Invitrogen™) was utilised to remove DNA from purified RNA . 10 μl buffer and 1 μl DNase were added to the RNA, and incubated for 30 minutes at 37 ºC. 2 μl DNAse inactivation solution were added, mixed and incubated at room temperature for 2 minutes. The contents were then centrifuged at 10,000 g for 2 minutes. The RNA supernatant was then transferred to a fresh tube.

4.2.4.4 Reverse transcription

Purified RNA was firstly quantified by a Nanodrop (Thermo scientific). The First-Strand cDNA Synthesis Using Superscript II RT kit (Thermo Scientific) was utilised for the reverse transcription reaction. 1000 ng RNA per sample, 1 μl of Oligo $(dT)_{12\text{-}18}$, and 1 μl dNTP mix were assembled in a sterile Eppendorf and made up to 12 μl with DEPC treated H2O. The mixture was heated to 65ºC for 5 minutes and quick chill on ice. 4 μl 5X cDNA buffer and 0.1 MDTT mix were added and incubated for 2 minutes at 42ºC. 1 μl of SuperScript II RT enzyme was then added. The mixture was incubated for 50 minutes at 42ºC followed by a last incubation for 15 minutes at 70ºC.

4.2.4.5 Real time-polymerase chain reaction

For RT-PCR reactions, primers were optimised for concentration, annealing temperature and efficiency. All primers used for RT-PCR are listed in Table 8. GAPDH was used as a reference gene to which data was normalised. SYBR green master mix was utilised. Reactions (10 μl each well) where assembled as follows: 5 μl SYBR Master mix, 0.5 μl of FW and RV primer (each at 10 μm), 2 μl of cDNA (at appropriate dilution), and 2 μl of H_20. The following cycling protocol was used: 95ºC for 7 minutes as the initial denaturation step, 40 cycles of 95ºC for 15 seconds and 60ºC for 30 seconds. Followed by 95ºC for 30 seconds and 65ºC for 10 seconds. Reactions were performed by real-time PCR machine ABI 7900 (Agilent Biotechnology).

Data analysis: To set the threshold, data was viewed on a log scale. The threshold level was set in the log region of amplification, where all amplification plots were parallel and above the background noise of the baseline. It was also checked that a single peak was obtained for the melting curves. For quantification of samples, this was determined as the ratio between quantities of day 0 versus all other days (day 1-5), mutant versus wild type (See Section 4.3.5) or knockout versus wild-type for inflammation assays (see section 4.3.7).

Normalised values were calculated by (Nolan *et al.*, 2006):

1. Delta Cq (wild-type) = Cq (wild-type) – Cq(Wild-type GAPDH)
2. Delta Cq (mutant) = Cq (mutant) – Cq (mutant GAPDH)

Then:

3. Deltadelta Cq = delta Cq (wild-type) – delta Cq (mutant)

The expression of the gene = 2^-deltadeltaCq

Therefore expression is = 2^ (3(=1-2))

4.2.4.6 High resolution in situ hybridisation of il34 in zebrafish embryos.

A. Probe design and synthesis

To generate RNA probes for whole mount *in-situ* hybridisation (WISH), the *il34* cDNA sequence was first obtained through the ENSEMBL database. The *il34* coding sequence is 642 bp long and therefore all of it was utilised (usually a 700-1000 bp in length, is desirable for generation of probes). Primer 3 was used to design primers that would amplify this region of cDNA. Primers where chosen away from the coding sequence and into UTRs, in order to make sure that all the cDNA is copied and included in PCR. The PCR product was amplified and subcloned into a TOPO TA. Colonies positive for the cassette were sent off for sequencing and the orientation was determined (sense and anti-sense strands).

To synthesize the probe, the plasmid was first linearized by cutting at the opposite end of the cassette to transcription using a restriction enzyme. The cassette was also checked not to have a restriction site at the same site as the digesting enzyme by analysing the sequence with NEBcutter V2.0. The restriction digest was constructed of 20 μg of plasmid DNA, 3 μl restriction enzyme and 20μl appropriate buffer. The reaction was made up to 200 μl H_2O and incubated at 37ºC for 2 hours. The cut plasmid was purified by phenol/chloroform extract, and re-suspended in H_20. 2 μl of uncut plasmid and 5 μl of cut plasmid were electrophoresed on a 1.5% gel to determine if linearization was complete.

To generate the riboprobe, 2000 ng cut plasmid, 4 μl transcription buffer, 4 μl DIG labelling mix, 2 μl of transcription enzyme (either T7, T3 or Sp6) and 2μl RNAase inhibitor were made up to 40 μl with H_2O, then incubated for 2 hours at 37ºC. Following incubation, 4μl DNAse was added and the mixture incubated for a further 15 minutes. 10 μl 7.5 M $NH_4C_2H_3O_2$ (ammonium acetate) and 60 μl Ethanol (both ice cold) were added to the transcription reaction and inverted to mix. The reaction was then centrifuged in a micro-centrifuge (13,000 g, 4ºC, and 15 minutes). The supernatant was discarded and the pellet washed with 100 μl ethanol (70%) and centrifuged again for 5 minutes. The supernatant was again discarded, the pellet air dried for 3 minutes and re-suspended in a 100 μl mixture of formamide and H_2O (70:30 respectively) then stored at -80ºC.

B. Embryo fixation

Larvae at 3dpf were utilised for whole mount *in situ* hybridisation (WISH). To fix larvae, they were first dechorionated and put into 1.5 ml microcentrifuge tubes in groups of 20. All E3 media was removed and 500 μl 4% PFA solution was added. The larvae were incubated on a rocker at room temperature for 2 hours. PFA was removed and replaced with 500 μl of 100% methanol, incubated at room temperature for 15 minutes and then stored at -20ºC until needed.

C. Whole Mount in In-Situ Hybridisation (WISH)

Day 1: Fixed larvae were rehydrated through a series of methanol washes each for 5 minutes: 75% methanol: 25% PBS, 50% methanol: 50% PBS, 25% methanol: 75% PBS, and 4 washes with 100% PBS-T (PBS + 0.1% Tween 20). Larvae were then digested with 10 μg/ml proteinase K, at room temperature for 40 minutes. The larvae were then fixed again in 4% PFA and incubated at room temperature for 20 minutes. Samples were then washed with PBS-T for 5 minutes, 5 times each. Samples were then cleared of the PBS-T and incubated in pre-heated PreHyb buffer (50% formamide, 5 x SSC solution, 0.5 mg/ml tRNA, 0.1% tween 20, 50 µg/mL Heparin, pH was adjusted to 6.0 with 1M citric acid) for 2-5hours at 70ºC. Samples were kept in a water bath. Following this incubation, PreHyb buffer was discarded, and replaced with ProbeHyb buffer (same as PreHyb with additional 1:200 dilution of probe in formamide). Samples were left to incubate overnight in a horizontal position on a heating blocking at 70ºC.

Day 2: Samples were briefly washed with WashHyb Buffer (PreHyb without tRNA and Heparin) at 70 ºC followed by washes (also at at 70 ºC) for 15 minutes each with a series HybWash as follows: 75% HybWash: 25% 2 x SSC, 50% HybWash: 50% 2xSSC, 25% HybWash: 75% 2 X SSC then 100% 2 x SSC. Samples were then washed twice with 0.2XSSC for 30 minutes at 70ºC. Samples were then given sequential washes of decreasing concentrations of 0.2 x SSC for 10 minutes at room temperature. Starting with 75% 0.2 x SSC: 25% PBS-T, then 50% 0.2 x SSC: 50% PBS-T, then 25% 0.2 x SSC: 75% PBS-T, followed by a final 10 minutes PBS-T wash. For blocking, each sample was incubated in blocking solution (2 mg/mL BSA), 2% sheep serum, all dissolved in PBS-T) for 2-5 hours

at room temperature. Each sample was then incubated in 500 μl Blocking buffer with a 1:5000 dilution of anti-dig antibody (Roche) and protected from light at 4 ºC overnight.

Day 3: The following day, samples were discarded of antibody solution and given a brief wash in PBT. This was followed by 6 additional washes for 15 minutes each. All larvae where then transferred to a 24-well plate on the last wash in order to start staining procedure. For staining, 3 x 5 minutes washes with NTMT buffer (0.1 M Tris HCl pH 9.5, 50 mM Mg Cl2, 0.1M NaCl, 0.1% Tween 20) at room temperature. Buffer was then exchanged for staining solution (3.5 μl and 4.5 μl, BCIP and NBT respectively, per ml of NTMT, Roche). Samples were monitored every 15 minutes for development of stain. Once stain had developed, the samples were washed 3 times with PBS-T. In order to remove any background, each sample was washed with 50% methanol, followed by incubation in 100% methanol, until all background had been cleared. Samples were then washed again with 50% methanol, then twice with PBS-T. 4% To re-fix larvae, PFA was added for 20 minutes at room temperature. Samples were washed 3 times with PBS-T, and placed into 75% glycerol and stored at 4 ºC.

Images: Photographs of larvae with WISH staining where taken using the SMZ1500 stereomicroscope, with a DS-Fi1 camera (both Nikon), at 20x magnification and Nikon Elements software.

4.2.5 Characterising the Expression and Inflammation of *il34* in Mutants

4.2.5.1 il34 expression in mutant adults

In order to determine loss of function in *il34* mutants, brains from 8-month old *il34*-/- individuals were collected and processed for cDNA. RT-PCR analysis on *il34*-/- and their *il34*+/+ siblings was performed.

4.2.5.2 Inflammation assays

The zebrafish was used as a model to study the role of *il34* as an inflammatory cytokine, through characterising its expression in response to injury and inflammation by caudal fin amputations. We also investigated the expression of its potential receptor *csf1ra* (colony stimulating factor 1 receptor) and the competing ligand *csf1a.* Additionally, we investigated the attenuation of two other common inflammatory signals *TNF-*α and *IL-1*β.

Amputation of the caudal fin was performed on 3 dpf larvae of homozygous (*il34*-/-) individuals. The caudal fin was amputated with a sterile scalpel, posterior to the muscle and notochord under anaesthesia with 0.016% tricaine in zebrafish water (Figure 55). Injured larvae, as well as uninjured ones (serving as control) were collected at various time points post-injury (2 hours, 4 hours, 8 hours and 24 hours). Following injury, larvae (20 for each condition; injured and uninjured, as well as for each time timepoint) were pooled and processed for RNA extractions as described in section 4.2.4.2. RT-PCR was then performed using SYBR green dye (refer to section 4.2.4.5). The list of primers used for RT-PCR can be found in the table below.

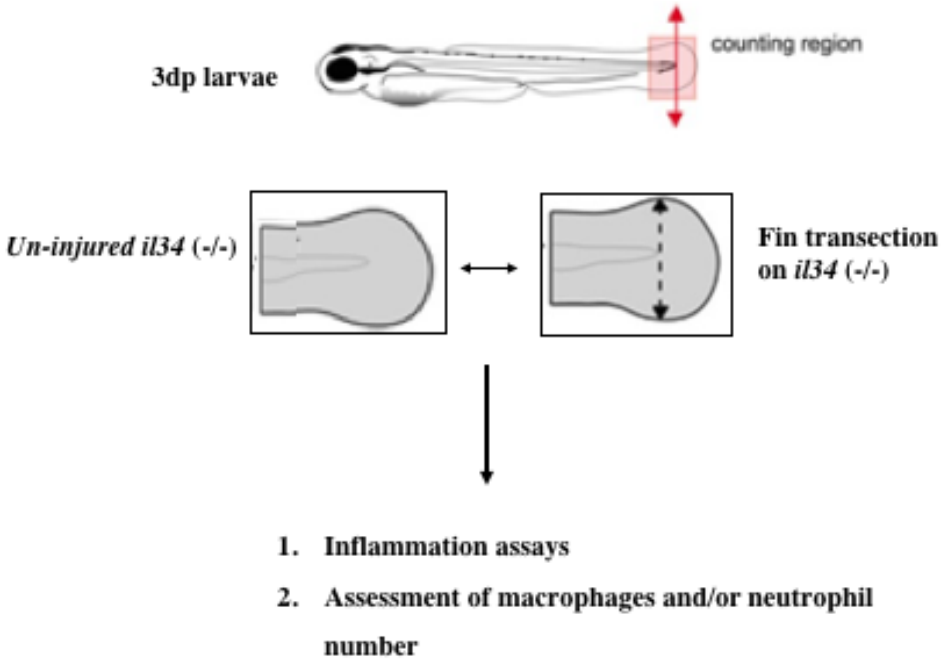

Figure 46: Schematic representation of caudal fin amputations in zebrafish. Caudal fins of homozygous ($il34^{-/-}$) from an F2 heterozygous ($il34^{+/-}$) in-cross, were amputated at 3dpf as shown. Injured and un-injured larvae were collected at several time points: 2hrs, 4hrs, 8hrs and 24hrs, and assessed for expression of the following :Il34, csf1ra, csf1a, TNF-α and IL-1β.

Table 8: List of primers for RT-qPCR of tail-fin injury assays.

	Forward (5'-3')	Reverse (5'-3')
Il34	TCAGACTGCGAAACATCAGC	TAATGCCCTGTTGACTCACG
EF1α	CAGCTGATCGTTGGAGTCAA	TGTATGCGCTGACTTCCTTG
GAPDH	GTGGAGTCTACTGGTGTCTTC	GTGCAGGAGGCATTGCTTACA
TNF-*α*	GCGCTTTTCTGAATCCTACG	TGCCCAGTCTGTCTCCTTCT
IL-1β	TGGACTTCGCAGCACAAAATG	GTTCACTTCACGCTCTTGGATG
Csf1a	Gene expression assay Dr03432535_m1 (Applied biosystems)	
Csf1ra	Gene expression assay Dr03125175_m1 (Applied biosystems)	

4.2.5.3 Assessment of neutrophil and macrophage number

For analysis of macrophages and neutrophils in *il34* genotypes, the transgenic reporter lines described in section 4.2.3.3 were used. Heterozygotes from the F1 generation for each respective line were incrossed, and 3 dpf larvae were anesthetized by immersion in E3 with 0.016% tricaine. Complete transection of the tailfin was performed using a microdissection scalpel in accordance with United Kingdom Home Office approval as previously described. Larvae recovered for the time interval indicated (4 hours for neutrophil counting, and 8 hours for macrophage counting).

Imaging: For imaging larvae were anesthetized in 0.016% tricaine and positioned in 24-well plates (Corning, Sigma), and covered with 1-2 mL of embryo water containing tricaine. Imaging was performed using a Nikon inverted microscope (Eclipse, TE2000) using a X1 objective, DS-Ri Camera at X20 magnification, and a GFP filter set. The number of fluorescent neutrophils and macrophages at the site of inflammation was counted by eye. Following counting, each individual embryo was genotyped.

4.2.6 Assesment of Cartilage and Bone Phenotype in *il34* Mutant Zebrafish

4.2.6.1 Von Kossa Stain

Von Kossa (calcium) staining is a technique used in histology to visualise calcium deposits. This technique uses the ability of calcium salts to transform into silver salts. Tissues are first treated with a solution of silver nitrate, which turns into silver phosphate when facilitated by a light source. These phosphates in turn bind to calcium present in the tissue, and silver is deposited. Staining is then visualized as metallic grey/brown deposits. We aimed to use this technique to visualise any abnormal development of bone in *il34* mutants versus their wild-type siblings.

For staining, 5 dpf larvae (around 20 per sample) were fixed in 4% PFA for around 2 hours at room temperature. After fixation, samples were rinsed three times in H_20 and 0.01% Tween. 1 mL of silver nitrate solution was added, and samples were left to incubate under a 60 W light bulb for 1 hour. Rinsing with H_20 and 0.01% tween was repeated to wash away any silver nitrate solution. Embryos were fixed in 2.5% sodium thiosulfate for around 10 minutes, and then rinsed again (3X) in H_20 and tween. This was then followed by fixing in 4% PFA for 30 mins at room temperature, and preservation in sequential glycerol solutions (25%, 50%, 75% and 100%). Embryos were kept at room temperature and covered in foil until images were taken.

4.2.6.2 Alcian Blue Staining

Alcian blue staining is a technique used to observe embryonic development of cartilaginous structures in embryos and complete larvae. In fish, Alcian blue can be used to observe cartilage from 2dpf onwards. The principal aim of carrying out this staining was to determine whether mutations in *il34* had any effects on cartilage development in homozygous embryos compared to their wild-type siblings.

5dpf larvae were fixed overnight in 4% PFA at 4ºC. The next day the larvae were washed twice in 0.1% PBS-T, and washed with sequential washes of methanol: 100%, 60% and 30% for 5 minutes each. Specimens were then transferred into Alcian blue staining solution

(0.1% Alcian Blue, 70 ethanol, 1% concentrated hydrochloric acid) and left to stain overnight at room temperature. Following overnight incubation in the stain, embryos where first rinsed in PBS-T and then bleached in 30% hydrogen peroxide for 10 minutes and on a hot plate at 37ºC. 30% saturated borate was then used to wash samples and help eliminate and residues of bleaching solution. Embryos were put into digestion solution (trypsin in 30% saturated borate solution) for 30 minutes at 37ºC until brains and eyes appeared translucent. Finally re-hydration through methanol series (5 minutes each) was performed and samples were put through a glycerol series (25%, 50%, 75% and 100%). Embryos were kept in room temperature in glycerol until images were taken. Zebrafish were imaged for both stains using the SMZ1500 stereomicroscope, with a DS-Fi1 camera (both Nikon), at 20 X magnification and Nikon Elements software.

4.2.7 Statistical Analysis

Data were analysed using GraphPad Prism (version 7.0) software (GraphPad). The numbers of experimental subjects for all experiments are donoted by the prefix n. Data is shown as the mean ± Standard error of the mean. All data analysed by t-test or one way ANOVA depending on the number of experimental groups. Significance values denoted as follow: Non-significant (ns): $p > 0.05$; *: $p<0.05$; **: $p<0.01$; ***: $p<0.001$; ****:$p<0.0001$

4.3 RESULTS

The aim of this chapter was to develop a zebrafish model to understand the role of IL-34 in both the development and function of the zebrafish. To achieve this, a zebrafish line deficient of IL-34 was generated by the CRISPR/Cas9 genome editing tool. The phenotype of the resulting individuals was assessed by investigating the spatial and temporal expression of the cytokine in larval individuals. Additionally, the contribution of Il-34 in the innate immune response was also analysed in both wild-type and loss of function mutants.

At the time the work was conducted, no other loss of function mutants for il34 existed in the literature. As a result this study represents the first characterisation of a loss of function mutant in zebrafish as well as the role of il34 in the innate immune response. The data presented here is therefore still in early stages, and further investigations need to be conducted to add to this repertoire.

4.3.1 Zebrafish Possess a Single Orthologue of Human IL-34

A search for the il34 protein of zebrafish (*Danio rerio),* in both ENSEMBL and NCBI databases, identified a single zebrafish orthologue of the human IL-34 (ENSDARG00000091003). The BLAST online tool was used to align both sequences, which showed that the zebrafish sequence has 30% protein and DNA identity to the human gene (Figure 56).

Figure 47: Clustal alignment of human and zebrafish IL-34. The human protein sequence (ENSG00000157368) aligned via clustal to its zebrafish orthologue (ENSDARG00000091003). The zebrafish sequence has 30% homology with that of humans.

The zebrafish *il34* gene encodes a single protein of 213 amino acids, is present on chromosome 18 (18, 527, 170-18, 543, 358), and is made up of 7 exons. The human IL-34 gene is present on chromosome 16 (70, 579, 895-70, 660, 682), contains 6 transcripts, 4 of which are protein coding and are also made up of 7 exons. It appeared that the gene has a general 7 exon/6 intron structure with an intron in the 5'UTR region, across both zebrafish and humans (Figure 57). Despite the conservation in the number of exons, exon size was different between both species. Additionally, compared to the zebrafish, the human IL-34 genes have a large untranslated region at the first coding exon (exon 2) and a large coding region in the last exon.

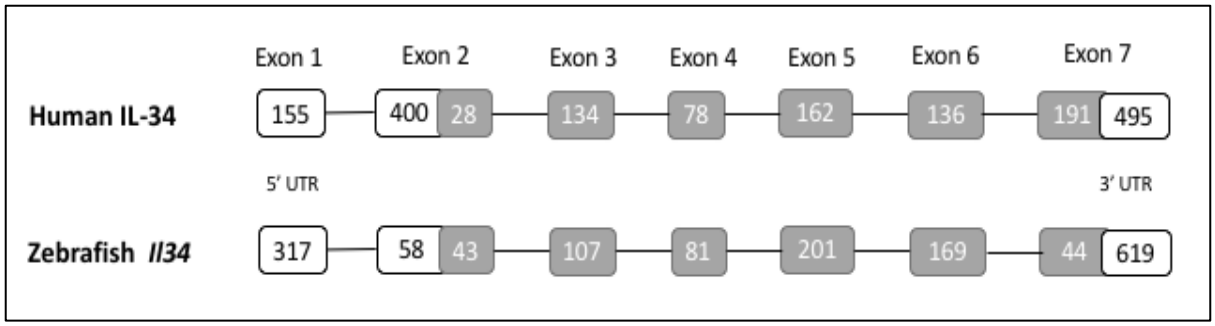

Figure 48: Exon alignment of human and zebrafish IL-34. Gene organization of human and zebrafish IL-34 molecules. Grey and white boxes represent amino acid coding regions and untranslated regions respectively. Bars represent introns, while exon sizes (bp) are numbered in the boxes.

Another important indicator of conserved function between orthologues, is gene synteny between the genomic loci of the gene of interest. The genomic loci of human and zebrafish *il34* were compared. A 500 kb stretch of zebrafish genomic locus was compared to a 900 kb stretch of human genomic locus, revealing gene synteny between them. The genes *MTSSIL, SF3B3, N4PB1, S1AH1,* and *LONP2* appear in both human and zebrafish loci. Although the gene order is reversed, *il34* is close to *SF383* in both species. This demonstrates that *il34* of zebrafish is a true orthologue of human. Figure 58 shows a graphical representation outlining the similarities and differences of both loci.

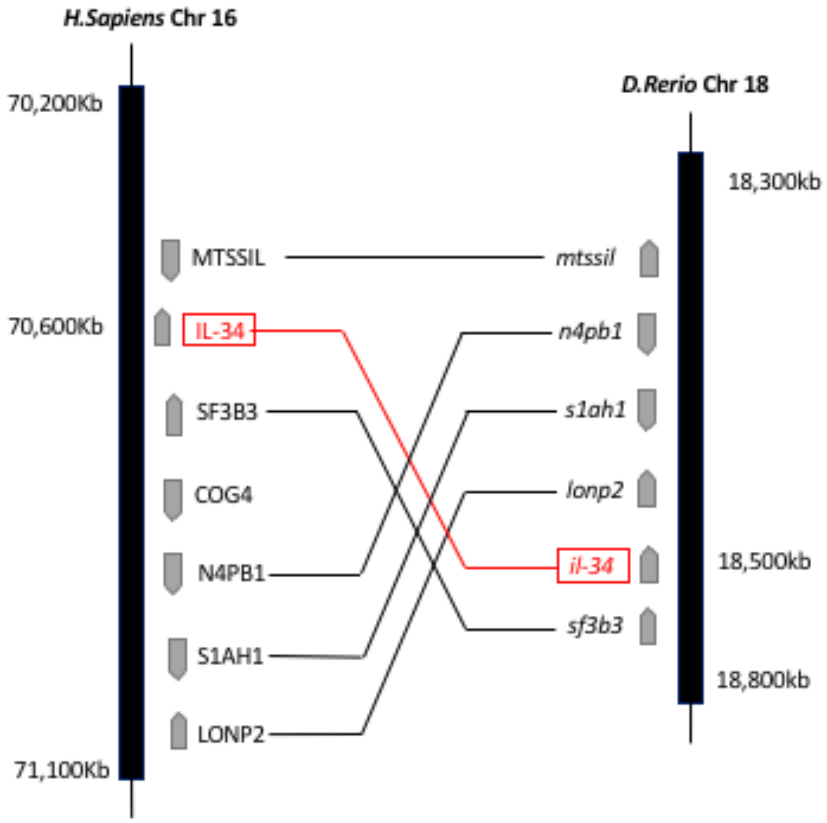

Figure 49: The genomic loci of IL-34 in human and zebrafish. Zebrafish and humans share conserved gene synteny with five genes (MTSSIL, SF3B3, N4PB1, S1AH1, and LONP2) remain localized within the same radius. This demonstrates that zebrafish il34 gene, is a true orthologue of the human IL-34. Arrows indicate transcriptional directions.

Taken together, the above factors indicate that homology between zebrafish and human IL-34 gene is relatively low, however the gene appears to be highly conserved across species. A similar pattern is observed for M-CSF (CSF-1). The M-CSF gene is highly conserved between zebrafish and humans with gene function in both species related to the mononuclear phagocyte system (Wang *et al*., 2013). As a result, given the relationship between M-CSF and Il-34 in the human monocyte/macrophage lineage and function, the zebrafish is a good model for the investigation of the role of il34 in immune and bone development.

4.3.2 Using the CRISPR/Cas9 System to Create an *il34* Mutant Line

4.3.2.1 Design and construction of il34 target sites

In order to generate a stable mutant line deficient of *il34,* the CRISPR/Cas9 system was utilised. To allow mutations caused by the CRISPR/Cas9 system to be identified easily, PAM sites close to large restriction sites were chosen. These are optimal sites to use for CRISPR as they are large and easily disrupted. Three restriction sites were chosen: *Mwo1, Bsl1* and *Bsr1*. The sites are GCNNNNNNNGC, CCNNNNNNNGG, ACTGGN, respectively with *BSl1* site containing natural PAM sites to which gRNA's can be targeted. *Il34* contained a number of these sites, and three guide RNA's were designed around these restriction sites. The aim was to generate a large deletion to eliminate, or cause a disruption in the coding sequence.

4.3.2.2 Testing the efficacy of CRISPR/Cas9

Any indels created by the CRISPR/Cas9 system and guide RNA will mutate the restriction site and prevent digestion. As can be seen from Figure 59, Guide RNA 2 induced a mutation. PCR products from un-injected single embryos were completely digested by *Bsr1* (Lanes 5-7). Digested PCR product from CRISPR/Cas9 injected samples (Lanes 8-17) showed incomplete digestion with the presence of uncut products, demonstrating that the CRISPR had medium efficacy. This confirms that the *BSrI* restriction site within *il34* exon 3, was disrupted and therefore the DNA fragment could not be digested. Figure 59 shows the restriction digest agarose gel image. Guide RNA's 1 and 3 did not induce any mutations and where thus eliminated as possible target sites or mutagenesis of *il34*.

Once the efficacy of the CRISPR was confirmed, 100 embryos were injected with gRNA–2 and Cas9, and raised to breeding age. In order to determine whether CRISPR mutations were transmitted to the germline, these F0 mosaic adults were crossed with wild-type and 8 embryos from each cross were analysed by PCR and analytical gel. Each digest was compared to a wild-type individual. Figure 60 shows representative digest for founder identification.

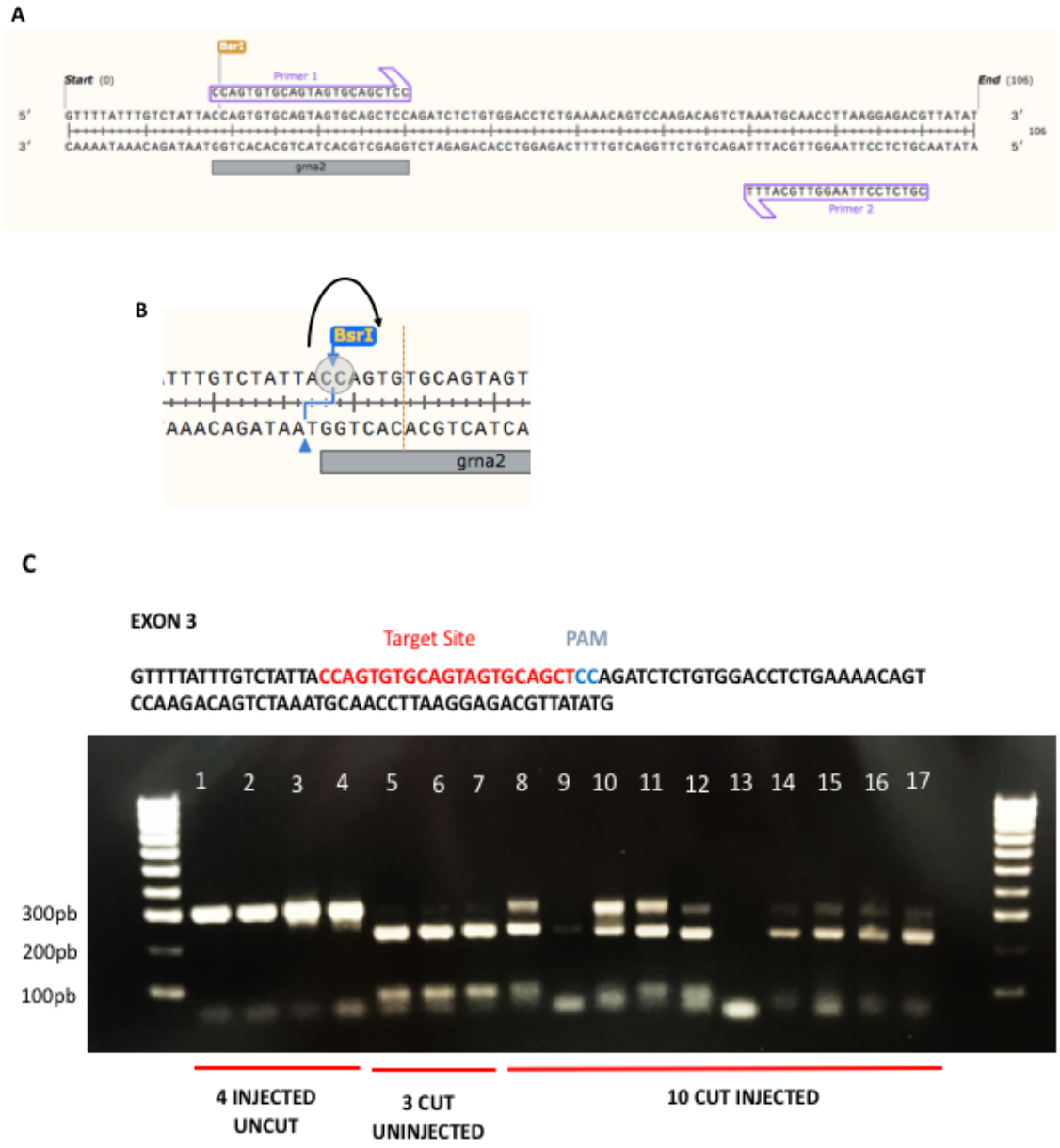

Figure 50: Design and efficacy of il34 gRNA-2 by CRISPR/Cas9 System. A) Schematic representation of il34 exon 3, with the guide RNA (gRNA2) designed complementary to the target site. The forward and reverse primers used to amplify the location of the target site are labelled as Primer 1 and Primer 2 respectively. B) The restriction site for BsrI is shown in detail. The restriction site is highlighted with a blue line, and its cut site labelled with a red line. The PAM site is shown in green with an arrow indicating the site where Cas9 will potentially cut the DNA. C: Analytical gel to test efficacy of CRISPR. PCR products of the target site from gDNA-2 from single embryos 24 hours post injection, were subjected to digestion by BsrI. The uncut PCR product of approximately 300 bp is shown in lanes 1-4. Un-injected controls cut with BsrI gave complete digestion, leaving two products of similar sizes at 250 bp mark (Lanes 5-7). CRISPR-injected embryos (Lanes 8-17) resulted in incomplete digestion in all embryos examined, implying BsrI site had been mutated by the CRISPR at medium efficacy.

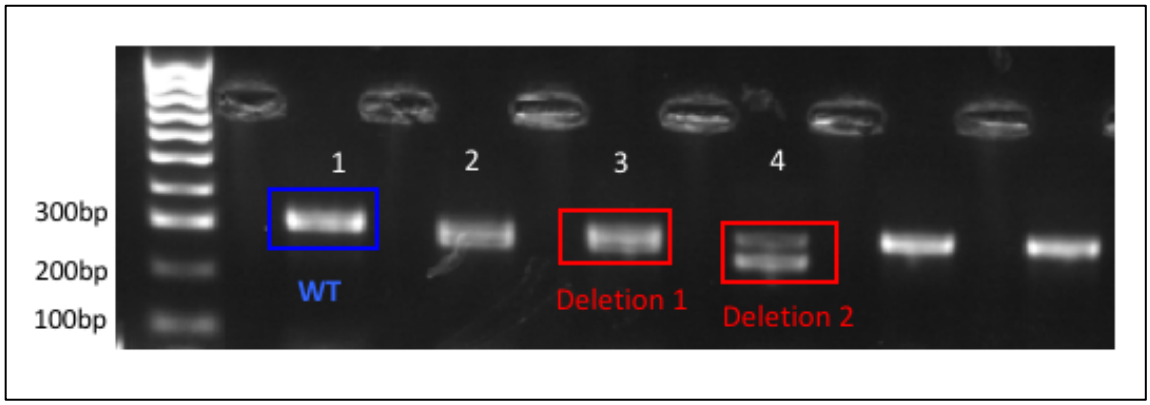

Figure 51: Analytical gel showing the identification of founders, F0 adults were outcrossed to wild-type to determine which individuals carry the heterozygous allele to their offspring. Two possible deletions were identified. PCR products from these where cloned into a vector and sent for sequencing to determine the exact nature of the mutations.

Although a deletion or insertion of 1bp is only required for a frameshift mutation to produce a premature stop codon, a large deletion or insertion would allow the resulting allele to be genotyped by analysing the PCR product size, without the need for restriction digests. Genotyping by PCR, is also considerably cost and time effective. The restriction digest identified two founders. The rest were non-transmitting individuals. One of the founders showed PCR products of two different sizes, possibly multiple deletions, implying that the founder transmitted an allele to the germ line containing a large deletion. The identified founders were outcrossed to wild-type fish and grown to adulthood producing the F1 generation.

In order to determine the mutations caused by this CRISPR, individuals from the F1 generation were out-crossed to wild-type. Embryos were collected 24 hpf to extract DNA, and PCR was performed to amplify the regions. Cloning was then performed by inserting the PCR products into the TOPO TA vector, and 20 samples were sent for direct sequencing. Table 9 shows the mutations generated by injection of gRNA2 and Cas9 protein and the resulting altered protein sequences. Two mutations were generated; a 25 pb deletion termed as MUTANT 1, and a 50 bp deletion/6 pb insertion termed as MUTANT 2. Since larger deletions are more likely to disrupt the protein function, this mutant was chosen for subsequent studies. This will also ensure time and cost-effective screening for mutations in the future.

Table 9: Table showing the mutations caused by the CRISPR/Cas9 system. Both the disrupted exon and resulting changes in protein sequences are shown for each. Red sequences indicated deletions, whilst blue sequences indicate insertions.

	WT Sequence	**Mutation**
Exon 3	GTTTTATTTGTCTATTACCAGTGTGCAGTAGTGC AGCTCCAGATCTCTGTGGACCTCTGAAAACAGTC CAAGACAGTCTAAATGCAACCTTAAGGAGACGTT ATATG	
Protein	MVQSECWLLRGLLGFICLLPVCSSAAPDLCGPLKTV QDSLNATLRRRYMKMHFPINYTVQVRYEEVFRLRN ISRLVNTSNEEEPVLPRDLQDLWLYVSQQGIKKVLR VLPERHPTRRKYLSDLENLFKKFETVFKEGNHEDQE NVRERPESLQTIWDHLTEQDYKGWKSVTPKSILDNC YRTMLCLFKECFTKEDDNYDYCEVYNRRKERKTT	
	Mutant 1 Sequence	
Exon 3	GTTTTATTTGTCTATTACCAGTGTGCAGTAGTGCA GCTCCAGATCTCTGTGGACCTCTGAAAACAGTCC AAGACAGTCTAAATGCAACCTTAAGGAGACGTTA TATG	23bp deletion
Protein	MVQSECWLLRGLLGFICLLPSLWTSENSPRQSKCNLKE TLYENALSH	
	Mutant 2 Sequence	
Exon 3	GTTTTATTTGTCTATTACCAGTGCAACCCTGCAGTA GTGCAGCTCCAGATCTCTGTGGACCTCTGAAAACA GTCCAAGACAGTCTAAATGCAACCTTAAGGAGACG TTATATG	6bp insertion, 50bp deletion
Protein	MVQSECWLLRGLLGFICLLPVQPKCNLKETLYENALSH	

4.3.3 Raising CRISPR Injected Zebrafish and Management of *il34* Mutant Line

Zebrafish homozygous for this deletion, ($il34^{-/-}$) used for all experiments in this thesis, were generated from an in-cross of F2 heterozygotes ($il34^{+/-}$). In-crosses of generations were kept to assess the phenotype of the homozygous mutant. Figure 61 shows a representative gel of genotyping for *il34* 50 pb deletion/6 bp insertion mutation. A product size of 300 bp was WT, whilst a product size of around 250 bp was a homozygous mutant. Products of both sizes were heterozygous. This method of genotyping the mutant line was used for subsequent generations and experiments.

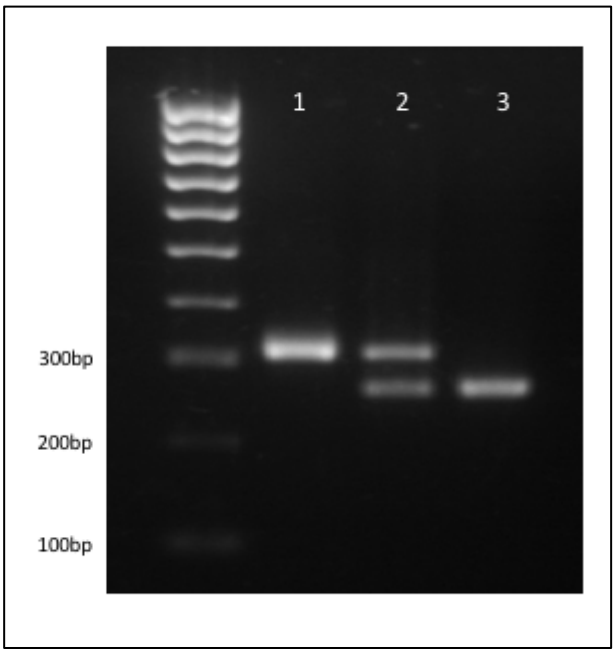

Figure 52: Gel illustrating il34 50bp deletion genotyping. Gel generated by genomic PCR of il34 50 bp deletion allele primers situated around the CRISPR targeted site. WT individuals produce a product of 300 bp (Lane 1), individuals homozygous for 50bp deletion ($il34^{-/-}$) show a product of 250 bp (Lane 3), while heterozygous 50 bp deletion ($il34^{-/+}$) individuals produce products of both sizes (Lane 2).

Embryos from each cross were monitored to check for any potential deformities or mortality. The following are some observations of each:

1. *Heterozygous outcross* - All individuals from a heterozygous outcross developed normally, with no apparent altered phenotype or mortalities.
2. *Heterozygous in-cross* – The embryos from a heterozygous in-cross, showed no apparent differences. However, the resulting homozygous adults appeared to be smaller in size than their wild-type siblings (43mm in length wild-type vs 28mm for homozygous) (Figure 62). The homozygous adults also appeared to have some difficulties in producing embryos, as embryo numbers were low when both pairing or marbling. All other wild-type or heterozygous adults appeared normal.
3. *Homozygous in-cross*- On the other hand, embryos from a homozygous in-cross exhibited some differences. Embryos showed a mortality rate of around 50% at 3 dpf, with only a few surviving individuals making it past day 5. Individuals also showed some deformities, including enlarged hearts or lack of circulation (Figure 62).

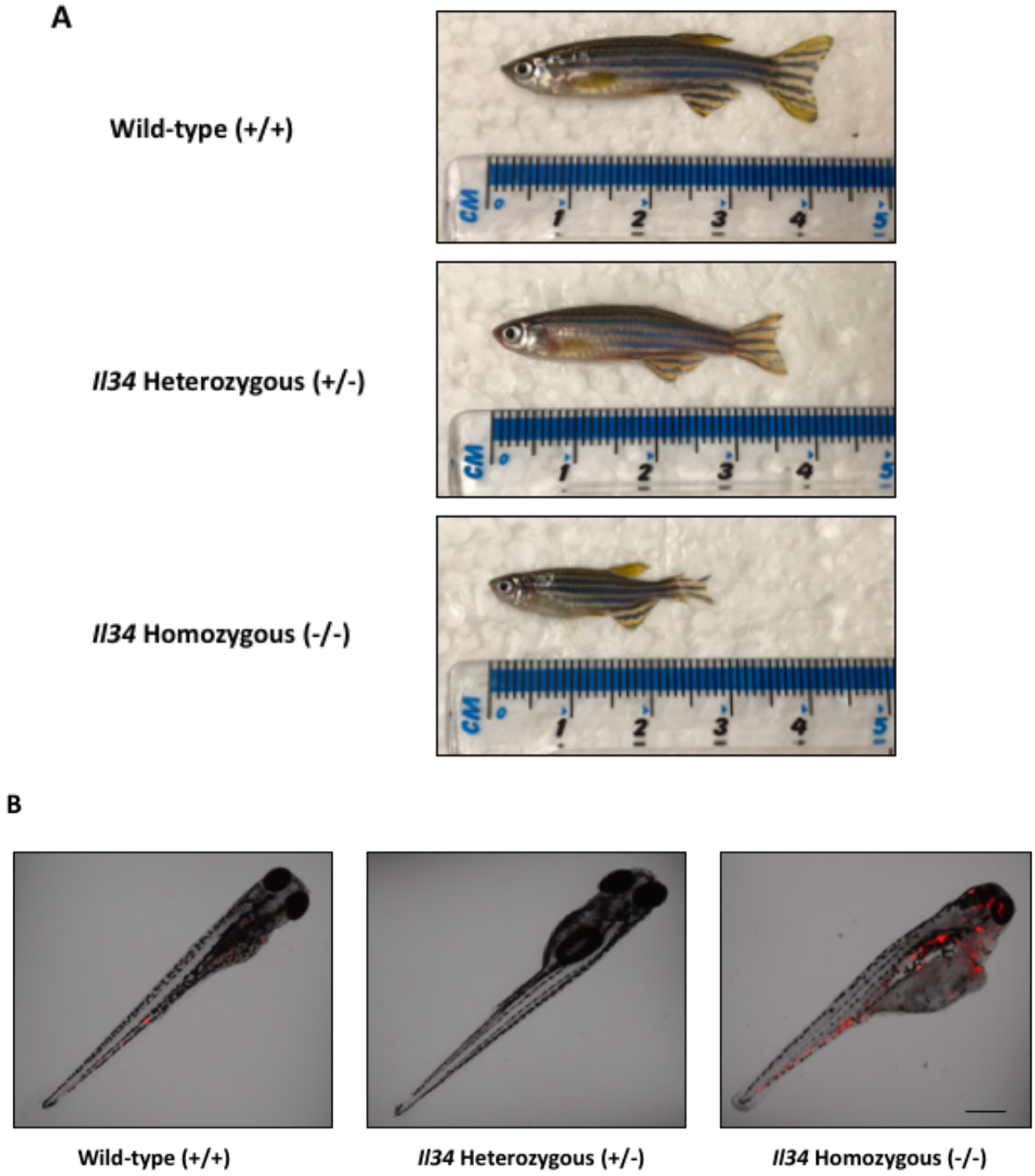

Figure 53: Photographs of morphological deformities in il34 mutants. (A) Representative Photographs of 50dpf individuals demonstrating that wild-type individuals do not display any gross morphological deformities, but il34$^{-/-}$ individuals exhibit a reduction in size. (B) 3dpf larvae showing defective development of homozygous embryos with visible heart aneurysm. Scale bar = 100 μm

4.3.4 The *il34* Transcript Undergoes Non-Sense Mediated Decay

Based on sequencing data, the *il34* allele (Mutant 2) underwent a frameshift mutation. A frame-shift mutation would change the reading frame and cause a change in the translation from the original. Thus a non-functional polypeptide would arise. Otherwise, a frame-shift mutation could also lead to a premature stop-codon altering the folding of the protein.

To investigate whether the mutation results in decreased *il34* mRNA levels, *il34* RT-qPCR was carried out in *il34*$^{-/-}$ and WT brains. Approximately 65% reduction in the transcript compared to WT controls (P<0.0001), was observed (Figure 63). This suggests that NMD is occurring in the homozygous fish and supports the assumption that the mutation results in loss of *il-34* protein expression.

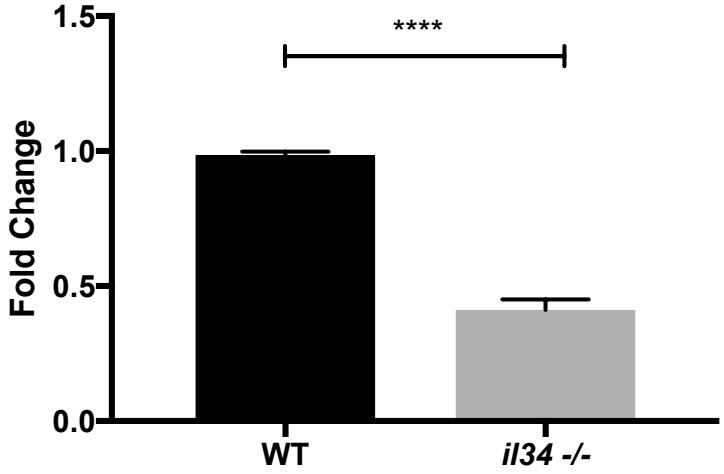

Figure 54: Expression of il34 in mutant vs wild-type zebrafish brains by RT-qPCR. Homozygous individuals have reduced il34 transcript levels in brain tissue compared to WT. **** $p < 0.001$ Unpaired T-test). Gapdh was used as a reference gene. Error bars represent ± SEM of n=3 triplicated samples.

4.3.5 Expression of *il34* in Wild-Type Zebrafish

4.3.5.1 Temporal expression of il34 in wild-type zebrafish.

Since no previous literature was available on the expression of il34 in wild-type zebrafish, to assess the temporal expression during development, RT-PCR was used to amplify a region of *il34* cDNA from 1 to 5 dpf as well as a selection of adult tissues. Expression of *il34* in WT embryos was detected as early as day 1 post fertilization, and at low levels for day 1-5 of embryogenesis (Figure 64).

Expression was similar in organs including brains from 3 months up to 24 months and organs such as spleen, liver, and heart (Figure 65) Some increased expression was observed for the gut and head kidney in adults.

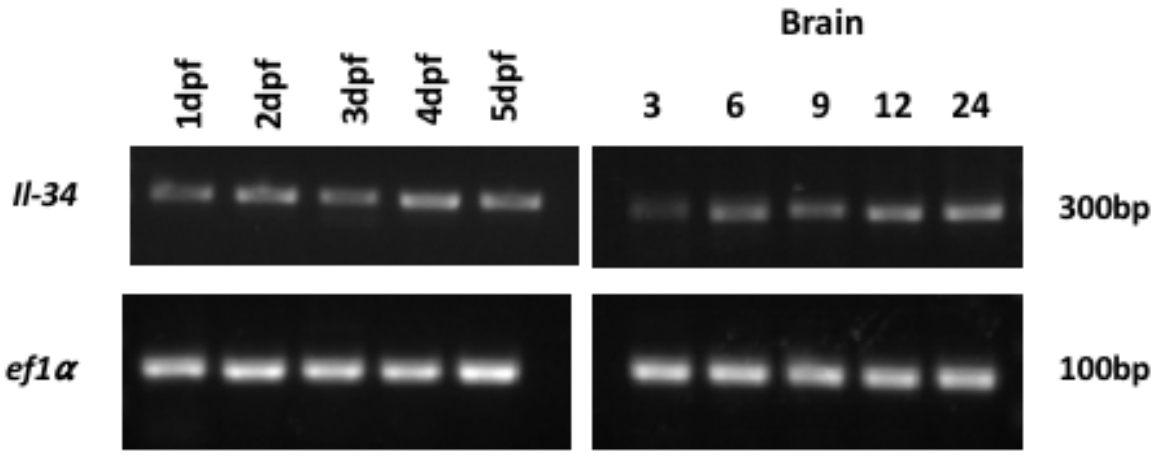

Figure 55: Expression of *il34* through development in wild-type zebrafish by PCR. Transcript levels of *il34* were measured throughout development from Day 1 to Day 5 by RT-PCR. Il34 expression was also confirmed in adult brains from 3 months to 24 months. Ef1α was utilised as a loading control.

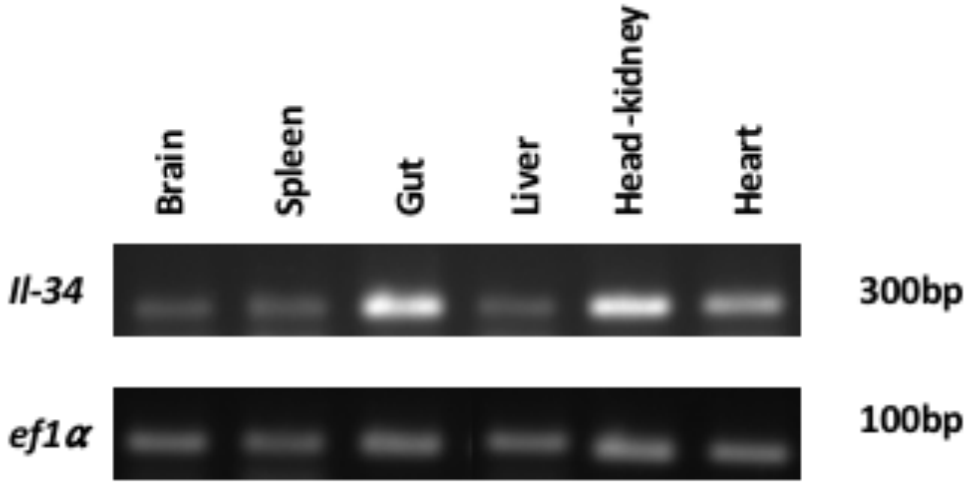

Figure 56: Expression of IL-34 in adult tissues of wild-type by RT-PCR. Expression was low throughout all tissues with higher levels seen in gut and head-kidney. Tissues were pooled from 3 individual fish at 18 months old. Ef1α was utilised as a loading control.

The expression of *il34* in the developmental stages was further investigated by RT-qPCR. cDNA from wild-type individuals was used to assess the temporal expression of *il34*. The data is presented as relative gene expression from day 1 to day 5 (Figure 66A) and as fold change compared with day 1 (Figure 66B). Results shows that the expression increases from day 1 till day 4, and is reduced again at day 5.

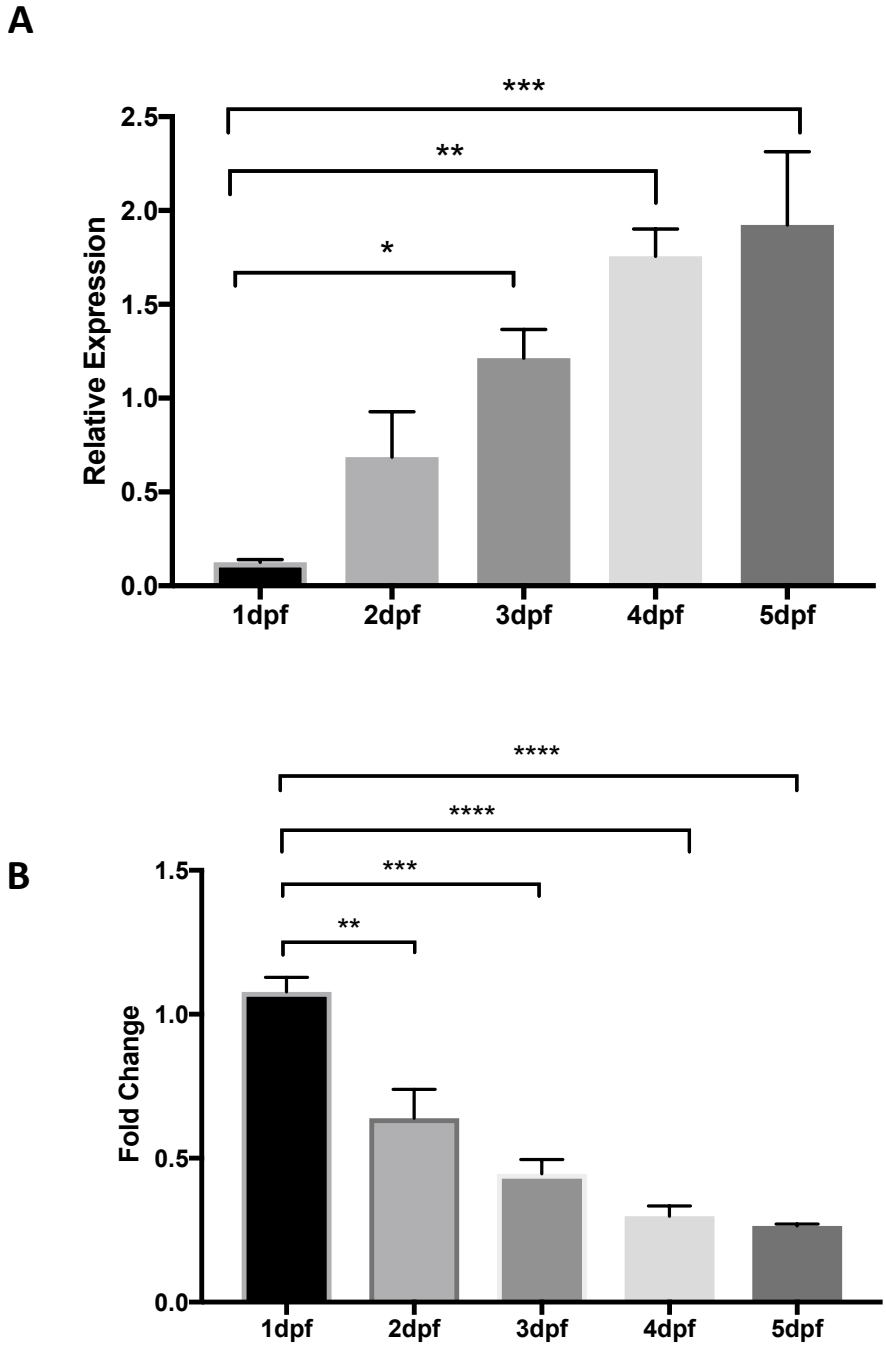

Figure 57: Expression of il34 in wild-type larvae from 1-5 dpf as determined by RT-qPCR. (A) Data shown as relative expression from day 1 to day 5and (B) data shown as fold change compared to day 1. Values were normalised to gapdh Error bars show ± SEM of triplicate samples (N=3). Analysis done by one-way ANOVA ** $p<0.01$, *** $p < 0.001$, **** $p<0.0001$.

4.3.5.2 Spatial expression and localization of il34 in wild-type zebrafish

Although both RT-PCR and RT-qPCR confirmed that *il34* is present within the first five days of development, these do not confirm the spatial expression. Therefore, to visualise the location and expression of *il34* in development of wild-type zebrafish, whole-mound *in situ* hybridisation (WISH) was utilised.

The design principles of WISH probes are described in detail in section 4.2.4.6. Since *il34* is a relatively small gene consisting of only 7 exons a WISH probe for *il34* was designed to target the whole protein coding region of the gene. Forward and reverse primers were designed to amplify the whole coding region of gene tagged with the T7 or SP6 promoter respectively (Figure 67). From this PCR product an antisense and sense control probe can be transcribed. Staining developed within 3 hours using the antisense WISH probe transcribed from the PCR product described. Within the same time scale, WISH performed with the sense control probe did not produce any staining, therefore indicating that staining produced with the antisense probe is specific for *il34*.

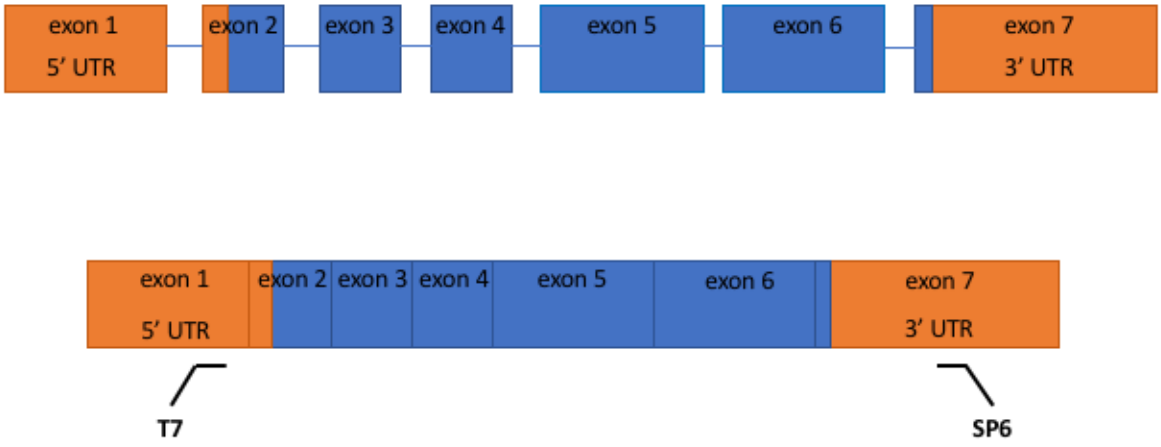

Figure 58: Design of WISH probe for *il34*. The gene and cDNA sequence of il34 are shown in this schematic. The location of the primers amplifying a region of the cDNA are also shown (T7 primer and SP6 primer). The resulting PCR product is used as a template from which the WISH probe is transcribed. Orange represents UTR and blue represents protein coding regions.

WISH was performed at 3 dpf larvae. From these observations, *il34* did not appear to be spatially restricted but rather appeared to be widespread and ubiquitously expressed. No other staining was detected using the control sense probe. Some marked expression appeared in the head of both control and experimental probes, but this was probably background staining which is characteristic, and often observed in zebrafish brain tissue. Dorsal views of the brains, did not reveal any site specific staining (Figure 68)

Additionally, since this was the first synthesised probe for *il34*, and no literature was available on the expression pattern of this cytokine in fish by WISH, an *L-plastin* WISH probe was added to serve as an additional control. *L-plastin* is a marker for the monocyte/macrophage lineage in zebrafish. The aim was to assess whether expression would follow a similar pattern. *L-plastin* could be seen in the posterior part of the embryo with enrichment in the posterior blood island (PBI).

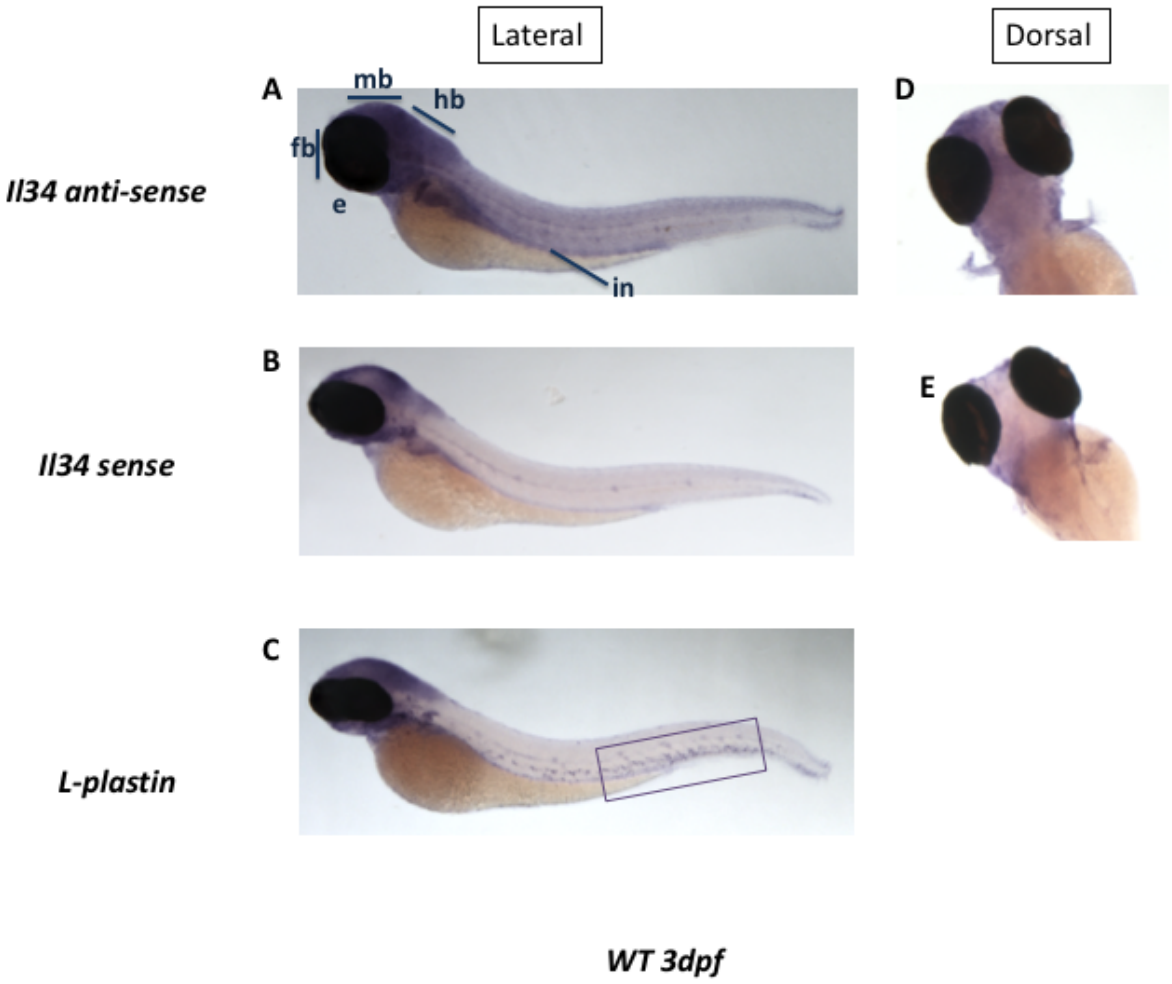

Figure 59: Whole-mount in-situ hybridization of *il34* expression in wild-type larvae at 3 dpf. A: Lateral view of 3dpf embryos stained with il34 experimental probe (anti-sense), B: il34 control probe (sense) and C: L-plastin probe (added control). D and E show dorsal views of the head/brain region for il34 anti-sense and sense probes respectively. The sense control probe for il34 showed no staining, indicating that the staining shown in the anti-sense strand is specific to il34. Abbreviations: FB – Fore-brain, MB – Mid-brain, HB-hind-brain, E- eyes, IN- intestine

4.3.6 Effect of *il34* Knockdown on Bone and Cartilage Development

To evaluate the effect of *il34* knockdown, on skeletal development, we assessed bone and cartilage formation in developing embryos. We used histological procedures to follow the development of the zebrafish skeleton by Von Kossa stain for detecting calcium deposition and mineralised structures, and Alcian blue stain for cartilage formation by proteoglycans. Specimens of zebrafish larvae collected at 5dpf were used.

No abnormal deposition or lack thereof was seen in the zebrafish by the Von Kossa stain. Ossification of branchio maxilla (MX), branchistegal ray (BS), opercle (OP), cleithrum (CL), and phargyneal teeth (PT), (Figure 69) do not show any significant changes. Cartilage deposition as seen by Alcian blue staining, was seen to be less reduced in mutant zebrafish. This was also determined by the intensity staining (Fig 69E) between wild-type and mutant fish. It must also be mentioned that at 5dpf, cartilage and bone mineralisation is still undergoing development and therefore any changes in colour or intensity observed, could be attributed to this. Additionally, mutant il34 -/- fish, survived for over 12 months at the time these experiments were conducted, suggesting that IL-34 mutation did not induce any detrimental changes that could have affected the survival of the mutants. However more data needs to be collected to better characterise the bone phenotype in both juvenile and adult zebrafish, to fully determine the effect of loss of Il-34.

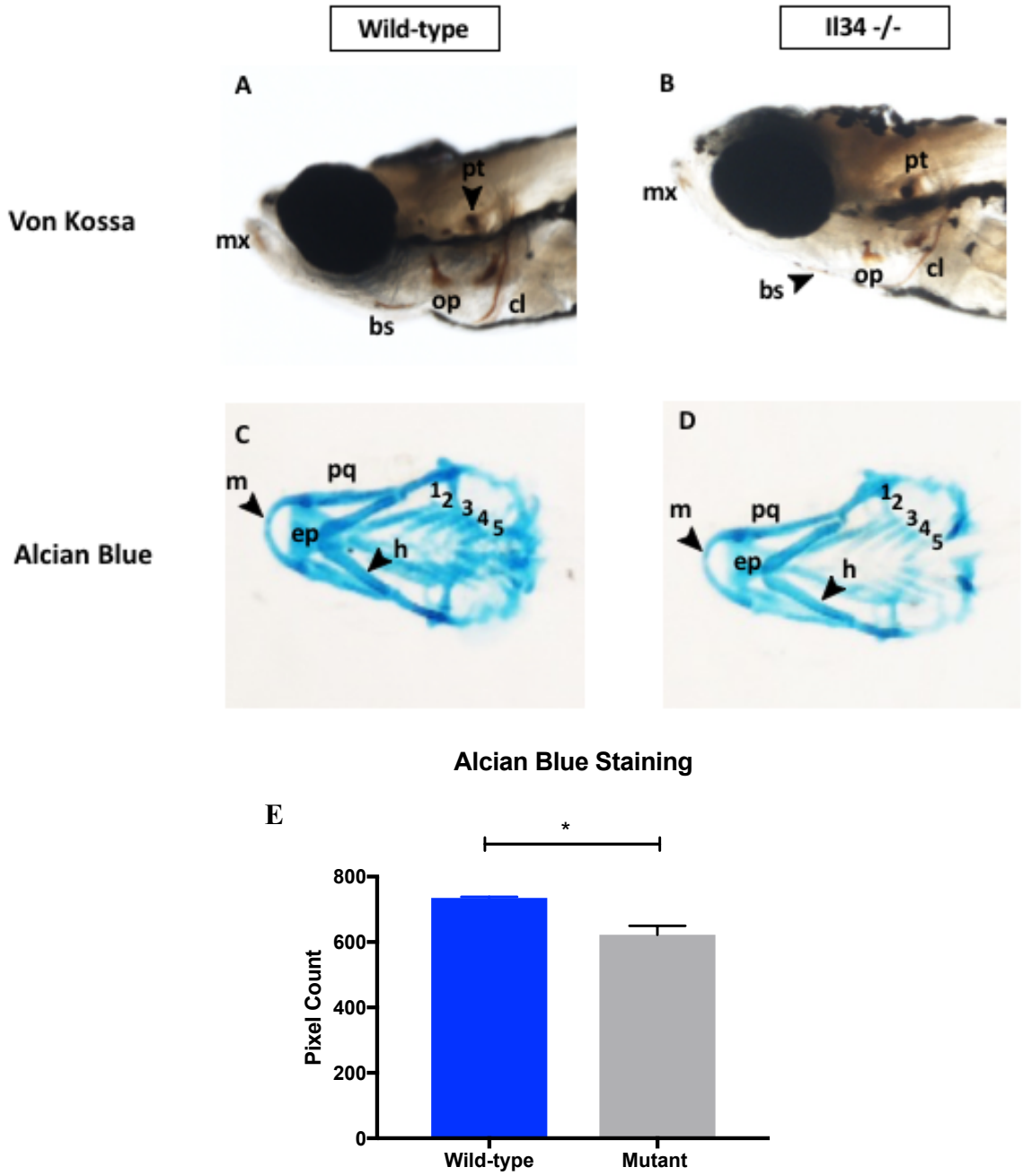

Figure 60: Von-Kossa and Alcian blue staining. A,B: Lateral views of wild-type and il34$^{-/-}$ embryos at 5 days post fertilization stained with Von-Kossa stain. Abbreviations: mx- branchio maxilla, bs- branchistegal ray, op- opercle, cl- cleithrum, pt -phargyneal teeth. C,D: Ventral view of stained with Alcian blue from wild-type (C) and il34-/- embryos at 5 dpf. Cartilage elements corresponding to the second and posterior arches (marked 1-5) appear to be reduced. E: Quantification of Alcian blue staining using Q-path as a measure of pixel density. Error bars show ± SEM of triplicate samples (N=3). Analysis done by unpaired T-test * $p<0.1$. Abbreviations: m – Meckel's cartilage, pq – palatoquadrate, ch – ceratohyal, ep – ethmoid plate

4.3.7 *il34* is Associated With the Inflammatory Environment in Zebrafish

After having assessed the expression of *il34* in developing zebrafish by both PCR and RT-qPCR, we conclude that *il34* mRNA is present at low levels in unstimulated larvae. Additionally, *in situ* hybridisation of wild-type larvae, did also not reveal any specific spatial expression of the gene at 3 dpf. As a result, we hypothesised that the expression and regulation of *il34* may be modulated in response to inflammatory stimulus, as already observed in the mammalian systems. In order to modulate inflammation in the zebrafish, we used a well-established tissue injury assay; the adult zebrafish tail (caudal) fin assay. This was chosen as the model of choice to study the role of immune cells in injury, as well as the signalling pathways controlling this regenerative process.

4.3.8 *il34* and its Association to Inflammation in Caudal Fin Assays

We first addressed the expression of *il34* at different time points in 3 dpf wild-type larvae under acute inflammatory conditions using the tail-fin model and quantitative PCR. We found that the mRNA levels of *il34* were not statistically significant between these time points, however, a slight trend towards upregulation was observed, peaking after 4 hours from the amputation. In unwounded embryos, there was no upregulation of gene expression, indicating that similar to mammalian counterparts, *il34* could also be a pro-inflammatory cytokine in the zebrafish (Figure 70A and 70B). In light of these results, we hypothesised that *il34* could be acting as an inflammatory cytokine showing early onset in the inflammatory response, and that its expression could be modulated by other inflammatory cytokines.

4.3.9 Expression of TNF-α and IL-1β is Upregulated in Wounded Zebrafish Tail-Fin.

This led us to investigate the expression of two genes encoding major pro-inflammatory molecules, namely TNF-α and IL-1β. These two cytokines were chosen as they are the main cytokines associated with initial response to inflammation, and are also linked to several major inflammatory diseases. Upon injury, mRNA levels of both cytokines increased with a peak expression at 4 hours post tail-fin amputation (Figure 70D and 70F). The expression appeared to increase significantly when compared to the uninjured zebrafish (Figure 70C and 70E) and appeared to resolve 24 hours from injury, consistent with a pattern seen in the caudal fin model.

4.3.10 Involvement of *csf-1* and *csf1-R* in Tail-Fin Injuries

Having determined that an inflammatory environment is established in response to tail fin injuries, we further addressed whether other molecules are involved. We investigated the macrophage colony stimulating factor 1 (*csf-1*) and its receptor *csf1-R*, given the major role played by these two in regulating and signalling macrophages, as well as owing to the fact that *csf1-r*, might potentially be the receptor for *il34*. Both cytokine and receptor appeared to be upregulated in response to injury with a peak expression at 8 hours for *csf1*, and a peak expression at 4 hours for *csf1-R* (Figure 70H and 70J). No increased expression was seen in uninjured zebrafish (Figure 70G and 70I).

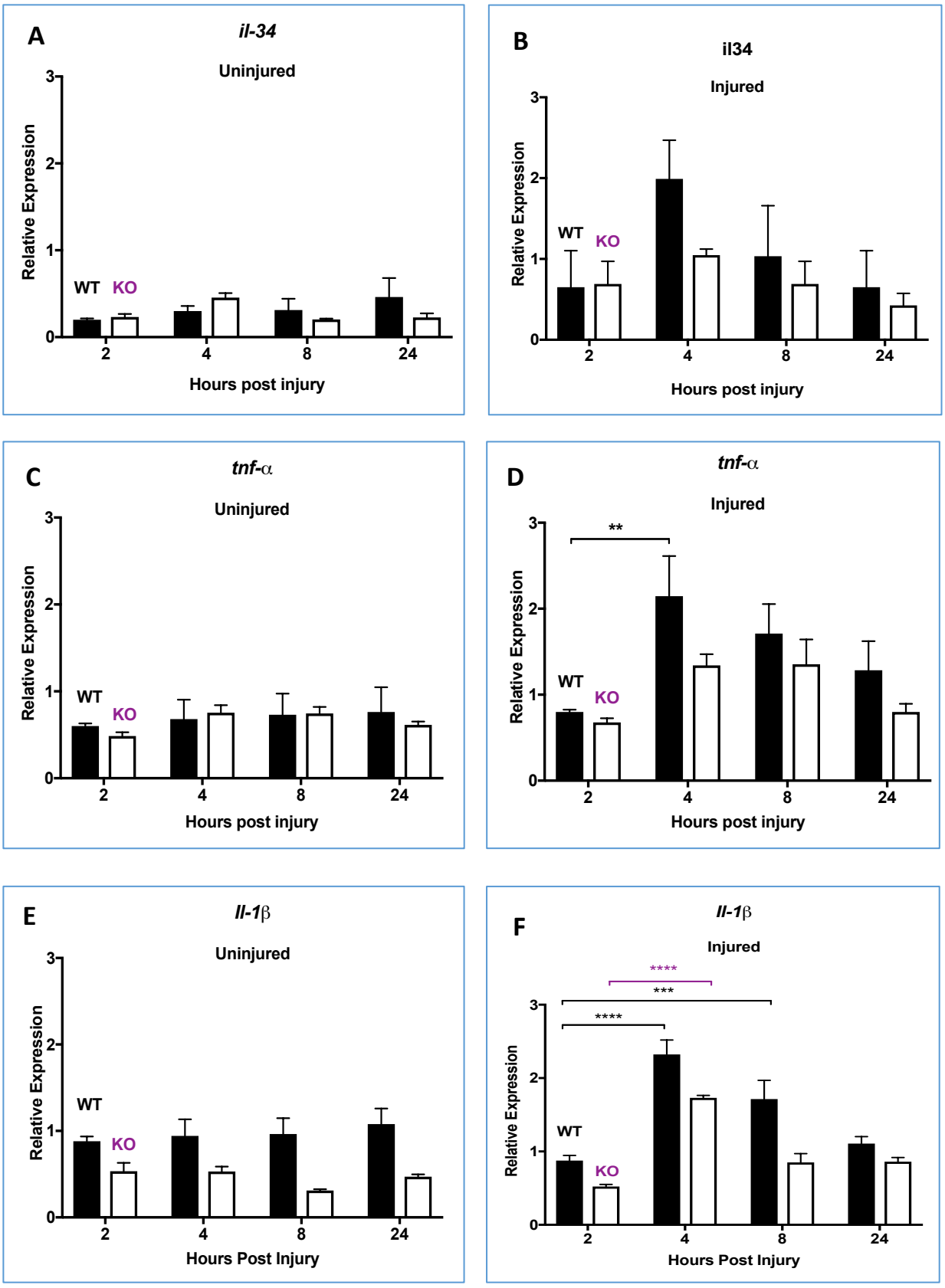
A
il-34
Uninjured
Relative Expression
WT
KO
Hours post injury
B
il34
Injured
Relative Expression
WT
KO
Hours post injury
C
tnf-α
Uninjured
Relative Expression
WT
KO
Hours post injury
D
tnf-α
Injured
**
Relative Expression
WT
KO
Hours post injury
E
Il-1β
Uninjured
Relative Expression
WT
KO
Hours Post Injury
F
Il-1β
Injured
****
***
****
Relative Expression
WT
KO
Hours Post Injury

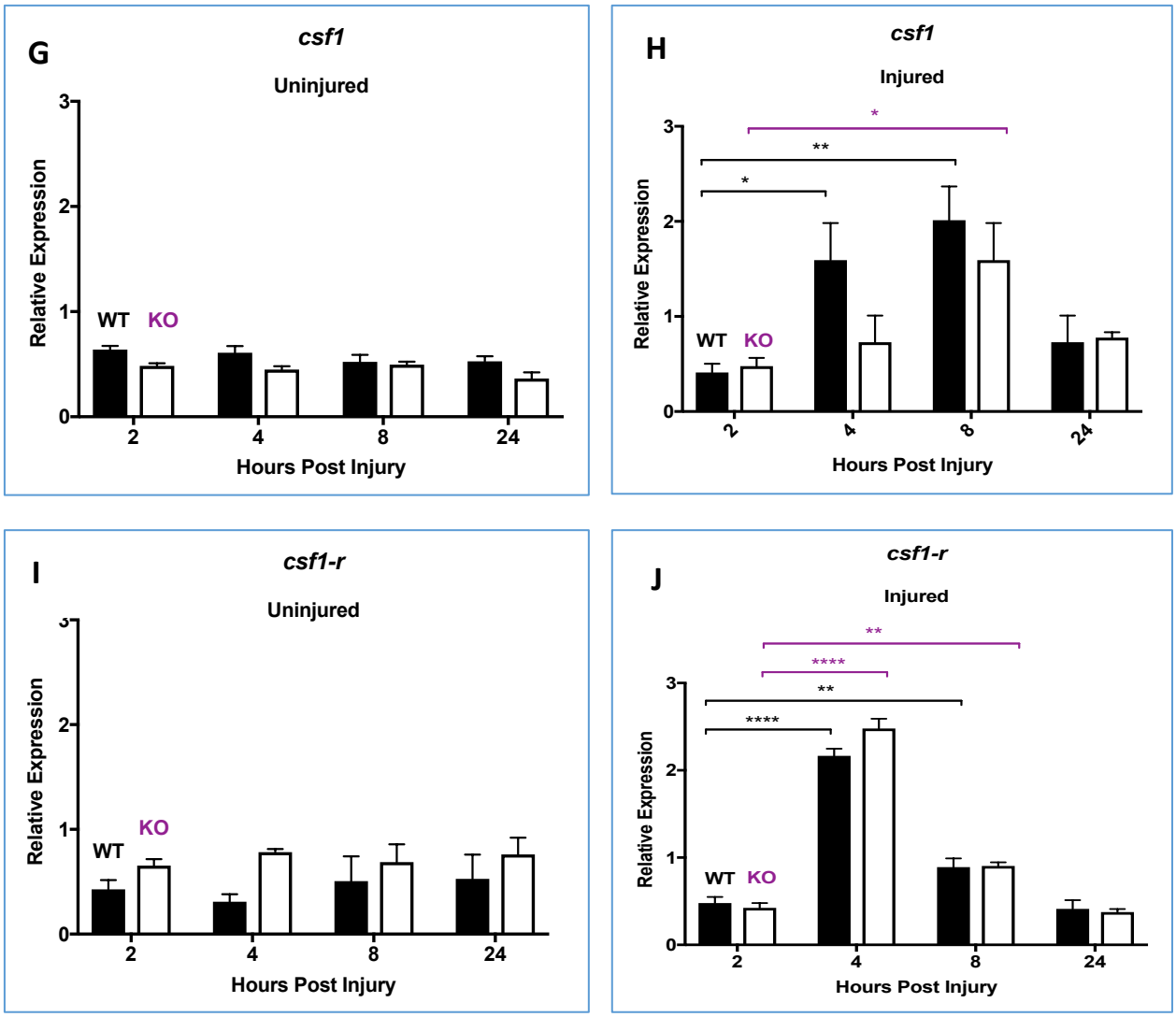

Figure 61: Expression of il34 and associated cytokines by zebrafish tail fin injuries. Tail fins from 3dpf wild-type and morphant larvae were injured, and mRNA levels of the indicated genes were determined by RT-qPCR of whole embryos at 2, 4, 8 and 24 hours post injury (30 embryos per time point), in comparison with uninjured embryos. Gene expression was normalized against gapdh. Each bar represents mean ± SEM of triplicated samples. To compare expression between time points, a Two-way ANOVA with Dunnett's multiple test was used. To compare relative gene expression between wild-type and knockout at each time point, a T-test with Mann-Whitney test was performed. For the t-test all p values were non-significant.. *p < 0.05, **p < 0.01, *** p < 0.001, **** p < 0.0001

In view of these observations, peak expression of both *il34* and *csf1-R* at 4 hours indicates that signalling of *il34* could be acting through *csf1-R* as already documented in humans and mice models. On the other hand, *csf1* which is known to signal through *csfl-R* does not peak at 4 hours but rather at 8 hours, suggesting that *il34* might be the primary pro-inflammatory molecule acting at the site of injury through the csf1-receptor before *csf1*, (or showing a greater affinity to the receptor). After observing this modulation of major pro-inflammatory cytokines, the recruitment of inflammatory cells at the site of injury was next analysed. The two main inflammatory cells are neutrophils and macrophages.

4.3.11 Neutrophils are Recruited During Fin Regeneration in Wild-Type Zebrafish

To study the response of neutrophil recruitment in response to an inflammatory stimulus, the established tail fin regeneration assay was again employed. The aim of this experiment was to compare neutrophil recruitment in wild-type and mutant zebrafish. However due to some technical complications encountered in the development of the il34 transgenic line, the mutant zebrafish could not be used for this analysis and as a result, only data for wild-type zebrafish is presented at this stage.

Tg(mpx:GFP)^{i114} embryos at 3dpf, were subject to tail-fin amputations from the end of the circulation. The injured embryos were viewed under a confocal microscope for 24 hours. Results showed that similar to previous studies, myeloid cells responded immediately and migrated to the wound via the circulation. However, the initiation of inflammation was faster than that observed for macrophages. Neutrophils show a higher motility than macrophages and are the first myeloid cells recruited to the site of injury, peaking at 4-6 hours before numbers decline by 24 hours. As expected, neutrophils migrated to the site of injury via the circulation with a peak accumulation at 4 hours, followed by a resolution complete by 24 hours from injury. Counting the fluorescence cells in individual fish that participated in the inflammatory response, confirmed that a neutrophil influx occurred in response to injury and was resolved within 24 hours (Figure 71).

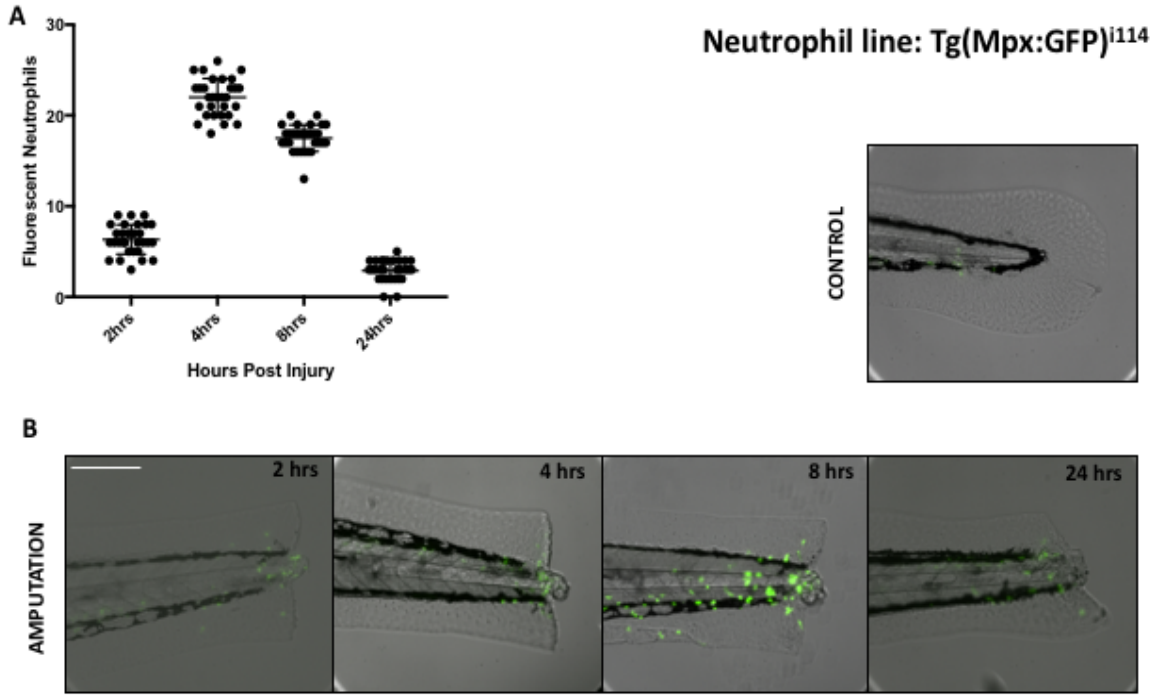

Figure 62: Time course of inflammation in Tg(mpx:gfp) neutrophil transgenic line. A) Tailfins of transgenic wild-type fish were transected at 3 dpf. At the time points indicated, individual fish where anesthetized and imaged as described. The number of fluorescent neutrophils at the site of injury (neutrophils counted after circulatory loop). Data points are shown for 30 individual fish per group in addition to mean ± SEM (n=30, 3 independent experiments). B: Images showing a single transgenic zebrafish larvae at the time points indicated following amputation of the tailfin and control. The accumulation and subsequent removal of fluorescent neutrophils can be seen. Scale bar = 150μm

4.3.12 Macrophage Recruitment is Altered in the Absence of *il34*

Since in mammalian systems IL-34 directs the differentiation and survival of monocytes and macrophages, (Foucher *et al.*, 2013; Ségaliny *et al.*, 2015) I wanted to investigate the effect of *il34* knockdown on the inflammatory response and macrophages in mutant zebrafish. To achieve this, caudal fin amputations were performed on 3 day embryos from a heterozygous (+/-) in-cross of the double transgenic line *tg*(fms: GFP). This line contains the heterozygous mutant *il34* allele, and GFP expression of macrophages is driven by the fms promoter. To visualize these inflammatory cells throughout injury, live images of the amputated caudal fins were taken at 8 hours post fin injuries (Figure 72). The 8 hour time-point was chosen as this is the optimal time for recruitment of macrophages to the site of injury.

In addition to characterizing the general inflammation throughout fin injury, we compared the inflammatory response by counting the number of macrophages at the site of injury, and determined how this correlated to the genotype of the fish. Macrophage numbers were counted from the end of the circulation, near the injured edge.

Consistent with a role in response to injury, accumulation of macrophages was observed at the wound. We demonstrate that the number of macrophages is altered depending on genotype with *il34*-/- individuals having the lowest number of macrophages at the site of injury in comparison to *il34* +/- or *il34* +/+. This result clearly reveals a direct association between knockdown of *il34* and recruitment of macrophages in response to an inflammatory environment.

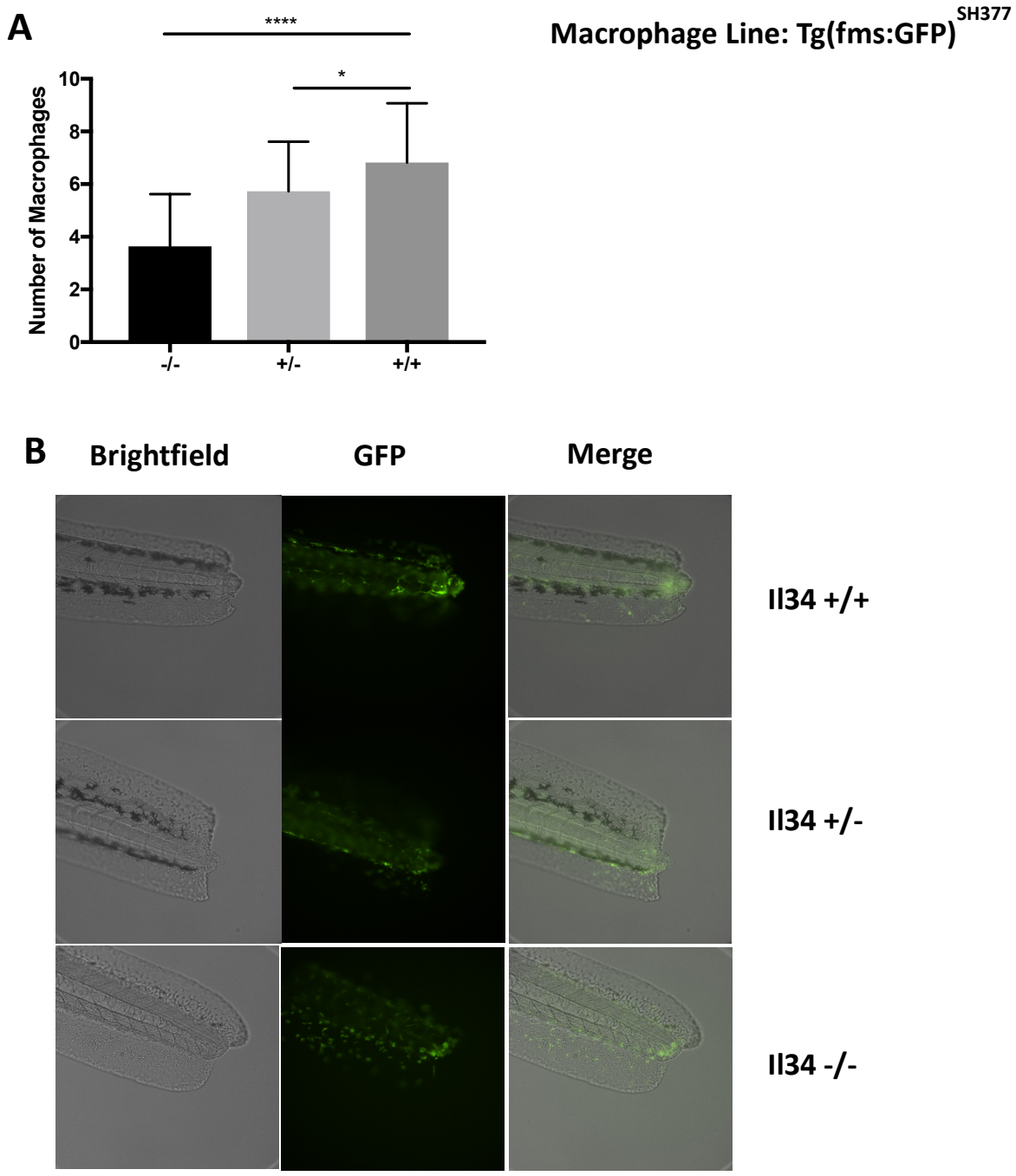

Figure 63: Knockdown of il34 reduces macrophage number in the transgenic line Tg(fms:GFP). (A) Tailfins of il34: fms:gfp transgenic larvae were amputated at 3 days post fertilization. Following 8 hours from injuries, individual fish where anesthetized and imaged as described. The number of fluorescent macrophages participating in the inflammatory response was assessed. Macrophage numbers where counted near the injured edge, after the circulatory loop. Individual larvae were then genotyped. The number of resulting fish per genotype is as follows: WT (+/+); 20, heterozygous (+/-); 30 and homozygous (-/-); 13. Data indicates mean ± SEM (n=3), $P < 0.0001$ for One-Way Anova. (B) Inverted microscopy images of single transgenic zebrafish larvae 8 hours after tailfin injury, comparing il34 WT (+/+), heterozygous (+/-) and homozygous (-/-) individuals. GFP labelled macrophages can be seen at the site of injury. Images are shown as projections of brightfield, GFP channel and summed Z-stacks. Scale bar = 200μm

4.4 SUMMARY

This study represents the first characterisation of *il34* expression in wild-type zebrafish as well as an analysis of *il34* loss of function model. A few loss of function *in vivo* models are currently present, however these only focus on the effect of *il34* on microglia deficiency. This is the first study attempting to investigate the deficiency of *il34* in relation to myeloid cells and inflammatory signalling.

Zebrafish were found to possess a single *il34* orthologue, with conserved gene synteny, whose expression was low, but consistent and not spatially restricted, at least during early development. CRISPR/Cas9 was employed to create a stable loss of function mutant. The resultant allele produced loss of protein function through non-sense mediated decay. Knockdown of *il34* did not lead to severe phenotypic defects, however juvenile homozygotes showed marked heart defects and early lethality.

We then aimed to investigate the role of *il34* in response to an inflammatory stimulus by tail fin injury assays. We describe the upregulation of *il34*, its potential receptor and other associated pro-inflammatory molecules in the cellular microenvironment in comparison to wild-type and mutant model. Furthermore, we report the first characterisation of *il34* in relation to macrophages in an inflammatory lesion. We document a decrease in the number of macrophages in homozygous mutants, elucidating the role of *il34* as a regulator of myeloid cells

CHAPTER 5

GENERAL DISCUSSION AND CONCLUSIONS

5.1 DISCUSSION

Following a decade from its discovery, IL-34 has been introduced as a newcomer into the family of interleukins with critical potential involvement in several diseases including autoimmune diseases or cancers. Il-34 is therefore emerging as a cytokine with promising clinical applications in diagnosis and treatment. In this thesis, the role of IL-34 in inflammation and in the progression of OS was investigated. The results highlight the importance of its signalling networks, and present new opportunities for therapeutic strategies.

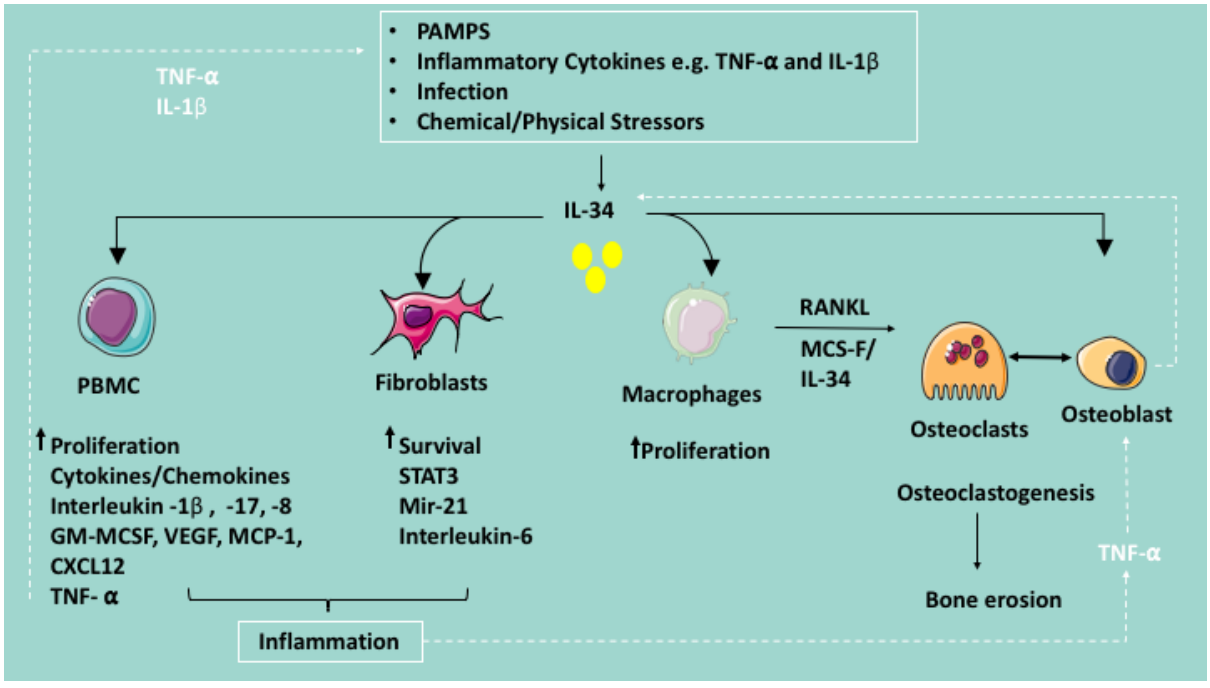

Figure 64: Schematic representation of the role of IL-34 in Inflammation. IL-34 expression can be induced by several stimuli including inflammatory cytokines, viral infection and pathogen associated patterns. IL-34 can act on a variety of cell types including synovial fibroblast and peripheral blood mononuclear cells (PBMC). IL-34 is associated with elevated expression of inflammatory cytokines inducing positive autocrine loops in amplifying the immune inflammatory response. IL-34 stimulates the proliferation of macrophages and their differentiation towards the M2 phenotype. Inflammatory process and the impact on macrophage differentiation lead to an increase of osteoclastogenesis and thus to an upmodulation of bone resorption. Adapted from Baghdadi et al., 2018.

SECTION I

Many aspects of the functions of IL-34 have so far been elucidated especially with regards to its role in myeloid biology. Despite this, there is still a lack of information about the secretory pathways and signals regulating the secretion of IL-34. The trafficking of this cytokine and its regulation both temporally and spatially to orchestrate responses is still unknown. Over recent years, extracellular vesicles are gaining attention as mediators of communication by regulating intracellular biological processes. Moreover, emerging evidencing is showing that extracellular vesicles play a role in supporting the tumour microenvironment niches by the transfer of oncogenic cargo between tumour cells or to neighbouring cells (Miller & Grunewald, 2015; Min, *et al*., 2016). Studies have shown that mesenchymal stem cells can modulate the proliferation of OS cells (Avril *et al*., 2016, Perrot *et al*., 2010) however the authors failed to identify any significant soluble factors produced by MSCs explaining the pro-proliferative effects on OS cells, leading to the conclusion that the effects observed might be due to EVs. These observations are strengthened by a study of Gabriel *et al*. who reported that undifferentiated MCSs and OS were not able to communicate via gap junctions therefore showing that direct cell to cell communication between these two cell types is not occurring (Tellez-Gabriel *et al*., 2017). EVs are consequently an additional mode of communication between OS cells and MSCs. Additionally, given the role of IL-34 in the pathogenesis of OS, our goal was to investigate whether IL-34 can be delivered by exosomes as part of the signalling and trafficking mechanism of OS, and how OS derived vesicles may impact stromal cells in the tumour microenvironment and consequently the tumour growth.

Exosomes were isolated and characterised from MG63 and KHOS osteosarcoma cell lines using ultracentrifugation. By using this method there were some differences in product yield from batch to batch, and quantification of exosomes presented some limitations throughout the studies. This highlights the problem in the field of EV research regarding the lack of standardization in current methodologies. For future studies it might be worth considering more rapid isolation techniques, such as ultrafiltration or size exclusion methods, so as to improve the efficacy of the preparation process, and optimize the quality of the finished material.

The use of TRPS allowed for the quantitative determination of sample size, size range and concentration. TRPS is a highly reliable technique for determining the size distribution of

cell-derived vesicles, due to its calibrated and consistent measurement. In TRPS the concentration is measured as a function of an already designated size range, this makes results standardisable and comparable (Maas *et al*., 2014). The detection of extracellular vesicles by TRPS showed a size range of 50-150 nm. Together with the presence of exosome specific markers CD9 and CD63, this demonstrates that OS cells release exosomes.

These observations are generally consistent with other studies that have reported the presence of exosomes from OS cell lines. OS derived vesicles have been so far isolated from canine OS cells; POS and HMPOS (Bracha *et al.,* 2018; Ruby *et al.*, 2017) and human OS; 143B and KHOS (Garimella *et al.*, 2014). Only a limited number of studies on exosomes derived from OS are currently present in the literature. To this date, these studies have focused on the content of the vesicles, showing that similar to other cancer types, they contain a pro-tumourigenic cargo, but the main mechanisms by which these function, still remain unexplored (Baglio *et al.*, 2017; Garimella *et al.*, 2014; Kovac *et al.*, 2015; Xu *et al.*, 2017).

Osteosarcoma derived exosomes promote the differentiation of mesenchymal stem cells towards adipocytes. Since stromal cells are a major component of the tumour microenvironment and known to modulate the growth and metastasis in OS, we investigated the role of OS derived exosomes on the differentiation of MSCs. Exosomes purified from KHOS, stimulated the differentiation of MSCs towards the adipogenic lineage, by upregulating the gene expression of AP2 and PPARG2. On the other hand, no effects were noted for chondroblastic differentiation whereas for osteoblastic differentiation, it was observed that the osteogenic markers decreased on day 7 when treating with OS derived vesicles. The significance of this observation is yet unknown and need to be investigated further. However previous studies have shown that this could be related to bone regeneration (Ekstrom 2013, Graneli 2016)

Mesenchymal stem cells differentiate into adipocytes through the two stages of adipogenesis, driven by transcription factors PPARG2 and the C/EBP family. Initially mesenchymal stem cells commit to the adipocyte lineage forming preadipocytes, which become mature adipocytes through terminal differentiation (Arimochi *et al*., 2016). Both

preadipocytes and mature adipocytes play numerous roles in tumour formation and progression of OS. They have been shown to provide pro-tumorigenic signals that promote cancer cell proliferation and

invasiveness by increasing STAT3 signalling mediated by matrix metalloproteinase 2/9 (MMP2/9) expression in tumour cells (Wang *et al*., 2017). KHOS cells could therefore facilitate the adipogenic differentiation establishing a cycle between adipocytes and OS tumour cells in favour of tumour promoting properties (Basu-Roy *et al*., 2016). These results highlight the properties of OS exosomes and their role as the main communicators for modulating the tumour microenvironment through modifications of the stroma.

How exosomes cause these significant changes in target cells remains an area of intensive research. More recently, one *in vivo* study described the generation of a preclinical mouse model of OS with exosome-mediated interactions between tumour cells and MSCs. The authors show that systemic injection of OS derived exosomes, educated MSCs in mice bearing OS xenografts to promote cancer growth and metastasis by activating the IL-6/STAT3 signalling pathway (Lagerweiji *et al*., 2018). These findings are relevant since immune modulation and tumour immune evasion are key mechanisms in malignant progression, and therefore suggest that cancer exosomes might directly or indirectly (via MSCs) influence the innate or adaptive immune components.

MSC derived exosomes can modulate the biological functions of OS. Our results show that MSC derived exosomes promoted the proliferation of OS cells *in vitro*, demonstrating the role of exosomes in cell-to-cell communication on tumour cell viability and progression. Proliferation was increased after treatment with BMSC on both KHOS and MG63 cells. We then observed the exchange of exosomes between MSC and cancer cells by monitoring their uptake over 24 hours using confocal microscopy. The functional properties of the mesenchymal derived exosomes on cancer, was investigated by looking into the cytokine profile of adipose and bone marrow derived stem cells. We demonstrated that several cytokines and chemokines such as Serpin E1, endoglin, IL-6, and FGF-19 were found. These data suggest that exosomes selectively carry certain cytokines and transfer them to recipient cells to bring about anti-tumour or pro-tumour effects. Such effects have

already been reported in breast cancer (Vallabhaneni *et al.*, 2015) and colon cancer (Zhu *et al.,* 2012).

There are three major mechanisms to explain how exosomes adhere to recipient cells to release their contents and bring about the desired effect. Exosomes first utilize the interaction of their various surface proteins and cellular receptors to adhere to target cells. Once bound, the exosomes may a) elicit signal transduction via the induction of intracellular signalling pathways, b) fuse with the cellular membrane to transfer the protein content into the cytoplasm of the recipient cells, or c) be endocytosed via phagocytosis (Zhang *et al.*, 2015). The complexity of these mechanisms is only beginning to emerge, and represents a significant area of exosome research that still needs to be refined.

To summarize, the results presented here indicate that despite the initial hypothesis, IL-34 may not be present in osteosarcoma derived vesicles and therefore it does not take participate in the pathogenesis of OS. Taken collectively however, the results suggest the hypothesis that cross-talk between OS cells and their microenvironment by secretion of exosomes is a crucial mechanism that can generate a specific sequence. First, cancer cells interact with MSCs via exosomes to modulate them, and in response, the modified MSCs participate in cancer progression through their own exosomes. Additionally, this may imply that the recipient MSCs may be employed for therapeutic use to improve bone regeneration (Chu *et al.*, 2018)

SECTION II

Based on previous work that demonstrated that IL-34 plays a key role in tumour development and chemoresistance (Baghdadi *et al*., 2016; Segaliny *et al*., 2015) we investigated the potential of targeting IL-34 in mouse model of OS using an IL-34 blocking antibody. There are currently no approved therapies based on the inhibition of IL-34. We hypothesised that using an IL-34 inhibitor, may have a therapeutic effect in treating cancers. By targeting IL-34, the communications between cancer cells and the tumour microenvironment can be hindered with the resulting functional impact being the inhibition of tumour proliferating cells, and/or the surrounding microenvironment through modulation of immune cells, and endothelial cells.

Blocking IL-34 had a therapeutic efficacy on the progression of osteosarcoma. On performing a dose response analysis, the results revealed that blocking IL-34 using a mouse monoclonal antibody significantly reduced tumour progression in allograft models of OS. Out of the four doses administered, the 4 mg/kg dose was the most effective. A higher dose failed to inhibit tumour growth with the same efficacy. This could mean that: i) an immune reaction is precluding the efficacy of the treatment, but this is probably unlikely as a slow inhibition of tumour growth was still observed, or ii) a more plausible explanation could be related to the pharmacodynamic properties of the antibody including its half-life, antibody degradation and elimination, or the equilibrium point between binding and release was reached.

In both syngeneic and xenogeneic models, a significant reduction in tumour volumes was observed following treatment with anti-Il-34 for 3-4 weeks (depending on the model). In parallel, an anti-human-IL-34 antibody was tested in the xenogeneic model, but in this case, no reduction of tumour growth was seen. This observation is in favour of a production of IL-34 by the tumour microenvironment. IL-34 blockade may be an effective approach to slow down tumour growth.

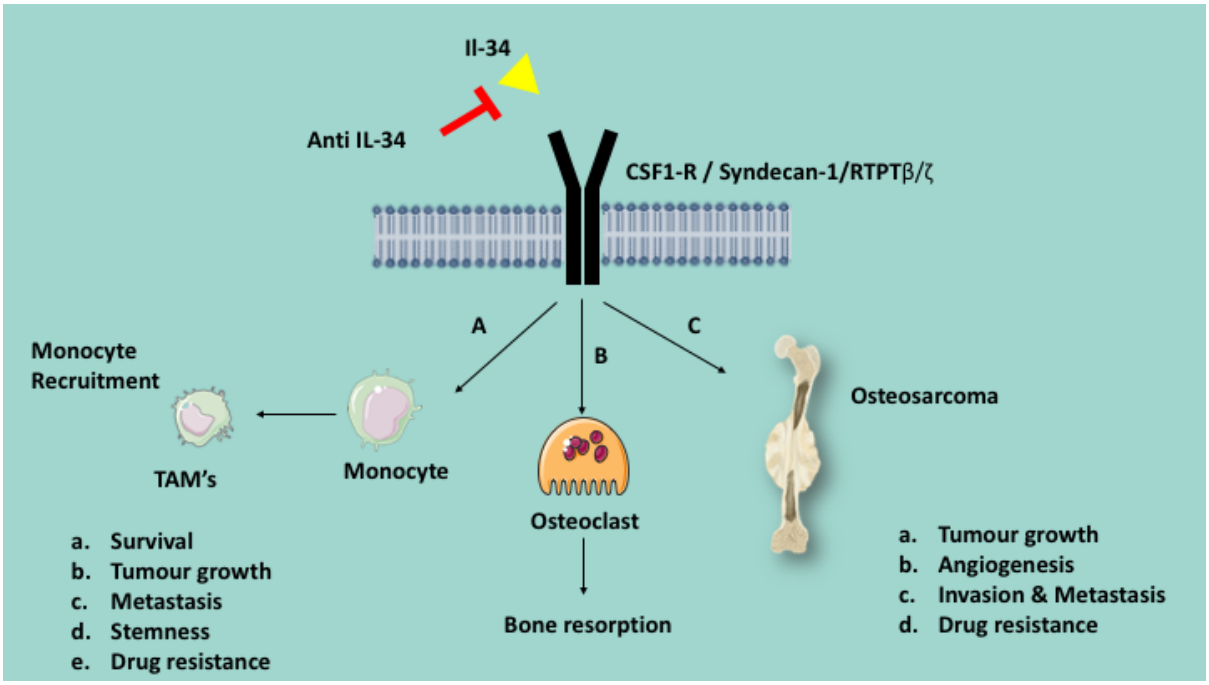

Figure 65: Schematic representation of how IL-34 can act as a therapeutic target in osteosarcoma. Using a blocking antibody, to block the interaction of IL-34 with its receptors can prevent the progression of osteosarcoma. **A)** Blocking IL-34 can reduce the infiltration of tissue associated macrophages into the tumour niche to bring about anti-tumour activities. B) In bone, IL-34 can facilitate osteoclastogenesis resulting in reduced formation of osteoclasts. (C) In osteosarcoma targeting the production of IL-34 in the tumour microenvironment may be effective against multi-agent chemotherapy and can lead to anti-tumour effects including a reduction in tumour growth, metastasis and angiogenesis.

On immunohistochemistry analysis, there were no significant effects on tumour cell proliferation (Ki67) or rate of apoptosis (Caspase-3) in either of the models. A few hypothesis could be proposed to explain this lack of a difference. Primarily, the tumours investigated in this study have a highly aggressive nature, (with MOS-J being more aggressive than MNNG-HOS), and therefore this would have had a limited effect on the proliferation rate.

A reduction in tissue vasculature was observed as marked by a decrease of the endothelial cell marker CD31. This highlights the critical role that Il-34 plays in promoting tumour angiogenesis (Segaliny *et al*., 2015). This difference was observed mostly in the MNNG-HOS model, with only a slight tendency detected in the MOS-J model, probably due to the aggressiveness of the tumours. It can be hypothesised that blocking IL-34 leads to a

reduction in angiogenesis by reducing the proliferation of endothelial cells or/and endothelial precursors.

Il-34 is known to modulate the FAK, Src and Akt and ERK1/2 signalling pathways in endothelial cells (Zhou *et al*., 2016) Indeed FAK is a critical mediator of integrin signalling with FAK knockout mice demonstrating its critical role in development of embryos and cancer progression (Sulzmaier *et al*., 2014). FAK also mediates the phosphorylation of Src and subsequently Src modulates the endothelial phenotype and angiogenesis (Pan *et al*., 2014). Similarly, Akt and ERK1/2 play critical roles in the regulation of endothelial cells and vascular homeostasis (Somanath *et al*., 2006). Therefore given the association of IL-34 to endothelial cells, this may explain the therapeutic benefit of treating with anti-IL-34.

Blocking IL-34 in osteosarcoma induced a dysregulation in M1/M2 macrophage subsets. A higher incidence of M1 macrophages was observed in treated groups compared to the control for both models. This increased infiltration and activation of anti-tumour M1 macrophages, can be attributed to high inflammation in the local environment of the tumour. Within the tumour cell microenvironment, several types of immune cells are present including T-lymphocytes, macrophages (M1 and M2), as well as sub-populations of B-lymphocytes and mast cells. OS cells are able to control the differentiation and recruitment of immune infiltrating cells to establish a local immunosuppressive environment that is able to promote tumour growth and metastasis, and increase drug resistance (Heymann *et al*., 2017).

The resident NK cells may secrete immune-activating cytokines such as IL-2, IFN-γ, and macrophage inflammatory protein (MIP)-1α, resulting in macrophage activation (Khawar *et al*., 2015) This may also lead to release of further cytokines from already activated macrophages present in the tumour tissue, such as TNF-α and IL-6. Additionally, immunosuppressive cytokines secreted by OS tumour cells such as TGF-β and IL-10 may be decreased, thus shifting the balance towards an activated immune response. This may attract more infiltrative NK and macrophages at the localized tumour site, thus increasing their migration and proliferation, and enhanced anti-tumour function (Bellora *et al*., 2010).

Buddingh *et al*., demonstrated that in OS, macrophages have both M1 anti-tumour, and M2 pro-tumour characteristics, and that the M2 macrophages are associated with bad prognosis (Buddingh *et al*., 2011). As previously described, increased IL-34 expression was found to facilitate the extravasation of mononuclear phagocytes and orient their polarisation towards an M2 phenotype (Segaliny *et al*., 2015). To determine the impact of blocking IL-34 on M2 macrophage subtypes, an M2 marker CD163 was utilised. Surprisingly, low numbers of CD163 infiltrating the tumour tissue were present in both control and treated groups. The CD163 analysed were not detected in the tumour mass but in connective tissue at the periphery. Tumour-associated macrophages (TAM) located in the periphery, of the M2 type and expressing CD163, but still in contact with the tumour have also been described in other tumours (Shabo *et al*., 2008). One plausible explanation for this low detection, is that low numbers of tumours were analysed, and therefore a bigger cohort would be needed for future experiments. Considering the low number of CD163 macrophages in the control groups, more data is required at this stage to fully elucidate the effect of anti-il34 on M2 macrophages. Another explanation is that changes in the microenvironment with the presence of *e.g*. IL-10 and TNF-α, both known to upregulate and downregulate CD163 respectively (Yang *et al*., 2015), may also play a role, and this would therefore merit further investigation.

At this stage these findings are clinically relevant and they indicate that anti-IL-34 antibodies may show promise in the treatment of patients with OS. Overall, the major challenge of these results is the aggressive nature of the models used, which consequently may have limited the effect of the treatment. The small animal numbers and high heterogeneity of OS tumours, could also explain the absence of significant differences. Thus further testing with an increase in animal numbers, as well as assessment of intermittent and continuous dosing of anti-IL34 antibody is needed.

Anti-Il34 antibody had no effect on bone remodelling, while its effect on metastasis is unknown. Due to the association between OS and development of metastasis, we aimed to assess the therapeutic effect of anti-IL-34 on inhibiting lung metastasis. Due to restrictions in the project licence, the short timing of the *in vivo* experiments did not allow for the assessment of the metastatic process. To provide a definitive conclusion on the efficacy of

blocking IL-34 as a therapeutic target, future studies should primarily aim to test the effect of blocking IL-34 on the development and progression of lung metastasis.

In this context, since associated alterations of bone remodelling play a central role in the development and progression of OS, we studied the effect of the blocking antibody on bone remodelling. The results indicate that the anti-IL-34 blocking antibody had no effect on bone architecture. The explanation for this could be attributed to two factors. The first is that tumour sizes investigated in the models where relatively small and not enough to induce OS associated bone remodelling. Secondly, bone mediated osteoclastogenesis occurs independently of IL-34, with the other major cytokine responsible being M-CSF. Together with RANKL and NF-κB, these cytokines induce osteoclastic differentiation (Baud'Huin *et al.,* 2010). MCS-F is also highly expressed in tumours with several tumour promoting functions (Chockalingam & Ghosh, 2014).

A bi-therapy treatment of anti-il34 and doxorubicin failed to act synergistically on tumour progression. Based on the results obtained, the combined therapy of anti-IL-34 with doxorubicin was evaluated. A combination of therapeutic regime would represent an additional therapeutic option, as both agents target different complementary pathways: anti-IL-34 targets mainly macrophages and vascular formation, while doxorubicin targets the proliferation of cancer cells.

The aim was to investigate whether combining both would induce a synergistic inhibition of primary tumours. The results show that a combination treatment had no significant synergistic effect on tumour progression than administering DOX or anti-IL-34 individually. While administering anti IL-34 alone had similar effect to previous experiments, there was a high variation in tumour volumes on administering the DOX. This high discrepancy can be attributed to problems when administering the DOX. This led to the unexpected results observed, and thus would need to be repeated in future experiments. Such analyses can also be rendered complicated due to several factors, including the high heterogeneity of tumours, the tumour microenvironment, and the host's immune system. An important factor for consideration at this stage is the dose timing of the treatment. In such studies, the timing of the treatment is highly important, and predicting how tumours will respond is currently elusive. Studies in the literature about administering more than

one drug for cancer treatment have demonstrated the importance of dose timing. A study by Ottewell *et al*., investigated the anti-tumour effect by administering zoledronic acid and doxorubicin in breast cancer subcutaneous tumours *in vivo*. This study supports the notion that initial priming of cells by one treatment, renders them more sensitive for subsequent exposure to a further treatment, when such treatments are administered time apart. Thus effects of combined treatments may manifest themselves over a few hours apart, increasing the anti- tumour effect when given in sequence. They also showed that administration of drugs in a particular treatment schedules initiated specific changes in gene expression of the tumours (Ottewell *et al*., 2008). Thus depending on the timing, the treatment outcomes can be vastly different even within the same tumour model.

Moreover, it is likely that populations of tumour infiltrating lymphocytes (TILs) and myeloid derived suppressor cells (MDSCs) are being modulated by these therapies, and understanding the underlying mechanisms behind this modulation are key to predicting the outcome (Bremnes *et al*., 2016). Therefore, further investigation with modulations in dose-timing is required. Apart from dose timing, the dose administration could need further adjustment. As already mentioned, the affinity of the antigen to the antibody, as well the amount of ligand present within the tumour tissue are two parameters that could affect the efficacy of the treatment.

Comparison of IL-34 conditional knockout mice with IL-34 mutant mice.

An IL-34 murine conditional knockout model was published by Wang et al., in 2014. In this model, the authors report that IL-34 expression was found mainly in the skin and the CNS and that it was produced mainly by keratinocytes. A deficiency of IL-34 resulted in impaired epidermal Langerhans Cells and microglia cell numbers (Wang *et al*., 2014). Based on the early data from the knockout model currently being developed, findings indicate that our preliminary results are in line with what was observed in the conditional model. Similarly, we also observed a decrease of Langerhans cells in the skin. Additionally we also report a decrease in number of immune cell populations in four major organs but most notably in the spleen. Our experiments also report a severe delay in bone mineral density that resulted in delayed growth of the mice. This phenotype was not reported in the

conditional knockout model, and therefore it is being hypothesised that IL-34 could be playing a role in in early very early development that is yet to be determined *(Schiavone et al., unpublished)*.

SECTION III

To study the role of IL-34 in bone development and the immune response, an il-34 mutant zebrafish line was generated. Up to date only a few studies on *il34* in zebrafish have been published. These studies mainly focus on the role of il34 in microglia and their early development. Two studies have shown that *il34* is required for early seeding of microglial progenitors in the brain (Kuil *et al*., 2018; Wu *et al.,* 2018). Taken together, these studies as well as the mouse model of KO IL-34, establish an essential role for *il34*, *csf1*, and *csf1r* axis in zebrafish development.

Using the CRISPR/Cas9 system, a zebrafish line mutated for *il34* was developed. The mutation was a 6 bp insertion and 50 bp deletion, that generated a frame-shift mutation resulting in non-sense mediated decay of *il34* protein. The generation of a stable mutant *il34* line using the CRISPR/Cas9 system highlights its importance as a highly efficient genome editing tool. Outcrossing two F0 founders for the generation of the F1 generation, and subsequent genotyping identified a 23 and 50 bp deletion. The 50 bp del allele was preferred due to the capacity to genotype by PCR alone, which eventually proved to be extremely cost and time effective. The time taken to generate heterozygous adults that could be utilised for in-cross experiments was between 6-9 months. The F1 adults then required direct sequencing to ascertain their mutation as F0 founders can still produce F1 individuals with different mutations if their germ line is a mosaic harbouring multiple mutations. One limitation of CRISPR/Cas9 system is off-target effects. Therefore the allele had to be outcrossed to remove any background mutations. Mutant alleles have traditionally been outcrossed to WT individuals until the F5 generation is reached. At this point, any confounding mutations are deemed to have been removed from the line, and therefore the adults can be utilised for experiments (Varshney *et al*., 2016*)*.

To determine the expression of IL-34 in steady state conditions, expression in wild type zebrafish was investigated. Expression analysis of WT tissue confirmed *il34* expression occurs at consistent levels throughout development, with earliest expression detected at 1 dpf. Expression in adult zebrafish was confirmed in several organs, including the brain and head kidney which are key tissues for pathology seen in KO mouse studies. Expression was additionally monitored through development by WISH. The staining for expression seemed overall ubiquitous with the majority of it concentrated in the head and skin, thus keeping in line with the observed expression pattern for microglia. As for the skin, il34 could be implicated in the development of colour pattern formation as observed in pigment models of zebrafish.

In the zebrafish *D. rerio* pattern development has been intensively studied. The general patterns are dark stripes comprising melanophores, with alternate light inter-stripes of yellow-orange xanthophores and abundant iridiophores. Collectively these three chromatophores are located in the hypodermis between the skin and the myotome, and are crucial pigments for the development of the skin pattern (Singh & Volhard, 2015). *Csf1r* mutants are deficient in xanthophores and have disorganised melanophores. These mutants fail to develop the normal stripe pattern characteristic of *Danio rerio* leading to impaired stripe formation in the trunk, as well as unstriped fins (Patterson *et al*., 2014). The skin phenotype for zebrafish deficient of *csf1* has been so far only studied in homologues of *csfl-a* including *kit* and *fms* mutants. These mutants encode genes for nuclear zinc protein that is required for stripe formation but not directly in pigment cells themselves; they regulates *csf1-a* expression that is necessary for the survival and migration of melanophores and xanthophores. Similarly, these mutants also show reduced expression of melanophores and xanthophores (Parichy, 2003; Rawls & Johnson, 2000).

This highlights the critical role of *csf1a* and *csf1r* cellular interactions in skin and stripe development in the zebrafish, and given their close similarity to *il34*, it could be possible that *il34* could play a role in the development of skin pigments. This is not the first time *il34* has been implicated in the skin. IL-34 mutant mice showed expression of *il34* in the skin and authors confirmed that it was produced by keratinocytes (Wang *et al.,* 2012). At this stage however, more detailed studies are required to elucidate the role, if any, of *il34* in the skin phenotype of zebrafish.

The phenotype of *il-34* mutants showed that il34 is required for development of the zebrafish. Heterozygote and homozygote adults showed a decrease in overall size. This reduction could be related to delayed development resulting in the observed growth difference, however at this stage more investigations would be required.

The KO mouse develops several bone complications with lack of mineralisation and severe osteopenia, leading to spontaneous spine fractures and eventually their early death (Schiavone *et al,* unpublished data). Given the lower weight-bearing demand on the skeleton in aquatic animals, it was hypothesised that the zebrafish would be a more suited model to assess the bone phenotype. Moreover, since zebrafish develop *ex utero* they are far easier to study than KO mice. Bone and cartilage phenotypes were evaluated at 5 dpf, but no major differences in structures were observed. This could be due to the fact that at day 5, bone mineralisation is still in the early stages and therefore later stages, post day 20 would be more ideal to investigate. Also if the mutation is causing a delay in development or an effect on vasculature, bone development is delayed even further resulting in the slow onset of ossification (Spoorendonk *et al.,* 2009). Adult stages should therefore be investigated in the future by either microCT analysis and/or histological assessment.

The mutant line was used to investigate the role of il34 in inflammation. By using the tail-fin injury assay we induced temporal induction of *il34* and other inflammatory cytokines, and subsequently compared their expression in wild type and mutant embryos. Expression of il34 in wild type zebrafish peaked at 4 hours and resolved within 24 hours from tissue injury, providing the first evidence that il34 is involved in the inflammatory response. This pattern of expression is consistent with that of other major inflammatory cytokines in contributing towards the initiation the immune response (Novoa & Figueras, 2012) Some expression was also detected in mutated individuals, indicating that perhaps at this stage the allele is only partially inactivated. Given the early time point analysed, there is the issue that it could be maternally expressed leading to residual WT transcript in the morphant. To further evaluate the status of *il34* expression in mutants, western blotting could be utilised, however this would require a functional antibody that is selective for *il34* in zebrafish and currently there are no antibodies of this specificity commercially available.

To demonstrate the onset of inflammation in this model, two other major pro-inflammatory cytokines were analysed. Upregulation of TNF-α and IL-1β in response to tissue injury confirms the role of these cytokines in initiating inflammation and in line with results of similar studies documenting the upregulation of these cytokines in the zebrafish injury model (Nguyen-Chi *et al.,* 2015). TNF-α and IL-1β have been shown to upregulate the expression of *il34* in both mice and humans through the induction of NF-ϰB and JNK pathways (Chemel *et al.,* 2012; Eda *et al.*, 2011).

Having established that *il34* is involved in the immune response, we demonstrate that expression of its competing ligand *csf1*, was upregulated after 8 hours from injury, while *csf1-R* expression was heightened at 4 hours in wounded embryos of both WT and *il34* mutants. In view of these observations, peak expression of both *il34* and *csf1-R* is at 4 hours thus suggesting that signalling of *il34* could be acting through *csf1-R* as already documented in human and mice models. On the other hand, *csf1* which is known to signal through *csfl-R* does not peak at 4 hours but rather at 8 hours, suggesting that *il34* might be the primary pro-inflammatory molecule acting at the site of injury through the csf1-receptor before csf1, (or showing a greater affinity to the receptor). Collectively, these results support the structural conservation of *il34* signalling between mammals and teleosts, alongside the induction of pro-inflammatory cytokines following injury and their ability to attenuate inflammation.

***il34* deficient zebrafish were used to study the macrophage and neutrophil dynamics.** We used transgenic zebrafish lines and the tail fin infection model to study the interactions of macrophages and neutrophils at the onset of inflammation and its subsequent resolution on tissue injury. In zebrafish, neutrophils can be identified as early as 48 hours post fertilisation. During the first several hours of fin amputation, neutrophils are the first group of cells to reach the wound. At this stage they are the predominant functional phagocytes, and the primary initiators of the immune response (Renshaw *et al.*, 2006). Zebrafish tail fin injuries were performed on 3 days post fertilisation larvae. The visualisation of neutrophils migrating to the injury site was possible by the use of a transgenic neutrophil line tg (*mpo:gfp)*. These cells can exit the vasculature and enter into the tailfin showing that their principal route of administration is through the circulation. Counting of GFP-labelled neutrophils at different time points enabled the quantification of the inflammatory response.

The counting of fluorescent cells confirmed the wave of neutrophil influx that resolved within 24 hours. Unfortunately at this stage the effect of *il34* deficiency on neutrophilic inflammation in the tailfin assay still needs to be determined, and will certainly be a priority for future work on the *il34* mutant line.

Using the same strategy, tracking of macrophages and their quantification was analysed in wild type and *il34* mutants using the transgenic line Tg (fms: gfp). Recruitment of macrophages occurs over a longer period than that of neutrophils. Macrophages become the dominant cells at around 6-8 hours from injury, with their main role being to resolve inflammation and facilitating tissue remodelling and regrowth (Petrie *et al.,* 2014). Here, for the first time, evidence is presented that a deficiency of *il34* resulted in decreased macrophage numbers collecting at the site of the wound. This reinforces the role of *il34* in the myeloid lineage and its direct relationship as a cytokine in the inflammatory response. Further work to better identify the events leading up to the observed effect, would have to look into the properties of these macrophages so as to improve our understanding of the behaviour and interaction of these cell populations in the absence of *il34*.

5.2 CONCLUSIONS

The objective of this thesis was to assess the role of IL-34 in terms of its functional role as a mediator of inflammation and in the pathogenesis of osteosarcoma. To better understand the functional role of the cytokine at the cellular level, we looked at extracellular membrane vesicles as mediators of intracellular communication. From here the role of these vesicles in modulating OS and the bone microenvironment was investigated. Following this, two animal models were used, a murine preclinical model to assess whether there is a therapeutic benefit of targeting IL-34 in osteosarcoma, and a knockout zebrafish model to study its role in activation/regulation of the immune system.

In this first chapter, we investigate the role of extracellular vesicles, derived from OS cells. Exosomes from OS cell lines did not contain any IL-34 but they induced the commitment of mesenchymal stem cells towards adipogenesis, therefore suggesting that OS exosomes can have an effect on differentiation and lineage abilities of stromal cells in tumour

microenvironment. Similarly, exosomes were also purified from bone marrow and adipose derived mesenchymal stem cells, and were able to induce the proliferation of OS cells. Characterisation of the components of these vesicles showed that these MSC derived exosomes contain a number of proteins associated with several biological processes including those related to tumour progression. Taken together, this chapter demonstrates that there is a cross talk occurring between OS cells and their microenvironment, via extracellular membrane vesicles, with the potential of modulating tumour associated responses.

In the second chapter, we used xenogeneic and syngeneic murine preclinical models of OS and showed that by using an anti-IL-34 blocking antibody, OS tumour growth was reduced, thus providing the first evidence of the therapeutic benefit of targeting IL-34 in the microenvironment of OS. Immunohistochemistry was used to investigate the tumour associated mechanisms of IL-34. Analysis revealed a reduction of vascularisation by the marker CD31, and increase in the M1 sub-type macrophages.

We then evaluated the potential therapeutic benefit of IL-34 blocking agent, and doxorubicin as a combination treatment in these preclinical models. These two treatments administered together, failed to act synergistically as determined tumour growth and histological analysis possibly due to dose timing. A better strategy for testing this combination therapy would be needed. In conclusion, the inhibition of IL-34 specific blocking antibodies demonstrates that the therapeutic benefit to abrogate IL-34 in OS and thus IL-34 may be a novel therapeutic target in bone associated diseases.

To study the role of il34 in terms of its contribution towards the immune phenotype, a knockout zebrafish line deficient of IL34 was generated. The generation of this line and subsequent phenotyping of IL-34 in wild type and mutant zebrafish are shown in Chapter 4. In this chapter the role of *il34* in response to an inflammatory stimuli was investigated. Upon inducing a wound, *il34* was seen to become upregulated, in addition to other associated pro-inflammatory molecules TNF-α and IL-1β, its competing cytokine *csfl-a* and its potential receptor *csfla-R*, thus confirming its role in the inflammatory environment in a new animal model. Furthermore, we report the first characterisation of *il34* in relation

to macrophages in an inflammatory lesion, where we document a decrease in the number of macrophages in morphants, elucidating the role of *il34* as a regulator of myeloid cells.

The work presented in this thesis has demonstrated how the use of animal models, have been extremely useful tools to highlights the relationship of IL-34 in inflammation and the pathogenesis of osteosarcoma. And even though such models were technically developed in parallel, together they have undoubtedly provided an excellent framework for understanding the connection between the inflammatory response and cancer. The zebrafish has proved to be a suitable study system to elucidate and visualise the physiological significance of IL-34 in inflammation. Whilst on the other hand, the mouse model has been a key tool to demonstrate how inflammation also comes into play in malignant tissue and the resulting therapeutic benefit of inhibiting IL-34 in a mouse model of OS.

5.3 FUTURE WORK

5.3.1 Extracellular vesicles in osteosarcoma

The work presented in the initial chapter of this thesis, although preliminary, sets the foundation for the role of extracellular vesicle mediated communication between tumour cells and the microenvironment. Further work on elucidating the mechanisms of these exosomes will be needed to establish their physiological role in OS. A comparison of other extracellular vesicles derived from additional OS cell lines will be firstly added to this study. These vesicles will be used to study the intracellular communication network between the tumour cells. Using analysis of cell proliferation, analyses of cell death; either by flow cytometry or caspase activity assay, and cell migration using scratch assays, the mechanistic basics of how the vesicles induce tumour progression and metastasis. Additionally, further work on how exosomes support the tumour microenvironment niches should be aimed at investigating other cell population found in the tumour microenvironment including monocytes and macrophages, osteoblasts and osteoclasts. Similarly, to better characterise the role of mesenchymal derived stem cells on osteosarcoma, additional work on the proliferation abilities, apoptosis, migration, invasion

and drug resistance should be carried out. The primary aim should be to investigate how healthy stromal cells are triggered to release exosomes that promote the malignant behaviour of cancer cells.

A significant addition to the work presented here, would be transcriptomic (miRNA and or/mRNA) and proteomic analysis (phosphorylated and non-phosphorylated proteins) on the exosomes content in order to compare profiles and determine the cargo content. Since EVs are considered as a direct derivative of their donor cells, cancer EV proteomics may reveal important information at the translational level, thereby significantly improving the accuracy of cancer diagnosis, as well that of patient prognosis.

5.3.2 IL-34 as a therapeutic treatment for osteosarcoma

The work presented in this thesis has shown that inhibition of IL-34 in the tumour microenvironment, appears to be a promising strategy for the treatment of osteosarcoma. Further work is needed to demonstrate the value of this therapeutic approach. *In vivo* experiments should primarily seek to investigate whether this treatment has any effect on the development of lung metastasis, therefore proof of concept should ideally be obtained in both models. Following that, further *in vivo* studies with an increased number of subjects should be carried out, so as to better define the mechanisms by which blocking Il-34 reduces tumour growth. Better characterization of the immune population in the resulting tumours, by a combination of histological analysis and flow cytometry should be considered. To determine at to what extent the treatment is efficient within the tumour environment, the levels of IL-34 in blood serum and/or specific tissues should be monitored.

The results, also strengthen the potential interest to enumerate and characterize the effect of anti-IL34 on circulating tumour cells (CTCs). CTCs play a key role in the metastatic process and could reflect the therapeutic response, thus leading to a strong clinical interest for OS patients. If treating with anti-IL34 continues to prove to be successful, a follow-up on the treatment regimen with respect to administering the antibody on its own, or as attempted here, in combination with chemotherapeutic agents will need to be carried out. A comprehensive study on the dose administration, binding characteristics and ultimately the pharmacokinetics of anti-IL-34 antibody, would allow further development for better

anti-tumour efficacy. Another key aspect to consider, is the combination of this treatment with other immune checkpoint inhibitors. Interaction with other immunotherapeutic treatments such as for example anti-PD-L1, could provide better efficacy in activating an anti-tumour immune response (Heymann *et al*., 2019)

5.3.3 Development of *il34* mutant zebrafish

The mutant zebrafish described in this thesis has proven to be a viable loss of function model for *il34*. The cytokine was identified as a participant in inflammation and a regulator of tissue resident macrophages, primarily affecting macrophage numbers at the site of injury.

Future work should focus on analyzing further wild type and mutant phenotypes in both juvenile and adult zebrafish. Analysis for morphological differences by histology at different timepoints, will elucidate more information on any pathological changes caused by the mutation. To address how the mutation affects the viability and development of the larvae, standard growth and survival curves can be implemented. Homozygous individuals showed a lack of circulation at 3 dpf. For this reason, development of vascularization in mutants should be elucidated in more detail.

To further demonstrate the loss of function of *il34*, immunoblotting and immunostaining (with/or without fluorescence) in mutant larvae would need to be performed. Up to date, there is no commercially available antibody specific for zebrafish il-34, and therefore developing such an antibody should be considered. This would also allow for the validation of tissue specific expression in organs for example in brain, head-kidney and spleen, and for expression following injury. Analysis of the bone phenotype should be extended to embryos at later stages including adults. Additional bone staining by for example alizarin red, immunohistochemistry by H&E and *in-situ* hybridization of juvenile embryos can be carried to identify the effect of loss of *il34* on bone development and mineralization. In adults radiography and microCT can be utilised to look for any bone abnormalities. Additionally expression of key bone-related markers, such as *runx2b* and *col1a1*, can be investigated.

In terms of the immune phenotype, the effect of il34 deficiency on neutrophil biology should primarily be demonstrated. Given the role of il34 as a regulator of myeloid precursors, it is plausible that similarly, il34 plays a role in neutrophilic inflammation. Understanding the morphological and functional features of inflammation and its resolution would help elucidate further the role of IL-34 in the innate immune system. For macrophages classical parameters analysed are the distribution, resolution, recruitment and shape of the cells, whilst for neutrophils there is also the added effect on phagocytosis, acidification and tracking. Unravelling these features would be key to obtain a comprehensive analysis of the role of IL-34 in inflammation and associated diseases. Gene to gene interactions in the inflammatory environment could be further elucidated by over expressing and inhibiting other members of the IL-34 pathway. RNA sequencing and transcriptome profiling could be used for expression profiles between wild type and mutant lines.

Macrophage transgenic lines would make it an ideal model for infection by bacteria. The zebrafish is an optimal model to study infectious diseases, by causing systemic invasive infection resembling human infections. An infection model (such as for example infection by *Staphylococcus* or *Cryptococcus*) would allow the analysis of bacterial and immune cell interactions during infection.

As zebrafish larvae have proven to be suitable for cancer studies, the mutant line could be used as a xenotransplantation model to study the behaviour of OS or other cancer cells. Cells can be injected into zebrafish larvae, to study their behaviour in the absence of Il34. This model could be used to investigate tumour-induced angiogenesis, intravasation and extravasation of tumour cells, metastatic potential and evaluation of cancer

REFERENCES

1. Ablain, J., Durand, E. M., Zhou, Y., Zon, L. I., Ablain, J., Durand, E. M., … Zon, L. I.. Resource A CRISPR / Cas9 Vector System for Tissue-Specific Gene Disruption in Zebrafish. *Developmental Cell*, ***32*****(6),** (2015)
2. Abo-al-ela, H. An introduction to selected innate immune-relevant genes in fish. Applied ecology and environmental research. **16(2)**, 955-976 (2018)
3. Andersen, T. L. *et al*. A physical mechanism for coupling bone resorption and formation in adult human bone. *Am. J. Pathol*. **174**, 239–247 (2009).
4. Arimochi, H., Sasaki, Y., Kitamura, A. & Yasutomo, K. Differentiation of preadipocytes and mature adipocytes requires PSMB8. *Sci. Rep*. **6**, 26791 (2016).
5. Atay, S. *et al*. Oncogenic KIT-containing exosomes increase gastrointestinal stromal tumor cell invasion. *Proc. Natl. Acad. Sci. U. S. A*. **111**, 711–6 (2014).
6. Auer, T. O. & Del Bene, F. CRISPR/Cas9 and TALEN-mediated knock-in approaches in zebrafish. *Methods* **69**, 142–150 (2014).
7. Avril, P. *et al*. Opposite Effects of Soluble Factors Secreted by Adipose Tissue on Proliferating and Quiescent Osteosarcoma Cells. *Plast. Reconstr. Surg*. **137**, 865–875 (2016).
8. Baghdadi, M. *et al*. Chemotherapy-induced IL34 enhances immunosuppression by tumor-associated macrophages and mediates survival of chemoresistant lung cancer cells. *Cancer Res*. **76**, 6030–6042 (2016).
9. Baghdadi, M. *et al*. High co-expression of IL-34 and M-CSF correlates with tumor progression and poor survival in lung cancers. *Sci. Rep*. **8**, 418 (2018).
10. Baghdadi, M. *et al*. Interleukin-34, a comprehensive review. *J. Leukoc. Biol*. **104**, 931–951 (2018).
11. Baglio, S. R. *et al*. Blocking Tumor-Educated MSC Paracrine Activity Halts Osteosarcoma Progression. *Clin. Cancer Res*. **23**, 3721–3733 (2017).
12. Bankhead, P. *et al*. QuPath: Open source software for digital pathology image analysis. *Sci. Rep*. **7**, 16878 (2017).
13. Barve, R. A. *et al*. Transcriptional profiling and pathway analysis of CSF-1 and IL-34 effects on human monocyte differentiation. *Cytokine* **63**, 10–17 (2013).

14. Basu-Roy, U. *et al*. PPARγ agonists promote differentiation of cancer stem cells by restraining YAP transcriptional activity. *Oncotarget* **7**, 60954–60970 (2016).
15. Baud'Huin, M. *et al*. Interleukin-34 is expressed by giant cell tumours of bone and plays a key role in RANKL-induced osteoclastogenesis. *J. Pathol.* **221**, 77–86 (2010).
16. Bauer, D. E., Canver, M. C., & Orkin, S. H. Generation of Genomic Deletions in Mammalian Cell Lines via CRISPR / Cas9, (January), 1–10. (2015).
17. Bellora, F. *et al*. The interaction of human natural killer cells with either unpolarized or polarized macrophages results in different functional outcomes. *Proc. Natl. Acad. Sci. U. S. A.* **107**, 21659–64 (2010).
18. Bhattacharya, A. *et al*. Tumor Vascular Maturation and Improved Drug Delivery Induced by Methylselenocysteine Leads to Therapeutic Synergy with Anticancer Drugs. *Clin. Cancer Res.* **14**, 3926–3932 (2008).
19. Bird, S. & Tafalla, C. Teleost Chemokines and Their Receptors. *Biology (Basel).* **4**, 756–784 (2015).
20. Bostrum, E. A. & Lundberg, P. The newly discovered cytokine IL-34 is expressed in gingival fibroblasts, shows enhanced expression by pro-inflammatory cytokines, and stimulates osteoclast differentiation. *PLoS One* **8**, 1–7 (2013).
21. Botter SM, Arlt MJE, Fuchs B (2015) Mammalian models of bone sarcomas. In: Heymann D (ed) Bone cancer, second edition, chapter 30. Elsevier, San Diego, pp 349–364. https://doi. org/10.1016/B978-0-12-416721-6.00030-3
22. Boulakirba, S. *et al*. IL-34 and CSF-1 display an equivalent macrophage differentiation ability but a different polarization potential. *Sci. Rep.* **8**, 256 (2018).
23. Bouxsein, M. L. *et al*. Guidelines for assessment of bone microstructure in rodents using micro-computed tomography. *J. Bone Miner. Res.* **25**, 1468–1486 (2010).
24. Bracha, S. *et al*. A Preliminary Proteomic Investigation of Circulating Exosomes and Discovery of Biomarkers Associated with the Progression of Osteosarcoma in a Clinical Model of Spontaneous Disease. *Transl. Oncol.* **11**, 1137–1146 (2018).
25. Bremnes, R. M. *et al*. The Role of Tumor-Infiltrating Lymphocytes in Development, Progression, and Prognosis of Non-Small Cell Lung Cancer. *J. Thorac. Oncol.* **11**, 789–800 (2016).

26. Broadhead, M. L., Clark, J. C. M., Myers, D. E., & Dass, C. R. The molecular pathogenesis of osteosarcoma: A review. *Sarcoma*, (20*11)*
27. Brown, H. K., Schiavone, K., Gouin, F., Heymann, M. & Heymann, D. Biology of Bone Sarcomas and New Therapeutic Developments. *Calcif. Tissue Int.* **102**, 174–195 (2017).
28. Brown, H. K., Schiavone, K., Tazzyman, S., Heymann, D. & Chico, T. J. Zebrafish xenograft models of cancer and metastasis for drug discovery. *Expert Opin. Drug Discov.* **12**, 379–389 (2017).
29. Buddingh, E. P. *et al.* Tumor-infiltrating macrophages are associated with metastasis suppression in high-grade osteosarcoma: A rationale for treatment with macrophage activating agents. *Clin. Cancer Res.* **17**, 2110–2119 (2011).
30. Casali, P. G. *et al.* Bone sarcomas: ESMO clinical practice guidelines for diagnosis, treatment and follow-up. *Ann. Oncol.* **25**, iii113–iii123 (2014).
31. Chan, C. K. F. *et al.* Clonal precursor of bone, cartilage, and hematopoietic niche stromal cells. *Proc. Natl. Acad. Sci. U. S. A.* **110**, 12643–8 (2013).
32. Chang, N., Sun, C., Gao, L., Zhu, D., Xu, X., Zhu, X., Xi, J. J. Genome editing with RNA-guided Cas9 nuclease in Zebrafish embryos. *Nature Publishing Group*, ***23*(4),** 465–472. (2013).
33. Chemel, M. *et al.* Bone Morphogenetic Protein 2 and Transforming Growth Factor β1 Inhibit the Expression of the Proinflammatory Cytokine IL-34 in Rheumatoid Arthritis Synovial Fibroblasts. *Am J Pathol* **187**, 156–162 (2017).
34. Chemel, M. *et al.* Interleukin 34 expression is associated with synovitis severity in rheumatoid arthritis patients. *Ann. Rheum. Dis.* **71**, 150–154 (2012).
35. Chen, C. *et al.* Aberrant activation of Wnt/B-catenin signaling drives proliferation of bone sarcoma cells. *Oncotarget* **6**, 17570–17583 (2015).
36. Chen, C.-H. *et al.* The Fractionated *Toona sinensis* Leaf Extract Induces Apoptosis of Human Osteosarcoma Cells and Inhibits Tumor Growth in a Murine Xenograft Model. *Integr. Cancer Ther.* **16**, 397–405 (2017).
37. Cherrier, B. *et al.* A New Experimental Rat Model of Osteosarcoma Established by Intrafemoral Tumor Cell Inoculation, Useful for Biology and Therapy Investigations. *Tumor Biol.* **26**, 121–130 (2005).
38. Chico, T. J. A., Ingham, P. W. & Crossman, D. C. Modeling Cardiovascular Disease in the Zebrafish. *Trends Cardiovasc. Med.* **18**, 150–155 (2008).

39. Chihara, T. *et al*. IL-34 and M-CSF share the receptor Fms but are not identical in biological activity and signal activation. *Cell Death Differ*. **17**, 1917–27 (2010).
40. Cho, J. A., Park, H., Lim, E. H. & Lee, K. W. Exosomes from breast cancer cells can convert adipose tissue-derived mesenchymal stem cells into myofibroblast-like cells. *Int. J. Oncol*. **40**, 130–138 (2012).
41. Chockalingam, S. & Ghosh, S. S. Macrophage colony-stimulating factor and cancer: a review. *Tumor Biol*. **35**, 10635–10644 (2014).
42. Chu, C. *et al*. Extracellular vesicle and mesenchymal stem cells in bone regeneration: recent progress and perspectives. (2018). doi:10.1002/jbm.a.36518
43. Ciccia, F. *et al*. IL-34 is overexpressed in the inflamed salivary glands of patients with Sjögren's syndrome and is associated with the local expansion of pro-inflammatory CD14brightCD16+monocytes. *Rheumatol*. **52**, 1009–1017 (2013).
44. Clayton, A. *et al*. Human tumor-derived exosomes down-modulate NKG2D expression. *J. Immunol*. **180**, 7249–58 (2008).
45. Clayton, A., Mitchell, J. P., Court, J., Mason, M. D. & Tabi, Z. Human Tumor-Derived Exosomes Selectively Impair Lymphocyte Responses to Interleukin-2. *Cancer Res*. **67**, 7458–7466 (2007).
46. Coffelt, S. B. *et al*. Angiopoietin-2 regulates gene expression in TIE2-expressing monocytes and augments their inherent proangiogenic functions. *Cancer Res*. **70**, 5270–5280 (2010).
47. Colombo, M., Raposo, G. & Théry, C. Biogenesis, Secretion, and Intercellular Interactions of Exosomes and Other Extracellular Vesicles. *Annu. Rev. Cell Dev. Biol* **30**, 255–289 (2014).
48. Corrò, C. *et al*. IL-8 and CXCR1 expression is associated with cancer stem cell-like properties of clear cell renal cancer. *J. Pathol* (2019). doi:10.1002/path.5267
49. Covaleda, L., Fuller, F. J. & Payne, S. L. EIAV S2 enhances pro-inflammatory cytokine and chemokine response in infected macrophages. *Virology* **397**, 217–223 (2010).
50. Dai, X.-M. *et al*. Targeted disruption of the mouse colony-stimulating factor 1 receptor gene results in osteopetrosis, mononuclear phagocyte deficiency, increased primitive progenitor cell frequencies, and reproductive defects. *Blood* **99**, 111-120 (2002).

51. Dee, C. T. *et al*. CD4-Transgenic Zebrafish Reveal Tissue-Resident Th2- and Regulatory T Cell-like Populations and Diverse Mononuclear Phagocytes. *J. Immunol*. **197**, 3520–3530 (2016).
52. Del Fattore, A. *et al*. Differential effects of extracellular vesicles secreted by mesenchymal stem cells from different sources on glioblastoma cells. *Expert Opin. Biol. Ther*. **15**, 495–504 (2015).
53. Duan, Z. *et al*. miR-15b modulates multidrug resistance in human osteosarcoma *in vitro* and *in vivo*. *Mol. Oncol*. **11**, 151–166 (2017).
54. Dujardin, F. *et al*. MDM2 and CDK4 immunohistochemistry is a valuable tool in the differential diagnosis of low-grade osteosarcomas and other primary fibro-osseous lesions of the bone. *Mod. Pathol*. **24**, 624–637 (2011).
55. Dumars, C. *et al*. Dysregulation of macrophage polarization is associated with the metastatic process in osteosarcoma. *Oncotarget*. **48**, 78343-78354 (2016).
56. Eda, H., Shimada, H., Beidler, D. R. & Monahan, J. B. Proinflammatory cytokines, IL-1β and TNF-α, induce expression of interleukin-34 mRNA via JNK- and p44/42 MAPK-NF-κB pathway but not p38 pathway in osteoblasts. *Rheumatol. Int*. **31**, 1525–1530 (2011).
57. Fabre, J. A. S. *et al*. The Interleukin-17 Family of Cytokines in Breast Cancer. *Int. J. Mol. Sci*. **19**, (2018).
58. Feng, Y., Santoriello, C., Mione, M., Hurlstone, A. & Martin, P. Live Imaging of Innate Immune Cell Sensing of Transformed Cells in Zebrafish Larvae: Parallels between Tumor Initiation and Wound Inflammation. *PLoS Biol*. **8**, e1000562 (2010).
59. Ferrari, A., Dirksen, U. & Bielack, S. Sarcomas of Soft Tissue and Bone. in *Progress in tumor research* **43**, 128–141 (2016).
60. Foucher, E. D. *et al*. IL-34 Induces the Differentiation of Human Monocytes into Immunosuppressive Macrophages. Antagonistic Effects of GM-CSF and IFN-Y *PLoS One* **8**, (2013).
61. Francis, M., Dennis, N., Charman, J., Lawrence, G. & Grimer, R. Bone and Soft Tissue Sarcomas UK Incidence and Survival : 1996 to 2010 November 2013. *Natl. Cancer Intell. Netw*. **2.0**, 1–14 (2013).
62. Franzè, E. *et al*. Interleukin-34 sustains pro-tumorigenic signals in colon cancer tissue. *Oncotarget* **9**, 3432–3445 (2018).

63. Fritzsching, B. *et al*. CD8+/FOXP3+-ratio in osteosarcoma microenvironment separates survivors from non-survivors: a multicenter validated retrospective study. *Oncoimmunology* **4**, e990800 (2015).
64. Garceau, V. *et al*. Pivotal Advance: Avian colony-stimulating factor 1 (CSF-1), interleukin-34 (IL-34), and CSF-1 receptor genes and gene products. *J. Leukoc. Biol* **87**, 753–764 (2010).
65. Garcia, S. *et al*. Colony-stimulating factor (CSF) 1 receptor blockade reduces inflammation in human and murine models of rheumatoid arthritis. *Arthritis Res. Ther*. **18**, 75 (2016).
66. Garimella, R. *et al*. Extracellular membrane vesicle derived from 143b osteosarcom cells contain pro-osteoclastogenic cargo: A nove communication mechanism in osteosarcoma bone microenvironment. *Transl. Oncol*. **7**, 331–340 (2014).
67. Giacomini, A., Ghedini, G. C., Presta, M. & Ronca, R. Long pentraxin 3: A novel multifaceted player in cancer. *Biochim. Biophys. Acta - Rev. Cancer* **1869**, 53–63 (2018).
68. Gobin, B. *et al*. New PI3K[alpha]-specific inhibitor, BYL719: therapeutic interest in osteosarcoma. *Bone Abstr*. (2013). doi:10.1530/boneabs.1.PP139
69. Gomez-Brouchet, A. *et al*. CD163-positive tumor-associated macrophages and CD8-positive cytotoxic lymphocytes are powerful diagnostic markers for the therapeutic stratification of osteosarcoma patients: An immunohistochemical analysis of the biopsies from the French OS2006 phase 3 trial. (2017). doi:10.1080/2162402X.2017.1331193
70. Grigoriadis, A. E., Schellander, K., Wang, Z. Q. & Wagner, E. F. Osteoblasts are target cells for transformation in c-fos transgenic mice. *J. Cell Biol*. **122**, 685–701 (1993).
71. Grimaud, E. *et al*. Bone remodelling and tumour grade modifications induced by interactions between bone and swarm rat chondrosarcoma. Histology and Histopathology, **17 (4)**. pp. 1103-1111. (2002).
72. Grimer R.J., Hogendoorn, P.C.W, Vanel, D,. WHO Classification of tumours of bone: introduction. In: Fletcher, C.D.M., Bridge, J.A., Hogendoorn, P.C.W., Mertens, F, Editors. World Health Organisation Classification of Bone Tumours of Soft Tissue and Bone. Lyon: IARC Press (2013).

73. Guijarro, M. V, Ghivizzani, S. C., Parker Gibbs, C. & Blanco Aparicio, C. Animal models in osteosarcoma. (2014). doi:10.3389/fonc.2014.00189
74. Henry, K. M., Loynes, C. A., Whyte, M. K. B. & Renshaw, S. A. Zebrafish as a model for the study of neutrophil biology. *J. Leukoc. Biol.* **94**, 633–642 (2013).
75. Heymann MF, Brown HK, Heymann D (2016). Drugs in early clinical development for the treatment of osteosarcoma. Expert Opin Investig Drugs 25:1265–1280. https://doi.org/10.1080/1 3543784.2016.1237503
76. Heymann, D. & Rédini, F. Bone sarcomas: pathogenesis and new therapeutic approaches. *IBMS Bonekey* **8**, 402–414 (2011).
77. Heymann, D. & Rédini, F. Targeted therapies for bone sarcomas. *Bonekey Rep.* **2**, 378 (2013).
78. Heymann, M.-F., Lézot, F. & Heymann, D. The contribution of immune infiltrates and the local microenvironment in the pathogenesis of osteosarcoma. *Cell. Immunol.* (2017). doi:10.1016/J.CELLIMM.2017.10.011
79. Howe, K. *et al.* The zebrafish reference genome sequence and its relationship to the human genome. *Nature* **496**, 498–503 (2013).
80. Humphries, B. A. *et al.* Plasminogen activator inhibitor 1 (PAI1) promotes actin cytoskeleton reorganization and glycolytic metabolism in triple negative breast cancer. *Mol. Cancer Res.* molcanres.0836.2018 (2019). doi:10.1158/1541-7786.MCR-18-0836
81. Huvos, A. Osteogenic osteosarcoma. In Huvos A (ed): Bone Tumors: Diagnosis. Treatment and Prognosis, 2nd ed. Philadelphia: WB Saunders (1991) ; 85-156.
82. Hwang, S. J. *et al.* Interleukin-34 produced by human fibroblast-like synovial cells in rheumatoid arthritis supports osteoclastogenesis. *Arthritis Res. Ther.* **14**, R14 (2012).
83. Inwald, E. C. *et al.* Ki-67 is a prognostic parameter in breast cancer patients: results of a large population-based cohort of a cancer registry. *Breast Cancer Res. Treat.* **139**, 539–52 (2013).
84. Jacques, C. *et al.* Small animal models for the study of bone sarcoma pathogenesis:characteristics, therapeutic interests and limitations. *J. Bone Oncol.* **12**, 7–13 (2018).

85. Jadus, M. R. *et al*. Macrophages can recognize and kill tumor cells bearing the membrane isoform of macrophage colony-stimulating factor. *Blood* **87**, 5232–5241 (1996).
86. Jerez, S. *et al*. Proteomic Analysis of Exosomes and Exosome-Free Conditioned Media From Human Osteosarcoma Cell Lines Reveals Secretion of Proteins Related to Tumor Progression. *J. Cell. Biochem.* **118**, 351–360 (2017).
87. Jian, Y. K., Zhu, H. Y., Wu, X. L. & Li, B. Thrombospondin 1 Triggers Osteosarcoma Cell Metastasis and Tumor Angiogenesis. *Oncol. Res. Featur. Preclin. Clin. Cancer Ther.* **27**, 211–218 (2019).
88. Joliat, M., Umeda, S., Lyons, B., Lynes, M. & Shultz, L. Establishment and characterization of a new osteogenic cell line (MOS-J) from a spontaneous C57BL/6J mouse osteosarcoma. *Fac. Res.* (2002).
89. Kettleborough, R. N. W. *et al*. A systematic genome-wide analysis of zebrafish protein-coding gene function. *Nature* **496**, 494–497 (2013).
90. Khawar, B., Abbasi, M. & Sheikh, N. A panoramic spectrum of complex interplay between the immune system and IL-32 during pathogenesis of various systemic infections and inflammation. *Eur. J. Med. Res.* **20**, 7 (2015).
91. Kovac, M. *et al*. Exome sequencing of osteosarcoma reveals mutation signatures reminiscent of BRCA deficiency. *Nat. Commun.* **6**, 1–9 (2015).
92. Knowles, H., Harris, A.L. Macrophages and the hypoxic tumour microenvironment. *Frontiers in Bioscience*. **12,** 4298-4314 (2007).
93. Kuil, L. E. *et al*. Reverse genetic screen reveals that Il34 facilitates yolk sac macrophage distribution and seeding of the brain. *bioRxiv* 406553 (2018). doi:10.1101/406553
94. Lagerweij, T., Pérez-Lanzón, M. & Baglio, S. R. A Preclinical Mouse Model of Osteosarcoma to Define the Extracellular Vesicle-mediated Communication Between Tumor and Mesenchymal Stem Cells. *J. Vis. Exp* 56932 (2018). doi:10.3791/56932
95. Lamoureux, F. *et al*. Selective inhibition of BET bromodomain epigenetic signalling interferes with the bone-associated tumour vicious cycle. *Nat. Commun.* **5**, 3511 (2014).

96. Lamoureux, F. *et al*. Therapeutic efficacy of soluble receptor activator of nuclear factor-kappa B-Fc delivered by nonviral gene transfer in a mouse model of osteolytic osteosarcoma. *Mol. Cancer Ther*. **7**, 3389–98 (2008).
97. Lamoureux, F. *et al*. Therapeutic relevance of osteoprotegerin gene therapy in osteosarcoma: Blockade of the vicious cycle between tumor cell proliferation and bone resorption. *Cancer Res*. **67**, 7308–7318 (2007).
98. Lee, J.-K. *et al*. Exosomes derived from mesenchymal stem cells suppress angiogenesis by down-regulating VEGF expression in breast cancer cells. *PLoS One* **8**, e84256 (2013).
99. Lee, K., Park, H., Lim, E. H. & Lee, K. W. Exosomes from breast cancer cells can convert adipose tissue-derived mesenchymal stem cells into myofibroblast-like cells. *Int. J. Oncol*. **40**, 130–138 (2011).
100. Lewis, C. & Murdoch, C. Macrophage responses to hypoxia: implications for tumor progression and anti-cancer therapies. *Am. J. Pathol*. **167**, 627–35 (2005).
101. Lieschke, G. J. & Currie, P. D. Animal models of human disease: zebrafish swim into view. *Nat. Rev. Genet*. **8**, 353–367 (2007).
102. Lin, E. Y., Nguyen, A. V, Russell, R. G. & Pollard, J. W. Colony-stimulating factor 1 promotes progression of mammary tumors to malignancy. *J. Exp. Med*. **193**, 727–40 (2001).
103. Lin, H.-H. *et al.* The macrophage F4/80 receptor is required for the induction of antigen-specific efferent regulatory T cells in peripheral tolerance. *J. Exp. Med.* **201**, 1615–1625 (2005).
104. Lin, H., Lee, E., Hestir, K., Leo, C., Huang, M., Bosch, E., Halenbeck, R., Wu, G., Zhou, A., Behrens, D., Hollenbaugh, D., Linnemann, T., Qin, M., Wong, J., Chu, K., Doberstein, S.K., Williams, L.T. Discovery of a Cytokine and Its Receptor by Functional Screening of the Extracellular Proteome Haishan. *Science*, **320,** 807-811 (2008).
105. Lin, P. P. *et al*. Targeted mutation of p53 and Rb in mesenchymal cells of the limb bud produces sarcomas in mice. *Carcinogenesis* **30**, 1789–1795 (2009).
106. Lindau, R. *et al*. Interleukin-34 is present at the fetal–maternal interface and induces immunoregulatory macrophages of a decidual phenotype in vitro. *Hum. Reprod*. **33**, 588–599 (2018).

107. Liu, Z.-L. *et al*. Extracellular vesicles-mediated signaling in the osteosarcoma microenvironment: Roles and potential therapeutic targets. *J. Bone Oncol*. **12**, 101–104 (2018).
108. Longhi, A., Errani, C., De Paolis, M., Mercuri, M. & Bacci, G. Primary bone osteosarcoma in the pediatric age: State of the art. *Cancer Treat. Rev*. **32**, 423–436 (2006).
109. Luetke, A., Meyers, P. A., Lewis, I. & Juergens, H. Osteosarcoma treatment - Where do we stand? A state of the art review. *Cancer Treat. Rev*. **40**, 523–532 (2014).
110. Lund, S. A., Giachelli, C. M. & Scatena, M. The role of osteopontin in inflammatory processes. *J. Cell Commun. Signal*. **3**, 311–22 (2009).
111. Maas, S. L. N., De Vrij, J. & Broekman, M. L. D. Quantification and Size-profiling of Extracellular Vesicles Using Tunable Resistive Pulse Sensing. *J. Vis. Exp.* 1–7 (2014). https://doi.org/10.3791/51623
112. Mackall, C. L., Meltzer, P. S. & Helman, L. J. Focus on sarcomas. *Cancer cell*. **2**, 175-178 (2002).
113. Macklin, R. *et al*. Extracellular vesicles secreted by highly metastatic clonal variants of osteosarcoma preferentially localize to the lungs and induce metastatic behaviour in poorly metastatic clones. *Oncotarget*. **7**, (2016).
114. Maekawa, N. *et al*. Immunohistochemical Analysis of PD-L1 Expression in Canine Malignant Cancers and PD-1 Expression on Lymphocytes in Canine Oral Melanoma. *PLoS One* **11**, e0157176 (2016).
115. Mantovani, A. & Sica, A. Macrophages, innate immunity and cancer: balance, tolerance, and diversity. *Curr. Opin. Immunol*. **22**, 231–237 (2010).
116. Mantovani, A., & Sica, A. (2010). Macrophages, innate immunity and cancer: balance, tolerance, and diversity. Current Opinion in Immunology, **22(2)**, 231–237.
117. Marina, N., Gebhardt, M., Teot, L. & Gorlick, R. Biology and therapeutic advances for pediatric osteosarcoma. *Oncologist* **9**, 422–441 (2004).
118. Martin, J. W., Squire, J. A. & Zielenska, M. The genetics of osteosarcoma. *Sarcoma* **2012**, (2012).
119. Meier, D. ; *et al*. Foscan and Foslip based photodynamic therapy in osteosarcoma in vitro and in intratibial mouse models. *J. Artic. Accept. Version Int. J. Cancer* **140**, 1680–1692

120. Melzer, C., Yang, Y. & Hass, R. Interaction of MSC with tumor cells. *Cell Commun. Signal.* **14**, 20 (2016).
121. Meyers PA, Schwartz CL, Krailo MD, et al. Osteosarcoma: the addition of muramyl tripeptide to chemotherapy improves overall survival++a report from the Children's Oncology Group.J Clin Oncol 2008;26:633-638.
122. Meyers, P. A. *et al.* Osteosarcoma: The addition of muramyl tripeptide to chemotherapy improves overall survival - A report from the children's oncology group. *J. Clin. Oncol.* **26**, 633–638 (2008).
123. Miller, I. V. & Grunewald, T. G. P. Tumour-derived exosomes: Tiny envelopes for big stories. *Biol. Cell* **107**, 287–305 (2015).
124. Min, L., Shen, J., Tu, C., Hornicek, F. & Duan, Z. The roles and implications of exosomes in sarcoma. *Cancer Metastasis Rev.* **35**, 377–390 (2016).
125. Miwa, S. *et al.* Current and Emerging Targets in Immunotherapy for Osteosarcoma. *J. Oncol.* **2019**, 1–8 (2019).
126. Mohseny, A. B., Hogendoorn, P. C. W. & Cleton-Jansen, A. M. Osteosarcoma models: From cell lines to zebrafish. *Sarcoma* **2012**, (2012).
127. Mori, K., Ando, K. & Heymann, D. Liposomal muramyl tripeptide phosphatidyl ethanolamine: a safe and effective agent against osteosarcoma pulmonary metastases. *Expert Rev. Anticancer Ther.* **8**, 151–159 (2008).
128. Muthana, M. *et al.* Macrophage Delivery of an Oncolytic Virus Abolishes Tumor Regrowth and Metastasis after Chemotherapy or Irradiation. *Cancer Res.* **73**, 490–495 (2013).
129. Mutsaers, A. J. & Walkley, C. R. Cells of origin in osteosarcoma: Mesenchymal stem cells or osteoblast committed cells? *Bone* **62**, 56–63 (2014).
130. Naeem, N., Mushtaq, S., Akhter, N., Hussain, M. & Hassan, U. Effectiveness Of Vascular Markers (immunohistochemical Stains) In Soft Tissue Sarcomas. *J. Coll. Physicians Surg. Pakistan* **28**, 352–356 (2018).
131. Nakamichi, Y., Udagawa, N. & Takahashi, N. IL-34 and CSF-1: Similarities and differences. *J. Bone Miner. Metab.* **31**, 486–495 (2013).
132. Nakashima, K. *et al.* The novel zinc finger-containing transcription factor Osterix is required for osteoblast differentiation and bone formation. *Cell* **108**, 17–29 (2002).

133. Nandi, S. *et al*. Receptor-type protein-tyrosine phosphataseζ is a functional receptor for interleukin-34. *J. Biol. Chem*. **288**, 21972–21986 (2013).
134. Nandi, S. *et al*. The CSF-1 receptor ligands IL-34 and CSF-1 exhibit distinct developmental brain expression patterns and regulate neural progenitor cell maintenance and maturation. *Dev. Biol*. **367**, 100–113 (2012).
135. Nasiadka, A. & Clark, M. D. Zebrafish Breeding in the Laboratory Environment. *ILAR J*. **53**, 161–168 (2012).
136. Nguyen-Chi, M. *et al.* Identification of polarized macrophage subsets in zebrafish. *Elife* **4**, (2015).
137. Nolan, T., Hands, R. E. & Bustin, S. A. Quantification of mRNA using real-time RT-PCR. *Nat. Protoc*. **1**, 1559–1582 (2006).
138. Novoa, B. & Figueras, A. Zebrafish: Model for the Study of Inflammation and the Innate Immune Response to Infectious Diseases. in 253–275 (Springer, New York, NY, 2012). doi:10.1007/978-1-4614-0106-3_15
139. Ono, M. *et al*. Exosomes from bone marrow mesenchymal stem cells contain a microRNA that promotes dormancy in metastatic breast cancer cells. *Sci. Signal*. **7**, ra63 (2014).
140. Ottewell, P. D. *et al.* Antitumor Effects of Doxorubicin Followed by Zoledronic Acid in a Mouse Model of Breast Cancer. *JNCI J. Natl. Cancer Inst.* **100**, 1167–1178 (2008).
141. Paget, S. The distribution of secondary growths in cancer of the breast. 1889. *Cancer Metastasis Rev*. **8**, 98–101 (1989).
142. Pan, C. C. *et al*. Src-mediated Post-translational Regulation of Endoglin Stability and Function Is Critical for Angiogenesis. *J. Biol. Chem*. **289**, 25486–25496 (2014).
143. Parichy, D. Evolution of danio pigment pattern development. *Heredity (Edinb).* **97**, 200–210 (2006).
144. Patterson, L. B., Bain, E. J. & Parichy, D. M. Pigment cell interactions and differential xanthophore recruitment underlying zebrafish stripe reiteration and Danio pattern evolution. *Nat. Commun.* **5**, 5299 (2014).
145. Peacock, B. *et al*. Extracellular vesicle microRNA cargo is correlated with HPV status in oropharyngeal carcinoma. *J. Oral Pathol. Med*. **47**, 954–963 (2018).
146. Perrot, P. *et al*. Safety concern between autologous fat graft, mesenchymal stem cell and osteosarcoma recurrence. *PLoS One* **5**, (2010).

147. Petrie, T. A. *et al*. Macrophages modulate adult zebrafish tail fin regeneration. *Development* **141**, 2581–91 (2014).
148. Picci, P. *et al*. Late sarcoma development after curettage and bone grafting of benign bone tumors. *Eur. J. Radiol.* **77**, 19–25 (2011).
149. Rawls, J. F. & Johnson, S. L. Zebrafish kit mutation reveals primary and secondary regulation of melanocyte development during fin stripe regeneration. *Development* **127**, 3715–3724 (2000).
150. Renshaw, S. A. *et al*. A transgenic zebrafish model of neutrophilic inflammation. (2006). doi:10.1182/blood-2006
151. Reyes-Cerpa, S. *et al*. Fish Cytokines and Immune Response. in *New Advances and Contributions to Fish Biology* (InTech, 2012). doi:10.5772/53504
152. Roccaro, A. M. *et al*. BM mesenchymal stromal cell–derived exosomes facilitate multiple myeloma progression. *J. Clin. Invest.* **123**, 1542 (2013).
153. Rodda, S. J. & McMahon, A. P. Distinct roles for Hedgehog and canonical Wnt signaling in specification, differentiation and maintenance of osteoblast progenitors. *Development* **133**, 3231–3244 (2006).
154. Rosen, G., Tan, C., Sanmaneechai, A., Beattie, E. J. Jr., Marcove, R., Murphy, M. L. The rationale for multiple drug chemotherapy in the treatment of osteogenic sarcoma. Cancer, **35**, 936-45. (1975).
155. Rosen, J. N., Sweeney, M. F. & Mably, J. D. Microinjection of zebrafish embryos to analyze gene function. *J. Vis. Exp.* (2009). doi:10.3791/1115
156. Ruby, C. E. *et al*. Exosomes from Osteosarcoma and normal osteoblast differ in proteomic cargo and immunomodulatory effects on T cells. *Exp. Cell Res.* **358**, 369–376 (2017).
157. Rupert, D. L. M., Claudio, V., Lässer, C. & Bally, M. Methods for the physical characterization and quantification of extracellular vesicles in biological samples. *Biochim. Biophys. Acta - Gen. Subj.* **1861**, 3164–3179 (2017).
158. Scholzen, T. and Gerdes, J. The Ki-67 protein: From the known and the unknown. *J. Cell. Physiol.*, **182:** 311-322. (2000), doi:10.1002/(SICI)1097-4652(200003)182:3<311::AID-JCP1>3.0.CO;2-9
159. Ségaliny, A. I. *et al*. IL-34 and M-CSF form a novel heteromeric cytokine and regulate the M-CSF receptor activation and localization. *Cytokine* **76**, 170–181 (2015).

160. Segaliny, A. I. *et al*. Interleukin-34 promotes tumor progression and metastatic process in osteosarcoma through induction of angiogenesis and macrophage recruitment. *Int. J. Cancer* **137**, 73–85 (2015).
161. Segaliny, A. I. *et al*. Syndecan-1 regulates the biological activities of interleukin-34. *Biochim. Biophys. Acta - Mol. Cell Res.* **1853**, 1010–1021 (2015).
162. Seth, A., Stemple, D. L. & Barroso, I. The emerging use of zebrafish to model metabolic disease. *Dis. Model. Mech.* **6**, 1080 (2013).
163. Shabo, I., Stål, O., Olsson, H., Doré, S. & Svanvik, J. Breast cancer expression of CD163, a macrophage scavenger receptor, is related to early distant recurrence and reduced patient survival. *Int. J. Cancer* **123**, 780–786 (2008).
164. Singh, A. P. & Nüsslein-Volhard, C. Zebrafish stripes as a model for vertebrate colour pattern formation. *Curr. Biol.* **25**, R81–R92 (2015).
165. Somanath, P. R., Razorenova, O. V, Chen, J. & Byzova, T. V. Akt1 in endothelial cell and angiogenesis. *Cell Cycle* **5**, 512–8 (2006).
166. Somm, E. & Jornayvaz, F. R. Fibroblast Growth Factor 15/19 – From Basic Functions to Therapeutic Perspectives. *Endocr. Rev.* **39**, 960–989 (2018).
167. Spoorendonk, K. M., Hammond, C. L., Huitema, L. F. A., Vanoevelen, J. & Schulte-Merker, S. Zebrafish as a unique model system in bone research: the power of genetics and *in vivo* imaging. *J. Appl. Ichthyol.* **26**, 219–224 (2010).
168. Stiller, C. A., Craft, A. W. & Corazziari, I. Survival of children with bone sarcoma in Europe since 1978: Results from the EUROCARE study. *Eur. J. Cancer* **37**, 760–766 (2001).
169. Strauss, S. J. *et al*. Report from the 4th European Bone Sarcoma Networking meeting: focus on osteosarcoma. *Clin. Sarcoma Res.* **8**, 17 (2018).
170. Sulzmaier, F. J., Jean, C. & Schlaepfer, D. D. FAK in cancer: mechanistic findings and clinical applications. *Nat. Rev. Cancer* **14**, 598–610 (2014).
171. Sundara, Y. T. *et al*. Increased PD-L1 and T-cell infiltration in the presence of HLA class I expression in metastatic high-grade osteosarcoma: a rationale for T-cell-based immunotherapy. *Cancer Immunol. Immunother.* **66**, 119–128 (2017).
172. Taniguchi, K. & Karin, M. IL-6 and related cytokines as the critical lynchpins between inflammation and cancer. *Semin. Immunol.* **26**, 54–74 (2014).

173. Tawbi, H. A. *et al*. Pembrolizumab in advanced soft-tissue sarcoma and bone sarcoma (SARC028): a multicentre, two-cohort, single-arm, open-label, phase 2 trial. *Lancet Oncol*. **18**, 1493–1501 (2017).
174. Tellez-Gabriel, M. *et al*. Analysis of gap junctional intercellular communications using a dielectrophoresis-based microchip. *Eur. J. Cell Biol*. **96**, 110–118 (2017).
175. Théry, C., Amigorena, S., Raposo, G. & Clayton, A. Isolation and Characterization of Exosomes from Cell Culture Supernatants and Biological Fluids. *Curr. Protoc. Cell Biol*. **30**, 3.22.1-3.22.29 (2006).
176. Tian, H. *et al*. Endoglin Mediates Vascular Maturation by Promoting Vascular Smooth Muscle Cell Migration and Spreading. *Arterioscler. Thromb. Vasc. Biol*. **37**, 1115–1126 (2017).
177. Tian, Y., Shen, H., Xia, L. & Lu, J. Elevated Serum and Synovial Fluid Levels of Interleukin-34 in Rheumatoid Arthritis: Possible Association with Disease Progression via Interleukin-17 Production. *J. Interf. Cytokine Res*. **33**, 398–401 (2013).
178. Torregiani, E., Roncuzzi, L., Perut, F., Zini, N. & Baldini, N. Multimodal transfer of MDR by exosomes in human osteosarcoma. *Int. J. Oncol*. **49**, 189–196 (2016).
179. Traver, D. *et al*. The zebrafish as a model organism to study development of the immune system. *Adv. Immunol*. **81**, 253–330 (2003).
180. Trede, N. S., Langenau, D. M., Traver, D., Look, A. T. & Zon, L. I. The Use of Zebrafish to Understand Immunity. *Immunity* **20**, 367–379 (2004).
181. Uluçkan, Ö., Segaliny, A., Botter, S., Santiago, J. M. & Mutsaers, A. J. Preclinical mouse models of osteosarcoma. *Bonekey Rep*. **4**, 670 (2015).
182. Valcz, G. *et al*. Perspective: bidirectional exosomal transport between cancer stem cells and their fibroblast-rich microenvironment during metastasis formation. *npj Breast Cancer* **4**, 18 (2018).
183. Varshney, G. K. *et al.* A high-throughput functional genomics workflow based on CRISPR/Cas9-mediated targeted mutagenesis in zebrafish. *Nat. Protoc.* **11**, 2357–2375 (2016).
184. Walkley, C. R. *et al*. Conditional mouse osteosarcoma, dependent on p53 loss and potentiated by loss of Rb, mimics the human disease. *Genes Dev*. **22**, 1662–1676 (2008).

185. Wang, T. *et* al. Identification of IL-34 in teleost fish: differential expression of rainbow trout IL-34, MCSF1 and MCSF2, ligands of the MCSF receptor. *Molecular Immunology*. **53**, 398-409 (2013).
186. Wang, Y. *et al*. Adipose-derived mesenchymal stem cells promote osteosarcoma proliferation and metastasis by activating the STAT3 pathway. *Oncotarget* **8**, 23803–23816 (2017).
187. Wang, Y. *et al*. IL-34 is a tissue-restricted ligand of CSF1R required for the development of Langerhans cells and microglia. *Nat. Immunol*. **13**, 753–760 (2012).
188. Webber, J. P. *et al*. Differentiation of tumour-promoting stromal myofibroblasts by cancer exosomes. *Oncogene* **34**, 290–302 (2015).
189. Webber, J., Yeung, V. & Clayton, A. Extracellular vesicles as modulators of the cancer microenvironment. *Semin. Cell Dev. Biol*. **40**, 27–34 (2015).
190. Wei, S. *et al*. Functional overlap but differential expression of CSF-1 and IL-34 in their CSF-1 receptor-mediated regulation of myeloid cells. *J. Leukoc. Biol*. **88**, 495–505 (2010).
191. Westrøm, S. *et al*. Evaluation of CD146 as Target for Radioimmunotherapy against Osteosarcoma. *PLoS One* **11**, e0165382 (2016).
192. Whelan, J. S. *et al*. EURAMOS-1, an international randomised study for osteosarcoma: Results from pre-randomisation treatment. *Ann. Oncol*. **26**, 407–414 (2015).
193. White, R., Rose, K. & Zon, L. Zebrafish cancer: the state of the art and the path forward. *Nat. Rev. Cancer* **13**, 624–636 (2013).
194. Wiktor-Jedrzejczak, W., Urbanowska, E., Aukerman, S. L., Pollard, J. W., Stanley, E. R., Ralph, P., Ansari, A. A., Sell, K. W. and Szperl, M. Correction by CSF-1 of defects in the osteopetrotic op/op mouse suggests local., developmental., and humoral requirements for this growth factor. *Exp. Hematol*. **19**, 1049-1054. (1991).
195. Wu, S. *et al*. Il34-Csf1r Pathway Regulates the Migration and Colonization of Microglial Precursors. *Dev. Cell* **46**, 552-563.e4 (2018).
196. Xu, J.-F. *et al*. Exosomes containing differential expression of microRNA and mRNA in osteosarcoma that can predict response to chemotherapy. *Oncotarget* **8**, 75968–75978 (2017).

197. Yamane, F. *et al*. CSF-1 receptor-mediated differentiation of a new type of monocytic cell with B cell-stimulating activity: its selective dependence on IL-34. *J. Leukoc. Biol.* **95**, 19–31 (2014).
198. Yang, J. *et al*. Recurrent LRP1-SNRNP25 and KCNMB4-CCND3 fusion genes promote tumor cell motility in human osteosarcoma. *J. Hematol. Oncol.* **7**, 76 (2014).
199. Yang, L. *et al*. CD163+ tumor-associated macrophage is a prognostic biomarker and is associated with therapeutic effect on malignant pleural effusion of lung cancer patients. *Oncotarget* **6**, 10592 (2015).
200. Yoshida, H. *et al*. The murine mutation osteopetrosis is in the coding region of the macrophage colony stimulating factor gene. *Nature* **345**, 442–444 (1990).
201. Yu, B., Zhang, X. & Li, X. Exosomes derived from mesenchymal stem cells. *Int. J. Mol. Sci.* **15**, 4142–4157 (2014).
202. Yu, H. & Rohan, T. Role of the Insulin-Like Growth Factor Family in Cancer Development and Progression. *J. Natl. Cancer Inst.* **92**, 1472–1489 (2000).
203. Yu, Y. *et al*. Tumor necrosis factor-α induces interleukin-34 expression through nuclear factor-ϰB activation in MC3T3-E1 osteoblastic cells. *Mol. Med. Rep.* **10**, 1371–1376 (2014).
204. Zhang, J. *et al*. Exosome and Exosomal MicroRNA: Trafficking, Sorting, and Function. *Genomics. Proteomics Bioinformatics* **13**, 17–24 (2015).
205. Zhang. Identification of the hematopoeitc stem cell niche. *Methods Mol. Biol.* **425**, 0–5 (2003).
206. Zheng, Y., Wang, G., Chen, R., Hua, Y. & Cai, Z. Mesenchymal stem cells in the osteosarcoma microenvironment: their biological properties, influence on tumour growth, and therapeutic implications. *Stem Cell Res. Ther.* **9**, 22 (2018).
207. Zhou, R. P. *et al*. Functions of interleukin-34 and its emerging association with rheumatoid arthritis. *Immunology* **149**, 362–373 (2016).
208. Zhou, Z.-F. *et al*. Calcium phosphate-phosphorylated adenosine hybrid microspheres for anti-osteosarcoma drug delivery and osteogenic differentiation. *Biomaterials* **121**, 1–14 (2017).
209. Zhu, W. *et al*. Exosomes derived from human bone marrow mesenchymal stem cells promote tumor growth in vivo. *Cancer Lett.* **315**, 28–37 (2012).

210. Zins, K. *et al*. Differential prognostic impact of interleukin-34 mRNA expression and infiltrating immune cell composition in intrinsic breast cancer subtypes. *Oncotarget* **9**, 23126–23148 (2018).

211. Zou, J. & Secombes, C. J. The Function of Fish Cytokines. *Biology (Basel)*. **5**, (2016).

212. Zwicker, S. *et al*. Interleukin 34: a new modulator of human and experimental inflammatory bowel disease. *Clin. Sci.* **129**, 281–290 (2015).

APPENDIX

Template of the image array for coordinate reference, followed by a table showing the human cytokine array coordinates.

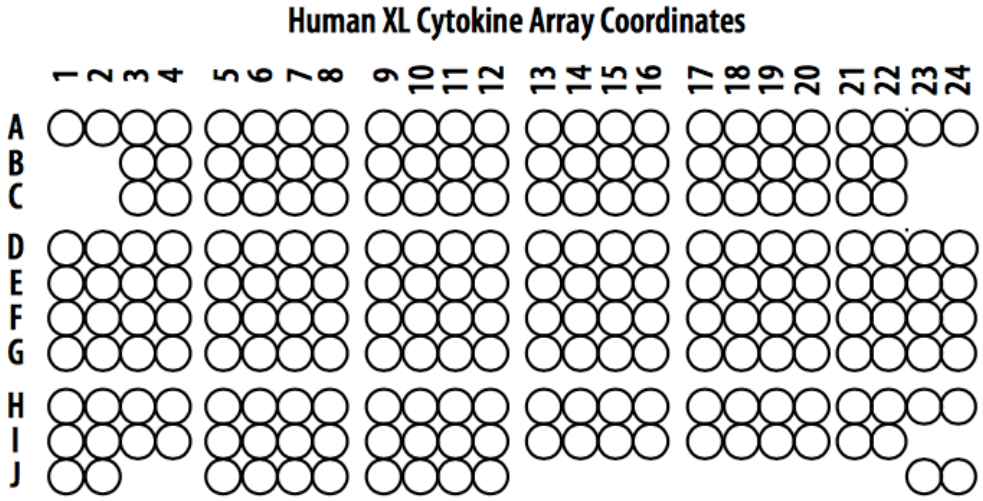

Coordinate	Analyte/Control	Entrez Gene ID	Alternate Nomenclature
A1, A2	Reference Spots	N/A	RS
A3, A4	Adiponectin	9370	Acrp30
A5, A6	Apolipoprotein A-I	335	ApoA1
A7, A8	Angiogenin	283	_____
A9, A10	Angiopoietin-1	284	Ang-1, ANGPT1
A11, A12	Angiopoietin-2	285	Ang-2, ANGPT2
A13, A14	BAFF	10673	BLyS, TNFSF13B
A15, A16	BDNF	627	Brain-derived Neurotrophic Factor
A17, A18	Complement Component C5/C5a	727	C5/C5a
A19, A20	CD14	929	_____
A21, A22	CD30	943	TNFRSF8
A23, A24	Reference Spots	N/A	RS
B3, B4	CD40 ligand	959	CD40L, TNFSF5, CD154, TRAP
B5, B6	Chitinase 3-like 1	1116	CHI3L1, YKL-40
B7, B8	Complement Factor D	1675	Adipsin, CFD

B9, B10	C-Reactive Protein	1401	CRP
B11, B12	Cripto-1	6997	Teratocarcinoma-derived Growth Factor
B13, B14	Cystatin C	1471	CST3, ARMD11
B15, B16	Dkk-1	22943	Dickkopf-1
B17, B18	DPPIV	1803	CD26, DPP4, Dipeptidyl-peptidase IV
B19, B20	EGF	1950	Epidermal Growth Factor
B21, B22	Emmprin	682	CD147, Basigin
C3, C4	ENA-78	6374	CXCL5
C5, C6	Endoglin	2022	CD105, ENG
C7, C8	Fas Ligand	356	TNFSF6, CD178, CD95L
C9, C10	FGF basic	2247	FGF-2
C11, C12	FGF-7	2252	KGF
C13, C14	FGF-19	9965	_____
C15, C16	Flt-3 Ligand	2323	FLT3LG
C17, C18	G-CSF	1440	CSF3
C19, C20	GDF-15	9518	MIC-1
C21, C22	GM-CSF	1437	CSF2
D1, D2	GROα	2919	CXCL1, MSGA-α
D3, D4	Growth Hormone	2688	GH, Somatotropin
D5, D6	HGF	3082	Scatter Factor, SF
D7, D8	ICAM-1	3383	CD54
D9, D10	IFN-γ	3458	IFNG
D11, D12	IGFBP-2	3485	_____

APPENDIX *CONTINUED*

Coordinate	**Analyte/Control**	**Entrez Gene ID**	**Alternate Nomenclature**
D13, D14	IGFBP-3	3486	_____
D15, D16	IL-1α	3552	IL-1F1
D17, D18	IL-1β	3553	IL-1F2
D19, D20	IL-1ra	3557	IL-1F3
D21, D22	IL-2	3558	_____
D23, D24	IL-3	3562	_____
E1, E2	IL-4	3565	_____
E3, E4	IL-5	3567	_____
E5, E6	IL-6	3569	_____
E7, E8	IL-8	3576	CXCL8
E9, E10	IL-10	3586	_____
E11, E12	IL-11	3589	_____

E13, E14	IL-12 p70	3593	_____
E15, E16	IL-13	3596	_____
E17, E18	IL-15	3600	_____
E19, E20	IL-16	3603	_____
E21, E22	IL-17A	3605	IL-17, CTLA8
E23, E24	IL-18 Bpa	10068	_____
F1, F2	IL-19	29949	_____
F3, F4	IL-22	50616	IL-TIF
F5, F6	IL-23	51561	IL-23A, SGRF
F7, F8	IL-24	11009	C49A, FISP, MDA-7, MOB-5, ST16
F9, F10	IL-27	246778	_____
F11, F12	IL-31	386653	_____
F13, F14	IL-32	9235	_____
F15, F16	IL-33	90865	C9orf26, DVS27, NF-HEV
F17, F18	IL-34	146433	C16orf77
F19, F20	IP-10	3627	CXCL10
F21, F22	I-TAC	6373	CXCL11, SCYB9B
F23, F24	Kallikrein 3	354	PSA, KLK3
G1, G2	Leptin	3952	OB
G3, G4	LIF	3976	_____
G5, G6	Lipocalin-2	3934	NGAL, LCN2, Siderocalin
G7, G8	MCP-1	6347	CCL2, MCAF
G9, G10	MCP-3	6354	CCL7, MARC
G11, G12	M-CSF	1435	CSF1
G13, G14	MIF	4282	_____
G15, G16	MIG	4283	CXCL9

APPENDIX *CONTINUED*

Coordinate	**Analyte/Control**	**Entrez Gene ID**	**Alternate Nomenclature**
G17, G18	MIP-1α/MIP-1β	6348/6351	CCL3/CCL4
G19, G20	MIP-3α	6364	CCL20, Exodus-1, LARC
G21, G22	MIP-3β	6363	CCL19, ELC
G23, G24	MMP-9	4318	CLG4B, Gelatinase B
H1, H2	Myeloperoxidase	4353	MPO, Lactoperoxidase
H3, H4	Osteopontin	6696	OPN
H5, H6	PDGF-AA	5154	_____
H7, H8	PDGF-AB/BB	5154/5155	_____
H9, H10	Pentraxin 3	5806	PTX3, TSG-14
H11, H12	PF4	5196	CXCL4
H13, H14	RAGE	177	_____

H15, H16	RANTES	6352	CCL5
H17, H18	RBP-4	5950	_____
H19, H20	Relaxin-2	6019	RLN2, RLXH2
H21, H22	Resistin	56729	ADSF, FIZZ3, RETN
H23, H24	SDF-1α	6387	CXCL12, PBSF
I1, I2	Serpin E1	5054	PAI-I, PAI-1, Nexin
I3, I4	SHBG	6462	ABP
I5, I6	ST2	9173	IL-1 R4, IL1RL1, ST2L
I7, I8	TARC	6361	CCL17
I9, I10	TFF3	7033	ITF, TFI
I11, I12	TfR	7037	CD71, TFR1, TFRC, TRFR
I13, I14	TGF-α	7039	TGFA
I15, I16	Thrombospondin-1	7057	THBS1, TSP-1
I17, I18	TNF-α	7124	TNFSF1A
I19, I20	uPAR	5329	PLAUR
I21, I22	VEGF	7422	BEGFA
J1, J2	Reference Spots	N/A	RS
J5, J6	Vitamin D BP	2638	VDB, DBP, VDBP
J7, J8	CD31	5175	PECAM-1
J9, J10	TIM-3	84868	HAVCR2
J11, J12	VCAM-1	7412	CD106
J23, J24	Negative Controls	N/A	Control (-)

SUB-CHAPTER 3.5

DEVELOPMENT OF IL-34 KNOCKOUT MICE

The data presented in this chapter was obtained in an experiment carried out by Dr F. Lézot and at the university of Nantes, France. The preparation and execution of the experiment, the data analysis and interpretation are entirely the work of Dr F. Lézot and his colleagues. Any contributions from colleagues in the collaboration, such as diagrams or calibrations, are explicitly referenced in the text. Flow cytometry analyses have been carried out in collaboration with Dr S. Dion and Dr M. Samson (IRSET, Inserm Unit 1085, Rennes, France). Skin analysis has been performed in collaboration with Prof. J.C. Lecron, University of Poitiers, France. The work presented here is currently still undergoing and is therefore still unpublished data (Unpublished, Schiavone *et al*).

3.5.1 METHODS

Il34 mutant mice were generated from embryonic stem cells carrying the targeted Il34 $^{tm1a(EUCOMM)Wtsi}$ allele designed to allow generation of either a null, LacZ reporter allele or a conditional floxed allele for subsequent Cre-mediated deletion. Clones carrying the targeted allele were introduced into C57BL/6J mice, and bred to CMV-Cre transgenic mice to remove the neo gene and generate Il34$^{LacZ/+}$ reporter mice in which exons 3-5 are deleted and replaced by an IRES-LacZ gene. Alternatively, mice could be bred to CAG-FLPe transgenic mice to remove the IRES-*LacZ*/*neo*^{r} cassette and generate mice carrying a conditional *Il34* allele in which exons 3-5 are flanked by *loxP* sites (*Il34*$^{f/+}$). Offspring were intercrossed to generate homozygote *Il34*$^{LacZ/LacZ}$ *or Il34*$^{f/f}$ mice (Wang *et al.,* 2012). Phenotyping of the model is currently focused on three main aspects: the immune phenotype, bone phenotype and skin phenotype.

3.5.2 RESULTS

3.5.2.1 Analysis of Immune Phenotype

Characterisation of immune cells in KO and WT mice was performed by FACS analysis from four organs: bone marrow, thymus, spleen and liver. For each organ, the analysis of total cell population, as well as of myeloid cells and lymphoid cells was performed.

Analysis of bone marrow cells showed no significant differences in the total cell population between wild-type and KO mice. (Figure 43A) However, IL-34 deficiency induced a significant decrease in the number of $CD19^{+}$ B lymphocytes, and a significant increase in $Gr1^{int}$ $CD11b^{+}$ monocytic lineage precursors. No difference was observed for $Ter119^{+}$ pro-erythroblast like cells myeloid precursors (MP), Lin^{-} hematopoetic stem cells and early lymphoid-committed precursors (LSK) (Figure 43B)

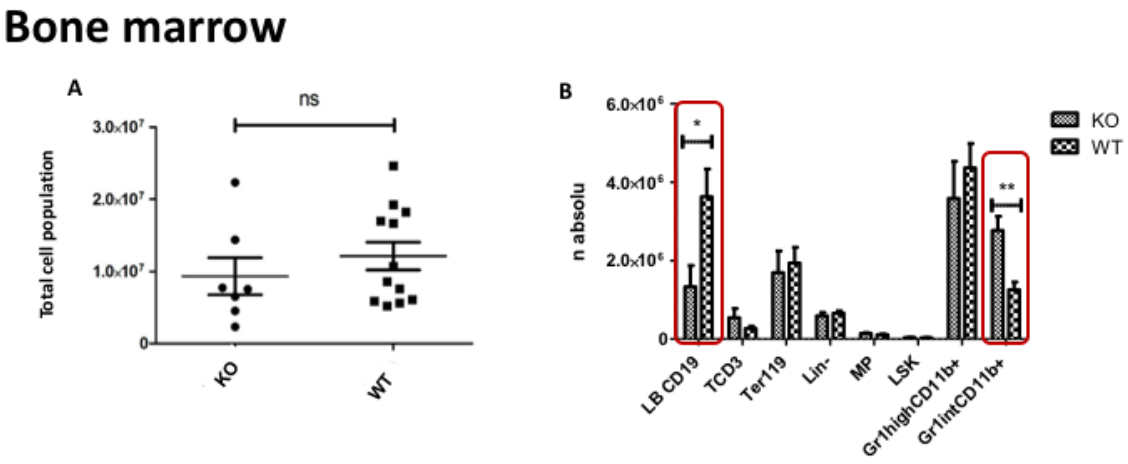

Figure 66: Immune characterisation of bone marrow cells in IL-34 KO mice. A) Quantification of the total immune cell populations in WT vs KO mice, and **B)** analysis of bone marrow cells CD19 (antigen for B-lymphocytes), CD3 (marker of T-cells) Ter119 (erythroid-specific marker), Lin (hematopoietic stem cells), MP (myeloid progenitor marker), LSK (lymphoid progenitor cell marker), $CD11b^{+}$ (marker of monocytes, dendritic cells and neutrophils).

In the thymus, a significant reduction in the total number of immune cells was present for KO mice. On further analysis, a decrease in thymocytes (pre T-lymphocytes) was detected by the marker CD3 (Figure 44)

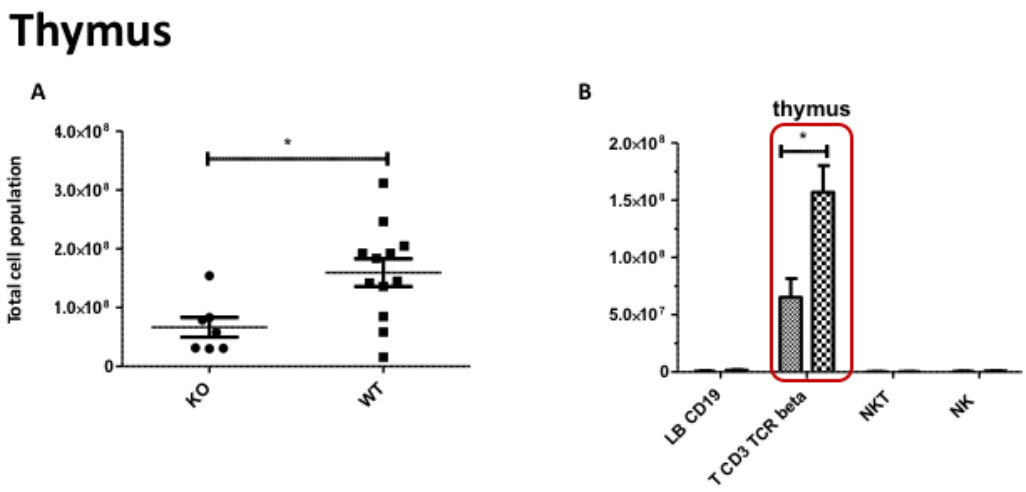

Figure 67: Immune characterisation of the thymus in IL-34 KO mice. A) Quantification of the total immune cell populations in WT vs KO mice, and B) analysis of CD19 (antigen for B-lymphocytes), CD3 (marker of T-cells), NKT (natural killer T-cells) and NK (natural killer cells).

The liver of IL-34 KO mice also showed a marked decrease in the total number of cell populations. Additionally, a decrease in dendritic cells ($CD11c^+$ cells), natural killer cells (NK) and B-cells surface marker (LB), as well as a tendency towards a decrease in resident macrophages (KC) was present in the KO mice in comparison to WT mice (Figure 45)

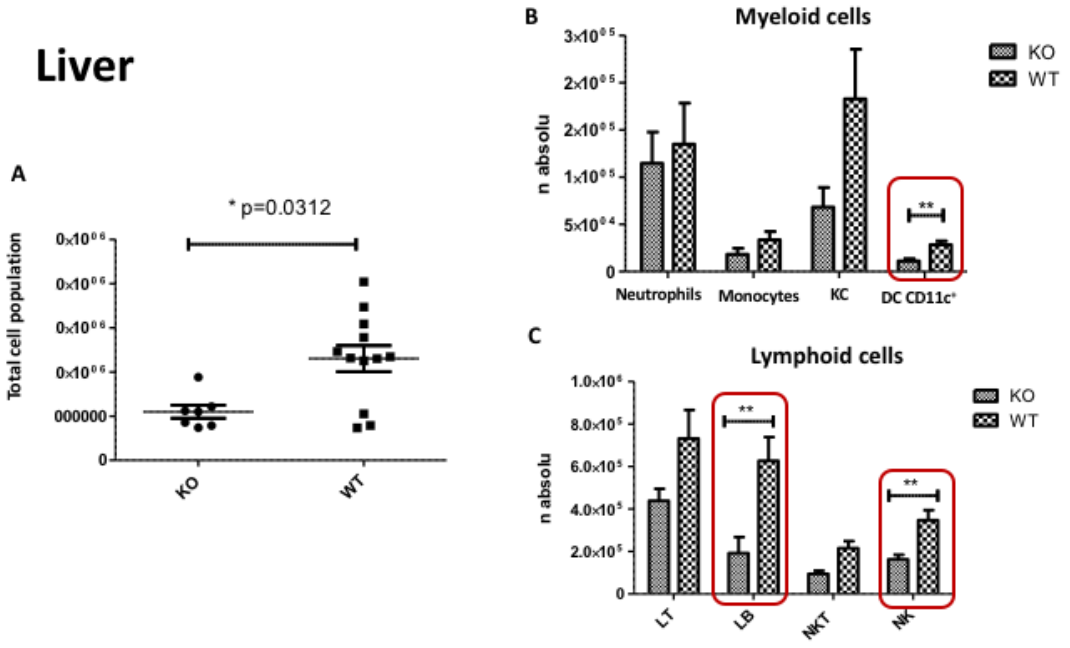

Figure 68: Immune characterisation of liver cells in IL-34 KO mice. A) Quantification of the total immune cell populations in WT vs KO mice, and B) analysis of myeloid cells including neutrophils, monocytes, KC (resident macrophages) and DC CD11c$^+$ (marker of dendritic cells). C) analysis of lymphoid cells including LT(marker of T-cells), LB(marker of B-cells), NKT (natural killer T-cells) and NK (natural killer cells).

The most notable difference in the immune cell populations however, was obtained in the spleen. In the spleen, a decrease for most cell populations was observed including natural killer cells (NK cells), natural killer T-cells (NKT), B-lymphocytes (CD19$^+$ cells), as well as a tendency towards a decrease in tissue resident macrophages (KC) and neutrophils (Figure 46).

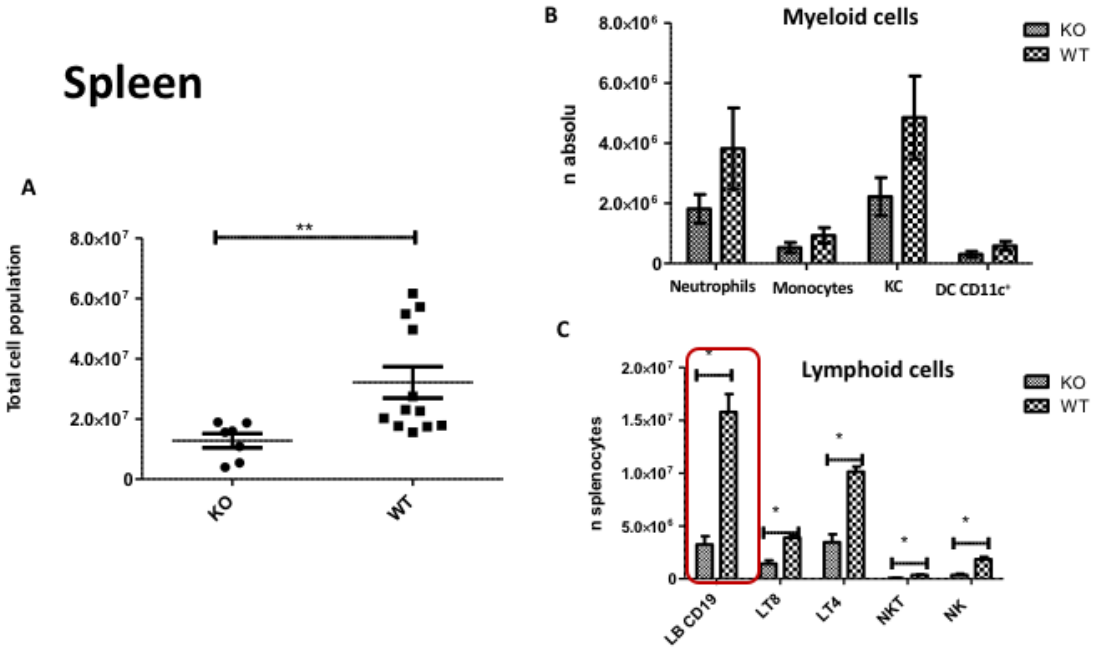

Figure 69: Immune characterisation of spleen cells in IL-34 KO mice. A) Quantification of the total immune cell populations in WT vs KO mice, and B) analysis of myeloid cells including neutrophils, monocytes, KC (resident macrophages) and DC CD11c⁺ (marker of dendritic cells). C) analysis of lymphoid cells including LBCD19 (marker of B-cells), LT8 (marker of T-cells), LT4 (marker of T-cells,) NKT (natural killer T-cells) and NK (natural killer cells).

3.5.2.2 Analysis of Bone Phenotype

Analysis of the bone phenotype carried out by microCT on 15-18 day old WT and KO mice, revealed a deficiency in mineralization of the skull in IL-34$^{-/-}$. (Figure 47). This delay in bone mineral density can be regarded as osteopenia, where the reduction in bone mineral content resulted in delayed growth of the mice, modification to head shape and fragile bones. Subsequently, this then resulted in spontaneous fractures in the spine.

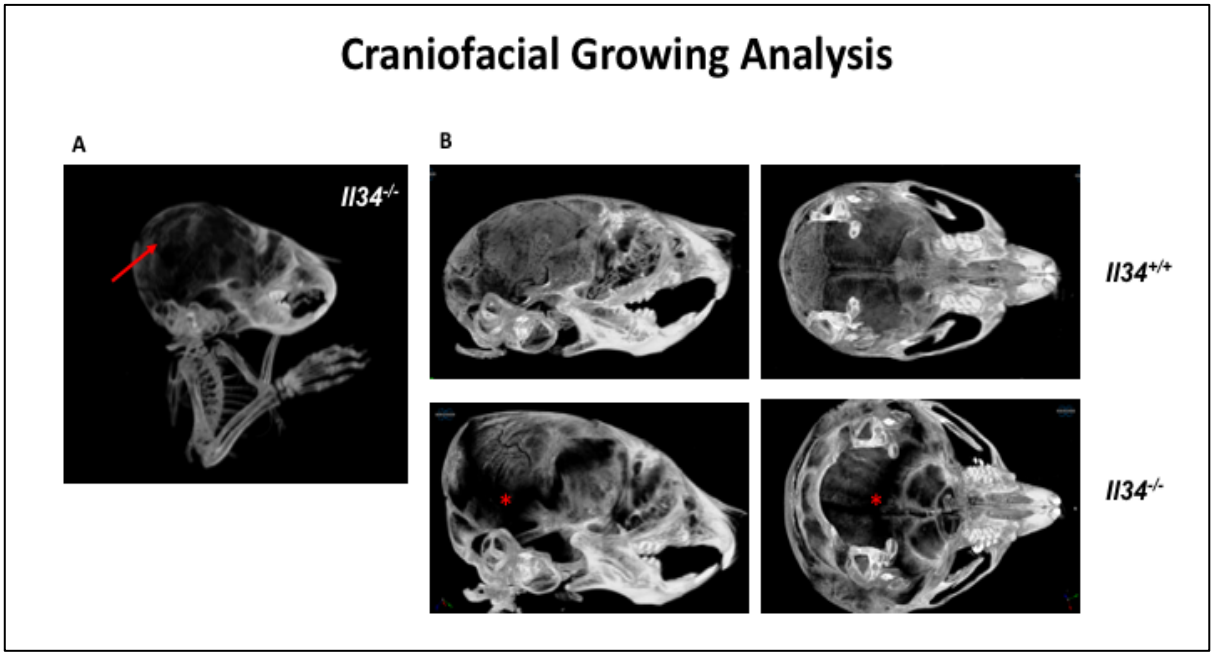

Figure 70: Analysis of craniofacial development in IL-34 knockout mice. **A)** MicroCT of 10 day old mouse showing lack of bone mineralisation in the skull as marked by the red arrow. **B)** Lateral and dorsal views of 15 day old mice skulls comparing wild-type and homozygous. Asterix indicate areas with loss of bone density.

Further analysis of the craniofacial phenotype in IL-34$^{-/-}$ knockout mice, showed that skeletal development was impaired. MicroCT analysis of horizontal growing as defined by the upper maxillary of the skull, vertical growth as determined by the cranial vault and defects in sagittal growing as observed in the zygomatic root width can be seen in Figure 48.

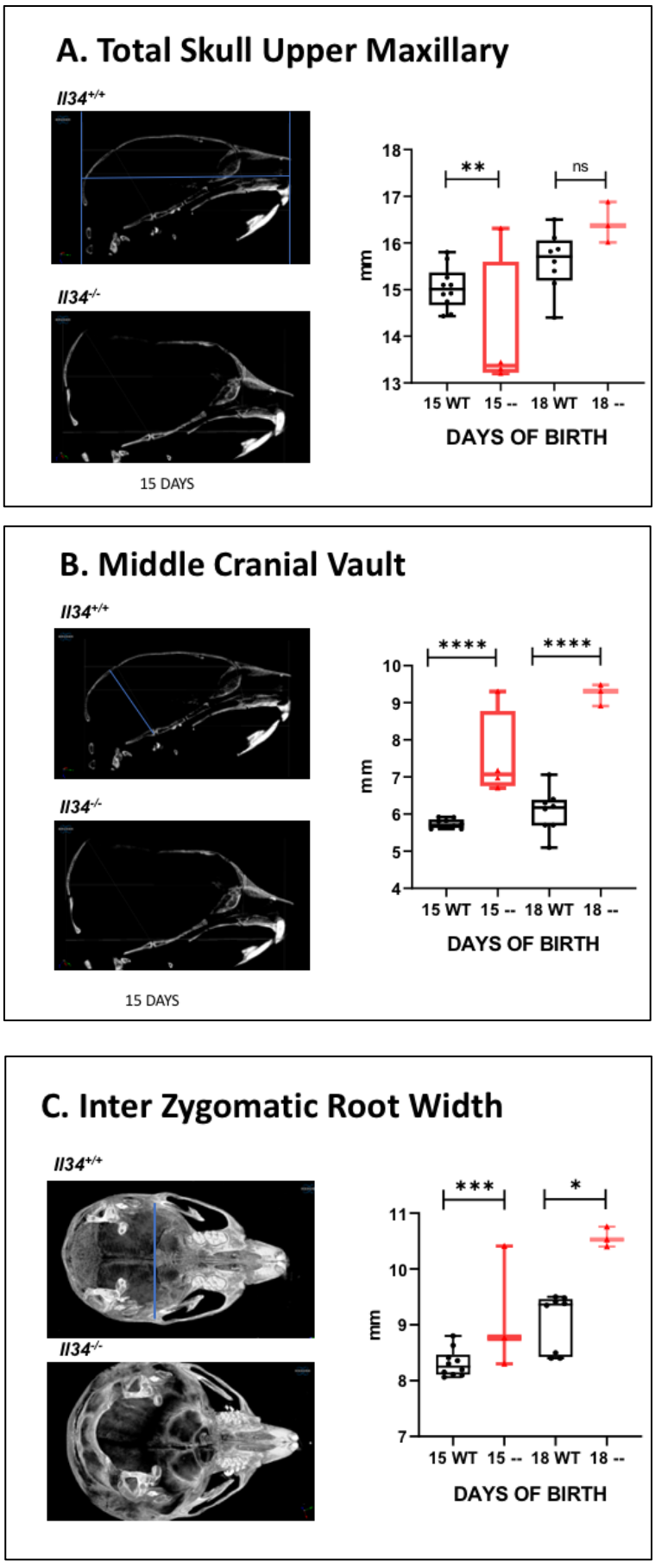

Figure 71: MicroCT images and quantification of craniofacial parameters in IL34 knockout mice. 15 day and 18 day old knockout mice were analysed in comparison with wild-type individuals for A) Total skull upper maxillary, B) middle cranial vault and C) inner zygomatic root width

To better understand the biological process associated with the bone loss observed in IL-34 KO mice, osteoclasts and osteoblasts were analysed by co-immunostaining: TRAP (staining of osteoclasts) and Osterix (staining of osteoblast precursors and mature osteoblasts) (Figure 49). A marked difference between IL-34 deficient and WT mice was observed, with an increase of both TRAP and OSX staining and a disappearance of the growth plate. This reason for this marked increase in osteoclasts and osteoblasts, is currently unknown and needs further evaluation, but it could be due to a dysregulation in bone remodelling. It is hypothesised that IL-34 may modulate the function of M-CSF.

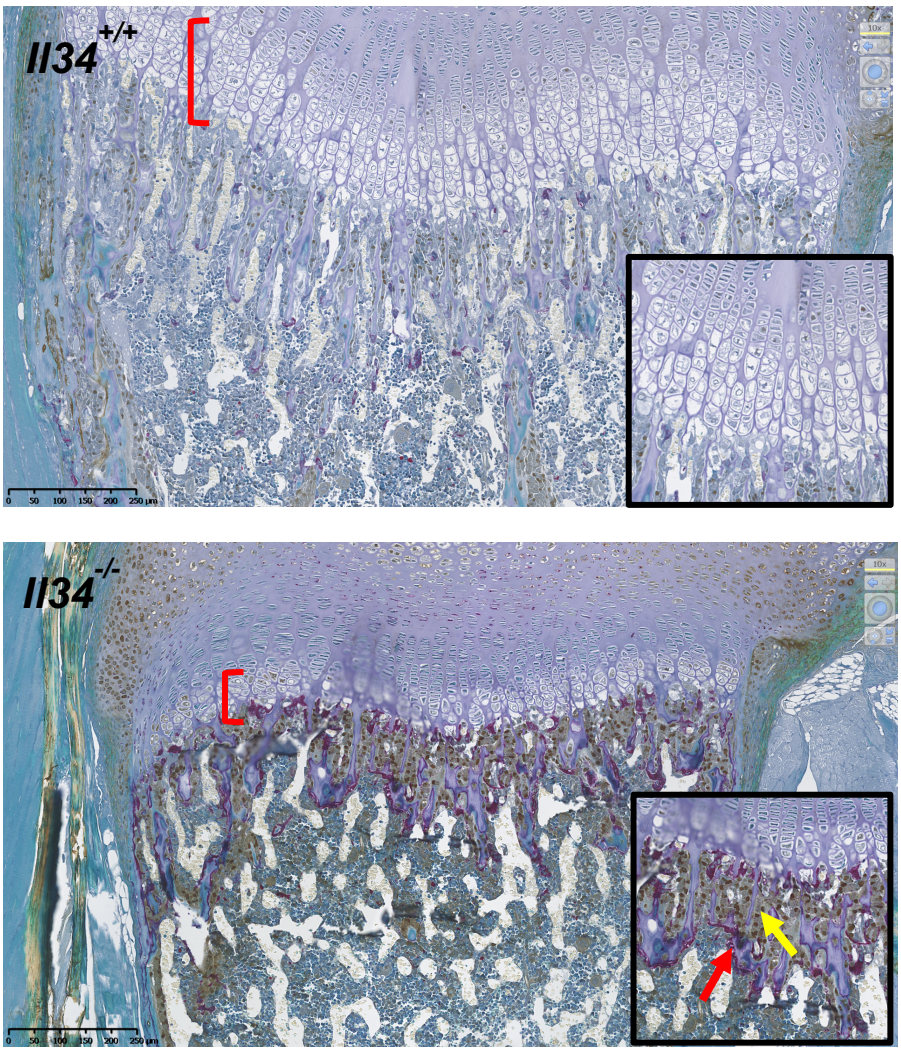

Figure 72: Immunohistological staining of TRAP (indicated in red arrow) and Osterix (indicated in yellow arrow) in IL-34$^{-/-}$ deficient and wild-type mice. Red bracket denotes the localisation and disappearance of the growth plate respectively.

3.5.2.3 Analysis of Skin Phenotype

On analysis of skin phenotype, there was no difference in the thickness of the epidermis or the dermis as determined by histology (Figure 50a-c). A significant decrease in the number of Langerhans cells was observed in the KO, as determined by immunohistochemistry and RT-qPCR for marker of langerin CD207 (Figure 50d-e).

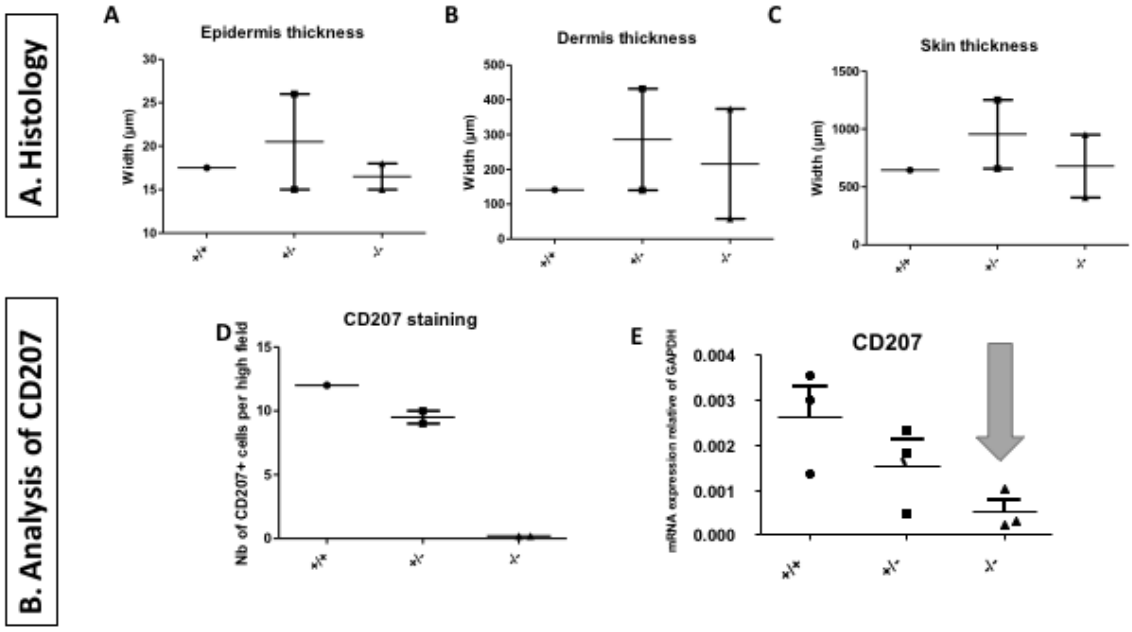

Figure 73: Analysis of skin phenotype for IL-34 knockout mice. A) Histological analysis of epidermal thickness **B)** dermal thickness and **C)** skin thickness. **D)** Immunohistochemistry analysis of CD207 in the epidermis **E)** RT-qPCR analysis of relative CD201 to GAPDH expression in the skin. +/+: IL-34$^{+/+}$; +/-: IL-34$^{+/-}$; -/-: IL-34$^{-/-}$.

Next genes responsible for epidermal differentiation (Keratin 1, Filaggrin and Involucrine) and dermal fibrosis (a-SMA, coll-a1 and coll-a3) were analysed by RT-qPCR. Results show that there was no difference in expression between wild type and heterozygous mutants, whereas for 1 out of every 3 homozygous mice investigated, there was an increased expression for each of the genes analysed. Therefore at this stage more repeats are required to obtain a complete cohort (Figure 51)

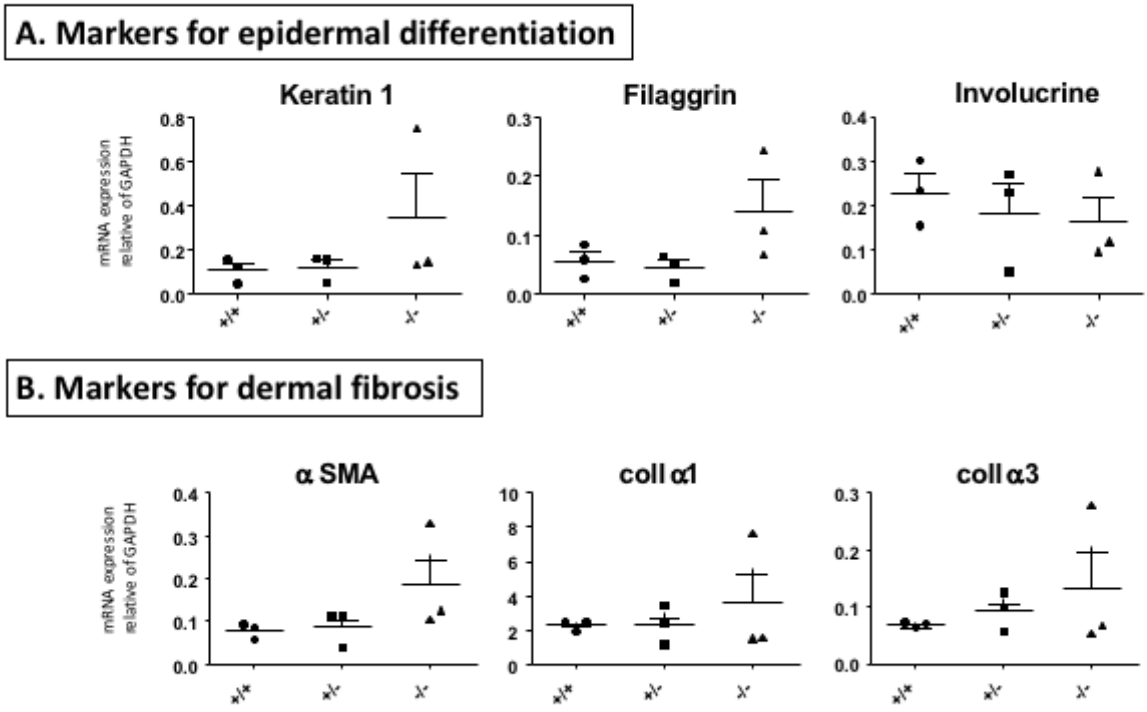

Figure 74: Analysis of skin phenotype for IL-34 deficient mice. A) RT-qPCR for markers of epidermal differentiation (Keratin 1, Filaggrin and Involucrine). **B)** RT-qPCR for markers of dermal fibrosis (a-SMA, coll-a1 and coll-a3). All relative gene expression was determined compared to GAPDH.

3.5.3 SUMMARY

The experiments reported here provide evidence that IL-34 has a considerable functional role in major cellular functions, including the development and maintenance of myeloid cell subsets, as well as possibly providing the first line of evidence for a de-regulation of lymphoid cells. The marked bone loss observed as a result of a delay in mineralization, rendered these mice non-viable thus strengthening the evidence consistent with a role for IL-34 in bone development.

These results led to the development of a zebrafish knockout model, as an additional model to address the limitations currently presenting with the mice knockouts. Most notably was the early lethality of the mice due to the spine fractures which did not allow for a longer time frame to assess the immune populations. Also, given the lower weight-bearing demand on the skeleton in aquatic animals, it was hypothesised that the zebrafish would be a more suited model to assess the bone phenotype, and thus by-pass the severe bone phenotype observed in these mice.